Modelling and analytical studies of magmatic-hydrothermal processes

Klyukin Yury Igorevich

Dissertation submitted to the faculty of the Virginia Polytechnic Institute and State University in partial fulfillment of the requirements for the degree of

Doctor of Philosophy
In
Geosciences

Robert J Bodnar
Esteban Gazel
Robert P. Lowell
Robert J. Tracy

December 8th
Blacksburg, VA

Keywords: Hydrothermal Fluid, Phase Equilibria, Numerical Model, Viscosity, Fluid Properties, Fluid Inclusions, Emerald, Raman spectrometry, Hiddenite

Modelling and analytical studies of magmatic-hydrothermal processes

Klyukin Yury Igorevich

ABSTRACT

Hydrothermal processes play a major role in transporting mass and energy in Earth's crust. These processes rely on hydrothermal fluid, which is dissolving, transporting and precipitating minerals and distribute heat. The composition of the hydrothermal fluid is specific for various geological settings, but in most cases it can be approximated by H_2O-NaCl-CO_2 fluid composition. The flow of hydrothermal fluid is controlled by differences in temperature, pressure and/or density of the fluid and hydraulic conductivity of the rock. In my work, I was focused on modeling of the hydrothermal fluid properties and experimental characterization of fluid that formed emerald deposit in North Carolina, USA. The dissertation based on the result of three separate projects.

The first project has been dedicated to characterization of the H_2O-NaCl hydrothermal fluid ability to transport mass and energy. This ability of the fluid is defined by a change in fluid density and enthalpy in response to changing pressure or temperature. In this project we quantified the derivatives of mass, enthalpy and SiO_2 solubility in wide range of pressure, temperature and composition (PTx) of H_2O-NaCl fluid. Our study indicated that the PT region in which fluid is most efficiently can transport mass and energy, located in the critical region near liquid-vapor phase boundary and the sensitivity to changing pressure-temperature conditions decrease with increasing salinity.

In second project we developed the revised H_2O-NaCl viscosity model. Revised model to calculate the viscosity of H_2O-NaCl reproduces experimental data with ±10 % precision in PTx range where experimental data available and follows expected trends outside of the range. This model is valid over the temperature range from the H_2O solidus (~0 °C) to ~1,000 °C, from ~0.1 MPa to ≤500 MPa, and for salinities from 0-100 wt.% NaCl.

The third project has been focused on the characterization of formation conditions of the emerald at North American Emerald Mine, Hiddenite, North Carolina, USA. The emerald formation conditions defined as 120-220 MPa, 450-625 °C using stable isotope, Raman spectrometry, and fluid inclusion analysis. Hydrothermal fluid had a composition of CO_2-H_2O±CH_4, which indicates mildly reducing environment of emerald growth.

DEDICATION

To my wife Ksenia and daughter Amber Anna, without whom this work would be probably finished faster but with less joy.

ACKNOWLEDGEMENTS

I would like to thank my advisor Bob Bodnar, for his guidance and support during my stay here. Esteban Gazel, Robert Tracy and Robert Lowell did a great work as committee members, providing professional recommendations.

Fellow graduate students gave useful advises and help: Adam Angel provided input regarding graphics; discussion of viscosity models with Shreya Singh led to understanding the demand for creating a revised model; Lowell Moore guided on how perform Raman calibration and routine analysis; Matt Sublett aided in early stages of work with North American Emerald Mine, performing analysis and sample preparation; Eszter Sendula did a tremendous work on sample selection.

I thank reviewers Axel Liebscher and David Dolejs for providing suggestions and comments that have improved project, introduced below in Chapter 1. Kayla Lewis confirmed that the Palliser and McKibbin model demonstrates unusual behavior that needs to be investigated. Robert McKibbin and Chris Palliser gave useful input concerning their model for the of H_2O-NaCl fluid viscosity. Jamie Hill, owner of the North American Emerald Mine, provided access and samples, and Ed Speer aided during field trips to the mine. Arthur Merschat provided the detailed geological map of the Appalachian region.

The office staff readiness to help is exceptional. I am particularly grateful for assistance given by Connie Lowe, her guidance regarding various aspects of graduate student work and life.

TABLE OF CONTENTS

LIST OF FIGURES

Figures Chapter 1

Figures Chapter 2

Figures Chapter 3

LIST OF TABLES

Tables Chapter 2

Tables Chapter 3

Tables Appendix B

Tables Appendix C

NOMENCLATURE

c_f – isobaric specific heat capacity of the fluid ($J \cdot kg^{-1} \cdot K^{-1}$)
c_r – isobaric specific heat capacity of the rock ($J \cdot kg^{-1} \cdot K^{-1}$)
F – fluxibility of the fluid ($J \cdot s \cdot m^{-5}$)
g – standard acceleration due to gravity (9.81 $m \cdot s^{-2}$)
h – specific enthalpy of the fluid ($J \cdot kg^{-1}$)
h^v – volumetric enthalpy of the fluid ($J \cdot m^{-3}$)
k – permeability (m^2)
m_{SiO2} – quartz solubility in H_2O-NaCl fluid per kg of H_2O ($mol \cdot kg^{-1}$ H_2O)
P – pressure (Pa), conversion factor: 1 bar = 10^5 Pa=10^{-1}MPa
T – temperature (K), conversion factor: K = °C + 273.15
t – time (s)
V – molar volume ($m^3 \cdot mol^{-1}$)
V – volume (m^3)
X – mol fraction
x – weight fraction
α – coefficient of isobaric thermal expansion (K^{-1})
β – coefficient of isothermal compressibility (Pa^{-1})
$\delta m^T_{SiO_2}$ – coefficient of isobaric change in quartz solubility (K^{-1})
$\delta m^P_{SiO_2}$ – coefficient of isothermal change in quartz solubility (bar^{-1})
η – dynamic viscosity (μPa·s), conversion factor: μPa·s =10^{-6} Pa·s
μ – chemical potential of the fluid ($J \cdot kg^{-1}$)
ρ – density of the fluid ($kg \cdot m^{-3}$)
ρ_r – density of the rock ($kg \cdot m^{-3}$)
$\vec{v}$ – mass flow rate per unit area vector ($kg \cdot m^{-2} \cdot s^{-1}$)
φ – flow connected porosity (dimensionless)
$\tilde{\chi}$ – reduced susceptibility (dimensionless)
∇ – gradient operator, (m^{-1}) $\frac{\partial}{\partial x} + \frac{\partial}{\partial y} + \frac{\partial}{\partial z}$

INTRODUCTION

Deposits are forming in various conditions, from weathering at the surface to magmatic crystallization in depth, but most of the deposits are formed by the hydrothermal fluid. The heat that transported by hydrothermal fluid found its application in geothermal power plants, located at geothermally active hydrothermal systems. The minerals and metals dissolved, transported and deposited by the hydrothermal fluid forming the deposits. The underlying process responsible for heat and mass transport is an interaction between fluid and rock. This interaction causes the heat exchange, changes in the composition of the hydrothermal fluid and alteration of the host rock.

An example of this interaction is given by Driesner (2013) – a seawater peculating through seafloor at Mid Ocean Ridge (MOR) conditions, is heated at the bottom of the system and then later released back to the ocean through hydrothermal vent often referred as black smokers. Black smokers frequently have a high concentration of base and precious metals. The process that is responsible for enrichment of black smokers in metals is next: the heated seawater is interacting with rocks of the seafloor in the base of the hydrothermal system and as a result, heated seawater is losing Mg and SO_4, but dissolving Cu from the host rock. Cu then transported with rising plume of the hydrothermal fluid and deposited, as hydrothermal fluid is cooling or mixing with cold seawater at sea bottom, precipitating Cu-bearing minerals.

The natural hydrothermal fluid has a multicomponent composition, which includes complexes of metals, various volatiles, salts and water (Yardley and Bodnar, 2014). As shown in the example with the MOR, the composition of the fluid dynamically changes. However, general composition of the hydrothermal fluid can be well approximated by H_2O-NaCl-CO_2.

As shown by Kesler (2005), seawater hydrothermal systems characterized by H_2O-NaCl with a low concentration of the NaCl, and traces of CO_2. The basinal hydrothermal system includes connate fluid, fluid formed during diagenetic reactions and meteoric recharge. While compositionally this fluid is similar to seawater hydrothermal fluid, it has higher salt content (up to 30 wt. %) and operates at lower temperatures. Magmatic-hydrothermal systems consist of fluid released from crystallizing magma, and their composition varies significantly. The hydrothermal fluid of such system can have salinity up to 70 wt. % or CO_2 of high concentration. The temperature of this system varies in significantly, reaching 700 °C. The metamorphic hydrothermal system characterized by CO_2-H_2O fluid composition, because these components are commonly released during the metamorphic reaction. In contrast with other hydrothermal systems, metamorphic hydrothermal fluid have a very low salt (or NaCl) content is due to the low solubility of the NaCl in the CO_2 phase.

The fluid flow is controlled by differences in temperature, pressure density of the fluid, and hydraulic conductivity of the rock. In my work I was focused on modeling of the H_2O-NaCl hydrothermal fluid properties, which would characterize seafloor, basinal and partially the magmatic hydrothermal systems. The emerald formation has been characterized in order to identify its origin – either metamorphic or magmatic, identify sources of beryllium and identify perspective regions where emerald mineralization may be discovered.

The first project has been focused on characterization of the H_2O-NaCl hydrothermal fluid ability to transport mass and heat. This ability of the fluid is limited by the scale of change in fluid density or enthalpy in response to changes in pressure or temperature. This change greatly varies, depending on pressure, temperature and composition (PTx) of the fluid. For pure H_2O there is a defined range of pressure and temperature where most of the physical and

thermodynamic properties changes by a large amount in the response to small changes in pressure or temperature. This region defined as a critical region. We implemented the concept of the critical region for the H_2O-NaCl system and modeled how this region is responding to change in salinity. Our study indicated that the critical region located near the liquid-vapor curve of the system at given composition, and the most efficiently hydrothermal fluid can transport mass and energy at low salinity. This project discussed in details in Chapter 1.

The second project has been dedicated to developing the revised H_2O-NaCl viscosity model. Viscosity is a crucial parameter for fluid flow and reactive transport models, where viscosity defines (among other parameters) mass flow in porous media. Most of existing viscosity models limited by the PTx which are lower than those of the seafloor and magmatic hydrothermal systems. The only one model that operates at high temperature and composition demonstrated an unusual behavior. This behavior was attributed to the governing equation and the way how this equation utilizes viscosity of pure H_2O. In response, we developed a revised H_2O-NaCl viscosity model that can reproduce experimental data better (±10 % error) and follows expected behavior in PTx range with no experimental data available. The review of existing models and developing of new model described in Chapter 2. Since its publication our model has been incorporated in multiple models simulating fluid flow.

The third project has been focused on experimental characterization of the emerald formation. Emerald is one of the most valuable gemstones, and it forms in unusual geological conditions. This gem is a green variety of beryl ($Be_3Al_2Si_6O_{18}$), in which green color defined by a trace amount of Cr and V substituting Al. The formation of emerald occurs in contradictory environment: Be is a highly incompatible element, most highly concentrated in highly evolved magmas and rocks, whereas Cr and V are compatible elements generally concentrated in ultramafic and other primitive magmas and rocks – thus, emerald formation implies unique conditions – where fluid derived from felsic magma or rock (high SiO_2 content) is interacting with ultramafic (low SiO_2) host rocks. In many cases, the origins of deposits remain unclear (Groat et al., 2008). One of the locations for which formation of the emerald was unclear is North American Emerald Mine, located in Alexander County, North Carolina, USA. In our study, we used fluid inclusion, mineralogical and stable isotope analyses and defined emerald formation conditions as 120-220 MPa, 450-625 °C. Hydrothermal fluid had a composition of CO_2-H_2O±CH_4, which indicates mildly reducing environment of emerald growth. These findings may help to identify new locations of the emerald. Detailed characterization of the emerald formation at North American Emerald Mine provided in Chapter 3

References

Driesner, T. (2013) The Molecular-Scale Fundament of Geothermal Fluid Thermodynamics, in: Stefansson, A., Driesner, T., Benezeth, P. (Eds.), Thermodynamics of Geothermal Fluids, pp. 5-33.

Groat, L.A., Giuliani, G., Marshall, D.D. and Turner, D. (2008) Emerald deposits and occurrences: A review. Ore Geology Reviews 34, 87-112.

Kesler, S.E. (2005) Ore-forming fluids. Elements 1, 13-18.

Yardley, B.W. and Bodnar, R.J. (2014) Fluids in the Continental Crust, Geochemical Perspectives. European Association of Geochemistry, p. 127.

CHAPTER 1

Klyukin, Y.I., Driesner, T., Steele-MacInnis, M., Lowell, R.P. and Bodnar, R.J. (2016) Effect of salinity on mass and energy transport by hydrothermal fluids based on the physical and thermodynamic properties of H_2O-NaCl. ***Geofluids*** 16, 585-603.

Effect of salinity on mass and energy transport by hydrothermal fluids based on the physical and thermodynamic properties of H_2O-NaCl.

Y.I. Klyukin [a], T. Driesner [b], M. Steele-MacInnis [c], R.P. Lowell [a] and R.J. Bodnar [a]

[a] Department of Geosciences, Virginia Tech, Blacksburg, VA, USA;
[b] Institute of Geochemistry and Petrology, ETH Zurich, Zurich, Switzerland;
[c] Department of Earth and Atmospheric Sciences, The University of Alberta, Alberta, Canada;

Abstract

Various thermodynamic properties of H_2O that are defined as pressure or temperature derivatives of some other variable, such as isothermal compressibility (β, pressure derivative of density), isobaric thermal expansion (α, temperature derivative of density), and specific isobaric heat capacity (c_f, temperature derivative of enthalpy), all show large magnitudes near the critical point, reflecting large variations in fluid density and specific enthalpy with small changes in temperature and pressure. As a result, mass (related to fluid density) and energy (related to fluid enthalpy) transport in this PT region are sensitive to changing PT conditions. Addition of NaCl to H_2O causes the region of anomalous behavior, here defined as the critical region, to migrate to higher temperatures and pressures. The critical region is defined as that region of PT space in which the dimensionless reduced susceptibility $\tilde{\chi} \geq 0.5$. When NaCl is added to H_2O, the critical region migrates to higher temperature and pressure. However, the absolute magnitudes of thermodynamic properties that are defined as temperature and/or pressure derivatives (α, β, and c_f) all decrease with increasing salinity. Thus, the mass and energy transporting capacities of hydrothermal fluids in the critical region become less sensitive to changing PT conditions as the salinity increases. For example, quartz solubility can be described as a function of fluid density, and because density becomes less sensitive to changing PT conditions as salinity increases, quartz solubility also becomes less sensitive to changing PT conditions as fluid salinity increases. Similarly, fluxibility describes the ability of a fluid to transport heat by buoyancy-driven convection, and fluxibility decreases with increasing salinity. Results of this study show that the mass and energy transport capacity of fluids in the Earth's crust are maximized in the critical region and that the sensitivity to changing PT conditions decreases with increasing salinity.

Keywords: Thermodynamics, H_2O-NaCl, heat capacity, isothermal compressibility, thermal expansion, quartz solubility, hydrothermal systems

1. Introduction

Fluids play a dominant role in mass and energy transport in the Earth's crust (Bredehoeft and Norton, 1990). During the last half century remarkable progress has been made in simulating

various chemical, physical and mechanical processes associated with the movement of fluids in the Earth. Mass and energy transport are quantitatively described by the equations for conservation of mass, momentum and energy.

Conservation of momentum associated with fluid flow is derived from the Darcy equation (Norton and Knight, 1977) according to (note that all symbols are defined in the section Nomenclature):

$$\vec{v} = -\frac{k\rho}{\eta}(\nabla P - \rho\vec{g}) \quad (1)$$

Similarly, conservation of mass is described by:

$$\frac{\partial \rho\varphi}{\partial t} = \nabla \cdot \vec{v} \quad (2)$$

Finally, conservation of energy according to Delaney (1982) is given by:

$$\left(\varphi\rho c_f + (1-\varphi)\rho_r c_r\right)\frac{\partial T}{\partial t} = -\nabla \cdot \left(\vec{v}h_f\right) + \nabla \cdot \lambda\nabla T \quad (3)$$

As shown by Equations (1) through (3), the variation in mass flux (Eq. (1)), fluid mass (Eq. (2)), and energy (Eq. (3)) with changing temperature and/or pressure all depend on the physical and thermodynamic properties of the fluid, including the fluid density and specific heat capacity. Thus, the ability of hydrothermal fluids in the Earth's crust to transport mass and energy varies as fluid density and/or enthalpy change in response to changing temperature and/or pressure.

Early workers applied these concepts to develop numerical models describing fluid flow in various types of hydrothermal systems, including those associated with shallow plutons (Cathles, 1981; Norton, 1979, 1982, 1984), submarine hydrothermal systems (Fehn and Cathles, 1979; Fehn et al., 1983; Patterson and Lowell, 1982), sedimentary environments (Cathles and Smith, 1983; Garven, 1985; Wood and Hewett, 1982) and others. A common feature of all of these pioneering modeling efforts is that the physical, thermodynamic and transport properties of the fluids were approximated based on the properties of pure H_2O. Although it was recognized that natural hydrothermal fluids are not pure H_2O but, rather, contain various amounts of dissolved salts and gases, experimental data and numerical models to predict the properties of these more complex fluids were unavailable.

Levelt Sengers et al. (1983) developed an equation of state (EOS) for the thermodynamic properties of H_2O in the limited pressure and temperature (*PT)* region from 644 to 693 K (370.85 to 419.85 °C) and pressures bounded by the 200 and 420 $kg \cdot m^{-3}$ isochores (lines of constant density). Subsequently, Johnson and Norton (1991) examined the thermodynamic properties of pure H_2O from 350-475 °C and 200-450 bars within the context of mass and energy transport in this "critical region" of *PT* space. The wedge-shaped *PT* region studied by Johnson and Norton (1991) (labeled as "Johnson & Norton, 1991" in Figure 1A) includes the *PTρ* region in which the EOS of Levelt Sengers et al. (1983) is valid, as well as adjacent *PT* space. According to Johnson and Norton (1991), approximately 20% of the *PT* grid covered in their study is within the *PT* window for the critical region modeled by Levelt Sengers et al. (1983). Johnson and Norton (1991) emphasized that various properties of H_2O [as well as other one-component fluid systems] exhibit anomalous behavior within the *PT* range of their investigation, such that the magnitude of the property changes by a large amount with a small change in temperature or pressure. Johnson and Norton (1991) used two different EOS to estimate the various properties of H_2O within their *PT* grid. Within the "critical region" (370.85 to 419.85 °C and pressures bounded by the 200 and 420 $kg \cdot m^{-3}$ isochores) the model of Levelt Sengers et al. (1983) was used, while the Haar et al. (1984) model was used for *PT* conditions outside of this region.

More recently, Anisimov et al. (2004) examined the behavior of aqueous solutions near the critical point of H_2O. These workers note that *"The properties of near-critical water are so*

drastically different from those of liquid water that one could almost consider it a different fluid: one that is highly compressible and expandable, low in viscosity, a low dielectric and a poor solvent for electrolytes, as opposed to liquid water with low compressibility and expansivity, but very high dielectric constant that makes it an excellent solvent for electrolytes."

In this study, we use the terms "liquid" and "vapor" to refer to aqueous fluids that have densities greater than and less than the critical density, respectively. The term supercritical fluid applies *sensu stricto* only to one-component fluids, and this term is not used to describe the two-component system H_2O-NaCl owing to inconsistencies in the literature concerning the definition of supercritical fluids in multi-component systems. Thus, according to Liebscher and Heinrich (2007), *"In two- or multi-component systems critical behavior occurs along critical curves and is no longer uniquely defined in terms of P and T. "Supercritical," as implying $P>P_c$ and $T>T_c$ therefore becomes meaningless."*

In order to define the "critical region," Anisimov et al. (2004) introduced a susceptibility factor, χ, that quantifies the isothermal rate of change of density with respect to chemical potential

$$\chi \equiv \left(\frac{\partial \rho}{\partial \mu}\right)_T \tag{4}$$

This relationship may also be written in terms of the isothermal compressibility as

$$\chi = \rho^2 \beta \tag{5}$$

Furthermore, Anisimov et al. (2004) defined the dimensionless reduced susceptibility as:

$$\tilde{\chi} = \rho^2 \beta \frac{P_{crit}}{\rho_{crit}^2} \tag{6}$$

These workers defined the critical region as that region of temperature and density space in which the reduced susceptibility, $\tilde{\chi}$ is ≥ 0.5.

Here, we adopt the suggestion of Anisimov et al. (2004), which was developed *sensu stricto* for a one-component system, to define the critical region for the two-component H_2O-NaCl system. As such, the region of *PT* space in which the reduced susceptibility $\tilde{\chi}$ for H_2O-NaCl fluid is ≥ 0.5 is used as a proxy to identify the critical region in which the fluids exhibit anomalous behavior. Note also that the region where $\tilde{\chi}$ is ≥ 0.5 for pure H_2O spans a wider *PT* region than the "critical region" of Johnson and Norton (1991) (Fig. 1A).

The mass transport capacity of hydrothermal fluids is related to the fluid density, and thermodynamic properties that describe the variation in density as a function of temperature and pressure are the coefficient of isothermal compressibility (β) that describes the pressure dependence of fluid density at constant temperature (Eq. (7)), and the coefficient of isobaric expansion (α) that describes the temperature dependence of fluid density at constant pressure (Eq. (8)). That is,

$$\beta \equiv \frac{1}{\rho}\left(\frac{\partial \rho}{\partial P}\right)_T \tag{7}$$

$$\alpha \equiv -\frac{1}{\rho}\left(\frac{\partial \rho}{\partial T}\right)_P \tag{8}$$

Within most of the one-phase liquid or vapor region for H_2O, the magnitudes of both α and β are relatively low, indicating small variations in density with small changes in pressure and/or temperature (Fig. 1B). However, in the critical region, both α and β attain large positive values because a small change in pressure or temperature results in a large change in density. The values of β and α reach infinity at the critical point of H_2O.

The specific isobaric heat capacity is an example of a fluid property related to the ability of a hydrothermal fluid to transport energy, as shown in Equation (3), and is defined as:

$$c_f \equiv \left(\frac{\partial h}{\partial T}\right)_P \quad (9)$$

As with isothermal compressibility (Eq. (7)) and isobaric expansivity (Eq. (8)) described above, the magnitude of the isobaric heat capacity of the fluid (c_f – $J \cdot kg^{-1} \cdot K^{-1}$) is relatively low over most of *PT* space, indicating small variation of specific enthalpy with small changes in temperature or pressure. However, the isobaric heat capacity of H_2O becomes infinite at the critical point and thus small changes in *T* result in large changes in specific enthalpy in the vicinity of the critical point (Fig. 1C).

Other properties of H_2O, including the isochoric heat capacity, Q and Y Born functions and thermal conductivity become infinite at the critical point, whereas apparent molal Helmholtz free energy, internal energy, enthalpy and entropy, the dielectric constant, the X Born function, dynamic and kinematic viscosity, thermal diffusivity, Prandtl number, the isochoric expansivity-compressibility coefficient and sound velocity all show large variation with small changes in pressure and/or temperature in the vicinity of the critical point (Johnson and Norton, 1991). In the following discussion, we consider the magnitude of isothermal compressibility (β), isobaric thermal expansion (α), and specific isobaric heat capacity (c_f) in the critical region. The magnitude of these three parameters is, in turn, a direct measure of the sensitivity of density to changing pressure (β) or temperature (α), or the sensitivity of enthalpy to pressure (c_f) because these properties are defined as temperature (α, c_f) or pressure (β) derivatives.

While the H_2O system provides a reasonable approximation of the composition of some low-salinity aqueous hydrothermal fluids, the single-component nature of the pure H_2O system results in a phase topology that differs significantly from that of natural, multi-component fluids. Specifically, in the one-component system H_2O, two fluid phases (liquid and vapor) only coexist along a line in *PT* space. Moreover, the liquid-vapor coexistence curve for H_2O terminates at the critical point (C.P.; Fig. 1A), beyond which only a single-phase fluid may exist. These topologic features of the H_2O system significantly restrict the *PT* region (and portion of the Earth's crust) where boiling or fluid immiscibility may occur. However, natural hydrothermal fluids contain variable amounts of salts and gases (Bodnar et al., 2014; Holloway, 1984; Roedder, 1972; Yardley and Bodnar, 2014). Recognizing this, Bodnar and Costain (1991) hypothesized that the *PT* region in which hydrothermal fluids might exhibit anomalous thermodynamic and transport properties should migrate in *PT* space as salts and/or gases are added to H_2O (Fig. 2). Similarly, in discussing the applicability of their results for pure H_2O to more complex natural compositions, Johnson and Norton (1991) state "*Hence, the critical region for this particular H_2O-NaCl solution will occur at correspondingly higher P-T conditions than those for pure H_2O, but the anomalous divergent behavior of solvent (and solute) properties and their effect on transport and chemical processes will, of course, persist.*" These workers did not indicate or recognize, however, that the anomalous behavior is expected to quickly reduce in magnitude as salt is added to the system.

While there are significant differences in phase topology and the meaning of the "critical point" when comparing one versus multi-component systems, it is generally thought that a region of anomalous behavior, as described for pure H_2O by Johnson and Norton (1991), also exists for multi-component fluids. We note that the critical point in the pure H_2O system represents a critical end point that occurs at the termination of the liquid-vapor coexistence curve, whereas a critical point in the H_2O-NaCl system is defined as the *PT* point along the isopleth that separates the one-phase region from the two-phase region where the bubble point curve (liquid + vapor ↔ liquid) and the dew point curve (liquid + vapor ↔ vapor) meet. As such, in the H_2O-NaCl system the critical point represents the unique condition at which *liquid = vapor*. Both Bodnar

and Costain (1991) and Johnson and Norton (1991) speculated that the region in which fluid properties would be most sensitive to changes in temperature or pressure would migrate in *PT* space as the fluid composition changed, but at that time the hypothesis could not be adequately tested owing to a lack of experimental and theoretical data for even the relatively simple two-component system H_2O-NaCl. In recent years algorithms have been developed to estimate the physical, thermodynamic and transport properties of more complex fluids, especially for the system H_2O-NaCl, at high temperatures and pressures. Thus, the numerical models of Anderko and Pitzer (1993), Palliser and McKibbin (1998a, b, c) , Lewis (2007), Driesner and Heinrich (2007) and Driesner (2007) allow estimation of the thermodynamic properties of the system H_2O-NaCl over a wide range of pressure-temperature-composition (*PT*X) conditions likely to be encountered in upper to mid-crustal hydrothermal systems. Here, we examine the properties of H_2O-NaCl fluids in the critical region and identify the *PT* conditions at which the mass and energy transport properties of the hydrothermal fluid are most sensitive to small changes in either temperature or pressure. The sensitivity is evidenced by large changes in either density or specific enthalpy with small variations in *P* or *T* as reflected by the magnitudes of the thermodynamic variables α, β, or c_f.

2. Model Description

We have employed the model of Driesner (2007) to estimate density, enthalpy and isobaric heat capacity of H_2O-NaCl fluids at *PT* conditions in the vicinity of the critical points for given fluid compositions (salinities). Calculations of the fluid properties are made at *PT* conditions outside of the two-phase envelope defined by the bubble-point – dew-point curve, i.e., in the H_2O-NaCl single-phase field, with positions of the phase boundaries predicted by the Driesner and Heinrich (2007) EOS. We note that Driesner (2007) used the International Association for the Properties of Steam IAPS-84 (Haar et al., 1984) formulation to estimate the properties of pure H_2O in the H_2O-NaCl model, whereas in the present study we use IAPWS-95 (Wagner and Pruß, 2002) to estimate properties for pure H_2O. The differences between the two formulations are insignificant for the purposes of this study. Thus, re-parametrization of Equation (5b) of Driesner and Heinrich (2007) to predict accurate densities close to the critical point of pure H_2O, as recommended by Driesner (2007) was not incorporated owing to the insignificant difference between the critical point *PT* position predicted by IAPS-84 (373.974 °C, 220.54915 bars) and that from IAPWS-95 (373.946 °C, 220.64 bars). Densities of the fluid in the critical region near the critical point are essentially independent of which model is used to calculate the properties of pure H_2O.

For the one-component H_2O system, the critical region envelops the critical isochore and occurs at pressures above and below the critical isochore. However, because the two-phase region in the H_2O-NaCl system extends to temperatures (and pressures) higher than the critical temperature (and pressure), the region of interest in this study is truncated by the isoplethal bubble-point – dew-point curve.

In order to examine effects of salinity on the thermodynamic and transport properties of hydrothermal fluids, values for pressure- and temperature-dependent fluid properties were calculated for various salinities in the H_2O-NaCl system. To illustrate the sensitivity of fluid density to changing pressure or temperature, the coefficients of isothermal compressibility (β; Eq. (7)) and isobaric expansion (α; Eq. (8)) were evaluated. To illustrate the effect of changing

temperature on energy (heat) transport, isobaric heat capacity (c_f), which describes the change in specific enthalpy with changing temperature at constant pressure Eq. (9), was examined.

Akinfiev and Diamond (2009) presented a model for quartz solubility in H_2O-NaCl-CO_2 fluids that includes a density-dependent solubility term. As such, the variation in solubility of quartz in H_2O-NaCl-CO_2 fluids over some *PT* range is related to the rate of change of fluid density over that same *PT* range. The temperature and pressure dependence of density is, in turn, a function of the salinity of the fluid, as shown below. Therefore, the *PT* region in which quartz dissolution/precipitation is most sensitive to changes in temperature and/or pressure can be evaluated by combining the results from this study with the quartz solubility model developed by Akinfiev and Diamond (2009).

To calculate the dynamic viscosity of the fluid, η, the IAPWS formulation 2008 for the viscosity for pure H_2O (Huber et al., 2009) was chosen along with the viscosity model of Klyukin et al. (2017) for H_2O-NaCl fluids. The commonly-used viscosity model of Palliser and McKibbin (1998c) predicts viscosities for salt solutions at temperatures higher than approximately 400 °C that are essentially independent of temperature and pressure, and show unexpected and abrupt changes in slope in *PT*X space and, therefore, was not used here.

The various EOS described above were coded in a VBA macro for MS Excel 2010. This macro requires as input the pressure, temperature and salinity of the fluid (*PTX*) or the density, temperature and salinity of the fluid (ρTX) to calculate density (ρ), pressure (P), specific enthalpy (h), isobaric specific heat capacity (c_f), quartz solubility (m_{SiO2}) and dynamic viscosity (η) at *PTX* conditions in the range from 0 to 5 kbar, 0 to 1000 °C.

3. Effect of Salinity on the Location of the *PT* Region of Anomalous Fluid Behavior

As NaCl is added to H_2O, the critical point migrates to higher temperatures and pressures (Bodnar and Costain, 1991; Sourirajan and Kennedy, 1962). For example, the critical point of a 5 wt. % NaCl fluid is at 422 °C and 337 bars, whereas the critical point for a 25 wt. % NaCl composition is 662 °C and 1123 bars (Driesner and Heinrich, 2007). In addition to migration of the critical point to higher temperatures and pressures, adding NaCl to H_2O also changes the topology of the critical region. Unlike for pure H_2O, the critical region for a given composition in the H_2O-NaCl system is asymmetrical in the sense that the critical region in the one-phase field is truncated at high T and low P by the bubble-point – dew-point curve isopleth that separates the one-phase region from the two-phase (liquid + vapor) region (Fig. 2, 3B).

In the pure H_2O system the isochores in the liquid field originate on the liquid-vapor coexistence curve, and the liquid density decreases with increasing temperature up to the critical point for pure H_2O. Then, as the density continues to decrease to values less than the critical density (322 kg·m^{-3}), the isochores originate along the liquid-vapor curve at progressively lower temperature (Fig. 3A), reaching 4.76 ×10^{-3} kg·m^{-3} at the triple point of H_2O (0.01 °C, 0.006 bars). Thus, two isochores originate at any *PT* point on the pure H_2O liquid + vapor coexistence curve, with the steeper isochore corresponding to the liquid phase extending into the liquid field with increasing temperature, and the less steep isochore corresponding to the vapor extending into the vapor field (Fig. 3A).

For a given composition in the H_2O-NaCl system, the bubble-point curve extends from the triple point where liquid and vapor are in equilibrium with H_2O-ice (or hydrohalite or halite for

higher salinities) to the critical point, and the dew-point curve extends from the critical point to the triple point where liquid and vapor are in equilibrium with halite. Isochores for that composition originate along the bubble-point – dew-point curve isopleth that separates the one-phase region from the two-phase (liquid + vapor) region (Fig. 3B). The density of the fluid decreases continuously along the bubble-point – dew-point curve isopleth in going from one triple point at low temperatures to the other triple point at high temperatures. For example, the density of a 5 wt. % NaCl liquid decreases from ~1050 $kg \cdot m^{-3}$ at low temperature to 486 $kg \cdot m^{-3}$ at the critical point (C.P in Fig. 3B). The density of the vapor phase decreases from the critical density (486 $kg \cdot m^{-3}$) to lower values with increasing temperature along the dew-point curve to its intersection with the liquid + vapor + halite (L+V+H) equilibrium curve (Fig. 3B). We note that details concerning the topology of the dew-point curve are poorly constrained at temperatures above about 700 °C and essentially unknown above 1000 °C. However, the principles of phase equilibria indicate that the temperature along the dew-point curve must eventually decrease such that the dew-point curve terminates on the liquid + vapor + halite coexistence curve (L+V+H) which, in turn, terminates at the triple point of NaCl (~801 °C; Fig. 3B).

A critical point in the H_2O-NaCl system represents the temperature and pressure along an isoplethal bubble-point – dew-point curve at which liquid equals vapor and the density equals the critical density – the critical isochore originates from this temperature and pressure and extends into the one-phase field. Commonly, the critical isochore is, for a given composition, considered as the arbitrary boundary in *PT* space (no phase boundary occurs) separating liquid (densities greater than the critical density) from vapor (densities less than the critical density). In terms of fluid inclusions (or any constant volume system), the critical isochore (ρ_{crit} in Fig. 3B) thus separates the *PT* trapping region in which fluid inclusions trapped in the one-phase field will homogenize to the liquid phase (by dissolution of vapor into liquid; *PT* conditions to the high pressure, low temperature side of the critical isochore), from the *PT* trapping conditions that will result in fluid inclusions that homogenize to the vapor phase (by dissolution of liquid into vapor; *PT* conditions to the low pressure, high temperature side of the critical isochore).

4. Effect of Salinity on Mass Transport Properties

The effect of fluid composition on mass transfer in hydrothermal systems may be illustrated by examining the effect of temperature and pressure on fluid density, because mass transport capacity of the fluid is a function of the fluid density. As such, we have calculated the coefficient of isothermal compressibility, β, (Eq. (7)) and the coefficient of isobaric thermal expansion, α, (Eq. (8)) for various salinities. For pure H_2O, the largest variations in density as a function of temperature or pressure (i.e., maximum values of α and β, occur in the vicinity of the critical point (Fig. 4), and α and β approach infinity at the critical point. These properties also show local maxima for H_2O-NaCl fluids. However, the maximum values of α and β decrease significantly with increasing salinity, indicating that fluid density becomes less sensitive to changing temperature or pressure as salinity increases (as predicted by fluid phase theory; e.g., Levelt Sengers (2000)). Figure 5 shows the variation in maximum values of α and β as a function of salinity, and was constructed by determining the maximum value for these parameters at various salinities. Thus, both α and β decrease by about two orders of magnitude as the salinity increases from ~0.1 to ≈5 wt. % NaCl (Fig. 5). Additionally, as salinity increases and the critical point migrates to higher temperatures and pressures, the *PT* region in which α and β reach their

maximum values also migrates to higher temperature and pressure (Figs. 6 and 7). However, unlike pure H_2O in which the coefficients of isothermal compressibility (β) and isobaric expansion (α) both show maxima precisely at the critical point, these maxima are not co-located for H_2O-NaCl solutions and neither maximum occurs precisely at the critical point for the given salinity. The reason(s) for the lack of agreement between *PT* positions for the maxima of isothermal compressibility (β) and isobaric expansion (α) and the critical point for the given composition are unknown. The disagreement could be an artifact of the EOS of Driesner (2007) or could reflect the asymmetry in density distribution in the vicinity of the critical point and critical isochore owing to the truncation of the low-density region by the dew-point curve (Fig. 3B).

With increasing salinity, the migration of the critical point to higher temperatures and pressure "outpaces" the migration of the *PT* region of maximum values of α and β (i.e., the region where the temperature and pressure derivatives of density are greatest) such that above about 5-10 wt% NaCl, the critical temperature and pressure both exceed the temperature and pressure at which the maxima of α and β occur (Figs. 6 and 7).

The coefficients of isothermal compressibility (β) and isobaric expansion (α) have maximum values that are located along and just above the two-phase (L+V) boundary. In order to identify the region in which the density of H_2O-NaCl fluids is most sensitive to changing temperature and pressure (i.e., shows anomalous behavior), α and β were calculated for various salinities (from 0 to 30 wt. % NaCl) along the phase boundary. The temperature and pressure at which maximum values for α and β are reached as a function of salinity are shown in Figure 8. Also shown in Figure 8 is the *PT* region in which the value $\tilde{\chi}$ is ≥ 0.5 at that salinity, and the critical points for that salinity. At low salinities, the temperature and pressure at which the maximum values of α and β occur for a given salinity are close to the critical temperature and pressure for that composition (i.e., lines representing the critical curve and the loci of maximum values for the coefficients are close together), but the temperature and pressure corresponding to the maxima diverge from the critical temperature and pressure at higher salinities (Fig. 8). The reasons for this divergence are not clear.

The *PT* region in which α and β show anomalous behavior ($\tilde{\chi} \geq 0.5$) expands with increasing salinity. This behavior likely reflects the fact that the reduced susceptibility $\tilde{\chi}$ (Eq. (6)) is related to the critical pressure, P_{crit}, and this value increases with increasing salinity (Fig. 8B) while the ratio of ρ^2/ρ^2_{crit} for fluids with density higher than the critical density is greater than unity. Thus, the *PT* region in which mass transport properties show anomalous behavior (i.e., large variation in density with small changes in the temperature or pressure) expands as the fluid salinity increases.

Although the region of *PT* space in which the reduced susceptibility $\tilde{\chi}$ is ≥ 0.5 expands with increasing salinity, the absolute values of α and β decrease with increasing salinity. Thus, the same change in temperature or pressure in the critical region for a high salinity fluid will have a smaller effect on the density than for a lower salinity fluid.

4.1 Quartz transport and deposition

The formation of hydrothermal ore deposits requires the dissolution, transport and eventual precipitation of ore and gangue minerals. While many hydrothermal fluids are able to transport sufficient amounts of ore-forming components to generate mineralization, formation of large, high-grade deposits requires a significant decrease in solubility over a relatively small distance

(or over a relatively small change in temperature and/or pressure) such that most of the ore metals are precipitated in a small volume of host rock. Simple temperature decrease may be insufficient to cause mineralization in some hydrothermal settings as the change in solubility with temperature for many ore minerals in many environments is small and, as a result, the ore minerals are distributed in a larger volume of rock to produce lower grades. Thus, formation of economic mineral deposits requires an effective depositional mechanism, one that results in deposition of all (or most) of the ore components over a small range of temperature and/or pressure, hence in a small volume. Thus, processes such as boiling (Drummond and Ohmoto, 1985; Stefánsson and Seward, 2003; 2004) or mixing (Bons et al., 2014; Drummond, 1981; Lester et al., 2012) are commonly invoked as depositional mechanisms owing to the large decrease in solubility that is commonly associated with these processes.

Temperature and/or pressure fluctuations can be effective depositional mechanisms for ore formation in hydrothermal settings if the temperature and/or pressure derivative of solubility is large. As an example of how salinity affects mass transport and deposition in hydrothermal systems, we consider the effect of salinity on quartz solubility (i.e., dissolved silica transport and deposition). Quartz is among the most common minerals precipitated from hydrothermal fluids, and much of our understanding of fluid compositions and temperatures in hydrothermal systems comes from studies of fluid inclusions contained in quartz. The model of Akinfiev and Diamond (2009) has been used here to demonstrate the effect of fluid composition on the solubility of SiO_2 in the H_2O-NaCl-CO_2 system, based on the following relationship:

$$\log m_{SiO_2} = A(T) + B(T) \log \frac{18.0152}{V^*_{H_2O}} + 2X_{H_2O} \qquad (10)$$

where *A(T)* and *B(T)* are polynomial functions of temperature from Manning (1994) describing quartz solubility in pure H_2O, and X_{H2O} and V^*_{H2O} are the mole fraction of H_2O and effective partial molar volume (Akinfiev and Diamond, 2009), of H_2O in the fluid, respectively. The value V^*_{H2O} is calculated from the relation $V_{mix} = X_{H2O}V^*_{H2O} + (1\text{-}X_{H2O})V_s$, where V_{mix} is the molar volume of the H_2O-NaCl fluid and V_s is the intrinsic volume of NaCl. According to Akinfiev and Diamond (2009) the intrinsic volume is an empircally-determined volume that "*may represent the sum of volumes of all NaCl species in solution.*" Thus, for a given fluid composition, quartz solubility is a function of fluid temperature and molar volume (density), and changes in quartz solubility are related to changes in fluid density. Changes in quartz solubility can therefore be described in a manner similar to that for α and β above.

To estimate relative changes in quartz solubility with changing temperature and pressure, temperature (δm^T_{SiO2}) and pressure (δm^P_{SiO2}) coefficients of quartz solubility in H_2O-NaCl fluid were determined. The equations describing the temperature and pressure coefficients of quartz solubility follow the same form as the equations for the coefficient of isothermal compressibility (β) that describes the pressure dependence of fluid density at constant temperature and has units of bar^{-1} (Eq. (7)), and the coefficient of isobaric expansion (α) that describes the temperature dependence of fluid density at constant pressure and has units of K^{-1} (Eq. (8)). The pressure coefficient (δm^P_{SiO2}) of quartz solubility is defined as the partial derivative of quartz solubility (in molal concentration, mol per kg of H_2O) with respect to pressure at constant temperature, multiplied by the inverse of quartz solubility at that *PT* condition and fluid salinity (bar^{-1}):

$$\delta m^P_{SiO_2} \equiv \frac{1}{m_{SiO_2}} \left(\frac{\partial m_{SiO_2}}{\partial P} \right)_T \qquad (11)$$

In a similar way, the temperature coefficient of quartz solubility (K^{-1}) is calculated according to:

$$\delta m^{T}_{SiO_2} \equiv -\frac{1}{m_{SiO_2}}\left(\frac{\partial m_{SiO_2}}{\partial T}\right)_P \quad (12)$$

The solubility of quartz is a function of density, and thus the relative change in quartz solubility with temperature and pressure is proportional to the relative change in fluid density over the same *PT* interval.

The temperature (δm^{T}_{SiO2}) and pressure (δm^{P}_{SiO2}) coefficients of quartz solubility were calculated for salinities ranging from 3.5 to 30 wt. % NaCl and are shown in Figures 9 and 10. At low salinity, quartz solubility shows the greatest dependence on temperature or pressure in the critical region and in the *PT* area located between the critical isochore and the bubble-point – dew-point curve. With increasing salinity, the temperature and pressure derivatives of quartz solubility decrease and the regions of maximum δm^{T}_{SiO2} and δm^{P}_{SiO2} move to higher temperatures and pressures. Stated differently, as the salinity increases, the *PT* region in which the solubility of quartz is most sensitive to changing temperature and/or pressure migrates to higher temperature and pressure. Note that at salinities of 3.5 and 10 wt. % NaCl the pressure (δm^{P}_{SiO2}) coefficient of quartz solubility shows a change from negative to positive values (Fig. 10A, B), corresponding to the change in solubility of quartz from prograde to retrograde in this *PTX* region (Akinfiev and Diamond, 2009).

4.2 Energy transport properties

The circulation of hydrothermal fluids plays an important role in energy (heat) transport in the Earth's crust (Bredehoeft and Norton, 1990). Advective heat transfer in hydrothermal systems associated with epizonal plutons results in cooling of the pluton and distribution of the thermal energy into the environment surrounding the heat source (Cathles, 1981; Norton and Knight, 1977). As shown by Equation (3), heat transfer by hydrothermal fluids is a function of the isobaric specific heat capacity of the fluid (c_f). The isobaric specific heat capacity approaches infinity at the critical point of H_2O (Fig. 1C), similar to the coefficient of isothermal compressibility (β) shown in Figure 1B. At temperatures and pressures greater than the critical point, isobaric heat capacity shows maximum values along and adjacent to the critical isochore for H_2O. As NaCl is added to H_2O, the *PT* region in which isobaric heat capacity reaches its maximum becomes asymmetrical and stretched along and above the phase boundary (Fig. 11), similar to the behavior of the coefficients of thermal expansion (α) and compressibility (β) shown in Figures 6 and 7, respectively. As the salinity increases, the magnitude of the near-critical isobaric specific heat capacity anomaly for a given salinity decreases. Stated differently, as the salinity increases, the magnitude of the temperature derivative of enthalpy of the fluid (heat capacity) in the critical region decreases, and the ability of the fluid to transport thermal energy is less sensitive to temperature change. We also note that at a given *PT* condition the enthalpy of the fluid decreases with increasing salinity (Driesner, 2007).

5. Effect of Salinity on Energy Transport in Submarine Hydrothermal Systems

Black smokers associated with submarine hydrothermal systems are characterized by fluids with salinity between 0.1 to ~8 wt. %. NaCl, and temperatures are typically in the range of 350±30 °C, and rarely exceeding 400 °C (e.g., Fontaine et al., 2007; Von Damm, 1995). The

water depth of most vent sites ranges from 1500 to 3500 m, sometimes reaching 5000 m, corresponding to hydrostatic pressures of ~150 to ~500 bars (Baker and German, 2004).

Submarine hydrothermal systems provide a good example of how fluid salinity might affect the ability of fluids to transport thermal energy. Lister (1995) introduced the term "fluxibility" ($J \cdot s \cdot m^{-5}$) to quantify the heat transport capacity of a buoyancy-driven fluid convecting in a hydrostatic pressure gradient $\vec{g}\rho_0$ (analogous to a submarine hydrothermal system) according to:

$$F = \frac{h^v(\rho_0 - \rho)}{\eta} \quad (13)$$

where, ρ refers to the density of a fluid of some salinity at the temperature and pressure of interest below the seafloor, and ρ_0 is the density of a 3.5 wt. % NaCl fluid at 4 °C and 2.5 km hydrostatic depth (~250 bar). Thus, fluxibility describes the amount of thermal energy transferred across a square meter interface of rock by one cubic meter of fluid per second. The term h^v is the volumetric enthalpy defined as:

$$h^v = \rho(h - h_0) \quad (14)$$

where h is the specific enthalpy of a fluid at the temperature, pressure and salinity of interest in the sub seafloor, and h_0 refers to the specific enthalpy of a 3.5 wt. % NaCl fluid at 4 °C and 2.5 km hydrostatic depth (~250 bar).

Jupp and Schultz (2000, 2004) adopted the approach presented by Lister (1995) to investigate balances of mass and energy transport in a convecting submarine hydrothermal system using the relationships described by Equation (13). Since fluxibility depends on fluid density, enthalpy, and dynamic viscosity, fluxibility will vary as the density, enthalpy and dynamic viscosity vary in response to changing temperature and pressure.

Jupp and Schultz (2004) report that fluxibility for pure H_2O is maximized at 400-500 °C, and pressure between 200-600 bars, conditions where the density of H_2O is close to or lower than the critical density of pure H_2O (Fig. 13A). These conditions approximately correspond to the critical region of pure H_2O in which the reduced susceptibility $\tilde{\chi}$ is ≥ 0.5 (Fig. 1A).

To evaluate the potential effect of salinity on energy transport in submarine hydrothermal systems, we have calculated fluxibility as a function of salinity using Equation (13), as did Jupp and Schultz (2004), but here we replace the density and enthalpy of pure H_2O with appropriate values for H_2O-NaCl. The specific enthalpy of the fluid was calculated using the EOS of Driesner (2007). Volumetric enthalpy and fluxibility for H_2O-NaCl fluids having salinities from 0 to 10 wt. % NaCl are shown in Figures 12 and 13, respectively. An upper limit of 10 wt. % NaCl was selected because submarine hydrothermal vent fluid rarely exceeds this salinity. With increasing salinity, the volumetric enthalpy (h^v; Eq. (14)) increases and the *PT* conditions of the maximum volumetric enthalpy migrate to higher temperatures (Fig. 12). For a constant salinity and pressure, the specific enthalpy (h) increases with increasing temperature, while the density (ρ) decreases with increasing temperature. Starting at lower temperatures, the relative increase in specific enthalpy is larger than the relative decrease in density, resulting in a net increase in volumetric enthalpy (h^v) with increasing temperature. Eventually, the contribution from density outweighs that from specific enthalpy, and the volumetric enthalpy decreases as the temperature increases further (Fig. 12). At pressures close to average seafloor conditions (260 bars), the volumetric enthalpy reaches maximum values at 350 to ~390 °C, depending on the salinity. At higher pressures the maximum volumetric enthalpy migrates to temperature of 400 to ~450 °C, depending on the salinity.

The difference between the fluxibility of an H_2O-NaCl fluid and that of pure H_2O at the same temperature and pressure is given by Equation (15):

$$Deviation = \frac{F_{P,T}^{H_2O-NaCl} - F_{P,T}^{H_2O}}{F_{P,T}^{H_2O}} \times 100 \quad (15)$$

The deviation in the fluxibility is defined as the percent difference in fluxibility of the H_2O-NaCl fluid relative to that of pure H_2O at the same temperature and pressure. Note that all deviations are negative (Fig. 14), indicating that saline fluid is less buoyant than pure water and thus has a lower fluxibility. The minimum deviation in fluxibility compared to pure H_2O (i.e., where the fluxibility of the salt solution is closest to that of pure H_2O) increases with increasing salinity, from roughly -5% difference for a salinity of 1 wt. % NaCl, to -17% difference for a salinity of 3.5 wt. % NaCl, up to -40 -45% difference for a salinity of 10 wt. % NaCl (Fig. 14). The minimum difference in fluxibility occurs at ~350 ° and the difference increases with increasing salinity.

In submarine hydrothermal systems, the fluid that circulates through hot seafloor is seawater, and this composition is reasonably well approximated by an H_2O-NaCl fluid with a salinity of 3.5 wt. % NaCl. Such a fluid may undergo phase separation close to the heat source where the PT conditions are in the two-fluid phase field for an H_2O-NaCl fluid with a salinity of 3.5 wt. % to produce a low-salinity, low-density fluid (vapor) and high-salinity, high-density fluid (liquid, or brine). The high density brine phase mostly remains at depth, while the lower salinity vapor migrates upwards towards the seafloor, perhaps continuing to exsolve small amounts of high salinity brine along the way and mixing with colder inflowing seawater (Han et al., 2013; Singh et al., 2013). Thus, in our calculations above, the low salinity fluids are the equivalent of the vapor phase generated at depth, and these fluids carry more heat energy and therefore result in high fluxibility.

6. Summary

The region of anomalous thermodynamic and physical properties in the H_2O-NaCl system (defined by large changes in the magnitude of pressure or temperature-derivative properties with small changes in temperature or pressure) migrates to higher temperature and pressure as the salinity of the fluid increases. However, unlike the pure H_2O system, the maxima in derivative properties for H_2O-NaCl do not occur at the critical temperature and pressure for a given composition, and also unlike the pure H_2O system, maxima for all thermodynamic properties for a given composition do not occur at the same temperature and pressure. Finally, the magnitude of the maxima for derivative properties and the gradient in *PT* space both decrease significantly with increasing salinity, such that variations in temperature or pressure for higher salinity hydrothermal fluids will have less of an effect on the energy and mass transport properties of the fluid, compared to lower salinity fluids. These results suggest that temperature and pressure are most likely to influence energy and mass transport in hydrothermal systems with low salinity fluids (less than about 10 wt. % NaCl) operating at ~375-450 °C and ~250-500 bars. These conditions are observed in submarine hydrothermal environments and during the mineralization stage in porphyry copper systems.

7. Acknowledgements

The authors thank Ksenia Klyukina for advice concerning coding of the numerical model, Adam Angel for assistance with graphics, Shreya Singh for discussions concerning fluid

viscosity and for providing code to calculate viscosity for the Palliser and McKibbin model. We also thank reviewers Axel Liebscher and David Dolejs for providing many suggestions and comments that have led to a significantly improved manuscript. This material is based on work supported in part by the National Science Foundation under Grant No. EAR-1019770 to RJB.

8. References

Akinfiev, N.N. and Diamond, L.W. (2009) A simple predictive model of quartz solubility in water-salt-CO_2 systems at temperatures up to 1000 °C and pressures up to 1000MPa. Geochim. Cosmochim. Acta 73, 1597-1608.

Anderko, A. and Pitzer, K.S. (1993) Equation-of-state representation of phase-equilibria and volumetric properties of the system NaCl-H_2O above 573 K. Geochim. Cosmochim. Acta 57, 1657-1680.

Anisimov, M.A., Sengers, J.V. and Levelt Sengers, J.M.H. (2004) Near-critical behavior of aqueous systems, in: Palmer, D.A., Fernandez-Prini R., Harvey Allan H. (Eds.), Aqueous Systems at Elevated Temperatures and Pressures: Physical Chemistry in Water, Steam and Hydrothermal Solutions. Elsevier Ltd, Amsterdam, pp. 29-72.

Baker, E.T. and German, C.R. (2004) On the global distribution of hydrothermal vent fields, in: German C. R., Lin J., M., P.L. (Eds.), Mid-ocean ridges, pp. 245-266.

Bodnar, R., Lecumberi-Sanchez, P., Moncada, D. and Steele-MacInnis, M. (2014) Fluid inclusions in hydrothermal ore deposits, in: Scott S. D. (Ed.), Treatise on Geochemistry, 2nd ed. Elsevier Ltd., Amsterdam, pp. 119-142.

Bodnar, R.J. and Costain, J.K. (1991) Effect of varying fluid composition on mass and energy - transport in the Earth's crust. Geophys. Res. Lett. 18, 983-986.

Bons, P.D., Fusswinkel, T., Gomez-Rivas, E., Markl, G., Wagner, T. and Walter, B. (2014) Fluid mixing from below in unconformity-related hydrothermal ore deposits. Geology 42, 1035-1038.

Bredehoeft, J.D. and Norton, D.L. (1990) Mass and Energy Transport in a Deforming Earth's Crust, in: Council, N.R. (Ed.), The Role of Fluids in Crustal Processes. The National Academies Press, Washington, DC, pp. 27-42.

Cathles, L.M. (1981) Fluid flow and genesis of hydrothermal ore deposits, in: Skinner, B.J. (Ed.), Economic Geology 75th Anniversary Volume. The Economic Geology publishing company, Lancaster, pp. 424-457.

Cathles, L.M. and Smith, A.T. (1983) Thermal constraints on the formation of Mississippi Valley-Type lead-zinc deposits and their implications for episodic basin dewatering and deposit genesis. Econ. Geol. 78, 983-1002.

Delaney, P.T. (1982) Rapid intrusion of magma into wet rock: Groundwater flow due to pore pressure increases. Journal of Geophysical Research: Solid Earth 87, 7739-7756.

Driesner, T. (2007) The system H_2O-NaCl. II. Correlations for molar volume, enthalpy, and isobaric heat capacity from 0 to 1000 °C, 1 to 5000 bar, and 0 to 1 X-NaCl. Geochim. Cosmochim. Acta 71, 4902-4919.

Driesner, T. and Heinrich, C.A. (2007) The system H_2O-NaCl. I. Correlation formulae for phase relations in temperature-pressure-composition space from 0 to 1000 °C, 0 to 5000 bar, and 0 to 1 XNaCl Geochim. Cosmochim. Acta 71, 4880-4901.

Drummond, S.E. (1981) Boiling and mixing of hydrothermal fluids: chemical effects on mineral precipitation. Pennsylvania State University.

Drummond, S.E. and Ohmoto, H. (1985) Chemical evolution and mineral deposition in boiling hydrothermal systems. Econ. Geol. 80, 126-147.

Fehn, U. and Cathles, L.M. (1979) Hydrothermal convection at slow-spreading mid-ocean ridges. Tectonophysics 55, 239-260.

Fehn, U., Green, K.E., Von Herzen, R.P. and Cathles, L.M. (1983) Numerical models for the hydrothermal field at the Galapagos Spreading Center. Journal of Geophysical Research: Solid Earth 88, 1033-1048.
Fontaine, F.J., Wilcock, W.S.D. and Butterfield, D.A. (2007) Physical controls on the salinity of mid-ocean ridge hydrothermal vent fluids. Earth Planet. Sci. Lett. 257, 132-145.
Garven, G. (1985) The role of regional fluid flow in the genesis of the Pine Point Deposit, Western Canada sedimentary basin. Econ. Geol. 80, 307-324.
Haar, L., Gallagher, J.S. and Kell, G.S. (1984) NBS/NRC steam tables: Thermodynamic and transport properties and computer programs for vapor and liquid states of water in SI units. Hemisphere, Washington DC.
Han, L., Lowell, R.P. and Lewis, K.C. (2013) The dynamics of two-phase hydrothermal systems at a seafloor pressure of 25 MPa. Journal of Geophysical Research: Solid Earth 118, 2635-2647.
Holloway, J.R. (1984) Graphite-CH_4-H_2O-CO_2 equilibria at low-grade metamorphic conditions. Geology 12, 455-458.
Huber, M., Perkins, R., Laesecke, A., Friend, D., Sengers, J., Assael, M., Metaxa, I., Vogel, E., Mareš, R. and Miyagawa, K. (2009) New international formulation for the viscosity of H_2O. Journal of Physical and Chemical Reference Data 38, 101-125.
Johnson, J.W. and Norton, D. (1991) Critical phenomena in hydrothermal systems - state, thermodynamic, electrostatic, and transport-properties of H_2O in the critical region. Am. J. Sci. 291, 541-648.
Jupp, T.E. and Schultz, A. (2004) Physical balances in subseafloor hydrothermal convection cells. Journal of Geophysical Research: Solid Earth 109, B05101.
Klyukin, Y.I., Lowell, R.P. and Bodnar, R.J. (2017) A revised empirical model to calculate the dynamic viscosity of H_2O-NaCl fluids at elevated temperatures and pressures (≤1000 °C, ≤500 MPa, 0–100 wt % NaCl). Fluid Phase Equilibria 433, 193-205.
Lester, D.R., Ord, A. and Hobbs, B.E. (2012) The mechanics of hydrothermal systems: II. Fluid mixing and chemical reactions. Ore Geol. Rev. 49, 45-71.
Levelt Sengers, J.M.H. (2000) Supercritical Fluids: Their properties and applications, in: Kiran E., Debenedetti P.G., Peters C.J. (Eds.), Supercritical Fluids. Springer Netherlands, pp. 1-30.
Levelt Sengers, J.M.H., Kamgar-Parsi, B., Balfour, F.W. and Sengers, J.V. (1983) Thermodynamic Properties of Steam in the Critical Region. Journal of Physical and Chemical Reference Data 12, 1-28.
Lewis, K.C. (2007) Numerical modeling of two-phase flow in the sodium chloride-water system with applications to seafloor hydrothermal systems, Earth and Atmospheric Sciences. Georgia Institute of Technology.
Liebscher, A. and Heinrich, C.A. (2007) Fluid–fluid interactions, in: Liebscher, A., Heinrich, C.A. (Eds.), Rev. Mineral. Geochem., pp. 1-14.
Lister, C. (1995) Heat transfer between magmas and hydrothermal systems, or, six lemmas in search of a theorem. Geophys. J. Int. 120, 45-59.
Manning, C.E. (1994) The solubility of quartz in H_2O in the lower crust and upper mantle. Geochim. Cosmochim. Acta 58, 4831-4839.
Norton, D.L. (1979) Transport phenomena in hydrothermal systems: the redistribution of chemical components around cooling magmas. Bull. Mineral. 102, 471-486.

Norton, D.L. (1982) Fluid and heat transport phenomena typical of copper-bearing pluton environments, in: Titley, S.R. (Ed.), Advances in Geology of the Porphyry Copper Deposits, Southwestern North America. University of Arizona Press, Tucson, Arizona, pp. 59-72.
Norton, D.L. (1984) Theory of hydrothermal systems. Annual Review of Earth and Planetary Sciences 12, 155-177.
Norton, D.L. and Knight, J.E. (1977) Transport phenomena in hydrothermal systems; cooling plutons. Am. J. Sci. 277, 937-981.
Palliser, C. and McKibbin, R. (1998a) A model for deep geothermal brines, I: T-p-X state-space description. Transport in Porous Media 33, 65-80.
Palliser, C. and McKibbin, R. (1998b) A model for deep geothermal brines, II: thermodynamic properties – density. Transport in Porous Media 33, 129-154.
Palliser, C. and McKibbin, R. (1998c) A model for deep geothermal brines, III: thermodynamic properties – enthalpy and viscosity. Transport in Porous Media 33, 155-171.
Patterson, P. and Lowell, R. (1982) Numerical models of hydrothermal circulation for the intrusion zone at an ocean ridge axis, in: Fanning K.A., F.T., M. (Eds.), The Dynamic Environment of the Ocean Floor. Lexington Books, Lexington, pp. 471-492.
Roedder, E. (1972) Composition of fluid inclusions.
Singh, S., Lowell, R.P. and Lewis, K.C. (2013) Numerical modeling of phase separation at Main Endeavour Field, Juan de Fuca Ridge. Geochem. Geophys. Geosyst. 14, 4021-4034.
Sourirajan, S. and Kennedy, G.C. (1962) The system H_2O-NaCl at elevated temperatures and pressures. Am. J. Sci. 260, 115-141.
Stefánsson, A. and Seward, T. (2003) Experimental determination of the stability and stoichiometry of sulphide complexes of silver (I) in hydrothermal solutions to 400 C. Geochim. Cosmochim. Acta 67, 1395-1413.
Stefánsson, A. and Seward, T. (2004) Gold (I) complexing in aqueous sulphide solutions to 500 °C at 500 bar. Geochim. Cosmochim. Acta 68, 4121-4143.
Von Damm, K.L. (1995) Controls on the chemistry and temporal variability of seafloor hydrothermal fluids, in: Humphris, S.E., Zierenberg, R.A., Mullineaux, L.S., Thomson, R.E. (Eds.), Seafloor Hydrothermal Systems: Physical, Chemical, Biological, and Geological Interactions. American Geophysical Union, Washington DC, pp. 222-247.
Wagner, W. and Pruß, A. (2002) The IAPWS formulation 1995 for the thermodynamic properties of ordinary water substance for general and scientific use. Journal of Physical and Chemical Reference Data 31, 387-535.
Wood, J. and Hewett, T. (1982) Fluid convection and mass transfer in porous sandstones - a theoretical model. Geochim. Cosmochim. Acta 46, 1707-1713.
Yardley, B.W. and Bodnar, R.J. (2014) Fluids in the Continental Crust, Geochemical Perspectives. European Association of Geochemistry, p. 127.

9. Figures

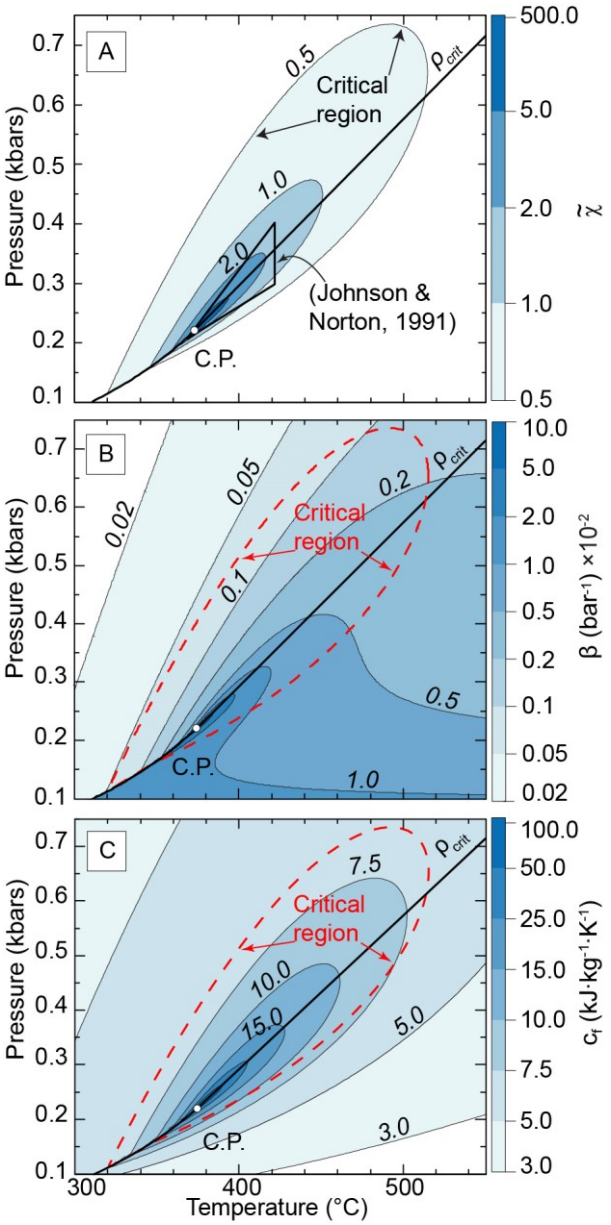

Figure 1. (A) Pressure-temperature diagram for pure H_2O, showing the critical region (shaded area) defined as the region of *PT* space in which the reduced susceptibility, $\tilde{\chi} \geq 0.5$. The wedge-shaped region represents the *PT* region examined by Johnson and Norton (1991) that extends from slightly less than the critical temperature (~374 °C) to 421.85 °C, and is bounded at lower and higher pressure by the 200 and 420 kg·m^{-3} isochores, respectively. Also shown is the *PT* projection of the critical isochore for H_2O (ρ_{crit}). (B) Coefficient of isothermal compressibility (β, bar^{-1}) ×10^{-2} for pure H_2O as a function of temperature and pressure. The critical isochore is shown by the solid black line labeled ρ_{crit} and the critical region is defined by the *PT* region enclosed by the dashed red line. (C) Isobaric specific heat capacity (c_f, kJ kg^{-1} K^{-1}) for pure H_2O as a function of temperature and pressure. The critical isochore is shown by the

solid black line labeled ρ_{crit} and the critical region is defined by the *PT* region enclosed by the dashed red line.

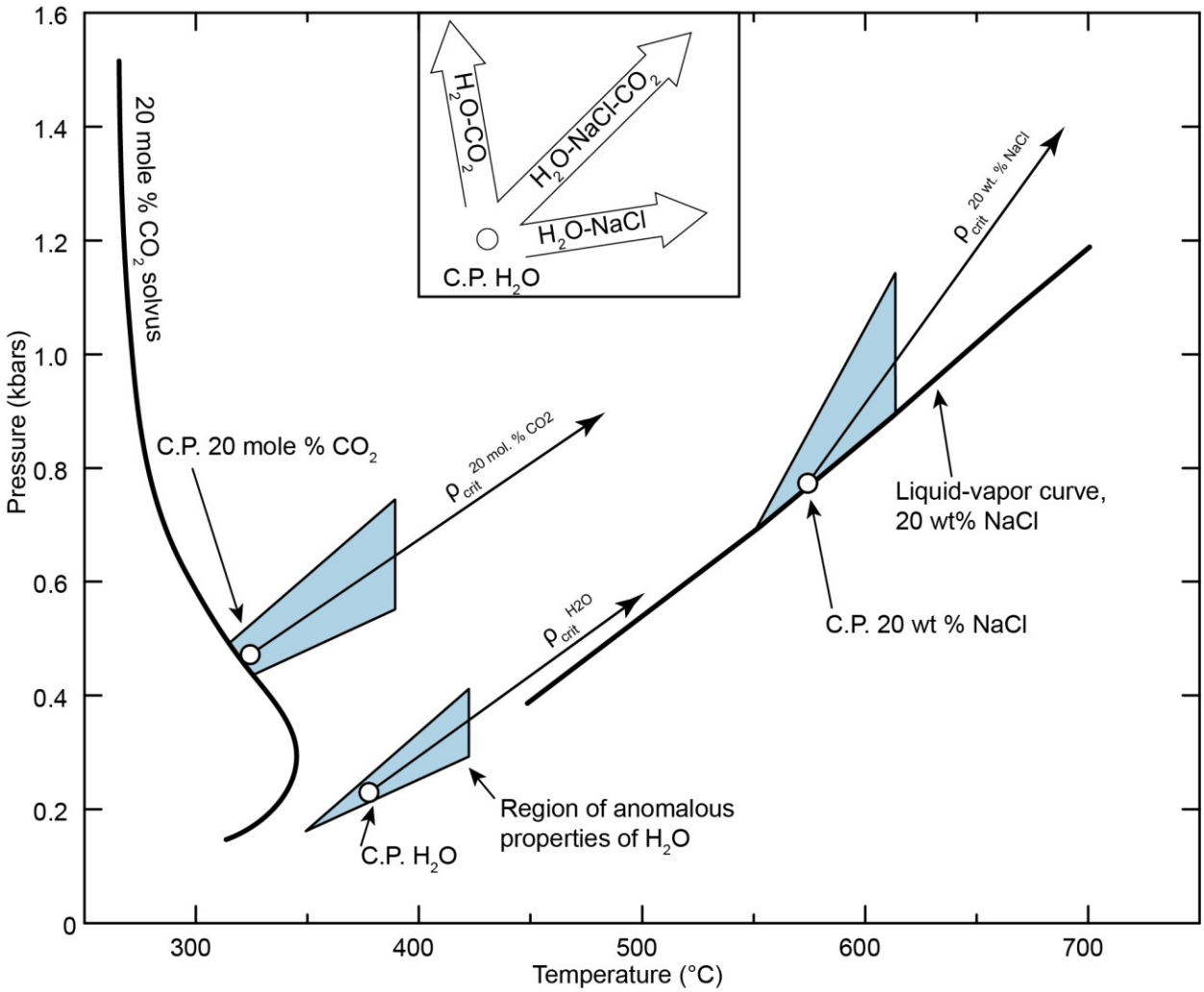

Figure 2. Pressure-temperature diagram showing the critical point (C.P. H_2O), critical isochore, and the wedge-shaped critical region for pure H_2O from Johnson and Norton (1991). Also shown is the bubble-point - dew-point curve for an H_2O-NaCl fluid containing 20 wt. % NaCl, and for an H_2O-CO_2 fluid containing 20 mol. % CO_2, as well as the critical point and critical isochore for these fluids. A schematic "critical region" analogous to that for pure H_2O is shown for each of the binary fluids. The inset shows the direction of shift in the *PT* coordinates of the critical points for different fluid compositions in the H_2O-NaCl, H_2O-CO_2 and H_2O-NaCl-CO_2 systems. After Bodnar and Costain (1991).

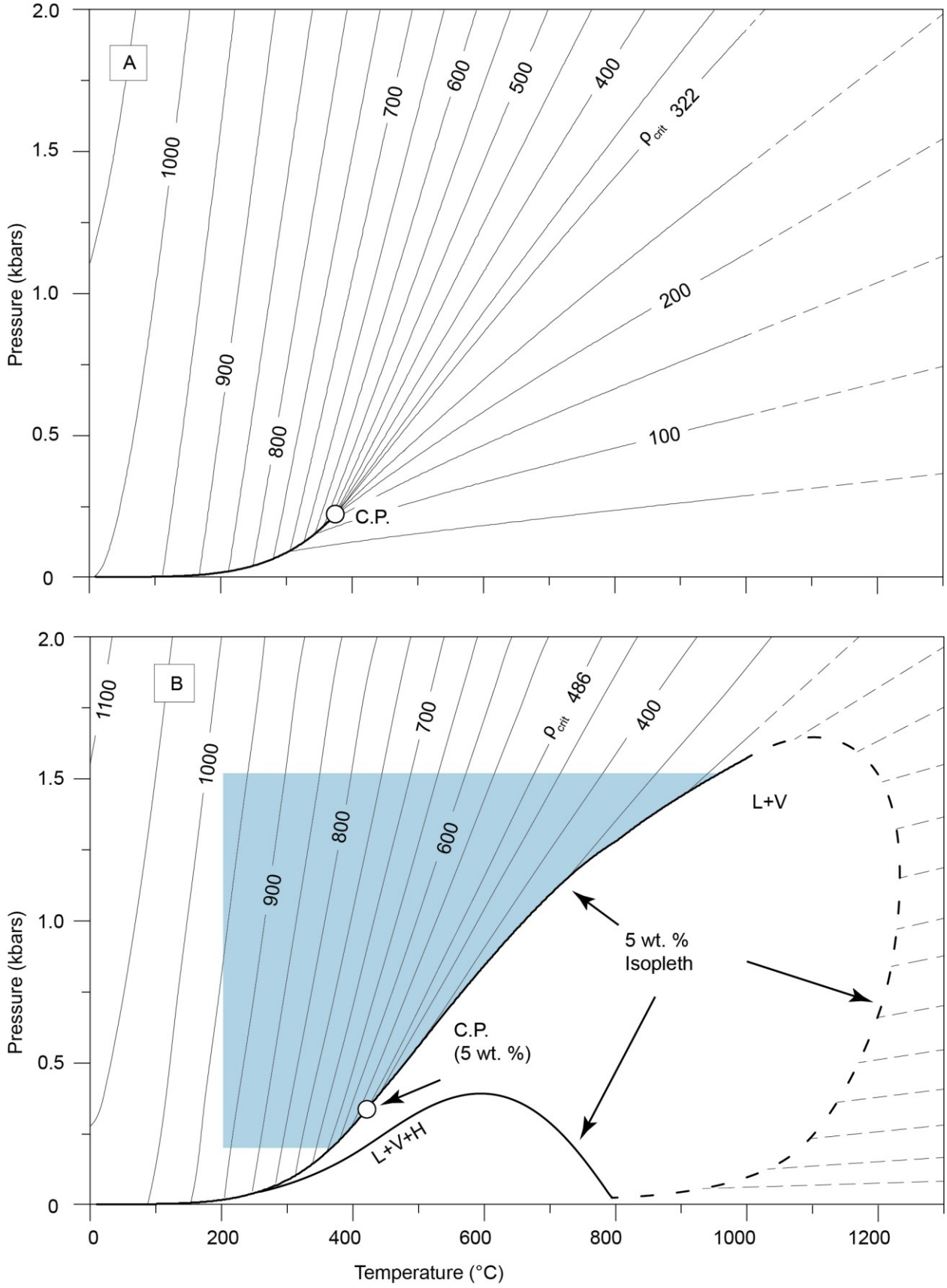
A
1000
900
800
700
600
500
400
P_{crit} 322
200
100
C.P.
Pressure (kbars)
2.0
1.5
1.0
0.5
0
B
1100
1000
900
800
700
600
P_{crit} 486
400
L+V
L
5 wt. %
Isopleth
C.P.
(5 wt. %)
L+V+H
Pressure (kbars)
Temperature (°C)
0
200
400
600
800
1000
1200

Figure 3 (A) Pressure-temperature diagram for pure H_2O showing the critical point (C.P.) at the termination of the liquid-vapor coexistence curve, and isochores (in $kg \cdot m^{-3}$), calculated from the IAPWS-95 EOS. Fluids with densities greater than the critical density of 322 $kg \cdot m^{-3}$ are considered liquids, and those with densities less than the critical density are vapor. (B) Pressure-temperature diagram for an H_2O-NaCl fluid with a salinity of 5 wt. % NaCl. The heavy solid lines show the 5 wt. % NaCl bubble-point – dew-point curve isopleth separating the one-phase region from the two-phase (liquid + vapor) field and the locus of triple points where liquid + vapor + halite (L+V+H) coexist. The lighter solid lines represent isochores (in $kg \cdot m^{-3}$) for a fluid of 5 wt. % NaCl, and the critical isochore separating liquid from vapor is labeled with the critical density of 486 $kg \cdot m^{-3}$. Phase boundaries and isochores were calculated using the EOS of Driesner and Heinrich (2007) and Driesner (2007), respectively. The 5 wt. % NaCl bubble-point – dew-point curve isopleth and the isochores for H_2O and H_2O-NaCl are dashed at high temperatures owing to lack of data in this region. The blue shaded area represents the *PT* region in the one-phase field in which physical and thermodynamic properties of the fluid were evaluated in this study and which includes the critical points for salinities ranging from 0 to ~30 wt.% NaCl.

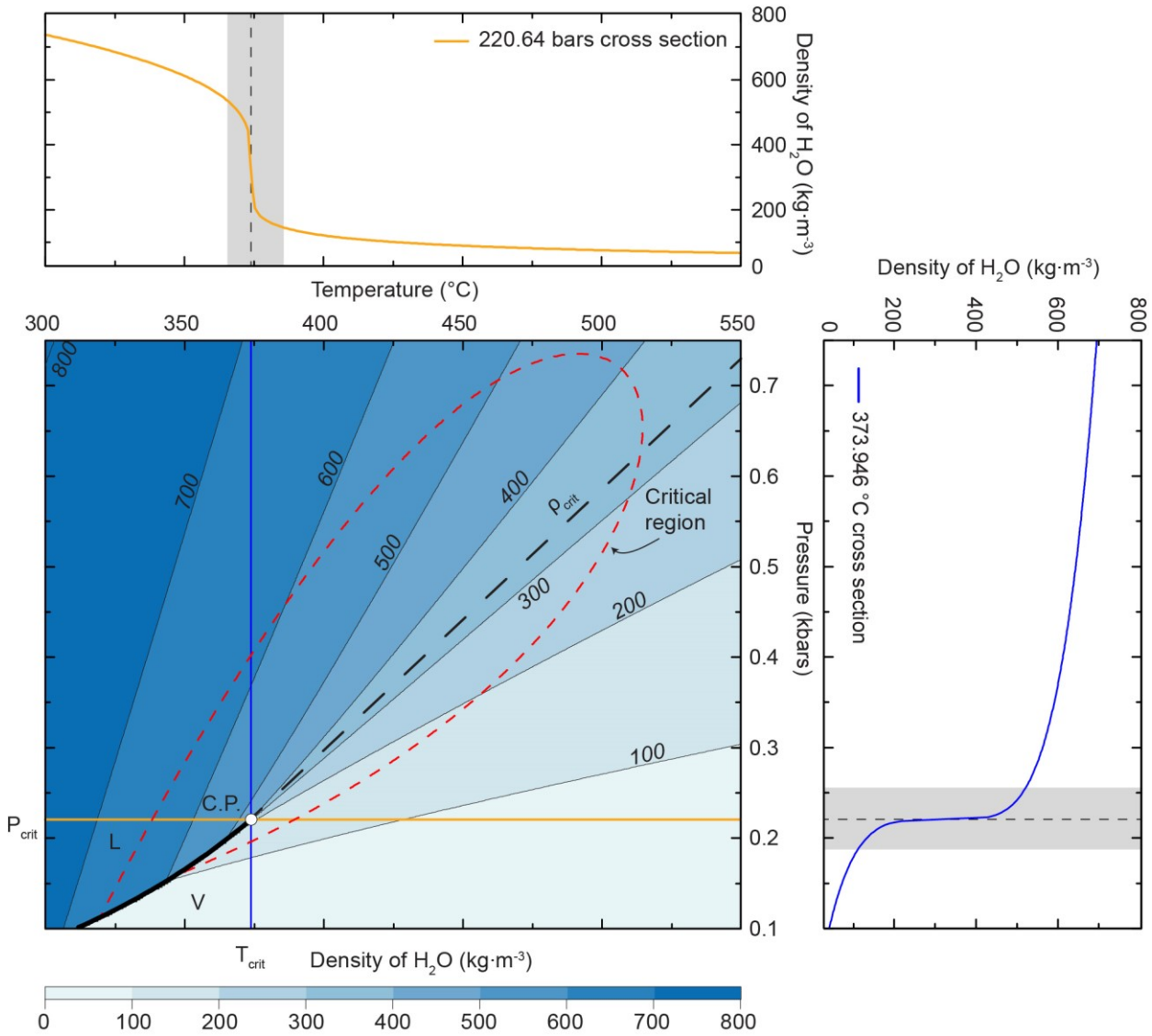

Figure 4. Variations in density of pure H_2O in temperature-pressure space. Temperature-density (top) and pressure-density (right) diagrams show the variation in density along the critical isobar (220.64 bars) and along the critical isotherm (373.946 °C), respectively. The temperature and pressure regions along the isobaric and isothermal projections in which the density is most sensitive to temperature or pressure changes are shaded. The dashed red line labeled "critical region" outlines the region of *PT* space in which $\tilde{\chi} \geq 0.5$. The critical isochore (ρ_{crit}) originates at the terminus of the H_2O liquid-vapor equilibrium curve (L-V), i.e., at the critical point (C.P.), and is shown by the dashed line.

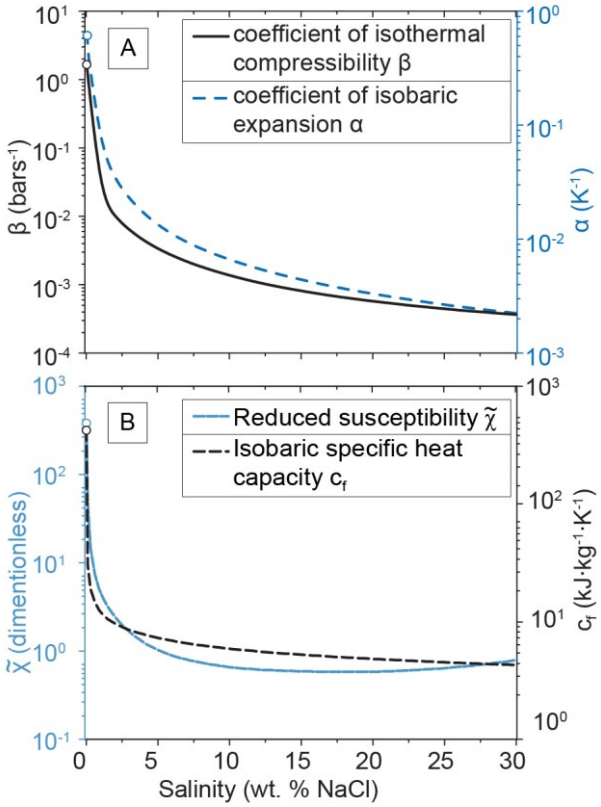

Figure 5. Maximum values of (A) the coefficients of isothermal compressibility (β, bar^{-1} left axis) and isobaric thermal expansion (α, K^{-1} right axis), and (B) reduced susceptibility ($\tilde{\chi}$ left axis) and isobaric specific heat capacity (c_f, kJ kg^{-1} K^{-1} right axis), all shown as a function of salinity within the *PT* range of interest (i.e. in the one phase fluid field at 200 to 900 °C and 0.15 to 1.7 kbar).

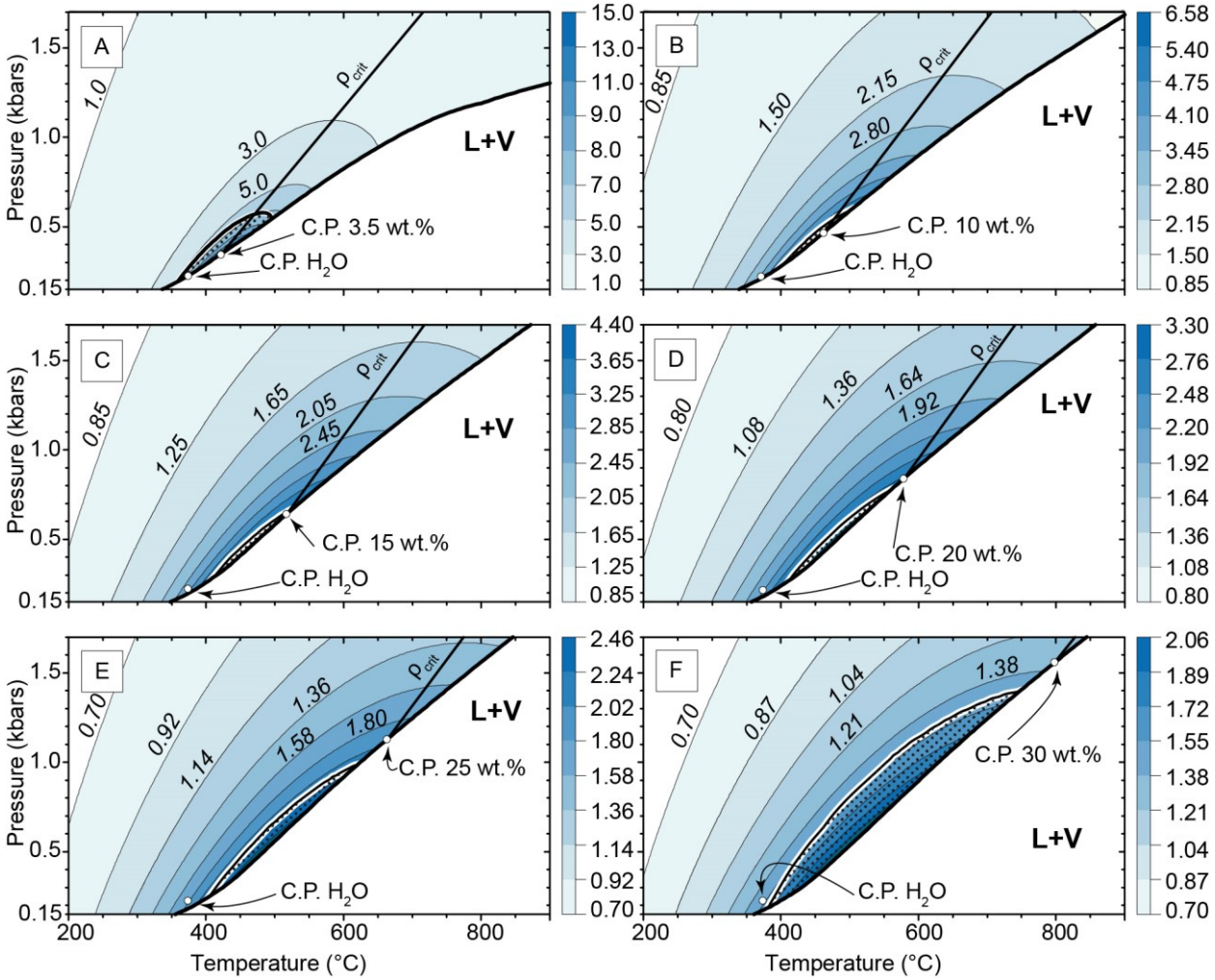

Figure 6. Contour diagrams showing the variation in magnitude of the coefficient of isobaric thermal expansion (α, K^{-1}) $\times 10^{-3}$ for salinities of 3.5, 10, 15, 20, 25 and 30 wt. % NaCl in the one-phase field. Also shown are the boundaries between the one-phase and two-phase (L+V) fields (heavy solid line), the critical point for H_2O (C.P. H_2O), the critical point for the given salinity, and the critical isochore for a given fluid composition (ρ_{crit}). The density of the critical isochore (ρ_{crit}) equals to 462, 542, 583, 617, 641 and 655 $kg \cdot m^{-3}$ for the 3.5, 10, 15, 20, 25 and 30 wt. % NaCl compositions, respectively. The stippled *PT* area immediately above the phase boundary represents the critical region, i.e., the region where $\tilde{\chi} \geq 0.5$. The color bar and the numbers along the right side of each panel correspond to the magnitude of the coefficient of isobaric thermal expansion (α, K^{-1}) $\times 10^{-3}$.

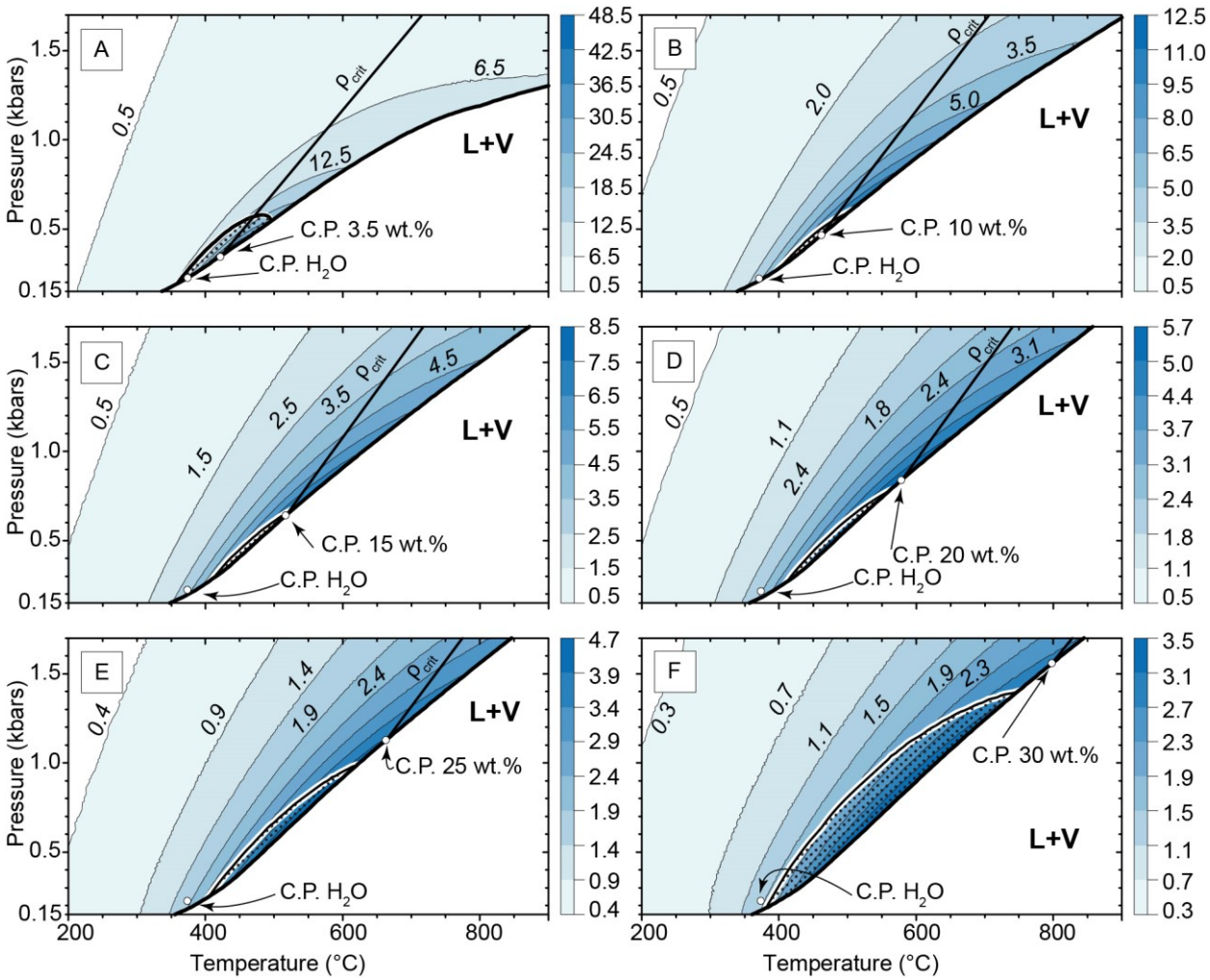

Figure 7. Contour diagrams showing the variation in magnitude of the coefficient of isothermal compressibility (β, bar^{-1}) × 10^{-4} for salinities of 3.5, 10, 15, 20, 25 and 30 wt. % NaCl in the one-phase field. Also shown are the boundaries between the one-phase and two-phase (L+V) fields (heavy solid line), the critical point for H_2O (C.P. H_2O), the critical point for the given salinity, and the critical isochore for a given fluid composition (ρ_{crit}). The density of the critical isochore (ρ_{crit}) equals to 462, 542, 583, 617, 641 and 655 $kg \cdot m^{-3}$ for the 3.5, 10, 15, 20, 25 and 30 wt. % NaCl compositions, respectively. The stippled *PT* area immediately above the phase boundary represents the critical region, i.e., the region where $\tilde{\chi} \geq 0.5$. The color bar and the numbers along the right side of each panel correspond to the magnitude of the coefficient of isothermal compressibility (β, bar^{-1}) × 10^{-4}.

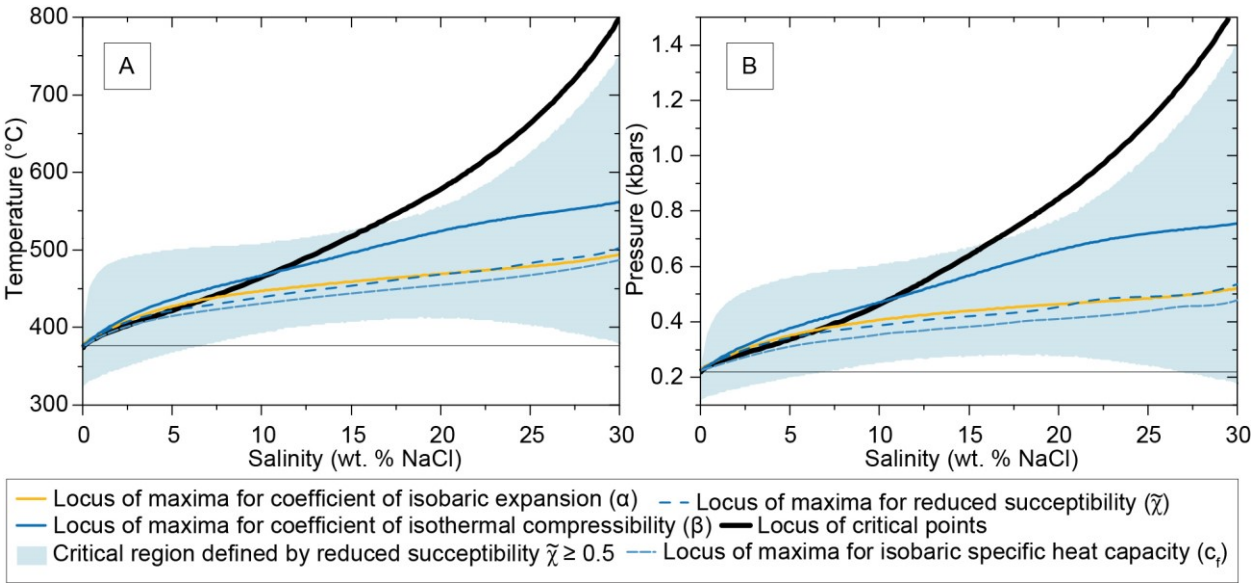

Figure 8. Relationship between temperature, pressure and the critical region in which maximum values of the coefficients of thermal expansion (α), isothermal compressibility (β), reduced susceptibility ($\tilde{\chi}$) and isobaric specific heat capacity (c_f) occur as a function of salinity in theone phase fluid field. (A) The temperature at which the maximum values of α, β, $\tilde{\chi}$ and c_f are observed as a function of salinity; the critical temperature as a function of salinity is also shown; (B) the pressure at which the maximum values of α, β, $\tilde{\chi}$ and c_f are observed as a function of salinity; the critical pressure as a function of salinity is also shown; shaded regions represent the temperature (A) and pressure (B) range of the critical region as a function of salinity, defined as the region in which reduced susceptibility, $\tilde{\chi} \geq 0.5$. Thin horizontal lines correspond to the critical temperature (373.946 °C) and critical pressure (220.64 bars) for pure H_2O on 8A and 8B, respectively

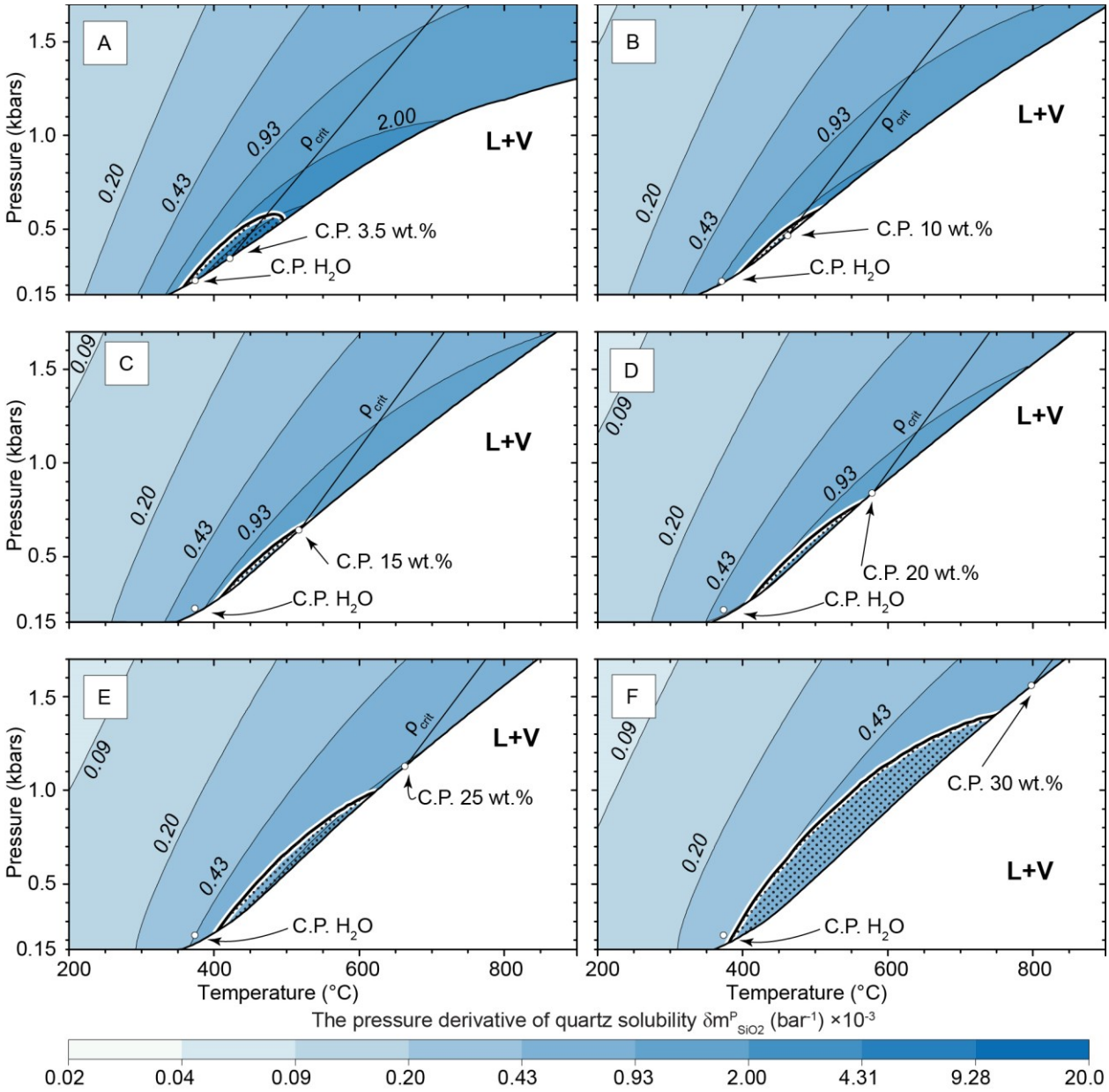

Figure 9. The pressure coefficient of quartz solubility (δm^P_{SiO2}, bar^{-1}) $\times 10^{-3}$ for salinities of 3.5, 10, 15, 20, 25 and 30 wt. % NaCl in the one-phase fluid field. Also shown are the boundaries between the one-phase and two-phase (L+V) fields, the critical point for H_2O (C.P. H_2O), the critical point for the given salinity, and the critical isochore for the given fluid composition (ρ_{crit}). The stippled *PT* area immediately above the phase boundary represents the critical region, i.e., the region where $\tilde{\chi} \geq 0.5$.

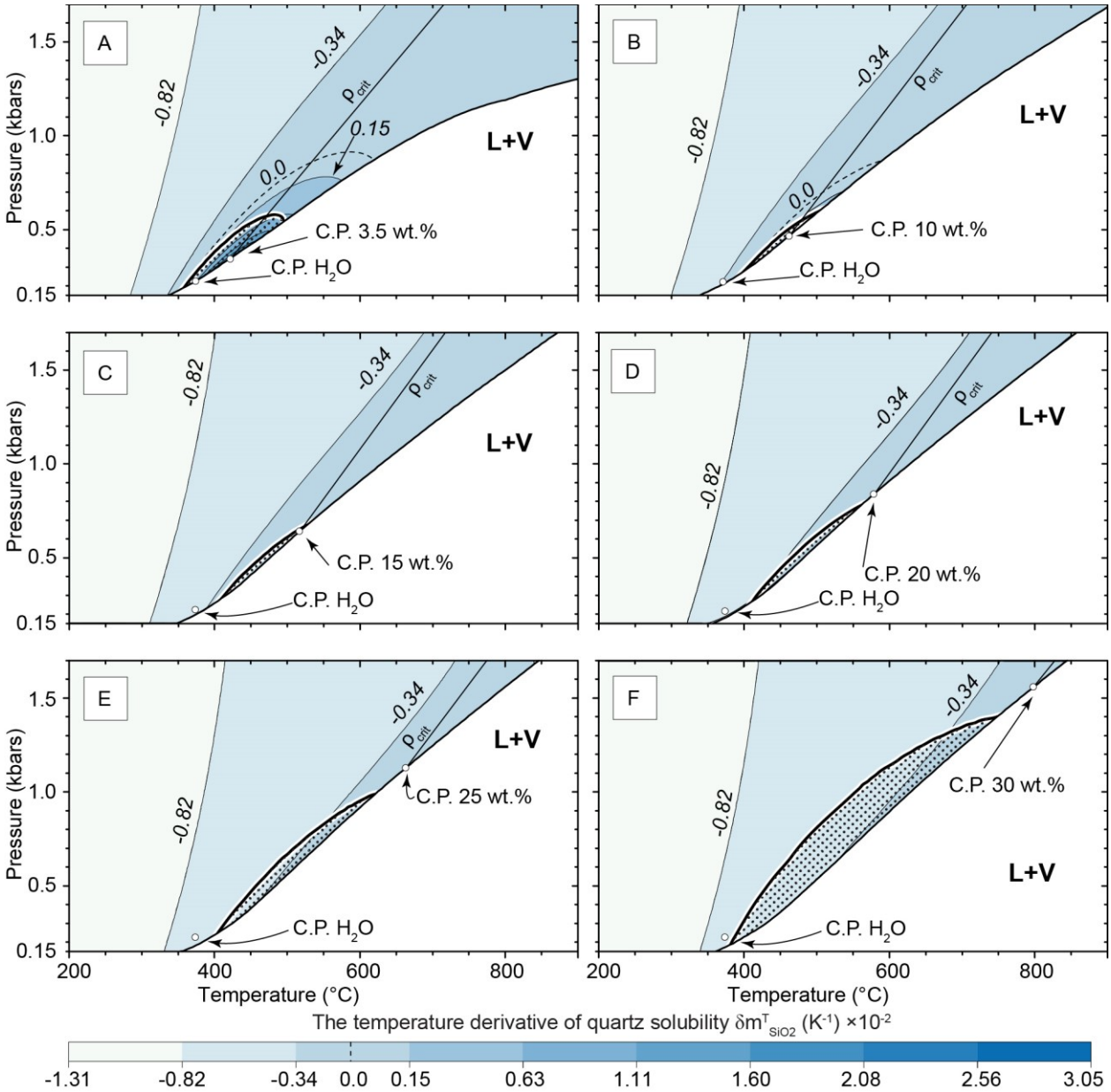

Figure 10. The temperature coefficient of quartz solubility (δm^T_{SiO2}, K^{-1}) ×10^{-2} for salinities of 3.5, 10, 15, 20, 25 and 30 wt. % NaCl in the one-phase fluid field. Also shown are the boundaries between the one-phase and two-phase (L+V) fields, the critical point for H_2O (C.P. H_2O), the critical point for the given salinity, and the critical isochore for the given fluid composition (ρ_{crit}). The stippled PT area immediately above the phase boundary represents the critical region, i.e., the region where $\tilde{\chi} \geq 0.5$. Note that δm^T_{SiO2} changes from being negative to positive inside PT area limited by thick dashed line corresponding to the region in which quartz solubility changes from prograde to retrograde.

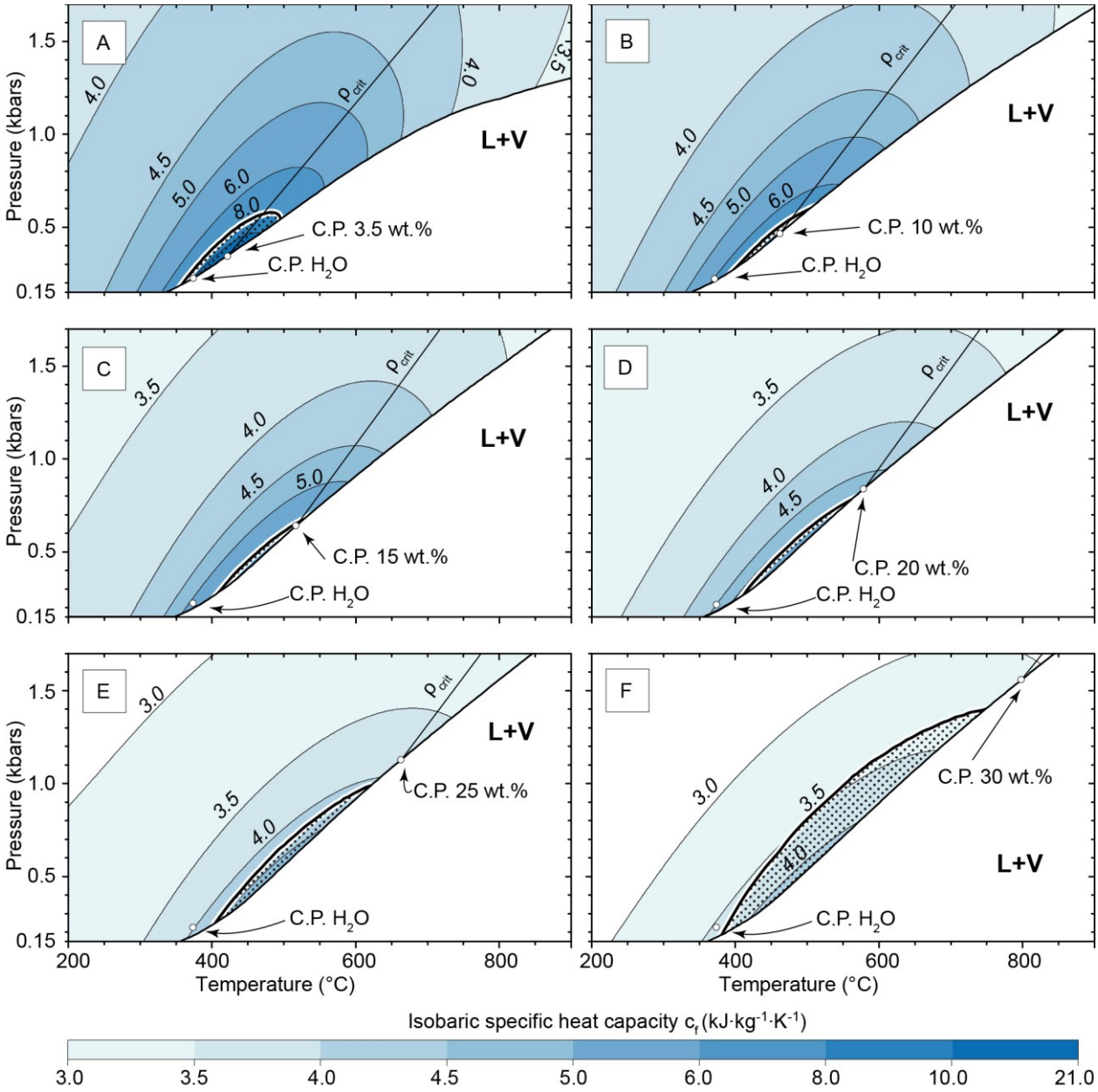

Figure 11. Contour diagrams showing the variation in isobaric specific heat capacity (c_f, $kJ \cdot kg^{-1} \cdot K^{-1}$) for salinities of 3.5, 10, 15, 20, 25 and 30 wt. % NaCl in the one-phase fluid field. Also shown are the boundaries between the one-phase and two-phase (L+V) fields (heavy solid line), the critical point for H_2O (C.P. H_2O), the critical point for the given salinity, and the critical isochore for the given fluid composition (ρ_{crit}). The stippled *PT* area immediately above the phase boundary represents the critical region, i.e., the region where $\tilde{\chi} \geq 0.5$.

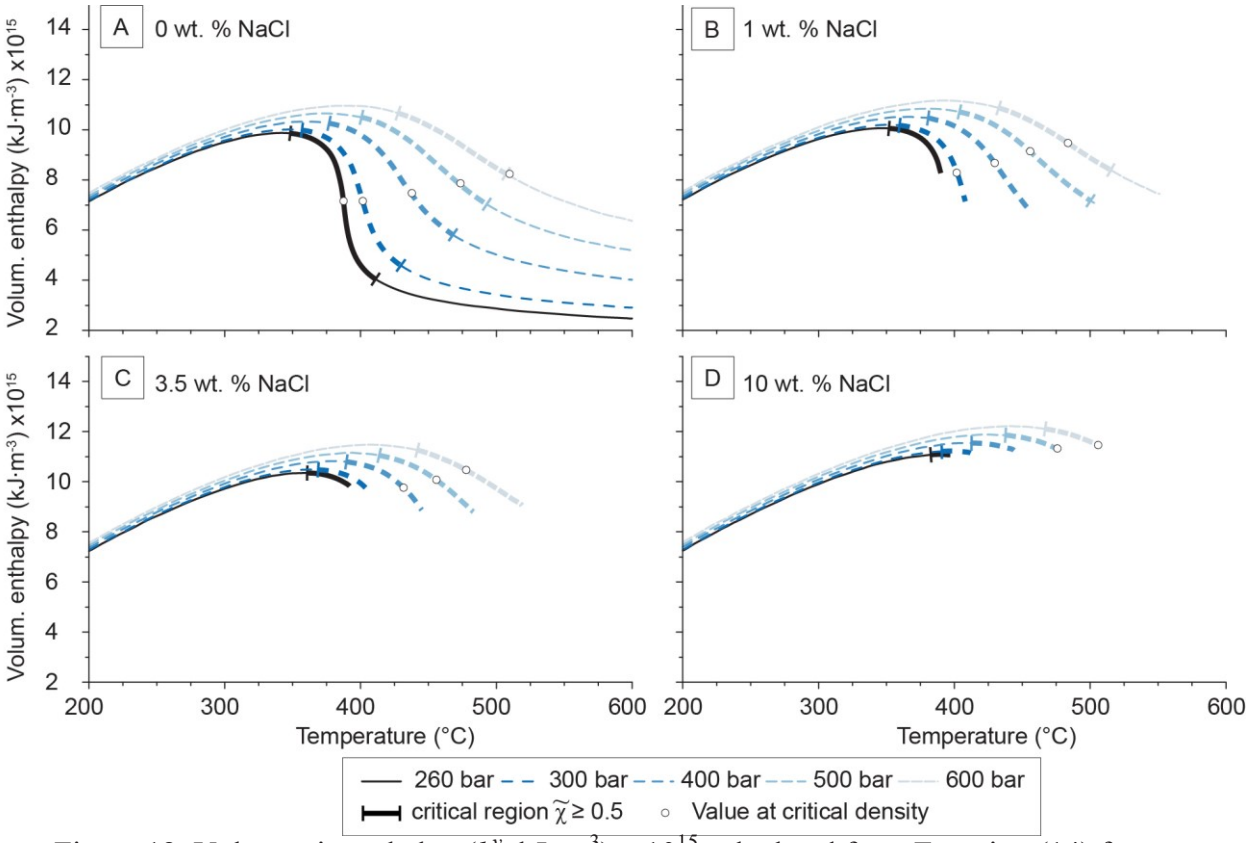

Figure 12. Volumetric enthalpy (h^v, kJ·m^{-3}) × 10^{15} calculated from Equation (14) for pure H_2O, 1, 3.5 and 10 wt. % NaCl solutions as a function of temperature at pressures of 260, 300, 400, 500 and 600 bars, plotted along isobars. All calculations are for fluids in the single-fluid-phase field. The open circle on each isobar represents the volumetric enthalpy and temperature on the critical isochore (density) for that pressure. For temperatures to the low-temperature side of the point representing the critical density, the fluids are in the liquid field (i.e., densities greater than the critical density), whereas for temperatures to the high-temperature side of the point representing the critical density the fluids are in the vapor field (i.e., densities less than the critical density). The heavy solid portion of the 260 bar isobar represents that portion of *PTX* space that is within the critical region.

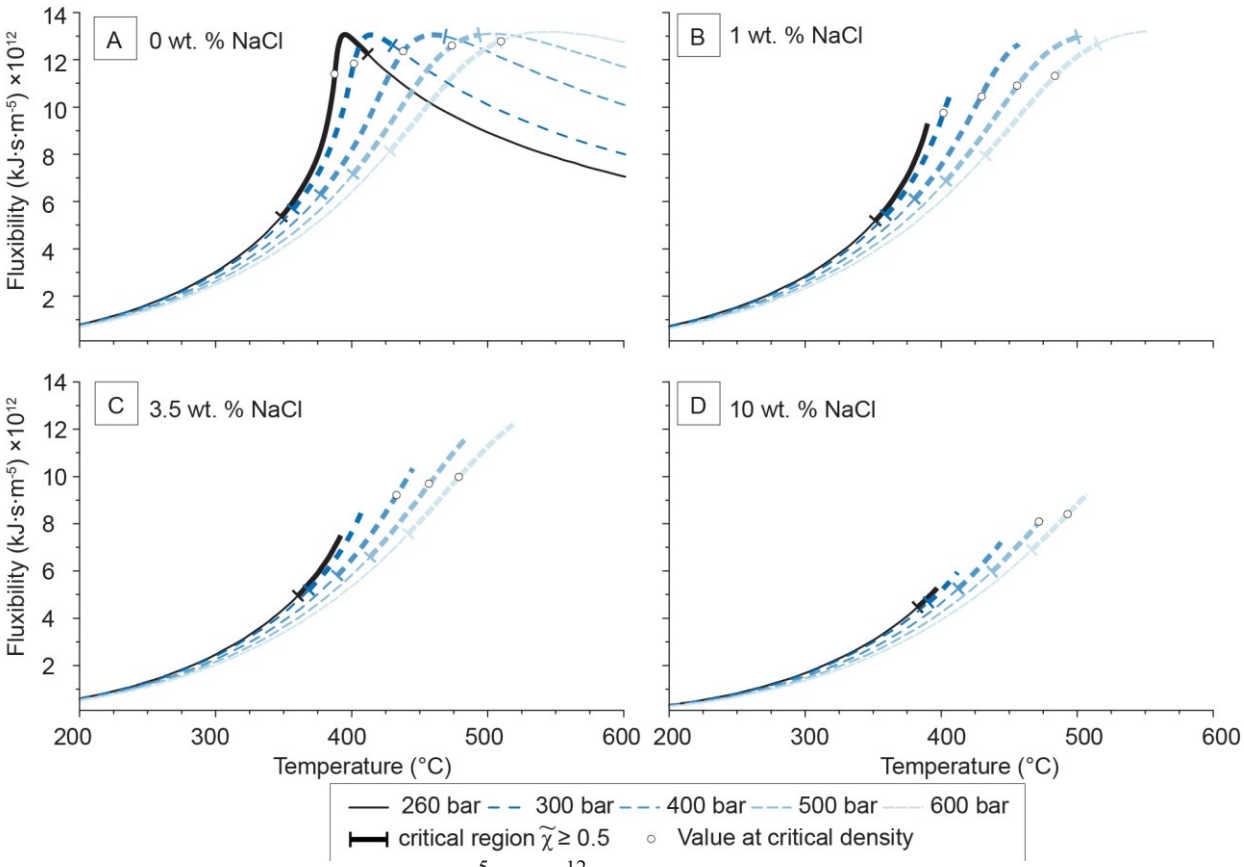

Figure 13. Fluxibility (F, kJ·s·m^{-5}) × 10^{12} for pure water, 1, 3.5 and 10 wt. % NaCl solutions as a function of temperature at pressures of 260, 300, 400, 500 and 600 bars, calculated using Equation (13). All calculations are for fluids in the single-fluid-phase field. The open circle on each isobar represents the fluxibility and temperature on the critical isochore (density) for that pressure. For temperatures to the low-temperature side of the point representing the critical density, the fluids are in the liquid field (i.e., densities greater than the critical density), whereas for temperatures to the high-temperature side of the point representing the critical density the fluids are in the vapor field (i.e., densities less than the critical density). The heavy solid portion of the 260 bar isobar represents that portion of PTX space that is within the critical region.

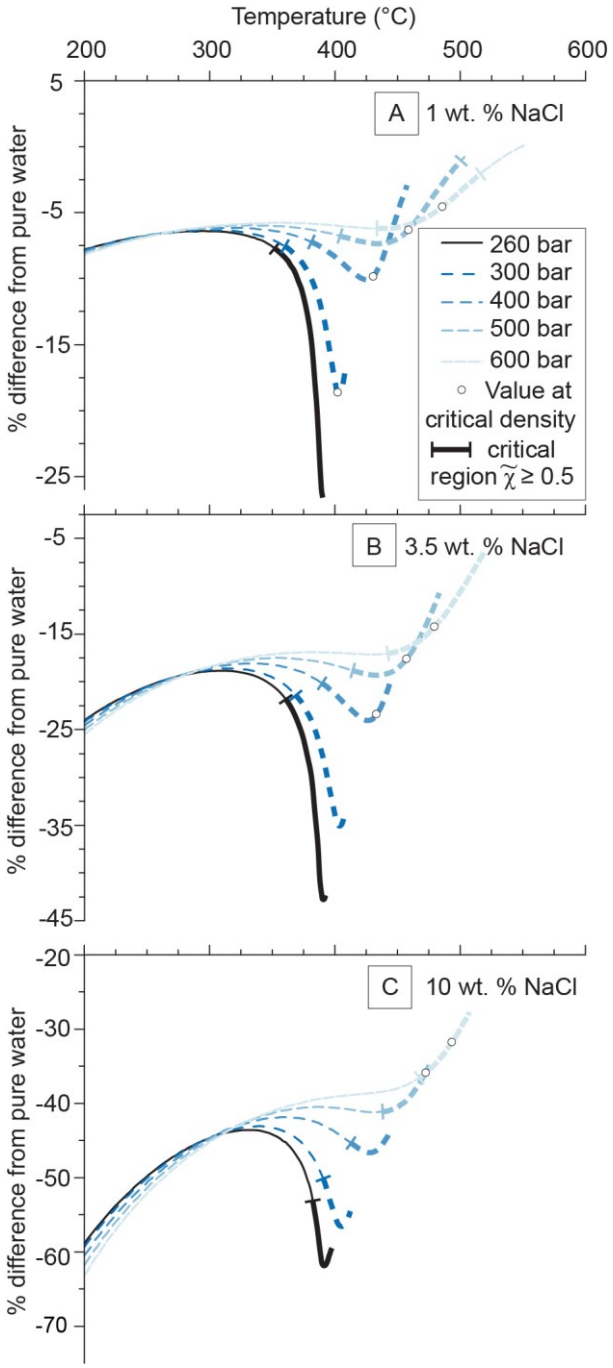

Figure 14. Percent difference between the fluxibility of H_2O-NaCl fluids and that for pure H_2O, calculated from Equation (15), as a function of temperature at pressures of 260, 300, 400, 500 and 600 bars. All calculations are for fluids in the single-fluid-phase field. Negative values indicate that saline fluids are less capable of transporting heat by buoyancy-driven convection in a hydrostatic pressure gradient $\vec{g}\rho_0$, compared to pure H_2O. The open circle on each isobar represents the difference in fluxibility at the critical density. For temperatures to the low-temperature side of the point representing the critical density, the fluids are in the liquid field (i.e., densities greater than the critical density), whereas for temperatures to the high-temperature side of the point representing the critical density the fluids are in the vapor field (i.e., densities less than the critical density). Note that the "% difference from pure water" scale (Y-axis) is

different on each diagram. The heavy solid portion of the 260 bar isobar represents that portion of *PTX* space that is within the critical region.

CHAPTER 2

Klyukin, Y.I., Lowell, R.P., Bodnar, R.J., 2017. A revised empirical model to calculate the dynamic viscosity of H_2O-NaCl fluids at elevated temperatures and pressures (≤1000 °C, ≤500 MPa, 0–100 wt % NaCl). ***Fluid Phase Equilibria***, 433: 193-205.

A revised empirical model to calculate the dynamic viscosity of H_2O-NaCl fluids at elevated temperatures and pressures (≤1000 °C, ≤500 MPa, 0–100 wt % NaCl).

Y.I. Klyukin [a], R.P. Lowell [a] and R.J. Bodnar [a]

[a.] Department of Geosciences, Virginia Tech, Blacksburg, VA 24061

Abstract

Examination of viscosities for the fluids in the system H_2O-NaCl predicted by the commonly-used model of Palliser and McKibbin has identified regions of pressure-temperature-salinity (PTx) space in which the model delivers values that are inconsistent with some experimental data and exhibits discontinuities and trends that are unexpected. Here, we describe a revised model to calculate viscosity of H_2O-NaCl fluids that shows good correlation with experimental values and shows trends that are consistent with known or expected behavior outside of the region where experimental data are available. The model described here is valid over the temperature range from the H_2O solidus (~0 °C) to ~1,000 °C, from ~0.1 MPa to ≤500 MPa, and for salinities from 0-100 wt.% NaCl.

Keywords H_2O-NaCl fluid, viscosity, transport properties, numerical model

1. Introduction

The circulation of fluids in the Earth's crust plays an important role in the transport of chemical constituents (mass) and heat (energy), and is the major control on the formation of hydrothermal ore deposits (Bredehoeft and Norton, 1990). In recent decades, our understanding of fluid circulation in response to thermal perturbations in the crust has advanced significantly through application of numerical fluid flow models. These models incorporate the transport equations that describe conservation of mass, energy and momentum of the system, and require as input the physical and thermodynamic properties of the circulating fluid. Early numerical simulations incorporated the properties of pure H_2O to simulate the natural fluid. For example, the properties of H_2O were used to approximate the hydrothermal fluid in studies of fluid circulation in systems associated with shallow continental plutons (Cathles, 1981; Norton, 1979, 1982, 1984), submarine hydrothermal systems (Fehn and Cathles, 1979; Fehn et al., 1983; Jupp and Schultz, 2000, 2004), and sedimentary environments (Cathles and Smith, 1983; Garven, 1985; Wood and Hewett, 1982). While most hydrothermal fluids are H_2O-rich, most also contain small to significant amounts of salts such as NaCl, KCl, $CaCl_2$, $FeCl_2$, etc. or volatiles such as CO_2 and CH_4 (Bodnar et al., 2014; Holloway, 1984; Roedder, 1972; Yardley and Bodnar, 2014).

While the one-component system H_2O is a reasonable approximation for the composition of some low-salinity aqueous hydrothermal fluids, the fact that H_2O is a one-component system results in a phase topology that differs significantly from that of multi-component fluids. An

important difference in phase topology of the one component H_2O system compared to multi-component fluid systems is that in a one component system liquid and vapor only coexist along the liquid-vapor curve that terminates at a critical end point (Figure 1a; C.P.), beyond which only a single-phase fluid may exist. Additionally, at temperatures above the critical temperature in a one-component system such as H_2O, all physical and thermodynamic properties of the fluid vary smoothly and continuously with changing temperature and pressure, and no discontinuities in fluid properties occur. Over the past several decades, a large experimental database describing the Pressure-Volume-Temperature-Composition (PVTx) properties of aqueous electrolyte systems has been generated, especially for the system H_2O-NaCl (Bischoff and Rosenbauer, 1988; Bodnar et al., 1985; Knight and Bodnar, 1989; Sourirajan and Kennedy, 1962). A complete summary of available experimental data thorugh 2008 is available in Valyashko (2008). The available experimental data have been used to develop algorithms to estimate the physical and thermodynamic properties of more complex fluids at high temperatures and pressures (Anderko and Pitzer, 1993; Driesner, 2007; Driesner and Heinrich, 2007; Palliser and McKibbin, 1998a, b, c; Tanger and Pitzer, 1989). These various algorithms have subsequently been incorporated into numerical fluid flow models (Lewis and Lowell, 2009; Weis et al., 2014) that describe the circulation of hydrothermal fluids in the crust.

One of the basic physical properties required to model fluid flow is the fluid viscosity. In most early models, the viscosity of pure H_2O was used. In the liquid region, the viscosity of pure H_2O decreases smoothly and continuously with increasing temperature at constant pressure above the critical pressure (22.064 MPa), up to approximately the PT conditions along the critical isochore (Figure 1a). With increasing temperature above the critical isochore, the viscosity shows a reversal and increases with increasing temperature at PT conditions to the low-pressure side of the critical isochore, i.e., in the vapor field (Fig. 1a). While use of the viscosity of pure H_2O in fluid flow models works reasonably well for low salinity fluids and at PT conditions that would be in the liquid field for pure H_2O (i.e., at pressure greater than the pressure on the liquid-vapor curve, or greater than the pressure on the critical isochore for a given temperature), the viscosity of pure H_2O is a poor analog for the viscosity of more saline fluids, especially at PT conditions in the vicinity of the pure H_2O liquid-vapor curve and at PT conditions that would be in the vapor field for pure H_2O.

The dynamic viscosity (η – Pa·s) is included in the expression for conservation of momentum associated with fluid flow. The conservation of momentum can be defined as (Norton and Knight, 1977):

$$\vec{\upsilon} = -\frac{k\rho}{\eta}(\nabla P - \rho\vec{g}) \quad (1)$$

Numerical models describing the viscosity for pure H_2O were developed within the International Association for the Properties of Steam (IAPS), which in 1989 became the International Association for the Properties of Water and Steam (IAPWS). The viscosity of H_2O established in 1964 was initially presented as a set of skeleton tables, together with recommended interpolation equations by Kestin and Whitelaw (1966). Later numerical models of the viscosity of H_2O included revisions to improve the accuracy of predictions (Kestin, 1980) and to better estimate the asymptotic divergent behavior of the viscosity near the critical point of water (Watson et al., 1980) (see Figure 1a). In the latest release of the IAPWS formulation 2008, the viscosity of pure H_2O is based on Huber et al. (2009) and replaces the IAPS formulation 1985 for the Viscosity of Ordinary Water substance issued in 2003 (Cooper and Dooley, 2008). The IAPWS 2008 formulation is based on the density of H_2O calculated by the IAPWS-95 model of water and steam properties developed by Wagner and Pruß (2002). The viscosity of

pure H_2O in the IAPWS formulation 2008 has estimated uncertainties between 1 and 7 %, and is limited in its PT range of applicability by the solidus of H_2O at low temperature, an upper temperature limit of 900 °C and an upper pressure limit varying from 1000 MPa at low temperatures to 300 MPa at high temperatures. The viscosity of H_2O predicted by the IAPWS formulation 2008 is shown on Figure 1a.

The most commonly used model to calculate the viscosity of H_2O-NaCl at elevated PT conditions is that of Palliser and McKibbin (1998c). During our earlier studies to investigate fluid flow in submarine hydrothermal systems (Han et al., 2013; Steele-MacInnis et al., 2012), we observed unexpected behavior that could be traced back to viscosities predicted by the Palliser and McKibbin (1998c) model. This motivated us to investigate further, leading to the development of a revised model for viscosity of H_2O-NaCl at elevated PT conditions. Here, we compare viscosities of H_2O-NaCl determined experimentally with those predicted by the Palliser and McKibbin (1998c) model (referred to hereafter as P&M model), examine trends in viscosity predicted by the P&M model outside of the range of experimental data, and propose a revised model that more faithfully reproduces the experimental data and displays smooth and expected extrapolation to PTx conditions outside of the range of experimental data.

2. Experimental and Modeling Studies of the Viscosity of H_2O-NaCl at Elevated PT Conditions

Experimental characterization of the viscosity of binary H_2O-NaCl solutions is limited to relatively low temperature (<350 °C) and low salinity (<27 wt. % NaCl) conditions, except for data for the viscosity of molten NaCl at ≥800 °C. A summary of experimental studies of the viscosity of H_2O-NaCl solutions, including the PTx range of the experiments, experimental method used and number of data points, is provided in Table 1. Numerical models to estimate the viscosity of H_2O-NaCl solutions are thus best constrained within the PTx range of the experimental data shown in Table 1, i.e., to approximately 300-350 °C and salinity less than 27 wt. % NaCl.

In addition to the P&M model, other models developed for the viscosity of aqueous solutions are those of Lencka et al. (1998), the TTG (Tammann-Tait-Gibson) model of Leyendekkers (1979), the model of Phillips et al. (1981) and that of Mao and Duan (2009) (hereafter referred to as M&D). The TTG and Lencka et al. (1998) models are designed to estimate the viscosity of complex multicomponent electrolyte solutions. Thus, both models include the H_2O-NaCl system as a sub-system of the H_2O + electrolytes system, but these models are generally not used in hydrothermal fluid flow simulations for various reasons. In the case of the model of Lencka et al. (1998), the EOS is limited to ≤300 °C and concentrations up to 30 m (i.e. for H_2O-NaCl, ~64 wt. % NaCl). The TTG model is not recommended to predict viscosities of H_2O-NaCl solutions because Kestin and Shankland (1984) showed that this model tends to underestimate viscosity at high pressure and low temperature conditions (compared to experimental data).

The models by Phillips et al. (1981) and Mao and Duan (2009) are based on almost the same experimental data that are listed in Table 1. These models are designed to estimate viscosity of any H_2O-electrolyte solution. For H_2O-NaCl solutions, both models are limited to temperatures ≤350 °C, and salinities up to 22.6 and 26 wt. % NaCl (5 and 6 mol kg^{-1} H_2O), and pressures up to 50 and 100 MPa, respectively. Mao and Duan (2009) report that their model agrees with experimental values to ≤1%, whereas the Phillips et al. (1981) report that their model reproduces experimental data to ≤2%.

An EOS that predicts the viscosity of H_2O-NaCl over the widest range of temperature and pressure for all salinities (0-100 % NaCl) is that of Palliser and McKibbin (1998c). This model has no stated PT limits over which the model is valid, but based on the manner in which the P&M model was developed, it follows that the pressure and temperature limits are defined by the EOS chosen to predict the viscosity of pure H_2O, which is then used in the P&M model to calculate viscosity of H_2O-NaCl. The P&M viscosity model for brines is composed of two separate equations, one designed to calculate the viscosity in the temperature range from 0 to 800 °C, and the other to calculate the viscosity at temperature ≥ 800 °C. For temperatures above 800 °C, viscosity is a linear function NaCl mass fraction, temperature, and the viscosity of pure H_2O at the same pressure and temperature. The viscosity at temperatures below 800 °C is described by a ninth order polynomial as a function of temperature:

$$\eta_b(P,T,x) = \frac{\eta_{H_2O}(T,P)\cdot(1+3x)\cdot\left(\frac{800-T}{800}\right)^9}{\left(\frac{800-T}{800}\right)^9+\left(\frac{T}{800}\right)^9} + \frac{(\eta_{H_2O}(T,P)\cdot(1-x)+\mu^{800}_{NaCl}\cdot x)\cdot\left(\frac{T}{800}\right)^9}{\left(\frac{800-T}{800}\right)^9+\left(\frac{T}{800}\right)^9} \quad (2)$$

where η_b is the dynamic viscosity of H_2O-NaCl fluid in kg m^{-1} s; η_{H_2O} is viscosity of pure water at given PT in kg m^{-1} s; η^{800}_{NaCl} is a constant corresponding to the viscosity of molten NaCl at 800 °C calculated by eq. 5.2 from P&M.

Viscosities of H_2O-NaCl fluids calculated using the P&M model for pressures of 22, 50 and 200 MPa are shown as a function of salinity and temperature on Figure 2, with several iso-viscosity lines plotted for reference. In some portions of PTx space the P&M model predicts viscosities that are unexpected, and these trends are a function of the nature of the algorithm used to calculate the viscosity. At pressures that are less than those on the pure H_2O liquid-vapor curve, or less than the pressure on the pure H_2O critical isochore, and higher than the pressure on the liquid + vapor + halite coexistence curve in the H_2O-NaCl system (hatched region in Figure 1b), most compositions in the H_2O-NaCl system are in the liquid field. However, the P&M model uses the viscosity of H_2O at the temperature and pressure of interest as a reference viscosity to calculate the viscosity of the H_2O-NaCl solution, and at PT conditions within the hatched area shown on Figure 1b pure H_2O is in the vapor field. Thus, because the model uses the viscosity of pure H_2O at the P and T of interest as the reference viscosity, and because the reference viscosity is for a "vapor" whereas the H_2O-NaCl fluid is a liquid, the viscosity is under-estimated in this PT region by the P&M model.

The P&M model also predicts viscosity trends that are unexpected in the temperature range from ~400 to 800 °C. The algorithm used to calculate viscosity in the P&M model and shown in equation (2) above can be broken down into two components, referred to here as the first term and second term on the right-hand side of Eq. (2). As shown in Figure 3, at temperatures less ~400 °C the viscosity is dominated by the first term of Eq. (2), whereas for temperatures between 400 and 800 °C the viscosity is dominated by the second term of Eq. (2). Moreover, owing to the form of the equation, between 400 and 800 °C the viscosity reaches a plateau and remains nearly constant with increasing temperature in this range (Figure 2, 3). Additionally, above 800 °C, a different form of relationship is used to calculate the viscosity in the P&M model, resulting in a significant and abrupt change in slope of iso-viscosity lines at 800 °C (Figure 2). Therefore, because viscosities of H_2O-NaCl fluids predicted by the P&M model show unexpected and, likely, incorrect trends in some regions of PTx space in which important hydrothermal processes in the crust occur, a new formulation to predict viscosities of H_2O-NaCl fluids was developed.

3. Model Development

The main criteria invoked to develop our model for the viscosity of H_2O-NaCl fluids over a wide range of PTx conditions relevant to crustal hydrothermal systems are (1) the model must accurately reproduce the viscosity of pure H_2O over the complete PT range, (2) the model must faithfully reproduce available experimental data for viscosities of H_2O-NaCl fluids and molten NaCl, (3) the model should predict smooth variations in viscosity with changing PTx conditions, and with no discontinuities or abrupt changes in trend (slope) in PTx space, and (4) the PTx region in which the model predicts viscosities that are consistent with a liquid (higher density), and the PTx region in which the model predicts viscosities that are consistent with a vapor (lower density) must be consistent with phase topology in the H_2O-NaCl system that defines PTx regions in which liquid and vapor exist. The viscosity of pure H_2O calculated using the IAPWS-2008 Formulation (Huber et al., 2009) (Fig. 4a) as well as experimentally determined viscosities of various H_2O-NaCl mixtures (Fig. 4b, c) (Kestin and Shankland, 1984; Pepinov et al., 1978; Semenyuk et al., 1977) are plotted on Figure 4 as a function of the fluid density. These, and additional experimental data listed in Table 1, have been used to develop and to test the degree to which the revised model reproduces experimental data.

Figure 4a shows the viscosity of pure H_2O as a function of density along several isobars ranging from 0.1 MPa to 150 MPa. The viscosity shows a smooth and consistent variation as a function of density along individual isobars, with a consistent offset towards higher density with increasing pressure. When NaCl is added to H_2O, the viscosity again varies in a smooth and expected manner as a function of density. Thus, the viscosity versus density trend for an H_2O-NaCl fluid with a salinity of 5 wt. % NaCl at a pressure of 10 MPa is offset to higher densities compared to the trend for pure H_2O at this same pressure (Fig. 4b). Moreover, the viscosity versus density trend for an H_2O-NaCl fluid with a salinity of 5 wt. % NaCl migrates to higher density with increasing pressure, analogous to the manner in which the trend for pure H_2O shown in Figure 4a migrates to higher densities. Finally, at a fixed pressure, the viscosity versus density trend migrates in a smooth and consistent manner to higher density with increasing salinity (Fig. 4c). The consistent manner in which the viscosity of H_2O-NaCl fluids varies with density as a function of changing salinity and pressure provides a basis for development of an algorithm to predict the viscosity of H_2O-NaCl fluids over a range of PTx conditions appropriate for crustal hydrothermal systems.

As shown on Figures 4b and 4c, the viscosity of an H_2O-NaCl fluid at a given pressure, temperature, and salinity (PTx) can be estimated from the viscosity of pure H_2O by determining the temperature at which pure H_2O has the same viscosity as that of the H_2O-NaCl fluid at the same pressure. Thus, the difference in density ($\Delta\rho$) between that of the H_2O-NaCl fluid at some pressure and that of pure H_2O having the same viscosity at that same pressure is converted into a temperature difference (ΔT). For example, Figure 5a shows the relationship between viscosity and density for pure H_2O and for an H_2O-NaCl fluid of some fixed salinity, both at the same pressure. At the conditions of interest (pressure and salinity of the H_2O-NaCl fluid), the viscosity of the H_2O-NaCl fluid is equal to the viscosity of pure H_2O having a density that is different from that of the H_2O-NaCl fluid. The density difference for these conditions is shown by ($\Delta\rho$). At the pressure of interest, the temperature at which H_2O will have the density estimated from $\Delta\rho$ may be calculated from the EOS. Then, the data shown in Figure 5a may be plotted in density-temperature space (Fig. 5b) to determine the temperature difference (ΔT) corresponding to the density difference ($\Delta\rho$). Thus, the viscosity of the H_2O-NaCl brine at some PTx condition is

equal to the viscosity of pure H_2O at that same pressure and equivalent temperature $T^* = T+\Delta T$ according to:

$$\eta_{H_2O}(T^*, P) = \eta_{brine}(x, T, P) \quad (3)$$

where η_{H_2O} is the dynamic viscosity of pure H_2O according to the IAPWS-2008 Formulation (Huber et al., 2009), η_{brine} is the viscosity of the H_2O-NaCl binary mixture of composition (x; mass fraction of NaCl) at the pressure (P; MPa) and temperature (T; °C) of interest. The equivalent temperature T^* at which pure H_2O has the same viscosity as that of the H_2O-NaCl fluid at the same pressure is described by the relationship:

$$T^* = e_1 + e_2 T \quad (4)$$

The temperature increment, ΔT, shows a nearly linear dependence with temperature (Fig. 5c), and is independent of pressure (Fig. 6).

Developing an empirical relationship describing the value of some fluid parameter for a multi-component fluid using the value of that same parameter for pure H_2O as a reference is a common approach that has been used successfully by other workers. For example, Haas (1976) proposed a logarithmic dependence between T and T^* in his numerical model to estimate volumetric properties of the system H_2O-NaCl up to 325 °C, while Driesner (2007) used a linear dependence between T and T^* to describe volumetric properties of H_2O-NaCl up to 1,000 °C. In the present study, we found that the relationship between T and T^* to calculate viscosity is best described by fitting the coefficients e_1 and e_2 described by polynomial functions as shown below:

$$e_1 = a_1 \cdot x^{a_2} \quad (5)$$

$$e_2 = 1 - b_1 \cdot T^{b_2} - b_3 \cdot x^{a_2} \cdot T^{b_2} \quad (6)$$

where x is the weight fraction of NaCl, T is temperature in °C, and fitting coefficients *a* and *b* are listed in Table 2. For pure H_2O, T^* calculated according to Eqs. 4-6 is equal to T, i.e., $\Delta T = 0$.

The temperature range over which this model for the viscosity of H_2O-NaCl is valid is limited by the temperature ranges over which (1) the IAPWS 2008 Formulation for the viscosity of pure H_2O and (2) the model of Driesner (2007) for the PVTx properties of H_2O-NaCl fluid are valid. Thus, this revised model for the viscosity of H_2O-NaCl is valid from the temperature of the H_2O solidus (0.01 °C at P = 0.01 MPa) to ~1,000 °C, assuming that $T^* \leq 900$ °C. The temperature limit $T^* \leq 900$ °C applies because this is the upper temperature limit for the IAPWS 2008 Formulation. The upper temperature limit of the model (1,000 °C) is constrained by the upper temperature limit of the Driesner (2007) model. The upper pressure limit for the revised viscosity model ranges from 500 MPa when the equivalent temperature T* is between 0-160 °C, 350 MPa when T* is between 160-600 °C, and 300 MPa when T* is between 600-900 °C. These upper pressure limits stem from constraints placed by the Driesner (2007) model for H_2O-NaCl and the IAPWS 2008 Formulation.

Figure 7 highlights the temperature-salinity (Tx) region in which the revised viscosity model is valid. The solid gray area in the upper left (T >900 °C and low salinity) of Figure 7a (also shown enlarged in Fig. 7b) depicts the region in which T^*>900 °C and, therefore, the model is not valid. The gray area shown along the bottom and right side of Figure 7a (low to moderate temperatures and all salinities) represents the Tx region in which T*<0.01 °C, and the model is also invalid in this region. The hatched region shown at moderate to high temperatures and salinities in Figure 7a (and along the right side of Fig. 7c) represents the liquid + halite (L+H) field. For T*≤160 °C the pressure limit for the model is 500 MPa, for T* ≤600 °C the pressure

limit is 350 MPa, and above 600 °C the pressure limit is 300 MPa. Insets show enlargements of regions (grey color) in which T* ≤ 0 °C (Fig. 7b) or >900 °C (Fig. 7c).

4. Comparison of Revised Model with the Model of Palliser and McKibbin

The viscosity of H_2O-NaCl solutions predicted by the revised model, and by the earlier P&M and M&D models, were compared with experimental data from the studies listed in Table 1 (experimental data and results of calculations are listed in Appendix A). Figure 8 shows the differences between the experimental viscosity and viscosity calculated by the revised model (Fig. 8a), and by the P&M (Fig. 8b) and M&D models (Fig. 8c). The scatter plots show that most calculated values show good agreement with experimental values and fall close to the 1:1 line. The hatched region indicates the area in which deviation from the 1:1 line is in the range ±5 %. The histograms shown by insets in Figure 8 show the percent difference (D) between the calculated and experimentally measured viscosity, calculated according to:

$$D = \frac{\eta_{ref} - \eta_{calc}}{\eta_{ref}} \cdot 100\% \qquad (7)$$

where η_{ref} is the experimentally measured viscosity and η_{calc} is the viscosity of H_2O-NaCl calculated using either the revised model or those of P&M or M&D. Viscosities predicted by the revised model agree with experimental values mostly within ±10%, whereas differences between experimental values and those predicted by the P&M model extend to -40% and to >20% (Fig. 8B), especially for higher salinity fluids. Most viscosities predicted by the M&D model reproduce experimental data to ±5%, with a few points up to >80% for PTx conditions at which pure H_2O is a vapor but the H_2O-NaCl fluid is a liquid (Fig. 8C).

Both the P&M and M&D models significantly under-estimate viscosities for the same data, especially for PT conditions that are within the hatched area shown in Figure 1b. In this case large difference results because the P&M and M&DMao and Duan (2009)Mao and Duan (2009)Mao and Duan (2009)Mao and Duan (2009) models both use the viscosity of H_2O at the temperature and pressure of interest as the reference viscosity. However, at pressures higher than those along the vapor + liquid + halite (P_{VLH}) coexistence curve and lower than the pressure on the H_2O liquid-vapor curve (P^L_S), the reference viscosity of H_2O that is used by P&M and M&D corresponds to that of a low density H_2O vapor phase, while at the same PT conditions the H_2O-NaCl phase is a high density liquid. Thus, these models underestimate the viscosity of the liquid phase at PT conditions close to the vapor + liquid + halite (P_{VLH}) coexistence curve for compositions such that H_2O-NaCl is in the one phase field.

The revised viscosity model reported here and the P&M model are valid at any salinity and thus can be used to estimate viscosity along the vapor-saturated halite liquidus. These two models were used to estimate viscosity at PTx conditions along the vapor + liquid + halite (VLH) coexistence curve. The compositions of the vapor and liquid phases in equilibrium with halite along the VLH coexistence curve are shown on Figure 9a. Note that, except for temperatures very close to the NaCl triple point (800.7 °C), the salinity of the vapor phase is <<1 wt. % NaCl, whereas the salinity of the liquid phase in equilibrium with vapor and halite varies from about 28 wt% NaCl at 100 °C to 100 wt. % NaCl at 800.7 °C. Viscosities of the liquid and vapor phases along the vapor + liquid + halite (P_{VLH}) coexistence curve predicted by the P&M model and by the revised model are shown in Figure 9b. Viscosities predicted for the vapor phase by both models are nearly identical as expected, because the concentration of NaCl in the vapor phase is very low (except very near the NaCl triple point temperature of 800.7 °C) and thus the viscosity of the vapor phase is nearly identical to that of pure H_2O. Conversely,

viscosities of the liquid phase predicted by the two models show different behavior. The P&M model underestimates the viscosity of the liquid phase and predicts a viscosity similar to that of the vapor at temperatures below ~300 °C because PT conditions along the vapor + liquid + halite coexistence curve in this region are in the vapor field for pure H_2O and the P&M model uses the viscosity of H_2O vapor as the reference viscosity for the calculations. The increase in viscosity of the liquid phase predicted by the P&M model at about 400 °C (Figure 9b) is related to the form of Eq. 2, as discussed above. The viscosity of a liquid is expected to decrease with increasing temperature in concert with decreasing density as temperature increases. Conversely, the viscosity of a liquid is expected to increase as the salinity increases and approaches the viscosity of the molten (H_2O-free) salt. These two competing effects for the liquid phase along the vapor + liquid + halite coexistence curve result in an initial decrease in viscosity with increasing temperature (and increasing salinity of the liquid), until the effect of increasing salinity overcomes the temperature effect at ~400 °C (corresponding to a salinity of ~45 wt.% NaCl). Thus, the viscosity of the liquid phase along the vapor + liquid + halite coexistence curve predicted by the present model is consistent with the known (or expected) relationship between viscosity, temperature and salinity, and shows a decrease in the viscosity with increasing the temperature, followed by an increase in the viscosity at higher temperatures, reflecting the effect of increasing NaCl concentration.

For further comparison of viscosities for H_2O-NaCl predicted by the P&M model and those predicted by the revised model described here, the viscosity at 50 MPa was calculated using both models over the range 100 - 1000 °C and salinity from 0-100 wt. % NaCl. At these conditions, the P&M model shows reversals in the magnitude of viscosity at ~400 °C that are not expected based on variations in density (or other fluid properties) at these conditions (Fig. 10a). Moreover, the P&M model shows discontinuities in iso-viscosity lines at high salinities and temperatures at 800 °C that are related to the form of the functions used to calculate viscosity above and below this temperature (Figs. 2; 10a). The revised model shows a systematic and expected decrease in viscosity with increasing temperature at any salinity and does not show any unexpected reversals or discontinuities in viscosity (Fig. 10b). Viscosities predicted by the two models are compared on Figure 10c, where the percent difference in viscosity is contoured in T-x space. The difference is calculated according to Eq. (7), where η_{ref} is the viscosity predicted by the P&M model and η_{calc} is the viscosity predicted by the revised model. Differences between the two models are small (between -4 to 10 %) for salinities less than about 20-30 wt. % NaCl and temperatures less than about 350 °C (Fig. 10c). At temperatures above 400 °C the difference in viscosity predicted by the two models for liquid H_2O-NaCl solutions varies between 55-85 %. For example, at a salinity of 50 wt. % NaCl and 500 °C and 50 MPa, the viscosity estimated by the P&M model is 765 μPa s and that predicted by the revised model is 145 μPa s (Fig. 10a, b). As discussed above and shown on Figure 1b, in the PT range in which the H_2O-NaCl solution is a liquid but pure H_2O is a vapor, the P&M model predicts a viscosity that is lower than that predicted by the revised model. Conversely, in the PT range in which both the H_2O-NaCl solution and pure H_2O have liquid-like densities, the P&M model predicts viscosities that are significantly higher than those predicted by the revised model. The temperature at which the P&M model transitions from under-estimating the viscosity of H_2O-NaCl to where it over-estimates the viscosity is about 400 °C (see Figs. 9b and 10). We note that the T-x range in which the largest differences are observed corresponds to the temperature and salinity conditions observed in many magmatic-hydrothermal ore deposits, such as the porphyry copper deposits,

and in the sub-seafloor portion of hydrothermal systems associated with magma emplacement at mid-ocean ridges.

Viscosities calculated with the current model for H_2O-NaCl fluids having salinities of 3.2 (seawater), 5, 10, 25, 50 and 75 wt. % NaCl and temperatures and pressures ranging between 100-1000 °C and 0-300 MPa, respectively, are shown in Figure 11. Note that viscosities have only been calculated for PTx conditions within the single-phase (liquid or vapor) fields.

As an example of the application of the revised model and potential implications for numerical modeling of fluid flow in hydrothermal systems, we have calculated the viscosities of hydrothermal fluids circulating through a submarine hydrothermal system using both the revised model and the P&M model. We have taken the temperature, pressure, fluid composition and density data along a sub-seafloor flow path from Steele-MacInnis et al. (2012) and show the viscosities calculated from the two models in Figure 12. The temperature distribution in the sub-seafloor after the system has been active for 80 years is shown in Figure 12 a. The salinity(ies) and temperatures of the fluid(s) along the fluid flow path A-B-C-D-E shown in Figure 12 are shown in Figures 12b, c. Calculated viscosities at the temperatures, pressures and salinities along the flow path are shown on Figure 12d. Along the portion of the flow path where the fluid is in the one phase field (A-C), viscosities predicted by the two models are similar. However, when the fluid undergoes immiscibility to produce a high salinity liquid in equilibrium with a low salinity vapor (C-D), the two models predict similar viscosities for the vapor phase, but the P&M model predicts a viscosity that is ~2x greater than that predicted by the revised model. Along the flow path from the sub-seafloor to the seafloor (D-E) the fluid is once again in the one-phase field and viscosities predicted by the two models are again similar. This example documents differences between the two models and potential implications for modeling hydrothermal systems, especially if high salinity fluids are involved and/or the PT conditions are in the region where the H_2O-NaCl fluid is a liquid and pure H_2O would be a vapor. In the example shown, the higher viscosities estimated by the P&M model for the brine (liquid) phase in the two-phase region would predict that more of the brine would remain at depth in the system, compared to the revised model in which the brine phase has a lower viscosity and would be more likely to be transported upwards towards the seafloor during hydrothermal circulation.

5. Summary

This study compares viscosities of H_2O-NaCl fluids predicted by the model of Palliser and McKibbin (1998c) (P&M model) with a revised model for viscosity developed here. The revised model incorporates an equivalent temperature T* at which the viscosity of pure H_2O has the same viscosity as that of an H_2O-NaCl fluid at the same pressure. This revised viscosity model shows better overall agreement with experimental data compared to the P&M model, and does not show unexpected trends in viscosity versus temperature or salinity that characterize the P&M model. The revised model can be used to simulate fluid flow in various geological environments over the range 0-1000 °C, ≤500 MPa and 0-100 wt. % NaCl. The revised model shows good agreement with the limited amount of experimental data available for H_2O-NaCl at elevated PTx conditions. As expected based on available data and our understanding of how the viscosity of aqueous fluids should change as temperature and pressure (density) change, an increase in temperature at constant Px (decrease in density) results in a decrease in viscosity, while an increase in salinity at constant PT or an increase in pressure at constant Tx both lead to an increase in density and a concomitant increase in viscosity.

6. Acknowledgments

This material is based on work supported in part by the National Science Foundation under Grant No. EAR-1019770 to RJB. We also thank Robert McKibbin and Chris Palliser for useful discussions concerning their model for the viscosity of H_2O-NaCl at elevated temperatures and pressures. Kayla Lewis confirmed that the values we were obtaining with the Palliser and McKibbin model were consistent with values predicted by that model in the FISHES modeling code. Shreya Singh made us aware of the fact that the Palliser and McKibbin model was predicting "unusual behavior" at high temperatures, and this motivated us to examine the model more closely.

7. References

Anderko, A. and Pitzer, K.S. (1993) Equation-of-state representation of phase-equilibria and volumetric properties of the system NaCl-H_2O above 573 K. Geochim. Cosmochim. Acta 57, 1657-1680.

Bischoff, J.L. and Rosenbauer, R.J. (1988) Liquid-vapor relations in the critical region of the system NaCl-H_2O from 380 to 415 °C: A refined determination of the critical point and two-phase boundary of seawater. Geochim. Cosmochim. Acta 52, 2121-2126.

Bodnar, R., Burnham, C. and Sterner, S. (1985) Synthetic fluid inclusions in natural quartz. III. Determination of phase equilibrium properties in the system H_2O-NaCl to 1000 °C and 1500 bars. Geochim. Cosmochim. Acta 49, 1861-1873.

Bodnar, R., Lecumberi-Sanchez, P., Moncada, D. and Steele-MacInnis, M. (2014) Fluid inclusions in hydrothermal ore deposits, in: Scott S. D. (Ed.), Treatise on Geochemistry, 2nd ed. Elsevier Ltd., Amsterdam, pp. 119-142.

Bredehoeft, J.D. and Norton, D.L. (1990) Mass and Energy Transport in a Deforming Earth's Crust, in: Council, N.R. (Ed.), The Role of Fluids in Crustal Processes. The National Academies Press, Washington, DC, pp. 27-42.

Cathles, L.M. (1981) Fluid flow and genesis of hydrothermal ore deposits, in: Skinner, B.J. (Ed.), Economic Geology 75th Anniversary Volume. The Economic Geology publishing company, Lancaster, pp. 424-457.

Cathles, L.M. and Smith, A.T. (1983) Thermal constraints on the formation of Mississippi Valley-Type lead-zinc deposits and their implications for episodic basin dewatering and deposit genesis. Econ. Geol. 78, 983-1002.

Cooper, J. and Dooley, R. (2008) Release of the IAPWS formulation 2008 for the viscosity of ordinary water substance. The International Association for the Properties of Water and Steam, Berlin, Germany.

Driesner, T. (2007) The system H_2O-NaCl. II. Correlations for molar volume, enthalpy, and isobaric heat capacity from 0 to 1000 °C, 1 to 5000 bar, and 0 to 1 X-NaCl. Geochim. Cosmochim. Acta 71, 4902-4919.

Driesner, T. and Heinrich, C.A. (2007) The system H_2O-NaCl. I. Correlation formulae for phase relations in temperature-pressure-composition space from 0 to 1000 °C, 0 to 5000 bar, and 0 to 1 XNaCl Geochim. Cosmochim. Acta 71, 4880-4901.

Fehn, U. and Cathles, L.M. (1979) Hydrothermal convection at slow-spreading mid-ocean ridges. Tectonophysics 55, 239-260.

Fehn, U., Green, K.E., Von Herzen, R.P. and Cathles, L.M. (1983) Numerical models for the hydrothermal field at the Galapagos Spreading Center. Journal of Geophysical Research: Solid Earth 88, 1033-1048.
Garven, G. (1985) The role of regional fluid flow in the genesis of the Pine Point Deposit, Western Canada sedimentary basin. Econ. Geol. 80, 307-324.
Haas, J.L. (1976) Physical properties of the coexisting phases and thermochemical properties of the H_2O component in boiling NaCl solutions. U. S. Geological Survey Bulletin 1421-A.
Han, L., Lowell, R.P. and Lewis, K.C. (2013) The dynamics of two-phase hydrothermal systems at a seafloor pressure of 25 MPa. Journal of Geophysical Research: Solid Earth 118, 2635-2647.
Haynes, W.M. (2014) CRC Handbook of Chemistry and Physics 94th ed. National Institute of Standards and Technology.
Holloway, J.R. (1984) Graphite-CH_4-H_2O-CO_2 equilibria at low-grade metamorphic conditions. Geology 12, 455-458.
Huber, M., Perkins, R., Laesecke, A., Friend, D., Sengers, J., Assael, M., Metaxa, I., Vogel, E., Mareš, R. and Miyagawa, K. (2009) New international formulation for the viscosity of H_2O. Journal of Physical and Chemical Reference Data 38, 101-125.
Ito, T., Kojima, N. and Nagashima, A. (1989) Redetermination of the viscosity of molten NaCl at elevated temperatures. International journal of thermophysics 10, 819-831.
Jupp, T.E. and Schultz, A. (2000) A thermodynamic explanation for black smoker temperatures. Nature 403, 880-883.
Jupp, T.E. and Schultz, A. (2004) Physical balances in subseafloor hydrothermal convection cells. Journal of Geophysical Research: Solid Earth 109, B05101.
Kestin, J. (1980) The Transport Properties of Water Substance, Water and steam: their properties and current industrial applications: proceedings of the 9th International Conference on the Properties of Steam, 10-14 September 1979. Pergamon, Technische Universität München, FRG, p. 283.
Kestin, J., Khalifa, H.E., Abe, Y., Grimes, C.E., Sookiazian, H. and Wakeham, W.A. (1978) Effect of pressure on the viscosity of aqueous sodium chloride solutions in the temperature range 20-150.degree.C. Journal of Chemical & Engineering Data 23, 328-336.
Kestin, J., Khalifa, H.E., Ro, S.-T. and Wakeham, W.A. (1977) Preliminary data on the pressure effect on the viscosity of sodium chloride-water solutions in the range 10-40.degree.C. Journal of Chemical & Engineering Data 22, 207-214.
Kestin, J. and Shankland, I.R. (1984) Viscosity of aqueous NaCl solutions in the temperature range 25–200 °C and in the pressure range 0.1–30 MPa. International Journal of Thermophysics 5, 241-263.
Kestin, J. and Whitelaw, J. (1966) Sixth international conference on the properties of steam—transport properties of water substance. Journal of Engineering for Gas Turbines and Power 88, 82-104.
Knight, C.L. and Bodnar, R.J. (1989) Synthetic fluid inclusions: IX. Critical PVTX properties of NaCl-H_2O solutions. Geochim. Cosmochim. Acta 53, 3-8.
Lencka, M.M., Anderko, A., Sanders, S.J. and Young, R.D. (1998) Modeling viscosity of multicomponent electrolyte solutions. International Journal of Thermophysics 19, 367-378.
Lewis, K.C. and Lowell, R.P. (2009) Numerical modeling of two-phase flow in the NaCl-H_2O system: Introduction of a numerical method and benchmarking. Journal of Geophysical Research: Solid Earth 114, B05202.

Leyendekkers, J.V. (1979) The viscosity of aqueous electrolyte solutions and the TTG model. Journal of Solution Chemistry 8, 853-869.
Mao, S. and Duan, Z. (2009) The viscosity of aqueous alkali-chloride solutions up to 623 K, 1,000 bar, and high ionic strength. International Journal of Thermophysics 30, 1510-1523.
Norton, D.L. (1979) Transport phenomena in hydrothermal systems: the redistribution of chemical components around cooling magmas. Bull. Mineral. 102, 471-486.
Norton, D.L. (1982) Fluid and heat transport phenomena typical of copper-bearing pluton environments, in: Titley, S.R. (Ed.), Advances in Geology of the Porphyry Copper Deposits, Southwestern North America. University of Arizona Press, Tucson, Arizona, pp. 59-72.
Norton, D.L. (1984) Theory of hydrothermal systems. Annual Review of Earth and Planetary Sciences 12, 155-177.
Norton, D.L. and Knight, J.E. (1977) Transport phenomena in hydrothermal systems; cooling plutons. Am. J. Sci. 277, 937-981.
Out, D.J.P. and Los, J.M. (1980) Viscosity of aqueous solutions of univalent electrolytes from 5 to 95°C. Journal of Solution Chemistry 9, 19-35.
Ozbek, H., Fair, J.A. and Phillips, S.L. (1977) Viscosity of aqueous sodium chloride solutions from 0 - 150° C.
Palliser, C. and McKibbin, R. (1998a) A model for deep geothermal brines, I: T-p-X state-space description. Transport in Porous Media 33, 65-80.
Palliser, C. and McKibbin, R. (1998b) A model for deep geothermal brines, II: thermodynamic properties – density. Transport in Porous Media 33, 129-154.
Palliser, C. and McKibbin, R. (1998c) A model for deep geothermal brines, III: thermodynamic properties – enthalpy and viscosity. Transport in Porous Media 33, 155-171.
Pepinov, R.I., Yusufova, V.D., Lobkova, N.V. and Panakhov, I.A. (1978) Experimental study of the viscosity of aqueous sodium chloride and sodium sulfate solutions at high temperature and pressures. High Temperature 16, 960-965.
Phillips, S.L., Igbene, A., Fair, J.A., Ozbek, H. and Tavana, M. (1981) A technical databook for geothermal energy utilization, Lawrence Berkeley National Laboratory, p. 46.
Roedder, E. (1972) Composition of fluid inclusions.
Semenyuk, E.N., Zarembo, V.I. and Fedorov, M.K. (1977) Apparatus for measuring viscoisties of electrolyte-solutions at temperatures of 273-673 K and pressures up to 200 MPa. Journal of Applied Chemistry of the USSR 50, 298-302.
Sourirajan, S. and Kennedy, G.C. (1962) The system H_2O-NaCl at elevated temperatures and pressures. Am. J. Sci. 260, 115-141.
Steele-MacInnis, M., Han, L., Lowell, R.P., Rimstidt, J.D. and Bodnar, R.J. (2012) The role of fluid phase immiscibility in quartz dissolution and precipitation in sub-seafloor hydrothermal systems. Earth Planet. Sci. Lett. 321, 139-151.
Tanger, J.C. and Pitzer, K.S. (1989) Thermodynamics of NaCl-H_2O: A new equation of state for the near-critical region and comparisons with other equations for adjoining regions. Geochim. Cosmochim. Acta 53, 973-987.
Valyashko, V.M. (2008) Hydrothermal Properties of Materials. Wiley.
Wagner, W. and Pruß, A. (2002) The IAPWS formulation 1995 for the thermodynamic properties of ordinary water substance for general and scientific use. Journal of Physical and Chemical Reference Data 31, 387-535.

Watson, J.T.R., Basu, R. and Sengers, J.V. (1980) An improved representative equation for the dynamic viscosity of water substance. Journal of Physical and Chemical Reference Data 9, 1255-1290.
Weis, P., Driesner, T., Coumou, D. and Geiger, S. (2014) Hydrothermal, multiphase convection of H_2O-NaCl fluids from ambient to magmatic temperatures: a new numerical scheme and benchmarks for code comparison. Geofluids 14, 347-371.
Wood, J. and Hewett, T. (1982) Fluid convection and mass transfer in porous sandstones - a theoretical model. Geochim. Cosmochim. Acta 46, 1707-1713.
Yardley, B.W. and Bodnar, R.J. (2014) Fluids in the Continental Crust, Geochemical Perspectives. European Association of Geochemistry, p. 127.

8. Tables

Table 1. Summary of experimental data for the viscosity of H_2O and H_2O-NaCl fluid

Salinity (wt. % NaCl)	Temperature (°C)	Pressure (bars)	Method	Uncertainty (%)	Number of data points	Reference
0.03-27.5	0-154	1-389.8	n.p.	n.p.	1161	(Ozbek et al., 1977)
0-6.8	0-300	100-1500	CAP	2	110	(Semenyuk et al., 1977)
0-24.7	10-40	1-311.6	OSD	0.3	166	(Kestin et al., 1977)
1-20	20-350	2-300	CAP	0.3	186	(Pepinov et al., 1978)
2.7-24	18-154	1-311.6	OSD	0.3	189	(Kestin et al., 1978)
0.6-6.5	5-95	1	Ub	0.02	60	(Out and Los, 1980)
5.9-26.1	24-201.5	1-321	OSD	0.2	381	(Kestin and Shankland, 1984)
0.1-26	20	1	n.p.	n.p.	23	(Haynes, 2014)
100	800-975	1	OSC	2.4	40	(Ito et al., 1989)

OSD: oscillating disc, Ub: Ubbelohde, CAP: capillary, n.p: not provided

Table 2. Coefficients for Equation (4)

	Value
a_1	-35.9858
a_2	0.80017
b_1	1e-6
b_2	-0.05239
b_3	1.32936

10. Figures

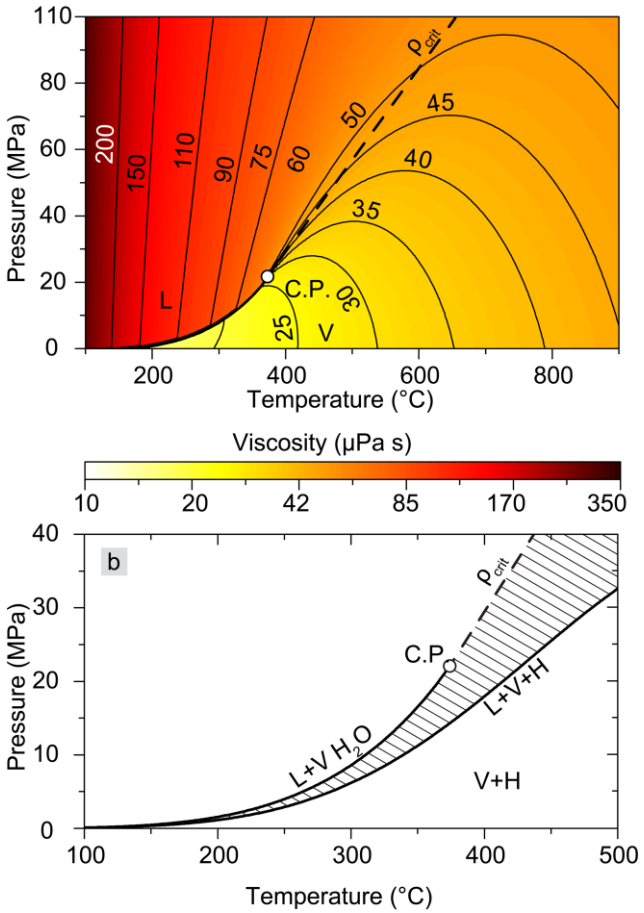

Figure 1. (A) Viscosity of pure H_2O in the PT range 0-100 MPa and 100-900 °C calculated using the Huber et al. (2009) model. C.P. is the critical point (373.946 °C, 22.064 MPa), L refers to the liquid phase (density greater than the critical density), V refers to the vapor phase (density less than the critical density), and ρ_{crit} indicates the critical isochore. (B) Pressure-Temperature plot showing the liquid-vapor coexistence curve of pure water (L+V H_2O) that terminates at the critical point (C.P.) and the critical isochore for H_2O (dashed line labeled ρ_{crit}). Also shown is the vapor + liquid + halite equilibrium curve (L+V+H) for H_2O-NaCl, and the field in which an H_2O-NaCl vapor phase and halite are in equilibrium (V+H). The hatched region defined by pressures less than the H_2O liquid-vapor curve and pressure along the critical isochore, and pressures greater than the pressure on the L+V+H curve identifies the region of PT space in which the P&M model may predict viscosities that are too low owing to the fact that in this PT region H_2O is a vapor (density less than the critical density) whereas many H_2O-NaCl compositions are liquid in this PT region.

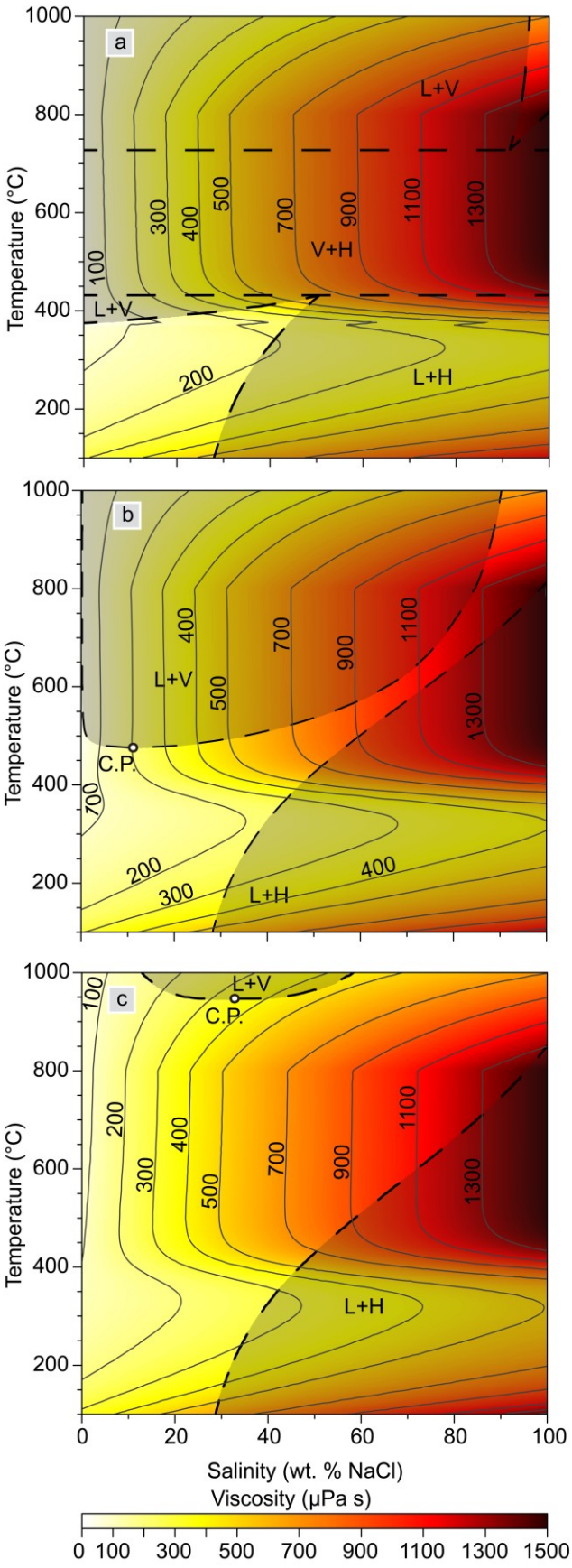
a
b
c
Temperature (°C)
Salinity (wt. % NaCl)
Viscosity (μPa s)
L+V
V+H
L+H
C.P.
0 100 300 500 700 900 1100 1300 1500

Figure 2. Viscosity of H_2O-NaCl fluids at 22 (A), 50 (B), and 200 (C) MPa in Temperature-Salinity (Tx) space calculated from the P&M model. The shaded regions in the lower right of the diagrams outlined by dashed lines represent the regions of Tx space in which two phases, either liquid + vapor (L+V) or liquid + halite (L+H), coexist and the model is not applicable in these regions of T-x space.

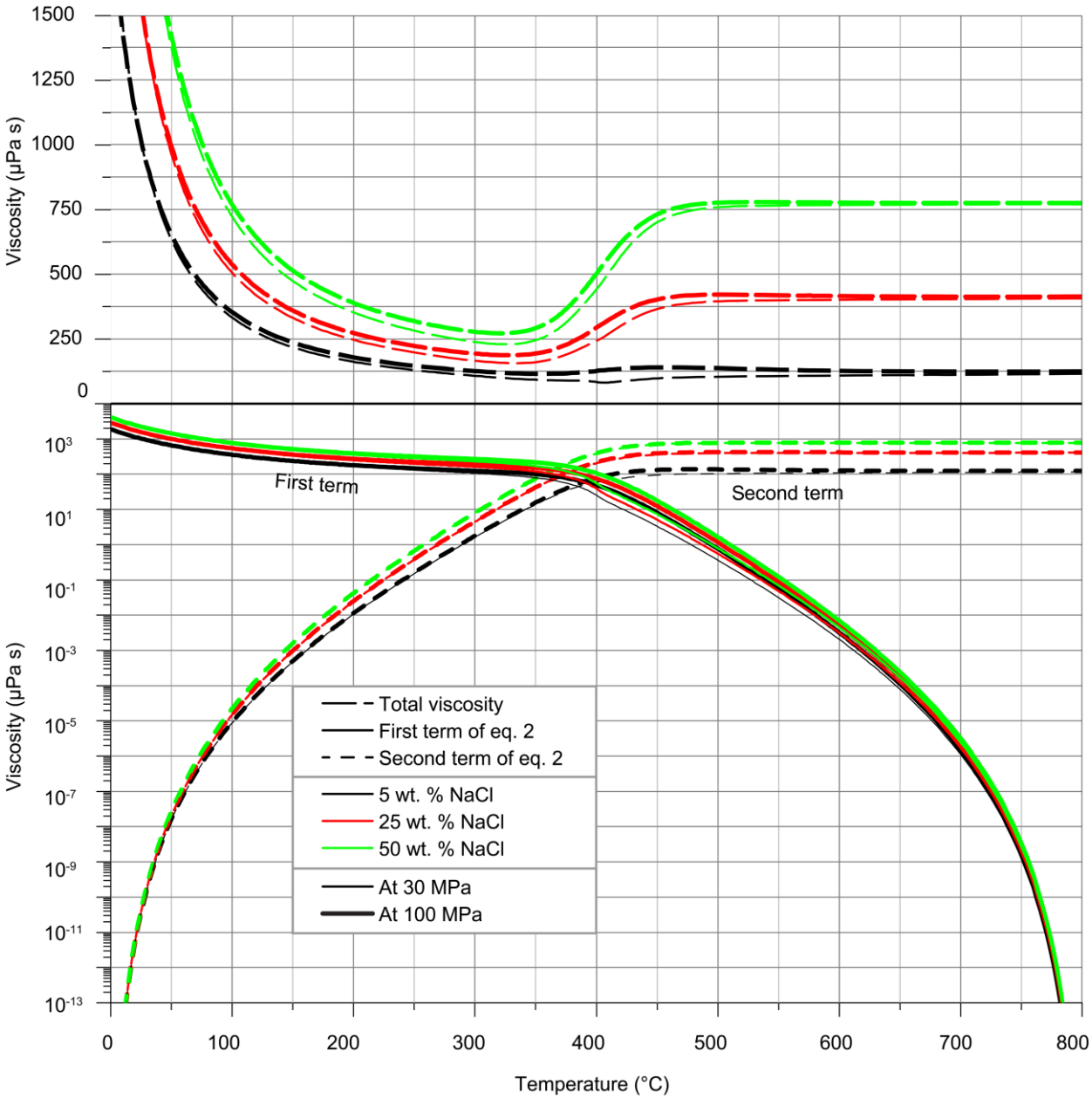

Figure 3. (top) Viscosity as a function of temperature predicted by equation (2) (P&M model) at 30 and 100 MPa for salinities of 5, 25 and 50 wt. % NaCl. (bottom) Contributions of the first (solid lines) and second (dashed lines) terms of equation 2 to the total viscosity (shown by dashed lines on the top graph) at different pressure and composition conditions. Note that the total viscosity is dominated by the contribution from the first term of equation 2 at temperatures less than about 400 °C and is dominated by the contribution from the second term of equation 2 at temperatures greater than about 400 °C.

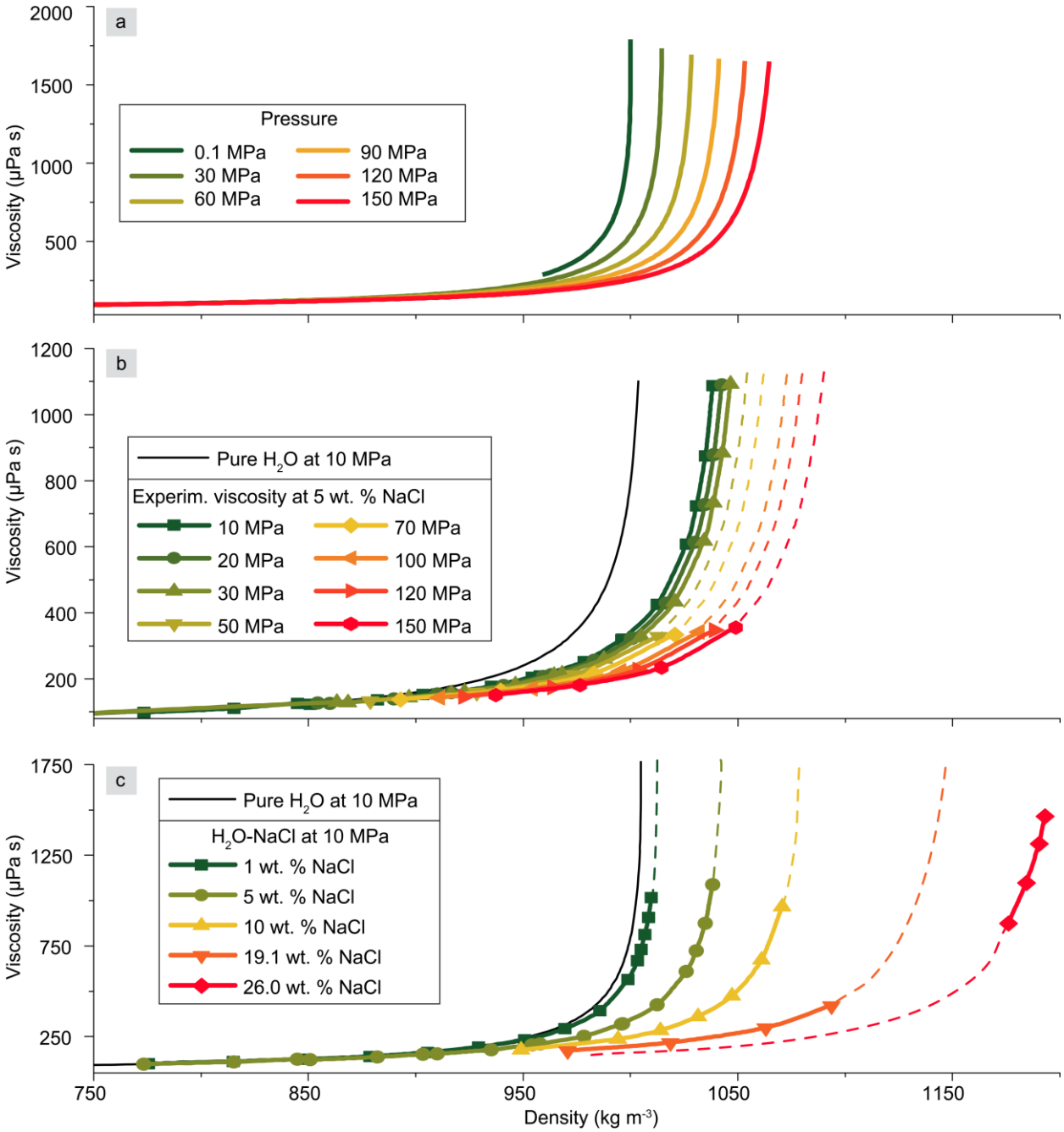

Figure 4. (A) Dynamic viscosity of H_2O as a function of density at various pressures calculated from the Huber et al. (2009) formulation; (B) experimentally determined viscosity as a function of density for a 5 wt. % NaCl solution at various pressures (Pepinov et al., 1978; Semenyuk et al., 1977). Dashed lines are viscosities calculated by the revised model and show the expected behavior of the viscosity as a function of PTx conditions; (C) experimentally determined viscosity at 10 MPa as a function of density for various salinities (Kestin and Shankland, 1984; Pepinov et al., 1978; Semenyuk et al., 1977). Dashed lines are viscosities calculated by the revised model and show the expected behavior of viscosity as a function of Pρx conditions. Note that a, b and c have different viscosity (Y) scales.

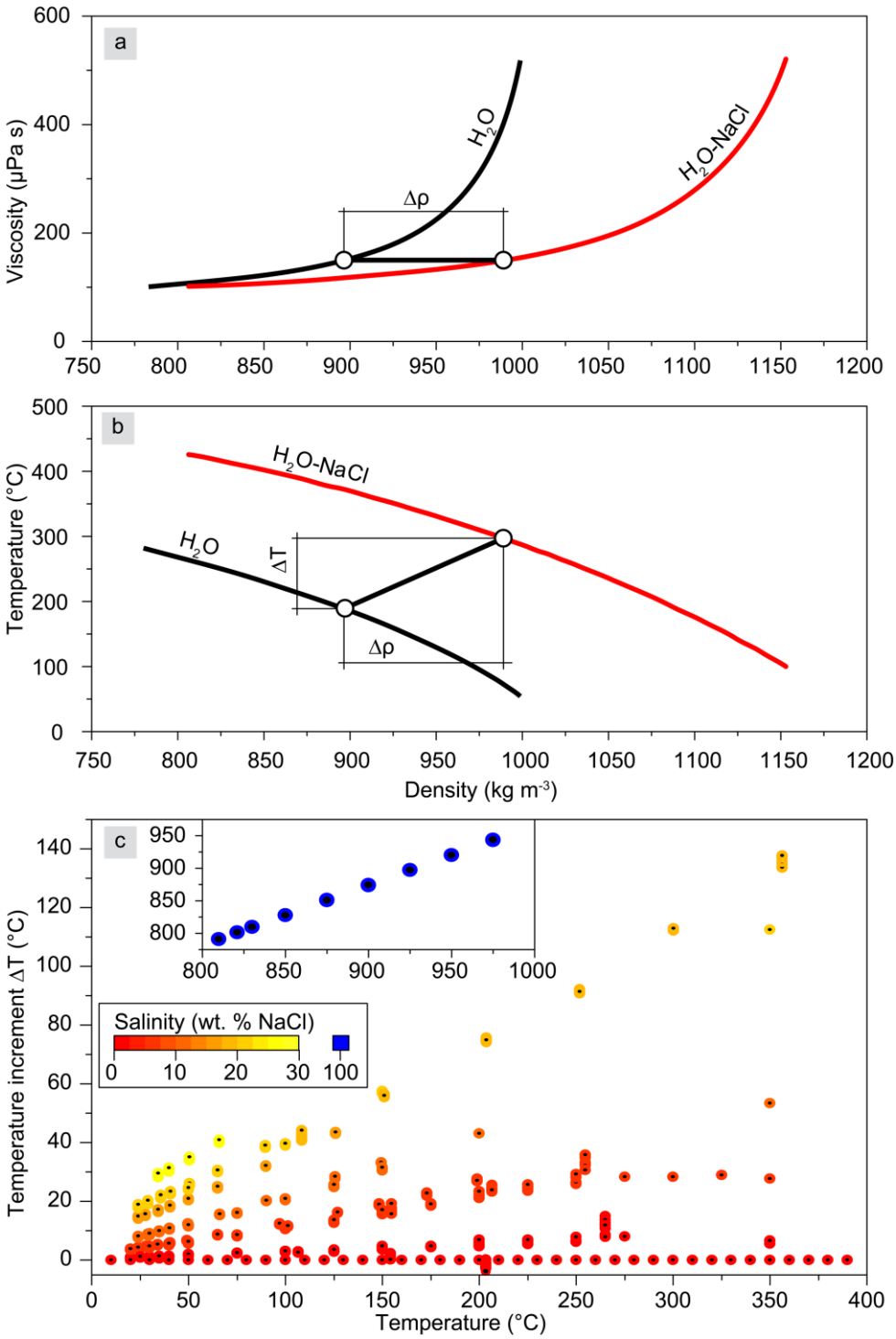

Figure 5. (A) Schematic representation showing the viscosity of pure H_2O (black line) and that of an H_2O-NaCl solution (red line), both as a function of density at the same pressure. A line connecting two iso-viscosity points on the two different curves defines the difference in density, $\Delta\rho$, of the two fluids having the same viscosity; (B) Temperature as a function of density for pure H_2O (black line) and for the same H_2O-NaCl fluid (red line) as in (A), plotted along isobars. The difference in density $\Delta\rho$ defined by the viscosity-density plot in (A) is converted into a temperature difference, ΔT; (C) The temperature increment, ΔT, plotted as a function of

temperature for various salinities obtained from experimental studies. The inset shows ΔT for pure liquid NaCl.

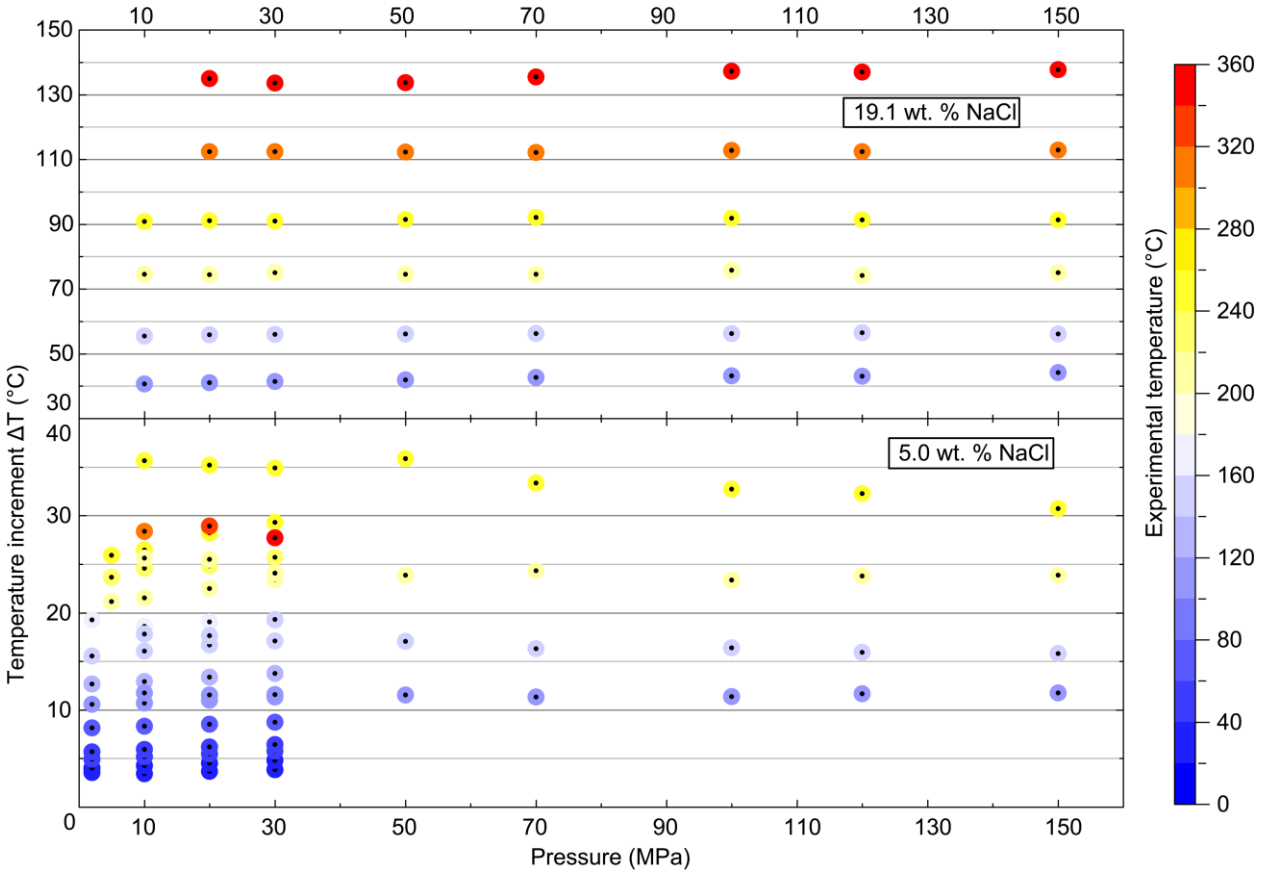

Figure 6. Temperature increment, ΔT, for various experimental temperatures as a function of pressure using data from (Pepinov et al., 1978; Semenyuk et al., 1977). ΔT does not show a pressure dependence; thus, Equation (3) can be used to calculate viscosities of H_2O and H_2O-NaCl fluids at constant pressure for input into Equation (3).

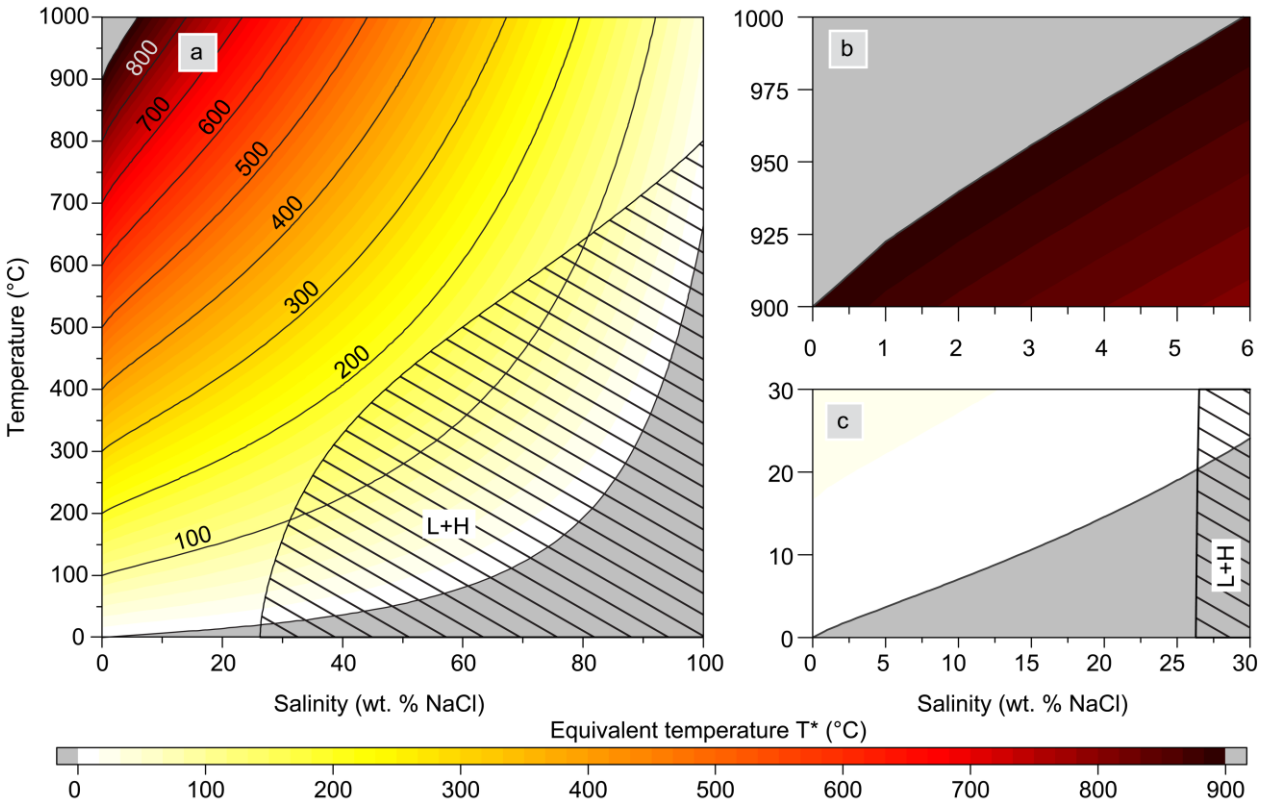

Figure 7. (A) T* calculated using Equations (4-6) plotted as a function of temperature and salinity. The grey shaded region indicates the region of Tx space in which T* is outside of the range in which the model of Huber et al. (2009) is valid. The hatched region represents the field in which liquid and halite (L+H) coexist.– (B) enlargement of the low salinity, high temperature region of Tx space where T* >900 °C (grey color) and the model described here is not valid. (C) enlargement of the high salinity, high temperature region of Tx space where T* ≤0.01°C °C (grey color) and the model described here is not valid.

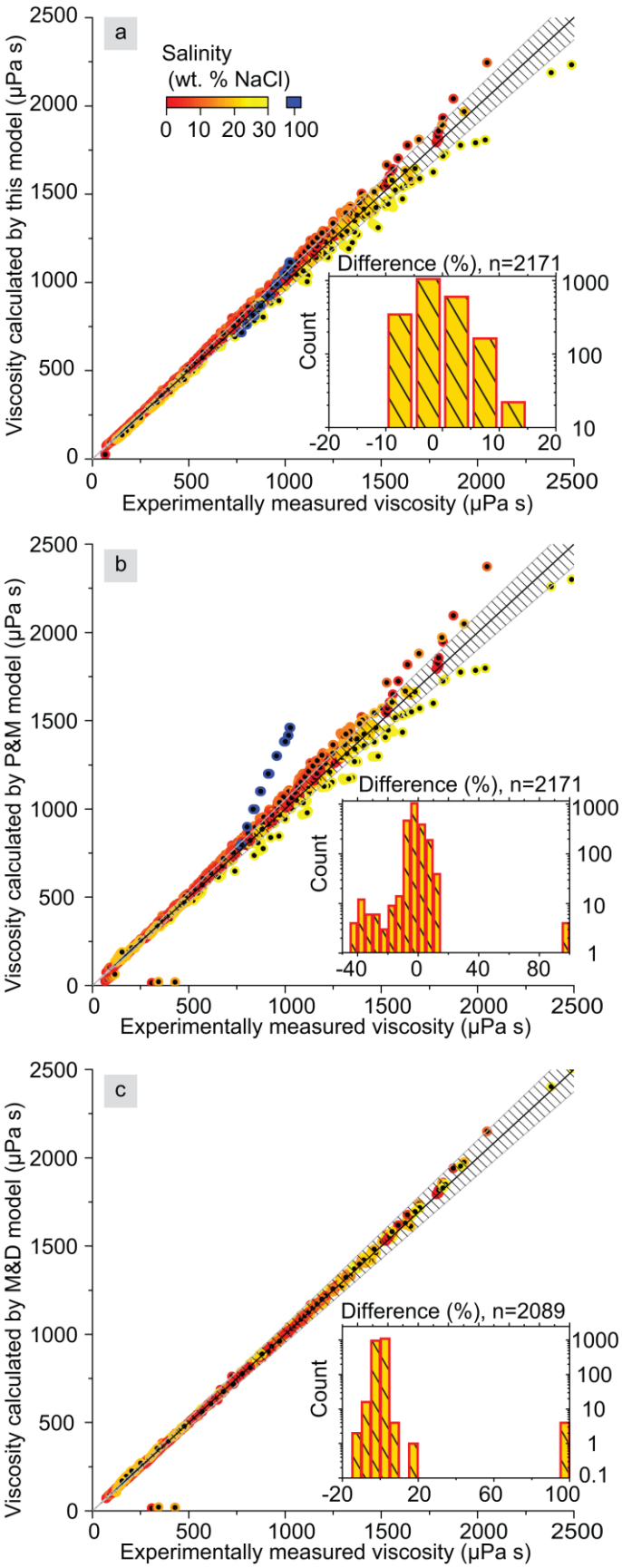
a
Salinity
(wt. % NaCl)
0 10 20 30 100
Difference (%), n=2171
Count
Viscosity calculated by this model (μPa s)
Experimentally measured viscosity (μPa s)
b
Difference (%), n=2171
Count
Viscosity calculated by P&M model (μPa s)
Experimentally measured viscosity (μPa s)
c
Difference (%), n=2089
Count
Viscosity calculated by M&D model (μPa s)
Experimentally measured viscosity (μPa s)

Figure 8. Relationship between experimentally determined viscosities of H_2O-NaCl and viscosity calculated by the revised model (A) the P&M model (B) and the Mao and Duan (2009) model (C). Experimental data are from the various studies listed in Table 1. Black line indicates 1:1 correlation, and the hatched region along the 1:1 line represents ±5 % difference from the 1:1 correlation. The color scale indicates the salinity. The histograms shown in insets show the percent difference between model predicted and experimental results (calculated for n points), calculated according to equation (7). Note the different scales for both axes on the different histograms.

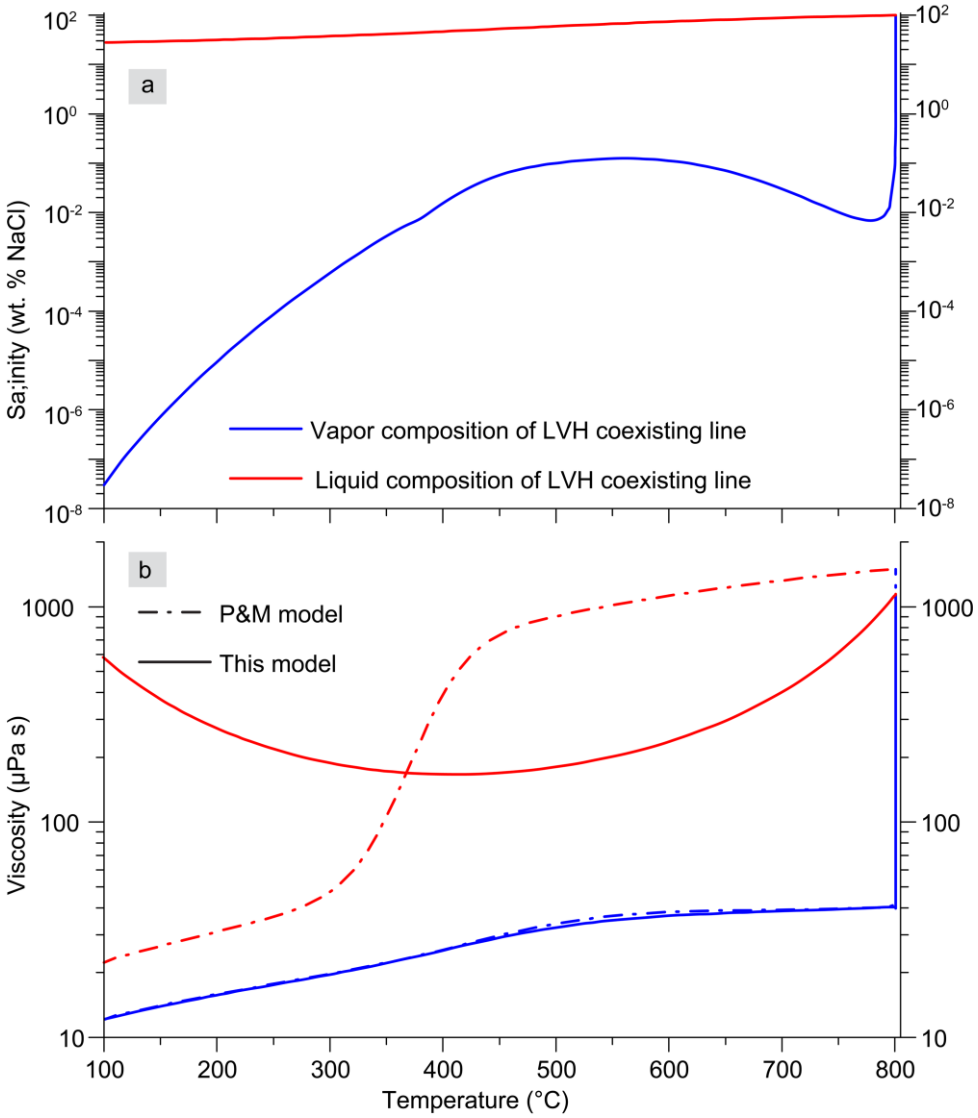

Figure 9. (A) Salinity of the vapor (blue line) and liquid (red line) phases in equilibrium with halite along the liquid-vapor-halite coexistence curve (L+V+H; see Figure 1b), calculated using the Driesner (2007) EOS. (B) Dynamic viscosity of the liquid and vapor phases along L+V+H curve shown in (A), calculated using the P&M model (dashed lines) and the revised model developed here (solid lines).

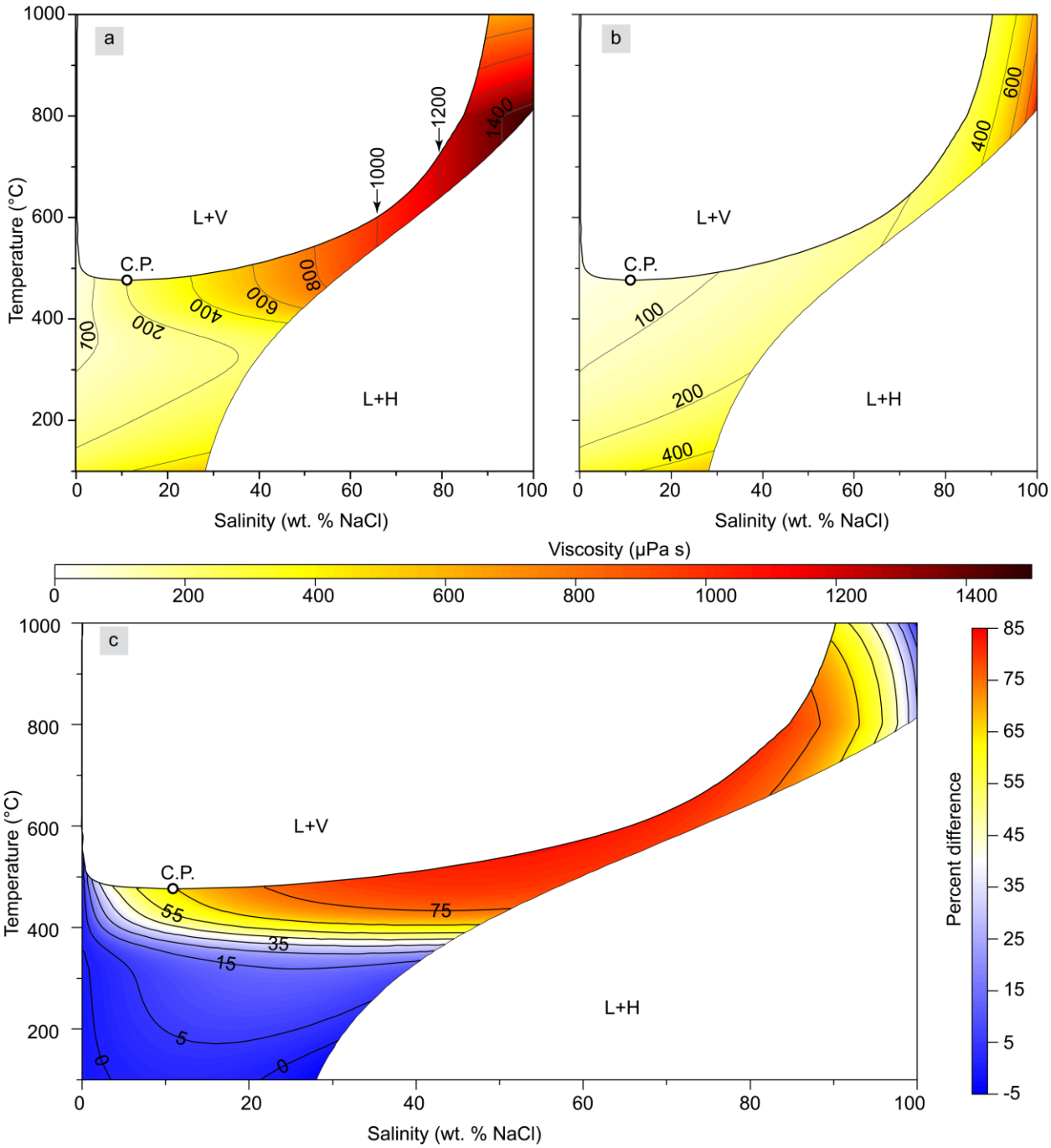

Figure 10. (A) Dynamic viscosity of H_2O-NaCl fluids calculated using the P&M model. (B) Dynamic viscosity of H_2O-NaCl fluids calculated with the present model. (C) Percent difference between viscosity predicted by the P&M model and the current model for various temperature and salinity conditions at 50 MPa. L+H represents the field in which liquid + halite coexist, L + V is the region in which liquid + vapor coexist. Small open circle labeled C.P. represents the critical point corresponding to the pressure of interest (50 MPa).

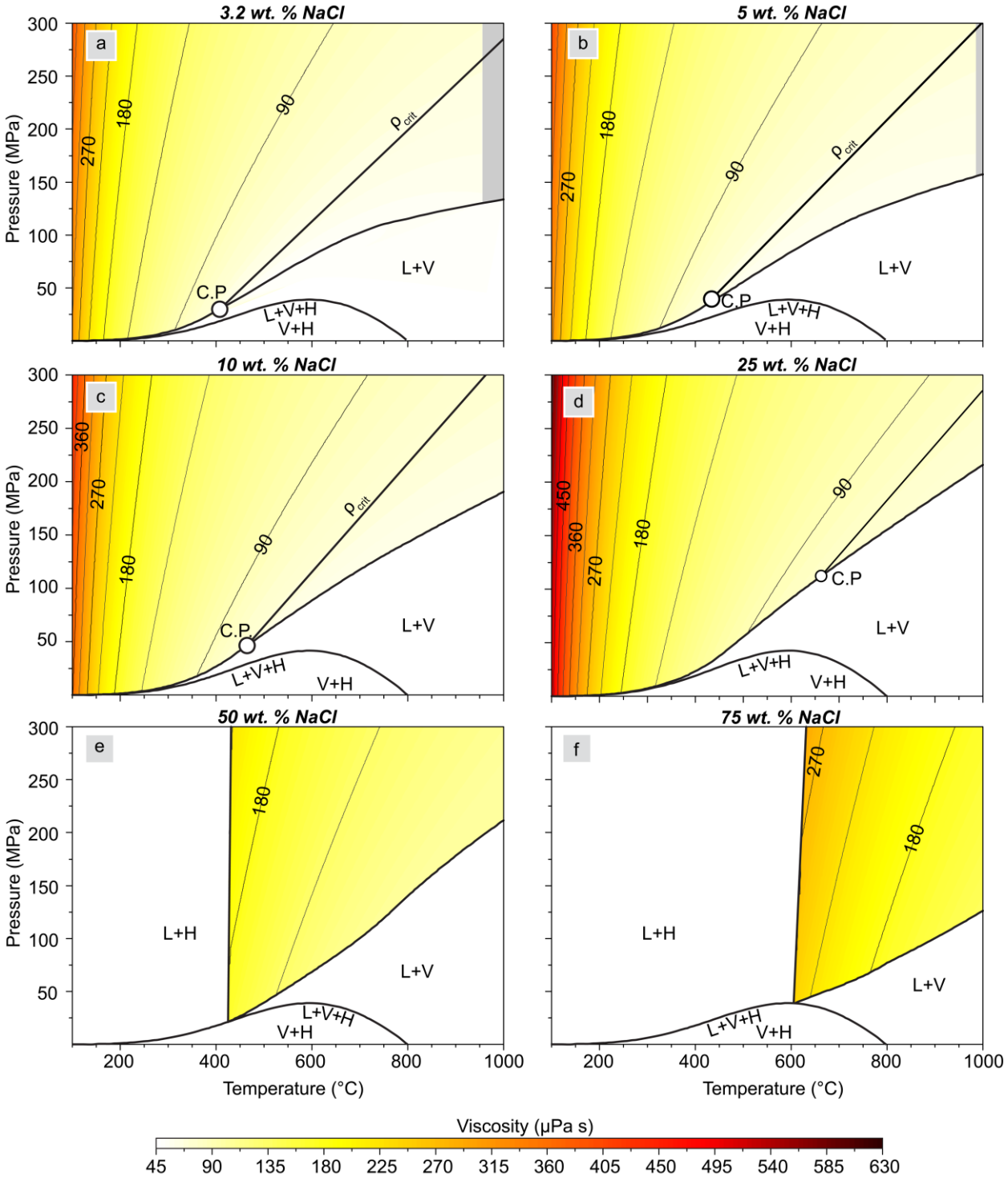

Figure 11. Dynamic viscosity calculated by the current model for salinities of 3.2, 5, 10, 25, 50 and 75 wt. % NaCl at pressures between 0 and 300 MPa. The grey region indicates the region where equivalent temperature T* is above 900 °C and the current model is not valid, L+V+H indicates the phase boundary along which liquid + vapor + halite coexist, V+H indicates the field in which vapor + halite coexist, L+V represents the region in which liquid + vapor coexist, and L + H indicates the region in which liquid + halite coexist. C.P. represents the critical point, and the line labeled ρ_{crit} that originates at the critical point represents the critical isochore.

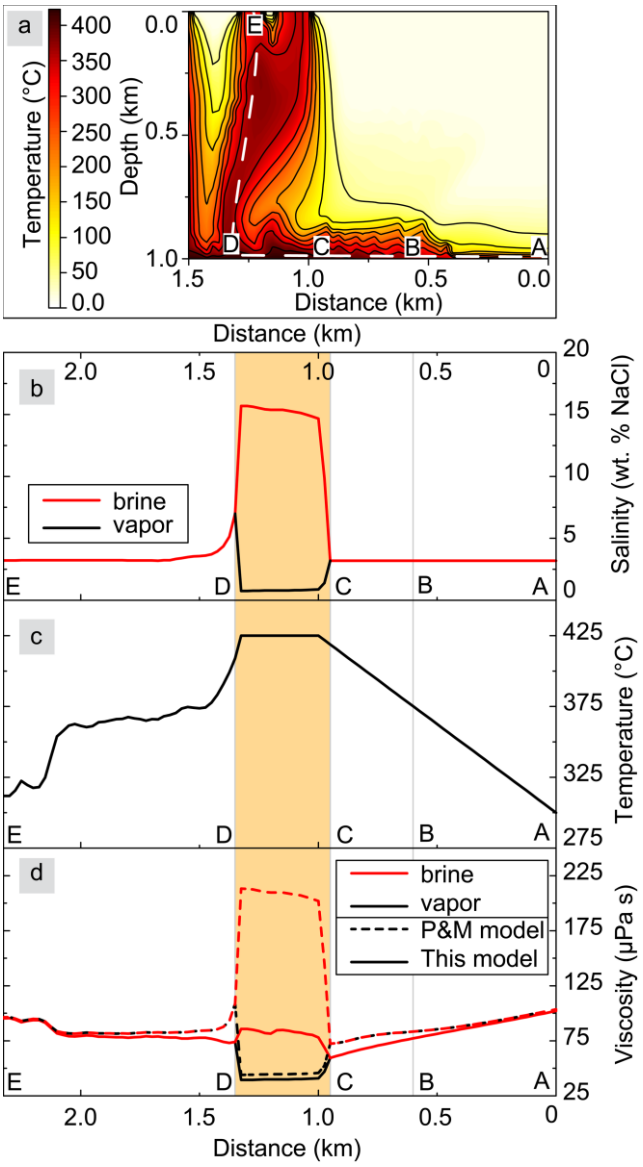

Figure 12 (A) The temperature distribution in the sub-seafloor at 80 years after emplacement of a magma body at a mid-ocean ridge (MOR) hydrothermal system from Steele-MacInnis et al. (2012). The top of the cross section represents the seafloor and the bottom left represents the center of the heat source that is beneath the lowest level shown. The letters A-E indicate points along the flow path with immiscibility occurring in the region C-D. Variation in salinity (B) temperature (C) and viscosity (D) of a hydrothermal fluid as it flows along the PT path in the subsurface at a mid-ocean ridge hydrothermal system. Immiscibility in the region C-D produces a high salinity, high-density brine and a low salinity, low-density vapor. Viscosities of the fluids along the flow path calculated from the revised model and the P&M model are shown as solid (revised model) and dashed (P&M) lines on d.

CHAPTER 3

This chapter is a scientific article in preparation to be submitted to ***Chemical Geology***

Physical and chemical conditions of emerald formation at the North American Emerald Mine, (North Carolina, USA)

Y.I. Klyukin [a], J.W. Miller [b], J Cox [c], and R.J. Bodnar [a]

[a] Department of Geosciences, Virginia Tech, 4044 Derring Hall, Blacksburg, VA 24061, USA
[b] Environmental Studies, University of North Carolina at Asheville, CPO 2330, Asheville, NC 28804, USA
[c] Department of Geology, University of Georgia, 210 Field Street, Athens, GA 30602, USA

Abstract

Emerald is a green variety of the beryl and is one of the most valuable gem minerals. Emerald deposits formed in diverse geological environments, and often origin of the deposit remains unknown or poorly characterized. North American Emerald Mine (NAEM), located in Hiddenite, North Carolina, USA, is one of the most significant emerald-producing sites in North America with more than 60,000 carats of emerald produced, including the 1,869-carat "NAEM Emerald" (19.5 cm length) and 858 carats "Empress Caroline". Gem-bearing pockets at NAEM located in the quartz veins. Quartz veins are discordant with hosting rocks - Devonian sillimanite grade metagraywacke rocks. We identified temperature and pressure of the formation, characterized the fluid composition and constrained possible sources of beryllium. The temperature of NAEM formation has been identified as 450-625 °C using stable isotopes of $\delta D/\delta^{18}O$ (450-520 °C) which overlapped with temperature range obtained from Raman carbonaceous material thermometry (450-625 °C). The $\delta^{18}O$ of the water estimated as ~11 ‰, the δD estimated approximately -55 ‰. This range of $\delta D/\delta^{18}O$ corresponds to either a peraluminous magmatic fluid source or a mixture of magmatic and metamorphic fluids. Pressure evaluated as 1.2-2.2 kbar, constrained by fluid inclusion analysis and temperature of the formation. The high density CO_2-H_2O±CH_4 fluid is responsible for emerald formation. The carbonaceous material has been found in mineral inclusions in emeralds and has been detected in albite/dolomite which formed in paragenetic association with the emerald. Up to 6 mol. % of CH_4 was detected in the vapor bubble of fluid inclusions at room temperature. CH_4 found only in the sample from the pocket with the "NAEM Emerald". We speculate that redox process, indicated by the presence of the carbonaceous material and CH_4 in the emerald is linked with the emerald formation. The absence of re-heating event evidence and tectonothermal history of the Cat Square terrane indicates that NAEM formation occurred after 315 MA during uplift and cooling of the Cat Square terrane.

Keywords:Cat Square terrane, Stable isotopes, Fluid inclusions, CO_2-H_2O-CH_4, Emerald

1. Introduction

The dark green variety of beryl ($Be_3Al_2Si_6O_{18}$) is referred to as emerald, and the color is the result of incorporation of trace amounts of Cr^{+3} and V^{+3} substituting for Al^{+3} in the beryl structure. The environment of formation of emerald deposits largely remains an enigma because Be required for beryl (emerald) formation tends to be more concentrated in felsic rocks or their metamorphic equivalents, while Cr and V are relatively more abundant in ultramafic/mafic rocks or their metamorphic equivalents. The differing geologic environments in which Be dominates compared to environments more favorable for Cr and V thus requires that felsic and mafic source rocks be located in close proximity to each other. Thus, according to Groat et al. (2008): "*unusual geologic and geochemical conditions are required for Be and Cr and/or V to meet. In the classic model, Be-bearing pegmatites interact with Cr-bearing ultramafic or mafic rocks"*.

Genetic classifications of emerald deposits generally distinguish between igneous-related (magmatic) and non-magmatic types. Igneous-related deposits include pegmatites and hydrothermal veins with a recognizable connection to granitic intrusions. Nonmagmatic types include deposits that may have an indirect connection to magmas or are associated with thrust/shear zones. However, some emerald deposits show characteristics common to both a magmatic and nonmagmatic origin. For example, (Marshall et al., 2016) characterized the Poona emerald deposit (Australia) as being enigmatic because it has characteristics of both magmatic and metamorphic origin. Based on similar cases Zwaan (2006) concludes: "*existing classifications are ambiguous and not particularly useful for understanding of the mechanisms and conditions that lead to formation of emerald".* Following this conclusion, Groat et al. (2008) suggested that stable isotopes (δD from beryl crystal channels and $\delta^{18}O$ of the beryl) could constrain the origin of the fluid and thus contribute to understanding deposit genesis.

Formation of the emerald deposits take place in wide range of PT conditions, geological settings and time. Giuliani et al. (2015) concluded that emerald deposits of magmatic origin are forming during oogenesis events, oldest deposits dated as early as Late Archean. Those of nonmagmatic origin formed in a result of fluid circulation in shear zones and thrust faults. Giuliani et al. (2015) defined sedimentary-metasomatic type which consists of Columbian emerald deposits exclusively. These deposits formed during convergence of Nazka and South American plates by circulation of basinal brines. Metamorphic-related deposits formed by fluid released during regional metamorphism, and demonstrate hydrothermal alteration.

In North Caroina emeralds found in Spruce Pine and near Hiddenite area. Emerald deposit at Spruce Pine occurs in biotite-chlorite schists and formed by fluid derived from desilicated Crabtree pegmatite.

The North American Emerald Mine (NAEM) (previously known as Rist mine and often referred to in the literature as Hiddenite) is located near Hiddenite, North Carolina, USA (Fig. 1C). The deposit was discovered in 1879 and is famous for the abundant green, gem-quality version of spodumene known as hiddenite as well as for deep-green emeralds (Mertie, 1959). Emerald production began in 1881, and the NAEM is considered to be the most significant North American emerald locality. The North American Emerald Mine has produced more than 60,000 karats, including the 1,869-carat "NAEM Emerald" (19.5 cm length) found in 2003, and now on exhibit at the Houston Museum of Natural Science. The mine operated between 1995 and 2012, after which it went on standby. Operations were continued for a short time in 2016 but the mine is currently inactive (as of October 2017).

Wise and Anderson (2006) studied the paragenesis and mineralogical composition at the NAEM deposit to develop a foundation for further studies of the deposit. These workers found

no evidence of a link between mineralization and an igneous intrusion. Wise and Anderson (2006) suggested that the NAEM formed at low pressure and temperatures in the range of 230-290 °C based on a preliminary study of fluid inclusions in vein quartz, reported by Lapointe et al. (2004). Boiling of an aqueous-carbonic fluid was suggested as the mechanism for the formation of emeralds at NAEM based on observations of platy calcite crystals, coeval quartz and abundance of open cavities (Wise and Anderson, 2006). In the present study, we extend these earlier studies of fluids responsible for emerald mineralization by characterizing the regional fluid inventory and comparing/contrasting regional fluids with fluids contained as fluid inclusions in emeralds and associated minerals from emerald-bearing pockets.

2. Geology

The North American Emerald Mine has hosted in sillimanite grade metamorphic rocks in the eastern Inner Piedmont (IP) Belt, Cat Square terrane. The Inner Piedmont Belt is one of the largest sillimanite grade terranes in the world (Merschat and Kalbas, 2002), extending from the Sauratown Mountain window, North Carolina, to the central Alabama Coastal Plain (Fig. 1A). Eastern IP Cat Square terrane rocks consist of aluminous schist and metagraywacke (Merschat et al., 2005) and have been dated as post-430 Ma. The Eastern Cat Square terrane is intruded by Devonian-Carboniferous age granitoids, including the Toluca (378 Ma), Cherryville Granites (375 Ma) and Walker Top (366 Ma, Fig. 1B, C) (Merschat et al., 2005). Several granitoids in the Cat Square terrane were described as being peraluminous (Merschat, 2009), including the Toluca, Walker Top and Cherryville Granites (Bier, 2001; Mapes, 2002; Merschat and Kalbas, 2002; Williams, 2000). In a later study (Byars, 2010) however, the Toluca and Walker Top Granites were identified as metaluminous, reflecting the compositional variability of the granites.

The NAEM deposit is hosted in sillimanite I metamorphic grade (sillimanite + muscovite) rocks (Byars, 2010), and is located within the Brindle Creek thrust sheet, between the Newton Window on the South/SouthEast and the Rocky Face (RF) granite pluton to the North/NorthWest. The RF pluton has been identified as part of the Toluca Granite complex based on petrographic and geochemical similarities (Goldsmith et al., 1988; Wilson et al., 2006). The Newton Window (NW) is a window within the Tugaloo terrane and is composed of biotite gneiss, biotite-hornblende gneiss, amphibolite and ultramafic rocks dipping to NorthWest and separated from the Cat Square terrane by the Brindle Creek fault. The NW has been dated as Cambrian by (Goldsmith et al., 1988) and as Mesoproterozoic in later studies (Merschat, 2009). Within a distance of ~3 km, the NAEM is flanked by two intrusions of Cherryville granite (Merschat, 2009). In describing the Brindle Creek thrust sheet, Hatcher (2002) concludes: "*The fact that the Walker Top and Toluca Granites are both catazonal plutons requires several millions to tens of millions of years for deposition and burial to depths where metamorphism at sillimanite-grade conditions and catazonal plutonism could occur. The maximum upper bound for the age of the paragneisses in the Brindle Creek thrust sheet thus may be 390 to 405 Ma… A subduction of the Tugaloo and Cat Square terranes beneath the Carolina terrane could provide the burial conditions needed to reach sillimanite-grade metamorphism by ~350 Ma and form the ~350 Ma plutonic suite*". Later studies assigned a Neoacadian (375-340 Ma) age for metamorphism in the Brindle Creek thrust sheet.

The country rocks in the vicinity of the NAEM are highly foliated biotite gneiss, interlayered with calc-silicate rocks. Sub-vertical massive Alpine fissure-type quartz veins are discordant with the country rocks. Quartz veins typically vary from 1 to 10 cm in width, rarely reaching 1.5

m. Some of the veins have cavities and some of the cavities are emerald bearing. Wise and Anderson (2006) identified four types of cavity assemblages: a) emerald-bearing (Fig. 2B); b) Cr-spodumene (hiddenite) cavities, characterized by clinochlore, graphite, pyrite, and chabazite-Ca; c) calcite-bearing (Fig. 2B); d) amethyst-bearing cavities. Quartz, muscovite and rutile are commonly observed in all cavities, while albite is observed only in emerald- and calcite-bearing cavities. Chabazite-Ca has been observed in Cr-spodumene- and amethyst-bearing cavities, which suggests later formation of these cavities because zeolite group minerals are only stable at low temperatures.

3. Methods

Samples were collected from emerald- and calcite-bearing cavities and from quartz veins located at various distances from the deposit to evaluate background (regional) fluid characteristics (Fig. 2A, Table 1). Double polished thick sections and mineral chips were prepared in order to conduct a detailed mineralogical and fluid inclusion (FI) study. Polished emerald chips and crystals were prepared by cutting crystals parallel to the *c* axis to preserve needle-shaped FIs elongated parallel to the *c* axis with length up to 0.5 mm. For carbonate minerals, cleavage chips were used to prevent leakage of FI during sample preparation (Goldstein, 2003).

Stable isotope analyses of δD, $\delta^{18}O$ and $\delta^{13}C$ were conducted in the Stable Isotope Laboratory in the Department of Geology at the University of Georgia. Carbon and oxygen from carbonate minerals were analyzed simultaneously, by reacting ~5 mg of each sample under vacuum in 100% phosphoric acid at 50 °C, producing CO_2 for further analysis. For $\delta^{18}O$ analysis of quartz, muscovite and rutile, samples were prepared by grinding to 1-2 mm, and a known mass of sample was reacted with BrF_5 under vacuum while heated with a variable power CO_2 laser (Synrad, 10.51-10.65 μm wavelength, 75W max power). The O_2 generated by the reaction is converted to CO_2 by reacting with heated graphite. δD was determined for finely ground muscovite from three cavities – one cavity was emerald-bearing and two did not contain emerald. The samples were dehydrated by heating with a gas torch under vacuum. The water generated during the dehydration reaction was collected in Pyrex tubes containing zinc granules, and the water and zinc in the sealed tubes were heated to 500 °C to produce H_2 gas. Both CO_2 and H_2 gas samples were analyzed on a Finnigan MAT 252 mass spectrometer along with CO_2 and H_2 generated from standard reference materials (UWG and NB2-28 for $\delta^{18}O$ and VSMOW and SLAP reacted with zinc under the same conditions as the samples for $\delta^{2}H$). For CO_2 generated from carbonate minerals, the laboratory standards were prepared and analyzed with each batch of samples.

Fluid inclusions were selected for analysis following the rigorous Fluid Inclusion Assemblage (FIA) protocol (Goldstein and Reynolds, 1994). As such, detailed petrographic examination was used to identify groups of fluid inclusions that were trapped at the same time. Most FIAs were composed of secondary inclusions trapped along well-defined fractures and, less commonly, were represented by isolated groups of FI or FI along growth features in crystals (Fig. 3). FIs in quartz usually have negative crystal shape, while FIs in other minerals (carbonates, rutile, tourmaline, apatite, emerald) have an irregular shape. FI in emerald are elongated along the c axis of the crystals and are interpreted as being primary based on growth features. Compositionally the FI contain mostly either high- or low density CO_2 and a smaller proportion of H_2O. H_2O-rich FIs are uncommon and are only observed in quartz and calcite.

Microthermometry was carried out on a Linkam THMS 600 heating/freezing stage in the Fluids Research Laboratory at Virginia Tech. The stage was calibrated at the melting temperature of solid CO_2 at -56.6 °C and the critical temperature of CO_2 at 31.1 °C using H_2O–CO_2 synthetic fluid inclusions (Sterner and Bodnar, 1984). The stage was calibrated at the critical temperature of H_2O (~374 °C) using pure H_2O synthetic inclusions at higher temperatures. Due to the abundance of CO_2-rich FI in all samples, most of the measurements were limited to temperatures less than about 35 °C to avoid decrepitation.

Raman spectroscopic analyses were conducted in the Vibrational Spectroscopy Laboratory in the Department of Geosciences at Virginia Tech using a JY Horiba LabRam HR (800 mm) spectrometer, with 1800 grooves/mm gratings and a slit width of 150 lm. The confocal aperture was set at 400 lm. Excitation was provided by a 514.57 nm Laser Physics 100S-514 Ar^+ laser. The instrument was calibrated at the beginning of each session using the peak position for metallic silicon, and peaks for Ne were collected simultaneously with the inclusion spectrum during analysis of individual inclusions. The density of CO_2 in FI was determined based on the temperature of homogenization of CO_2 (T_h^{CO2}) and based on the Fermi diad splitting (Fig. 4A). Density was obtained from $T_h^{CO}{}_2$ using PVT data for CO_2 in the NIST standard reference database (Lemmon et al., 2013). Densities were obtained from the measured Fermi diad using the relationship developed by Lamadrid et al. (2017). Some samples contained solid inclusions of carbonaceous material (CM) and as well as CM trapped in FIs. Raman thermometry was performed according to Beyssac et al. (2002) to estimate the formation temperature based on the ratio of D_1, D_2, and G peak areas (Fig. 4C). The temperature dependence of CM peak characteristics is shown in Fig. 4D, and the two highlighted CM spectra at 443° and 604°C are similar to Raman spectra commonly observed in NAEM samples as shown in Fig. 4C.

Elemental analysis of the fluid inclusions was carried in the LA-ICP-MS lab at Virginia Tech using an Agilent 7500ce quadrupole ICP-MS coupled to a Coherent GeoLasPro 193nm excimer laser ablation system. NIST610 standard reference material glass was used as the analytical standard and was analyzed two times at the beginning and end of each analytical session. Isotopes (elements) analyzed included ^{7}Li, ^{9}Be, ^{11}B, ^{23}Na, ^{25}Mg, ^{27}Al, ^{28}Si, ^{39}K, ^{40}Ca, ^{49}Ti, ^{51}V, ^{52}Cr, ^{55}Mn, ^{56}Fe, ^{85}Rb, ^{88}Sr, ^{140}Ce and ^{153}Eu. Data were reduced using AMS software (Mutchler et al., 2008) assuming a 5 wt. % salinity for the fluid inclusions. LA-ICP-MS analyses were performed on FI hosted in rutile, emerald, quartz, and dolomite, but the only FI in quartz provided results that could be quantified. In all cases the concentrations of elements analyzed was below the detection limit in CO_2-rich inclusions.

4. Results

Owing to the lack of newly-discovered, undisturbed cavities at the NAEM during the course of this study, we were unable to conduct detailed studies of the mineral paragenesis. Thus, we adopt the generalized paragenetic association for cavity mineralization described by (Wise and Anderson, 2006) for emerald- and calcite-bearing cavities (Fig. 2B).

A quartz sample (NAEM030916-4; Fig. 2A,) collected east of the open pit contained sillimanite needles, which is indicative of sillimanite grade regional metamorphism (Merschat, 2009). This quartz vein is not related to emerald/hiddenite mineralization at the NAEM deposit and presumably formed prior to NAEM mineralization. This sample is assumed to represent quartz generation Q_0 which we included in the paragenetic association of Wise and Anderson (2006) (Fig. 2B). Q_0 quartz is fine-grained with inclusions of rutile aggregates that are <2 mm

long. Most quartz samples collected from the open pit or provided by the mine operator are identified as Q_2 and Q_3 generations. Two samples of calcite-bearing cavity material were collected. One sample (HID2015-12) was collected from a pocket on the eastern side of the open pit, and the other sample (HID2015-18) was provided by the mine operator and was collected from an unspecified location in the pit. The samples contain muscovite, rutile, and quartz in addition to calcite. One sample (HID2016-19) was collected from a newly discovered emerald pocket hosted in saprolite a few hundred meters from the main pit and contained muscovite, emerald, quartz, rutile, tourmaline, and quartz.

5. Characterization of fluid and solid inclusions

5.1 General Characteristics

Fluid inclusion analysis revealed 3 common fluid inclusion types: (1) low density CO_2 (Fig. 3A-E; G-I), (2) high density FIs containing both liquid and vapor CO_2 at room temperature (Fig. 3F); both of these types contain less than 20 vol. % H_2O. The third type contains a low to moderate salinity aqueous solution and a vapor bubble, and are observed in quartz and calcite only. The CO_2-bearing FIs are the most common types in all samples except calcite, where H_2O-NaCl FIs are dominant (Fig. 3J).

The salinity of the aqueous phase in CO_2-rich inclusions ranges from 0-4 eq. wt. % NaCl based on a few observations of clathrate melting in dolomite and rutile from sample HID2016-19. In other samples, the salinity could not be estimated owing to lack of visible H_2O during an examination at room temperature or lack of clathrate formation during cooling. Aqueous FIAs without detectable CO_2 are hosted in Q_2 quartz and have salinity between 4.5-7 eq. wt. % NaCl. A single FIA in Q_3 quartz (HID2016-19) has salinity ≤9.9 eq. wt. % NaCl.

The bulk density of CO_2-rich FIs was estimated by assuming that the inclusions contain between 10-30 vol. % of the aqueous phase based on the observation that a thin film of water is sometimes observed along the walls or in "fingers" extending from the main FI in irregularly shaped FIs. The salinity of aqueous (non-CO_2-bearing) FI was calculated using equations in Bodnar and Vityk (1994), and density of the fluid was calculated using the SoWat model (Driesner, 2007). Isochores for CO_2-H_2O inclusions were calculated using the Fluids program in the Perplex software package (Connolly, 2009).

Solid inclusions of the carbonaceous material (CM) were observed in emerald as well as in albite and dolomite formed in paragenetic association with emerald (sample Spear-8). Solid inclusions identified, as well as daughter/trapped minerals in FI, are listed in Table 2.

6. Distribution of fluid and solid inclusions according to host phase

6.1 Emerald

Emeralds contain FIAs composed of primary, ≤0.5 mm long needle-like shaped FIs that are aligned parallel to the *c* axis (**Fig. 3G**), as well as randomly oriented secondary FI (Fig. 3H). Primary FIAs in some samples are accompanied by solid inclusions of carbonaceous material (CM, Raman spectra Fig. 4C), and CM may also be present in FIs as a trapped phase (Fig. 3G). CM is found mostly in emerald, but in sample Spear 8 solid inclusions of CM occur not only in emerald but also in coexisting dolomite and albite and along grain boundaries. Secondary FIAs

in emerald have compositions similar to primary FIAs – with high density CO_2 and sometimes containing a small fraction of water (Fig. 3H). The density of CO_2 in emerald-hosted FIs ranges from 0.55 to 0.95 g cm^{-3} (Fig. 5B).

Raman analysis of FI in emerald from sample NAEM030619-8 (this sample came from the same cavity that produced the 1,869-carat "NAEM Emerald") indicated the presence of 4-7 mol. % CH_4 and 93-96 mol. % CO_2 in inclusions that also contained CM. Other emerald samples do not show the presence of methane. The presence of CM indicates that the emerald-forming fluid is carbon saturated and that the fluid is relatively reducing. The C-O-H fluid composition for FI in quartz, rutile, and emerald is shown in Fig. 7A, assuming 20 vol. % H_2O in the FIs. The position of the carbon saturation surface depends on both temperature and pressure; the carbon-saturated curve moves towards the H_2O apex as temperature decreases, while a decrease in pressure has the opposite effect. Thus, a high temperature carbon-saturated fluid may become oversaturated in carbon during cooling and would precipitate CM. Secondary FIs in emerald do not show detectable CH_4 or CM, indicating the evolution of the fluid towards more oxidizing conditions.

The temperature of formation of CM in emerald (HID2016-19, NAEM030916-8, and Spear_8) and in albite and dolomite formed in genetic association with emerald (Spear_8) was evaluated by Raman CM thermometry. Estimated temperature varies between 450-625 °C for CM in emerald, and 500-625 °C for CM in albite/dolomite (Fig. 8A, inset). Using this temperature constraint and the isochores for the FI determined as described above to determine a pressure correction indicates a pressure of emerald formation of 1.2-2.2 kbar.

6.2 Quartz

FIs from different quartz generations show no significant or systematic differences in composition. The density of CO_2 in Q_0, Q_2, and Q_2/Q_3 generation quartz shows two dominant ranges in density (Fig. 5C). One is characterized by low density (0.1-0.4 g cm^{-3}) and the other has a higher density (0.6-0.95 g cm^{-3}). Low density CO_2-rich FI and aqueous FI are observed only in quartz (Fig. 5, Table 3), indicating that a low density CO_2–rich fluid and an aqueous fluid are not associated with emerald formation. Aqueous inclusions hosted in quartz that were analyzed by LA-ICP-MS show three distinct fluid types: NaCl-dominated, $CaCl_2$-dominated and KCl-dominated. Using the temperature constraint obtained from CM Raman thermometry and from the stable isotope study described below, the pressure of formation is 1-2.3 kbar for the high density FI, and 0.8-1.7 for the low density CO_2-rich fluid inclusions (Fig 6A).

6.3 Dravite

A single dravite crystal (HID2016-19) examined contains zircon inclusions near the base of the crystal that led to fracturing of the tourmaline around inclusions. Only one FIA was observed in the crystal (Fig. 3B) and it is characterized by high pressure CO_2-rich fluid inclusions (Fig. 5A, Table 3).

6.4 Rutile

A rutile sample (HID2016-19) contains large cavities (>5 mm in length) in the center of the crystal that, presumably, represents a FI that leaked following trapping. This observation is

supported by an abundance of FIs >50 μm forming a decrepitation halo (Fig. 3E) around the original FI and the presence of high-density CO_2-rich fluid inclusions (Fig. 3C, Fig. 5A).

6.5 Carbonates

Dolomite contains CO_2-rich FIs, often containing visible H_2O (Fig. 3I). Density varies between 0.6-1.0 g cm^{-3}. Calcite hosts only aqueous fluid inclusions, which either contain only liquid or with small bubbles that homogenized at temperatures <70 °C (Fig. 3J), indicating the formation of the calcite in a low-temperature environment (assuming that the pressures are not unusually high).

6.6 Apatite

Only one sample of apatite was studied (NAEM09.9), represented by a crystal <4 mm in length. The apatite crystal hosted only a few FIAs, two of which were analyzed (Fig. 5A) and found to contain high density CO_2-rich FIs.

7. Stable isotopic composition of minerals

Textural relationships observed in hand samples and in thin sections suggest that the minerals quartz, rutile and muscovite from both the emerald-bearing cavity (HID2016-16) and from the calcite-bearing cavities (HID2015-9, HID2015-12) were formed contemporaneously and in equilibrium. This result allowed us to constrain the formation temperature and original $\delta D/\delta^{18}O$ of the fluid using known isotopic partitioning between quartz-rutile and muscovite-rutile pairs, and between these minerals and water. Mineral/water isotope fractionation factors (Friedman and O'Neil, 1977) were used to calculate the temperature at which the $\delta^{18}O$ of the fluid in equilibrium with each mineral pair would be equal. The results are reasonably consistent and suggest a temperature between 450-520 °C (Fig. 8A). This temperature range overlaps the range in temperature estimated based on Raman CM thermometry, and we conclude that both of these thermometers provide a reliable temperature of formation for Q_2 quartz as well as for the coexisting and contemporaneous rutile, muscovite, albite, dolomite, and emerald. The $\delta^{18}O$ of the water from which these minerals precipitated ranged between ~11-12 ‰, consistent with either a peraluminous magmatic fluid source or a mixture of magmatic and metamorphic fluids (Fig. 8B).

The temperature of formation of the NAEM carbonates was previously estimated to be 250-350 °C (unpublished, Horne & Miller) based on Ca/Mg partitioning (Anovitz and Essene, 1987). Adopting this temperature estimate and isotope fractionation factors for O and C between calcite-CO_2 (Friedman and O'Neil, 1977) and dolomite-CO_2 systems (Ohmoto and Rye, 1979), we estimated the carbon and oxygen isotopic composition of the fluid that precipitated the carbonates (Fig. 8C). The oxygen isotopic composition ($\delta^{18}O$) of calcite and dolomite ranged from 11– 15.5 and from 13.3 – 12.7, respectively. The carbon isotopic composition ($\delta^{13}C$) ranged from -7.8 – -3.7 in calcite and from -11.1– -4.4 in dolomite. The calculated oxygen isotopic composition ($\delta^{18}O$) of CO_2 in equilibrium with calcite and dolomite at 250-350°C ranged from 0.2 to 6 for calcite and from 2.4 to 6.5 for dolomite. The carbon isotopic composition ($\delta^{13}C$) of the fluid ranged from -9.9 to -4.4 for calcite and from -12.6 to -4.4 for fluids in equilibrium with dolomite at 250-350 °C.

8. Conditions of Emerald Mineralization at the North American Emerald Mine

A main goal of this research was to determine the physical and chemical characteristics of fluids associated with emerald mineralization and to compare these features to those of background fluids in the region. To accomplish this, samples were collected from emerald-bearing pockets, from veins and vugs in close association with emerald-bearing pockets, and from outcrops several hundred meters to over a kilometer away from known mineralization. All samples contain abundant CO_2-rich FI, and the only significant difference observed is that FI in emerald contain 4-7 mol. % CH_4. Methane was not detected in FI from other hosts. Additionally, emerald and associated albite and dolomite contain carbonaceous material (graphite) as trapped mineral in FI or as mineral inclusions. Carbonaceous material was not observed in samples collected at some distance from mineralized pockets.

Formation of emerald requires a source for Be to form beryl as well as trace amounts of the chromophores Cr and/or V that give emerald its characteristic dark green color. The source(s) of Be, Cr and V to form emeralds in the NAEM deposit is unknown and it is only possible to speculate on the sources based on rock compositions and nearness to the NAEM deposit. The classic model of emerald formation states that ultramafic or mafic rocks or their analogs (Giuliani et al., 1993; Groat et al., 2008; Marshall et al., 2003) are the source of Cr and V owing to their relatively higher concentrations in these rocks compared to more felsic varieties. Conversely, beryllium tends to enriched in peraluminous granitoid bodies, compared to mafic rocks (Evensen and London, 2002; London and Evensen, 2002). As such, most models for emerald formation invoke two distinct metal sources – a mafic/ultramafic source for Cr and V and a more silica-rich source to for Be. Several meta/peraluminous granitoid bodies have been identified in the vicinity of the NAEM, including the Walker Top, Toluca and Cherryville granites (Fig. 1C). Based on the close spatial association with NAEM (Fig. 1C), the Toluca Granite, located north of the deposit, and the Cherryville granite, located between emerald occurrences, appear to be good candidates for the sources of Be. The source of Cr and V to form the emerald is even more speculative. Wise and Anderson (2006) report that country rocks at NAEM include quartz-biotite gneiss and biotite schist interlayered with massive, green calc-silicate rock. The NAEM is hosted in metagraywackes with mafic pods, and additional amphibolites and biotite gneisses within the Newton Window outcrop within about 5 km of the deposit (Fig. 1C); any of these may have served as the source of Cr and V. To our knowledge, data for Be, Cr and V abundances in these potential source rocks are not available.

While few data are available at the temperature and pressure conditions inferred for emerald formation at NAEM, it is generally assumed that Be is more soluble, and more mobile, than Cr and V in hydrothermal fluids. Wood (1992) conducted a theoretical study of Be solubility in fluids in equilibrium with phenakite (Be_2SiO_4) and bertrandite ($Be_4Si_2O_7(OH)_2$) up to 300°C At these conditions, Be can be transported in hydrothermal fluids as complexes of Be^{+2} with Cl^- F^-, CO_3^-, OH^- and SO_4^{-2}. Solubility of Be in aqueous fluids in equilibrium with phenakite and bertrandite is highly temperature dependent, with a_{Be} decreasing from ~10^{-4} at 300°C to ~10^{-9} at 100°C (Wood, 1992). Be shows the highest solubility as fluoride complexes (Wood (1992) at low temperatures and low pH. As the temperature increases from 100°C to 300°C, carbonate ligands become more important for beryllium transport, especially at higher pH. The highest Be solubilities at 300°C occur in ~neutral to alkaline solutions as $BeCO_3F^-$ complexes. Wood (1992) also suggested that aqueous aluminum-fluoride complexes play a significant role in Be transport

at elevated temperatures. Few studies have been conducted on Be^{+2} transport in hydrothermal fluids at temperatures above 300°C, and these are summarized in Barton and Young (2002). These studies support work of Wood (1992) that concluded that fluoride complexes are important at high temperature. However, Wise and Anderson (2006) found low concentrations of F in muscovite (0.0-0.05 atoms per formula unit, apfu) and in tourmaline (0.0-0.21 apfu) from NAEM, arguing against Be transport as a fluoride complex. The low concentrations of F in muscovite and tourmaline may indicate that beryllium was transported as carbonate, chloride or other complexes at the NAEM deposit. The $BeCl^{+}$ complex is effective for beryllium transport at low pH, but Wood (1992) concludes that chloride complexes are not important in the transport of Be at temperatures ≤300°C, but does not preclude the possibility that chloride complexes may be more important at higher temperatures.

Wise and Anderson (2006) determined the concentration of Cr and V in emerald from the NAEM. While both are present, the Cr concentration in emerald is significantly higher than that of V (0.01-0.023 apfu for Cr, 0.00-0.006 for V). In oxidizing environments, such as surface waters and groundwater, hexavalent chromium is highly soluble and mobile, whereas trivalent chromium is relatively immobile. Watenphul et al. (2014) note that chromium occurs in the trivalent state in the Earth's crust and mantle, and these workers showed that acidic chloride fluids can transport significant amounts of Cr^{+3} as aquo-hydroxy-chloride complexes at elevated pressures and temperatures of 400-700°C. At these temperatures chromium solubility is highest at low pH.

Emeralds in the NAEM are texturally in equilibrium with albite, dolomite and muscovite, and solid inclusions of carbonaceous material (CM) or graphite were observed in emerald, albite and dolomite. CM was only observed in minerals in close spatial association with emerald mineralization and was not observed in "far field" samples collected hundreds of meters to over a kilometer from known mineralization. This suggests that oxidation/reduction may play a role in emerald formation. Giuliani et al. (1995) and Ottaway et al. (1994) similarly reported that reduction of sulfate to sulfide occurred during emerald deposition. As Cr and V only substitute for aluminum in the beryl structure as trivalent cations, a reducing environment would favor the trivalent form of Cr over the hexavalent form (although most workers conclude that hexavalent Cr is not present in crustal and mantle environments).

Fig. 7A shows compositions of fluids in equilibrium with graphite in the C-O-H system at 450°C and 1.2 and 1.7 kbars, and at 650°C and 1.5 and 2.2 kbars (corresponding to the inferred range in PT conditions during emerald deposition). Also shown are the fluid compositions corresponding to various oxygen fugacity conditions, all relative to NNO at the same PT condition. Fig. 7B is an enlargement of the area shown in the box in Fig. 7A, along with >700 data points corresponding to compositions of fluid inclusions from this study. All compositions fall to the left of the line labeled $X_0 = 0.33$ represents oxidized fluid and those to the right of $X_0 = 0.33$ line is reduced fluid. According to Schmidt (2018) Cr^{3+} is stable in equilibrium with graphite at 400-600°C at oxygen fugacity conditions corresponding to the NNO oxygen fugacity buffer. We note that the only significant difference observed between FI in minerals from emerald-bearing pockets compared to those from non-emerald-bearing pockets and from far-field quartz veins is that methane was detected during Raman analysis of FI from emerald-bearing pockets but was not detected in other samples. This suggests that redox processes may have been associated with emerald deposition, but insufficient evidence is available to test or confirm this interpretation.

The metamorphic history in the vicinity of the North American Emerald Mine is reasonably well constrained as a result of many field, laboratory and geochronology studies over the past half-century or more. The deposit is hosted within the Brindle Creek thrust sheet, and the metamorphic path determined by several workers (Byars, 2010; Gatewood, 2007; Merschat et al., 2005; Merschat and Kalbas, 2002) indicates a clockwise PT path reaching peak metamorphic conditions during the Neoacadian at 360-340 Ma, followed by Alleghanian retrograde metamorphism (330-315 Ma, Fig. 9A). In this study, we estimate that emeralds in NAEM deposit formed at 450-625 °C and 1.2 -2.2 kbar (Fig. 6C). Based on the absence of evidence for later re-heating and on the tectonothermal history of the Cat Square terrane, we speculate that mineralization occurred during uplift and cooling after 315 Ma, during the waning stages of the Alleghanian orogeny (Fig. 9B). At this time, PT conditions would have been just below the granite wet solidus (Fig. 9B).

Both the regional background (metamorphic?) fluid and the fluids associated with NAEM mineralization are characterized by a CO_2-H_2O±CH_4 volatile phase of varying density. As noted above, CH_4 was only detected in FI in minerals from emerald-bearing pockets. Later, low salinity H_2O-NaCl-$CaCl_2$-KCl brines entered the system, perhaps as the rocks cooled and fractures developed, allowing H_2O-rich brines to enter the environment where emerald formation took place. While Wise and Anderson (2006) suggested boiling conditions during formation of the emeralds based on a FI study and the presence of tabular "poker-chip" calcite, we did not observe any fluid inclusion evidence of boiling associated with emerald deposition. Our results suggest that emerald deposition was likely the result of a decrease in temperature and pH increase (reducing Be solubility), perhaps combined with changing oxidation state of the fluid. It is worth noting that fluid inclusions in quartz from the pocket that produced the 1869-carat "NAEM Emerald" are the only inclusions in which CH_4 was detected, further supporting the importance of redox processes during formation of emeralds at the NAEM deposit. Because Be and Cr complexes become less stable as pH increases, pH changes may have also contributed to emerald deposition. Stable isotope data and compositions of fluid inclusions are consistent with a magmatic fluid exsolved from a peraluminous magma, or a mixture of metamorphic and magmatic fluids.

9. Acknowledgements

We thank Jamie Hill, owner of the North American Emerald Mine, for providing access and samples used in this study, and Ed Speer for his interest and support during this study. We also thank Arthur Merschat for providing the geological map of the Appalachian region, Eszter Sendula for help in sample selection and D. Mattew Sublett for analyses in early stage of the project. This material is based in part on work supported by the National Science Foundation under grant number 1624589 from the Petrology and Geochemistry Program.

10. References

Anovitz, L.M. and Essene, E.J. (1987) Phase-Equilibria in the System $CaCO_3$-$MgCO_3$-$FeCO_3$. Journal of Petrology 28, 389-414.

Barton, M.D. and Young, S. (2002) Non-pegmatitic Deposits of Beryllium: Mineralogy, Geology, Phase Equilibria and Origin, in: Grew, E.S. (Ed.), Beryllium: Mineralogy, Petrology and Geochemistry, pp. 591-691.

Beyssac, O., Goffe, B., Chopin, C. and Rouzaud, J.N. (2002) Raman spectra of carbonaceous material in metasediments: a new geothermometer. Journal of Metamorphic Geology 20, 859-871.

Bier, S.E. (2001) Geology of the southeastern South Mountains, North Carolina. University of Tennessee, Knoxville.

Bodnar, R. and Vityk, M.O. (1994) Interpretation of microthermometric data for H2O-NaCl fluid inclusions. Fluid inclusions in minerals: Methods and applications, 117-130.

Byars, H.E. (2010) Tectonic evolution of the west-central portion of the Newton window, North Carolina Inner Piedmont: Timing and implications for the emplacement of the Paleozoic Vale charnockite, Walker Top Granite, and mafic complexes. University of Tennessee.

Connolly, J.A.D. (2009) The geodynamic equation of state: What and how. Geochem Geophy Geosy 10, Q10014

Driesner, T. (2007) The system H_2O-NaCl. II. Correlations for molar volume, enthalpy, and isobaric heat capacity from 0 to 1000 °C, 1 to 5000 bar, and 0 to 1 X-NaCl. Geochim. Cosmochim. Acta 71, 4902-4919.

Evensen, J.M. and London, D. (2002) Experimental silicate mineral/melt partition coefficients for beryllium and the crustal Be cycle from migmatite to pegmatite. Geochimica Et Cosmochimica Acta 66, 2239-2265.

Friedman, I. and O'Neil, J.R. (1977) Data of geochemistry: Compilation of stable isotope fractionation factors of geochemical interest. US Government Printing Office.

Gatewood, M.P. (2007) Tectonics of the Northeastern Inner Piedmont, Northwestern NC, from Detailed Geologic Mapping, Geochronologic, Geochemical, and Petrologic Studies with Structural Analyses of Ductile Fault Zones. University of Tennessee - Knoxville, p. 263.

Giuliani, G., Branquet, Y., Fallick, A., Groat, L. and Marshall, D. (2015) Emerald deposits around the world, their similarities and their differences. InColor Special Issue, 56-69.

Giuliani, G., Cheilletz, A., Arboleda, C., Carrillo, V., Rueda, F. and Baker, J.H. (1995) An Evaporitic Origin of the Parent Brines of Colombian Emeralds - Fluid Inclusion and Sulfur Isotope Evidence. European Journal of Mineralogy 7, 151-165.

Giuliani, G., Cheilletz, A., Sheppard, S. and Arboleda, C. (1993) Geochemistry and origin of the emerald deposits of Colombia, in: Hach-Ali, F., Torres-Ruiz, Gervilla (Eds.), Biennial SGA Meeting Current research in geology applied to ore deposits, Grenade, pp. 105-108.

Goldsmith, R., Milton, D.J. and Horton J.W. Jr (1988) Geologic Map of the Charlotte 1°x2° Quadrangle, North Carolina and South Carolina, Miscellaneous Investigations Series Map I-1251-E. U.S. Geological Survey.

Goldstein, R.H. (2003) Petrographic analysis of fluid inclusions, in: Samson, I., Anderson, A.J., Marshall, D. (Eds.), Fluid inclusions: Analysis and interpretation, Vancouver, Canada, pp. 9-53.

Goldstein, R.H. and Reynolds, T.J. (1994) Systematics of fluid inclusions in diagenetic minerals, Sepm short course 31. SEPM.
Groat, L.A., Giuliani, G., Marshall, D.D. and Turner, D. (2008) Emerald deposits and occurrences: A review. Ore Geology Reviews 34, 87-112.
Hatcher, R.D., Bream, B.R. and Merschat, A.J. (2007) Tectonic map of the southern and central Appalachians: A tale of three orogens and a complete Wilson cycle. Geological Society of America Memoirs 200, 595-632.
Hatcher, R.D.J. (2002) An Inner Piedmont primer, in: Robert D. Hatcher, J., Bream, B.R. (Eds.), Inner Piedmont geology in the South Mountains–Blue Ridge Foothills and the southwestern Brushy Mountains, central-western North Carolina: Annual field trip guidebook, pp. 1-16.
Huizenga, J.M. (2005) COH, an Excel spreadsheet for composition calculations in the C-O-H fluid system. Computers & Geosciences 31, 797-800.
Kouketsu, Y., Mizukami, T., Mori, H., Endo, S., Aoya, M., Hara, H., Nakamura, D. and Wallis, S. (2014) A new approach to develop the Raman carbonaceous material geothermometer for low-grade metamorphism using peak width. Island Arc 23, 33-50.
Lamadrid, H.M., Moore, L.R., Moncada, D., Rimstidt, J.D., Burruss, R.C. and Bodnar, R.J. (2017) Reassessment of the Raman CO2 densimeter. Chemical Geology 450, 210-222.
Lapointe, M., Anderson, A.J. and Wise, M. (2004) Fluid inclusion constraints on the formation of emerald-bearing quartz veins at the Rist tract, Hiddenite, North Carolina, Atlantic Geoscience Society 2004 Colloquium & Annual General Meeting, Moncton, New Brunswick, p. 146.
Lemmon, E., McLinden, M. and Friend, D. (2013) Thermophysical properties of fluid systems in NIST chemistry webbook, NIST standard reference database, vol 69. National Institute of Standards and Technology, Gaithersburg, MD 20899.
London, D. and Evensen, J.M. (2002) Beryllium in Silicic Magmas and the Origin of Beryl-Bearing Pegmatites, Reviews in Mineralogy and Geochemistry, pp. 445-486.
Mapes, R.W. (2002) Geochemistry and geochronology of mid-Paleozoic granitic plutonism in the
southern Appalachian Piedmont terrane, North Carolina-South Carolina-Georgia. Vanderbilt University, Nashville, TN, p. 150.
Marshall, D., Downes, P.J., Ellis, S., Greene, R., Loughrey, L. and Jones, P. (2016) Pressure-Temperature-Fluid Constraints for the Poona Emerald Deposits, Western Australia: Fluid Inclusion and Stable Isotope Studies. Minerals 6.
Marshall, D., Groat, L., Giuliani, G., Murphy, D., Mattey, D., Ercit, T.S., Wise, M.A., Wengzynowski, W. and Eaton, W.D. (2003) Pressure, temperature and fluid conditions during emerald precipitation, southeastern Yukon, Canada: fluid inclusion and stable isotope evidence. Chemical Geology 194, 187-199.
Merschat, A.J. (2009) Assembling the Blue Ridge and Inner Piedmont: Insights Into the Nature and Timing of Terrane Accretion in the Southern Appalachian Orogen from Geologic Mapping, Stratigraphy, Kinematic Analysis, Petrology, Geochemistry, and Modern Geochronology. University of Tennessee - Knoxville, p. 455.
Merschat, A.J., Hatcher, R.D. and Davis, T.L. (2005) The northern Inner Piedmont, southern Appalachians, USA: kinematics of transpression and SW-directed mid-crustal flow. Journal of Structural Geology 27, 1252-1281.
Merschat, A.J. and Kalbas, J.L. (2002) Geology of the southwestern Brushy Mountains, North Carolina Inner Piedmont: A summary and synthesis of recent studies, in: Hatcher, R.D.J.,

Bream, B.R. (Eds.), Inner Piedmont geology in the South Mountains–Blue Ridge Foothills and the southwestern Brushy Mountains, central-western North Carolina: Annual field trip guidebook, pp. 101-126.
Mertie, J.B., Jr (1959) Quartz crystal deposits of southwestern Virginia and western North Carolina. USGPO.
Mutchler, S., Fedele, L. and Bodnar, R. (2008) Analysis Management System (AMS) for reduction of laser ablation ICPMS data, Laser-Ablation-ICPMS in the Earth sciences: Current practices and outstanding issues. Mineralogical Association of Canada Quebec, pp. 318-327.
Ohmoto, H. and Rye, R. (1979) Carbon and sulfur isotopes, in: Barnes, H. (Ed.), Geochemistry of Hydrothermal Ore Deposits. Wiley Interscience, New York, pp. 509-567.
Ottaway, T.L., Wicks, F.J., Bryndzia, L.T., Kyser, T.K. and Spooner, E.T.C. (1994) Formation of the Muzo Hydrothermal Emerald Deposit in Colombia. Nature 369, 552-554.
Schmidt, C. (2018) Formation of hydrothermal tin deposits: Raman spectroscopic evidence for an important role of aqueous Sn(IV) species. Geochimica et Cosmochimica Acta 220, 499-511.
Sheppard, S.M.F.F.E. (1986) Characterization and isotopic variations in natural waters. Reviews in Mineralogy and Geochemistry 16, 165-183.
Sterner, S.M. and Bodnar, R.J. (1984) Synthetic fluid inclusions in natural quartz I. Compositional types synthesized and applications to experimental geochemistry. Geochimica et Cosmochimica Acta 48, 2659-2668.
Watenphul, A., Schmidt, C. and Jahn, S. (2014) Cr(III) solubility in aqueous fluids at high pressures and temperatures. Geochimica Et Cosmochimica Acta 126, 212-227.
Williams, S.T. (2000) Structure, stratigraphy, and migmatization in the southwestern South Mountains, North Carolina. University of Tennessee, Knoxville.
Wilson, C.G., Hatcher R.D., J. and Bream, B.R. (2006) The nature and origin of Inner Piedmont Taconian and Neoacadian magmatism: synthesis of recent and new geochemical data, Southeastern Section 55th Annual Meeting, Knoxville, Tennessee, p. 73.
Wise, M.A. and Anderson, A.J. (2006) The emerald- and spodumene-bearing quartz veins of the Rist emerald mine, Hiddenite, North Carolina. Canadian Mineralogist 44, 1529-1541.
Wood, S.A. (1992) Theoretical Prediction of Speciation and Solubility of Beryllium in Hydrothermal Solution to 300 °C at Saturated Vapor-Pressure - Application to Bertrandite Phenakite Deposits. Ore Geology Reviews 7, 249-278.
Zwaan, J.C. (2006) Gemmology, geology and origin of the Sandawana emerald deposits, Zimbabwe.

11. Tables

Table 1. Sample descriptions and summary of analyses performed on each sample.

Sample #	Description	Location *	FI host mineral	Graphite observed	H & O isotopes measured	C & O isotopes measured
HID2015_2	quartz vein in leucocratic rock	1	Qtz		Qtz	
HID2015_3	Carbonate alteration adjacent to quartz vein	1	Qtz			Dol
HID2015_4	Aggregate of carbonate crystals	1				Cal
HID2015_6	Quartz vein with large quartz crystals and adjacent small carbonate and mica crystals	1	Qtz			
HID2015_8	Smoky quartz crystal with later biotite-quartz growth aggregate	1	Qtz		Qtz	
HID2015_9	Muscovite-carbonate-rutile mineralization in open fracture	1	Dol		Ru, Mu	Dol
HID2015_11	Quartz-carbonate sample	1	Dol			Dol
HID2015_12	Mix from calcite bearing pocket	1			Ru, Mu	Cal
HID2015_13	Quartz vein in leucocratic rock	1			Qtz	
HID2015_17	Quartz aggregate from quartz pocket	2			Qtz	
HID2015_18	Aggregates of micas, carbonates, quartz, rutile, provided by mine operator	1				Dol
HID2016_19	Crystal mixture from emerald pocket. Mica, clays, quartz, carbonates, emeralds	new excavation 6	Dol, Ru, Tur, Em, Qtz	Em	Ru, Mu, Qtz	Dol
NAEM 030916-2	"S.Yadkin River" quartz with rutile from concordant vein away from mineralization	4			Qtz	
NAEM 030916-4	Quartz vein concordant with host	5	Qtz		Qtz	
NAEM 030916-7	Quartz from the pocket that produced the NAEM Emerald	1			Qtz	
NAEM 030916-8	Quartz with included emerald from the pocket that produced the NAEM Emerald	1	Em, Qtz	Em	Qtz	
58A	Dolomite and quartz grain in emerald	1	Dol, Em, Qtz			

Spear 8 em	Small chip of emerald with associated albite and carbonate	1		Ab, Dol, Em		
NAEM09.9	Dolomite chips	1	Dol	Dol		
NAEM apatite	Apatite crystal 2mm in length	1	Ap			

* The numbers in "Location" column referring to locations on the Fig 2a

Ab – albite; Ap – Apatitie; Cal – calcite; Dol – dolomite; Em – emerald; Mu – muscovite; Qtz – quartz; Ru – rutile; Tur – tourmaline (dravite).

Table 2. Mineral inclusions identified in NAEM minerals and fluid inclusions

Host mineral	Mineral inclusions	Daughter/trapped minerals in FI
Emerald	Albite, rutile, magnetite*, siderite/dolomite*, carbonaceous material	Carbonaceous material
Dolomite	Rutile, muscovite	
Calcite	Pyrite	
Quartz	Rutile, sillimanite**, muscovite	Nahcolite, dawsonite
Tourmaline	Zircon	
Rutile	Carbonates	
Muscovite	Carbonates	
Apatite	Zircon	

* Observed in single crystal forming solid mineral inclusions with magnetite, siderite/dolomite and rutile

** Sillimanite present in Q_0 quartz vein sample without a clear genetic association with the NAEM deposit

Table 3. Fluid inclusion data.

Sample #	Host mineral	FIA type	Average density (g/cm3)	Average salinity (wt. % NaCl eq)	Th for aqueous FIAs
58A	Carbonate	CO_2-H_2O	0.74±0.04 (2)		
	Emerald	CO_2-H_2O	0.77±0.08 (4)		
	Quartz Q2	CO_2-H_2O	0.09 (1)		
HID2015-2a	Quartz Q2	CO_2-H_2O	0.88±0.03 (3)		
			0.04±0 (2)		
HID2015-3	Quartz Q2	CO_2-H_2O	0.8 (1)		
HID2015-6	Quartz Q2	CO_2-H_2O	0.27±0.06 (28)		
			0.77±0.1 (130)		
		H_2O-NaCl	0.93 (1)	4.6 (1)	167 (1)
HID2015-8	Quartz Q2	H_2O-NaCl	0.92±0.01 (2)	6.9 (2)	207±13 (4)
HID2015-9	Dolomite	CO_2-H_2O	0.87±0.12 (2)		
HID2015-11	Dolomite	CO_2-H_2O	0.79±0.07 (2)		
HID2016-19	Dolomite	CO_2-H_2O	0.88 (1)		
	Rutile	CO_2-H_2O	0.98±0.03 (2)	3.7±0.8 (2)	
			0.6 (1)	4.1	
	Dravite	CO_2-H_2O	0.64 (1)		
	Emerald	CO_2-H_2O	0.79±0.07 (4)		
			0.44 (1)		
	Quartz Q3/Q2	CO_2-H_2O	0.67 (1)		
		H_2O-NaCl	0.93 (1)	9.9 (1)	215 (1)
NAEM Apatite	Apatite	CO_2-H_2O	0.94±0.03 (2)		
NAEM030916-4	Quartz Q0	CO_2-H_2O	0.06 (1)		
			0.43±0.05 (2)		
			0.82 (1)		
NAEM030916-8	Emerald	CO_2-H_2O-CH_4	0.74±0.07 (4)		
	Quartz Q2	CO_2-H_2O	0.81±0.02 (3)		
NAEM09.9	Dolomite	CO_2-H_2O	0.72±0 (2)		

Compositions of CO_2-rich FI assume that FI contain 20 vol. % water at room temperature. The total number of Fluid Inclusion Assemblages (FIA) analyzed is shown in parenthesis; approximately 3-5 inclusions were analyzed in each FIA. The standard deviation is estimated for samples in which more than 1 FIA was analyzed.

12. Figures

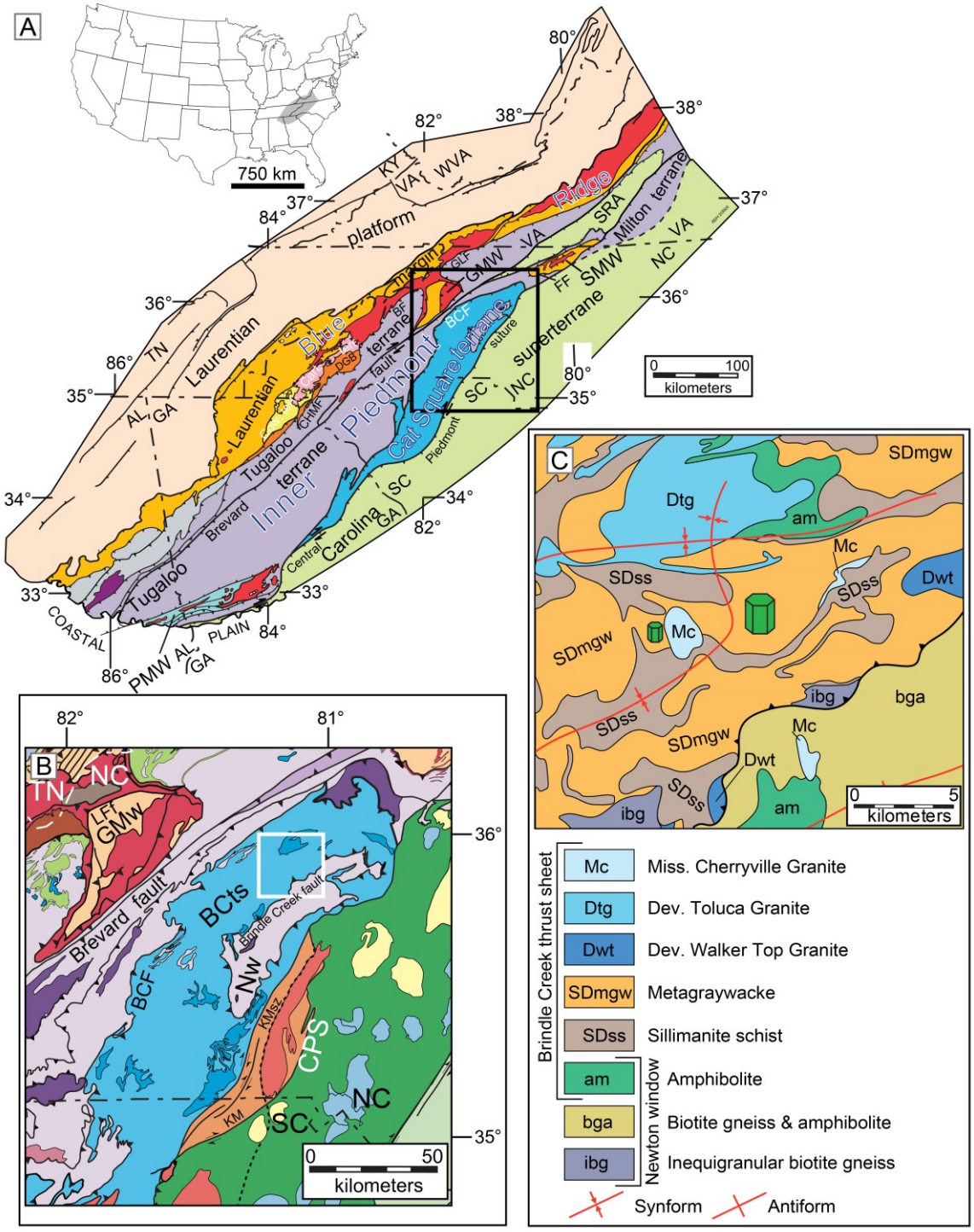

Figure 1. Regional and local geology in the vicinity of the North American Emerald Mine, Alexander County, North Carolina, USA. Note that maps A, B and C are from different sources, resulting in slight differences in the details shown in Figures 1A-C. (A). General tectonic map of the southern Appalachians showing major geological features. The black rectangle indicates the

area shown in inset 1B. BCF– Brindle Creek fault. BF–Burnsville fault. Cart. terr.–Cartoogechaye terrane. CHMF–Chattahoochee-Holland Mountain fault. Cow. terr.–Cowrock terrane. DGB–Dahlonega gold belt. FF–Forbush fault. GLF–Gossan Lead fault. GMW–Grandfather Mountain window. MH–Mars Hill terrane. NW–Newton window. SRA–Smith River allochthon. SMW–Sauratown Mountain window. PMW–Pine Mountain window. Light gray–Probable western Tugaloo terrane rocks in Alabama and Georgia. Purple–Ordovician Elkahatchee Quartz Diorite, modified after Merschat (2009). (B). Map of the northern Cat Square terrane, after Hatcher et al. (2007); the white square indicates the area in the vicinity of the NAEM deposit shown in (C). BCF– Brindle Creek fault; BCts– Brindle Creek thrust sheet; GMw – Grandfather Mountain window; KM – Kings Mountain belt; KMsz – Kings Mountain shear zone; LFf – Linville Falls fault; Nw – Newton window. (C). Detailed geologic map of the area in the immediate vicinity of the NAEM near the contact between the Brindle Creek thrust sheet and the Newton window, modified after Goldsmith et al. (1988) and Merschat (2009). The large emerald in the center indicates the location of the NAEM and the smaller emerald to the left is the location of the Adams Property within the town of Hiddenite.

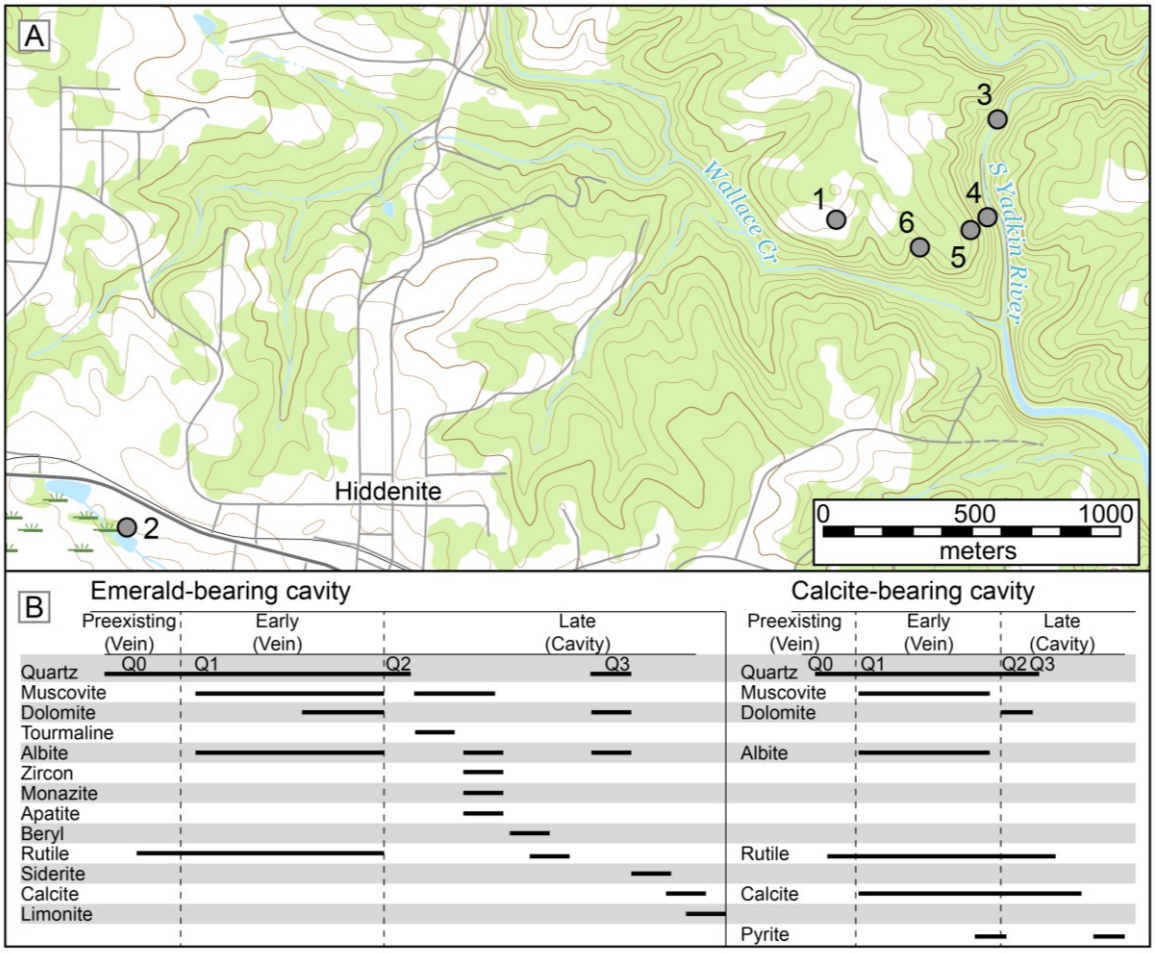

Figure 2. (A). Topographic map showing sample locations. Samples 1 and 3-6 were collected at the NAEM and nearby, and sample 2 was collected from the Adam's property in the town of Hiddenite. (B). Mineral paragenesis in emerald- and calcite-bearing pockets. Q0-Q3 indicates the various generations of quartz. Modified after Wise and Anderson (2006).

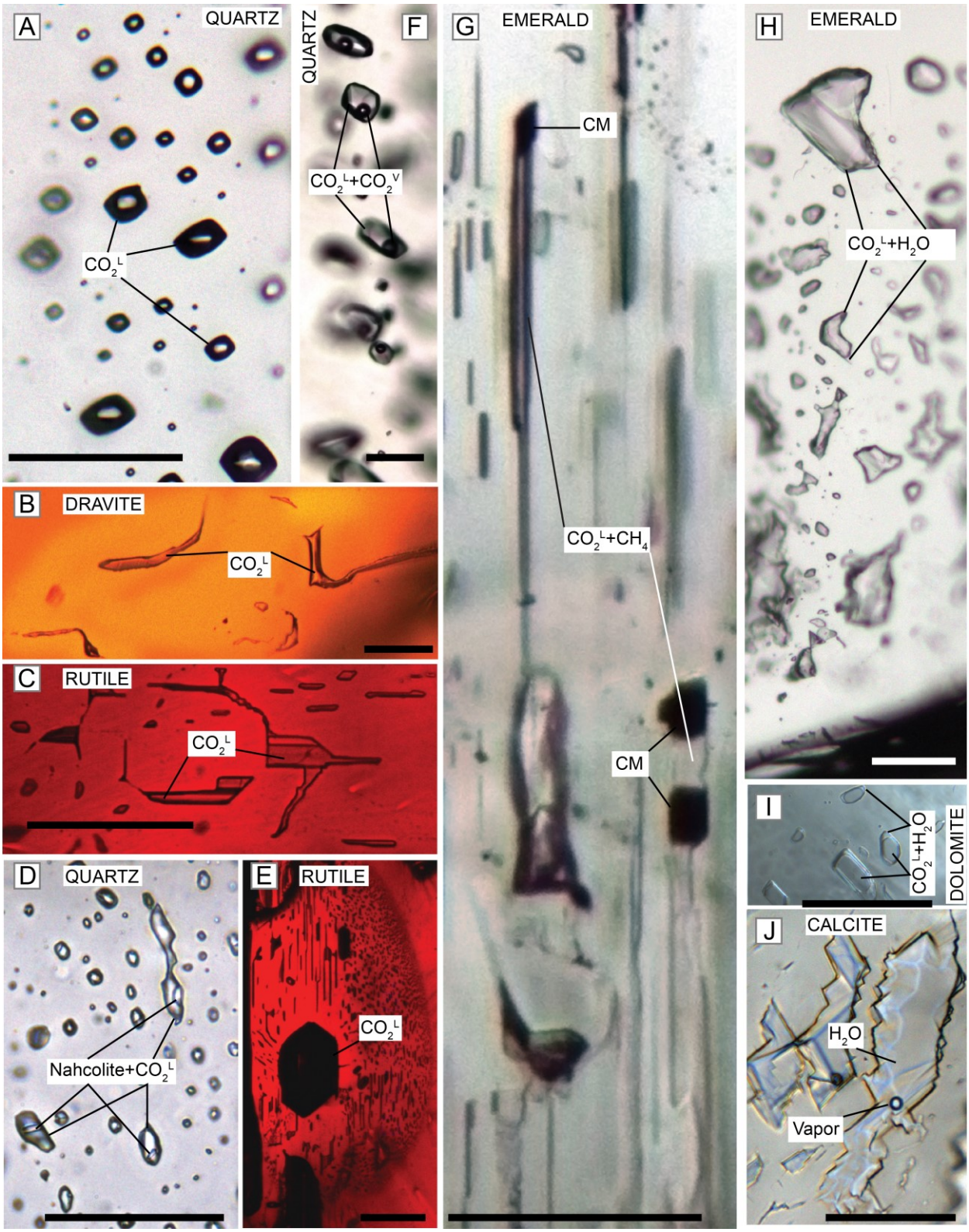

Figure 3. Fluid inclusion types observed in various minerals from the NAEM deposit. CM represents carbonaceous material, L & V correspond to liquid and vapor CO_2, respectively. Multifocal photomerging was used in order to illustrate fluid inclusions located at different depths within the field of view. The scale bar equals 50 microns in all photos. (A). Liquid CO_2

fluid inclusions in quartz (Q_2/Q_3) in sample HID2016-19; (B) Liquid CO_2 fluid inclusions in dravite in sample HID2016-19; (C, E) Liquid CO_2 fluid inclusions in rutile in sample HID2016-19, (E) shows decrepitation halo around large liquid CO_2 fluid inclusion; (D) Liquid CO_2 fluid inclusions in quartz (Q_2) with daughter phase identified as nahcolite ($NaHCO_3$), sample HID2015-3 (F) Two phase fluid inclusions in quartz (Q_2) in sample HID2015-8; (G) Liquid CO_2-CH_4 fluid inclusions in emerald with trapped carbonaceous mineral (CM) in sample NAEM030916-8 (H) liquid CO_2 fluid inclusions with visible thin film of H_2O, in emerald in sample 58A; (I) Liquid CO_2-H_2O fluid inclusions in dolomite, in sampleHID2016-19 (J) H_2O two phase fluid inclusions in calcite in sample HID2016-19.

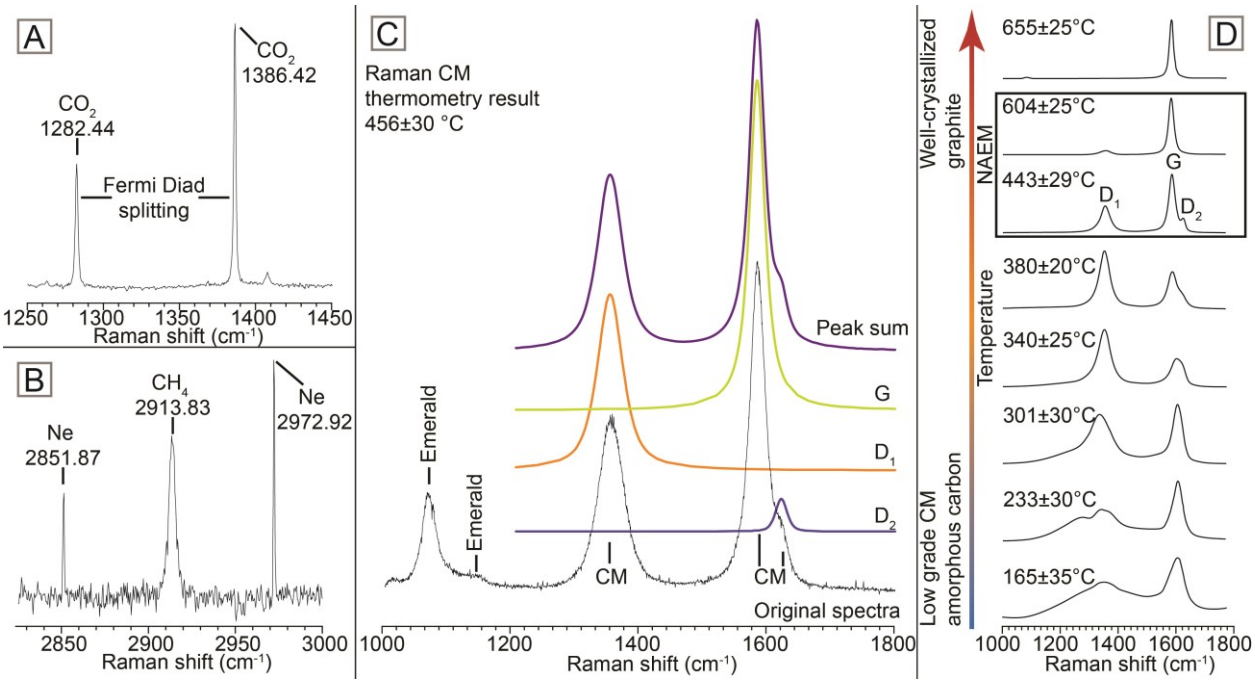

Figure 4. Raman spectra of phases observed in fluid inclusions. (A). Raman spectrum of CO_2 showing the Fermi Diad that is used to determine the CO_2 density; (B). Raman spectrum of methane (CH_4) in a FI in emerald sample NAEM030916-4; also shown are two Ne peaks that are used to calibrate peak position; (C). Raman spectra of carbonaceous material (CM) in emerald. The original spectrum at the bottom is deconvoluted to show the D_1, G, D_2 bands needed to estimate the CM formation temperature according to Beyssac et al. (2002); (D). Variation in the Raman spectrum of CM as a function of temperature, after Kouketsu et al. (2014). The spectra shown in the black box for 443°C and 604°C are similar to those obtained from Raman analysis of CM in NAEM samples.

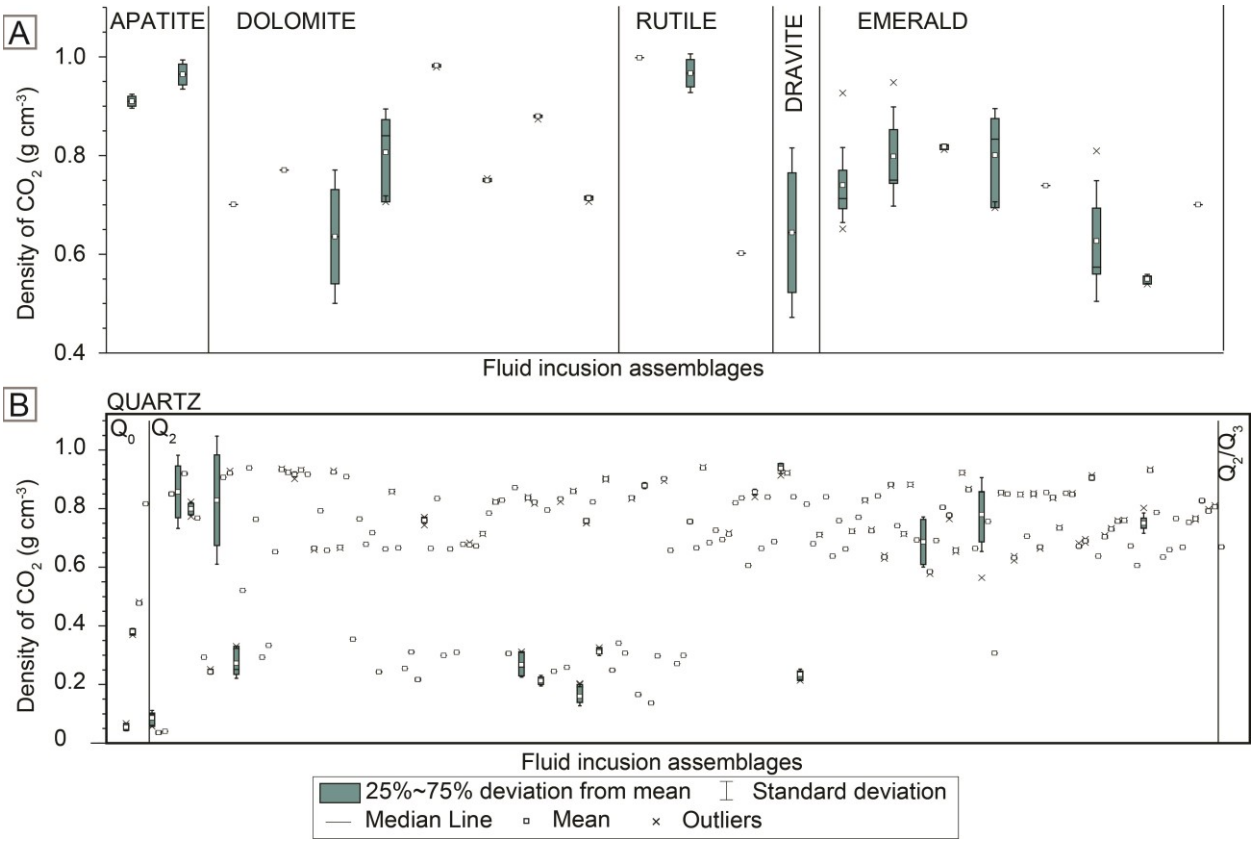

Figure 5.Densities obtained from well-constrained Fluid Inclusion Assemblages (FIAs) in dolomite, rutile, apatite, dravite, emerald (A) and quartz (B) of Q_0, Q_2 and Q_2/Q_3 generations. Crossed points above/below bars indicate outliers. Note different vertical scale for each figure.

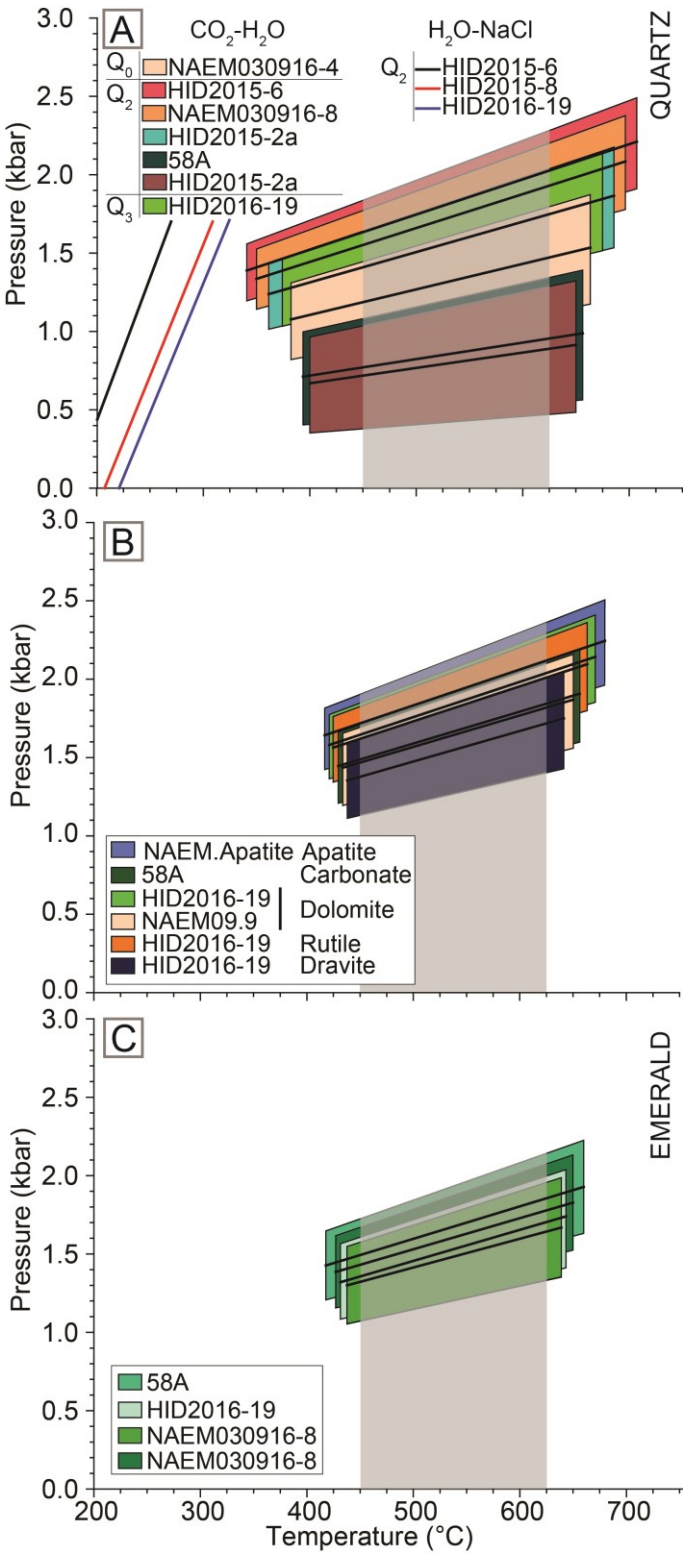

Figure 6. Pressure-temperature diagram showing isochores based on average homogenization temperatures or densities of fluid inclusions in each sample. FIAs with similar densities are grouped together, and sample HID2015-2a contains both high density and low density FIAs that are plotted separately. For each sample, the black line represents the isochore

assuming that the CO_2-H_2O FIs contain 20 vol. % H_2O at room temperature, and the colored rectangles show the range in isochore location assuming 10 and 30 vol. % H_2O. The gray shaded area represents the temperature range estimated by Raman CM thermometry. (A). FIA in quartz. (B) FIA in apatite, carbonate (composition not determined), dolomite, rutile and dravite. (C). FIA in emerald.

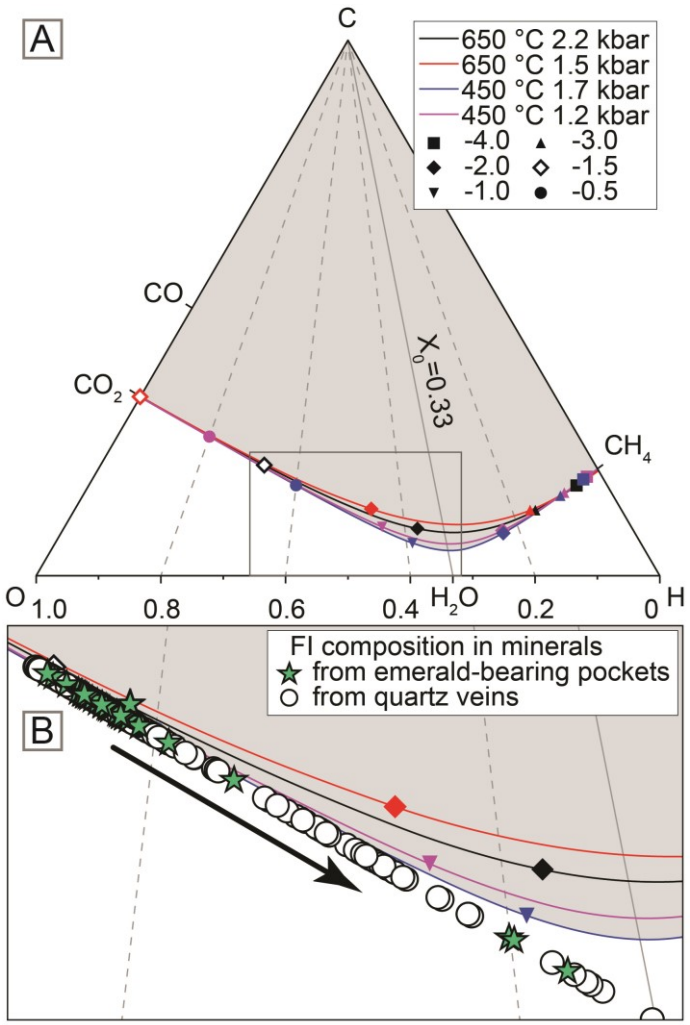

Figure 7. (A). Ternary C-O-H diagram showing the fluid composition during emerald formation based on the model of (Huizenga, 2005). Colored lines indicate the composition of C-O-H fluid in equilibrium with graphite at different pressure-temperature conditions. Symbol shape indicates the oxygen fugacity of the fluid relative to NNO at the same temperature. Color of the symbol corresponds to lines indicating compositions of fluid in equilibrium with graphite. The gray shaded area represents the range in compositions at which carbon is oversaturated (graphite is present), fluids at $X_0<0.33$ is referred to as a reduced fluid, and those at $X_0>0.33$ are considered to be oxidized fluids; (B). Enlargement of the area shown in the box in Fig. 7A, with individual FI compositions (>700 points) plotted. To estimate the composition we assume that CO_2-rich FIs contain 20 vol. % H_2O at room temperature. Star symbol indicates FI composition hosted either in emerald or in minerals found in emerald-bearing pockets. Open circles represent compositions of FI hosted in minerals that are not spatially associated with emerald mineralization.

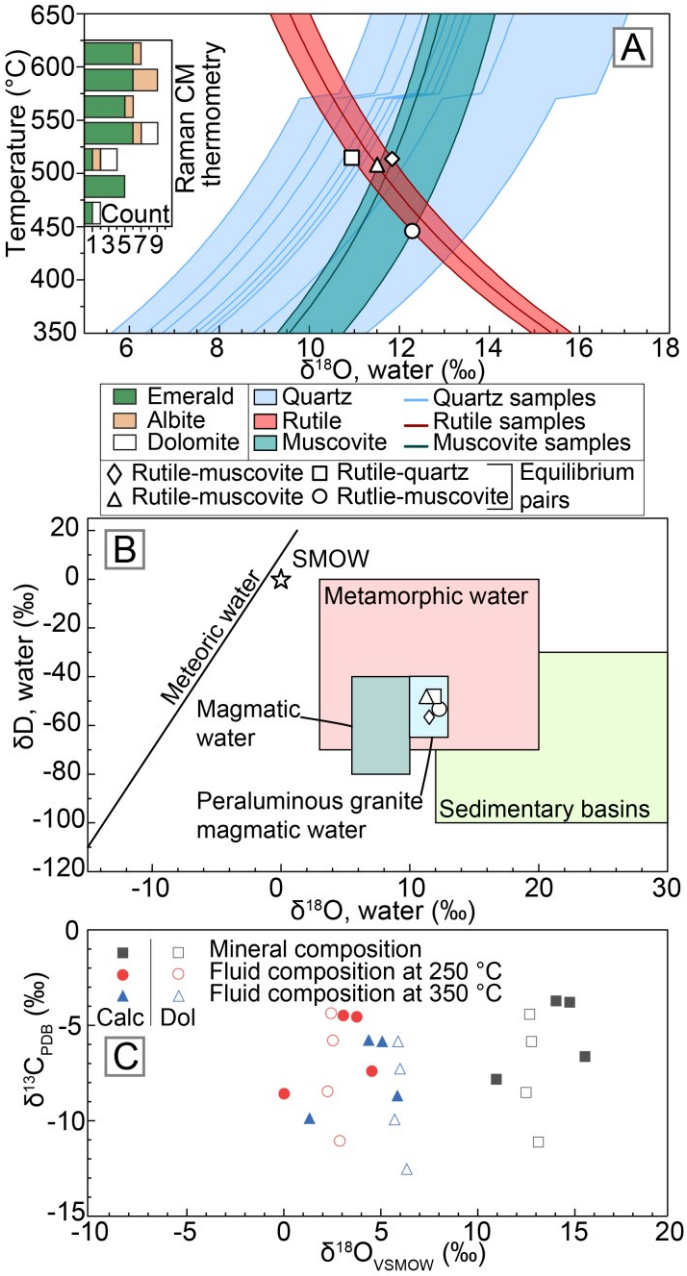

Figure 8. (A). Temperature versus $\delta^{18}O$ of water in equilibrium with quartz (light blue area), muscovite (turquoise colored area) and rutile (red area); Temperatures and water compositions calculated based on analysis of minerals coexisting in textural equilibrium indicate a formation temperature of 450-520 °C and fluid $\delta^{18}O$ between 10.9-12.3. Inset histogram shows temperatures estimated by Raman thermometry of carbonaceous material (CM) from mineral and fluid inclusions hosted in emerald (4 samples), dolomite (1 sample) and albite (1 sample); (B). δD vs $\delta^{18}O$ composition of the fluid based on rutile-muscovite and rutile-quartz pairs from 3 samples. The δD-$\delta^{18}O$ data are consistent with a metamorphic water source, or a mixture of metamorphic water and magmatic water derived from a peraluminous granite. Modified after Sheppard (1986); (C). $\delta^{13}C$ vs $\delta^{18}O$ composition of calcite (calc) and dolomite (dol) samples as

well as the isotopic composition of CO_2 at 250 °C (red symbols) and 350 °C (blue symbols) (Friedman and O'Neil, 1977) and (Ohmoto and Rye, 1979).

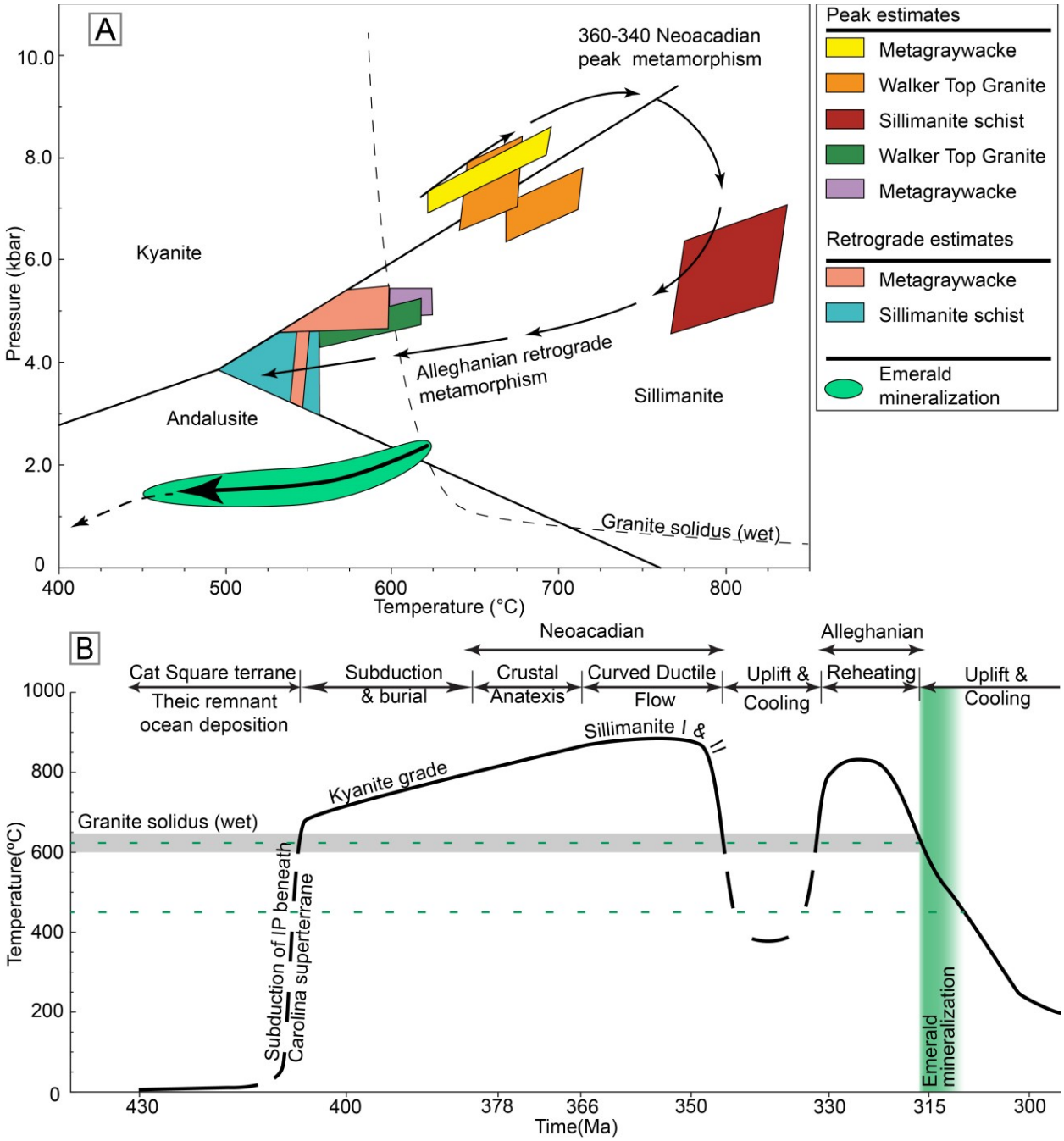

Figure 9. (A). Projected pressure-temperature metamorphic path for the Cat Square terrane (Brindle Creek trust sheet), with the inferred NAEM formation PT conditions. The PT path is modified after (Merschat and Kalbas, 2002) and (Byars, 2010). The bright green area that extends from the andalusite-sillimanite boundary to lower temperatures is the PT region of emerald formation inferred from fluid inclusion, stable isotope and CM Raman thermometry data; (B). Tectonothermal history of the Cat Square terrane, after (Byars, 2010). The timing of NAEM formation is based on NAEM formation temperature and PT path of the Cat Square terrane from (A), which indicates that NAEM formation occurred during Alleghanian retrograde metamorphism.

APPENDIX

1. Appendix A

Code of the program used to evaluate properties of the H_2O-NaCl fluid. The program developed in MS Excel Visual Basic Application and designed to both extend functions of MS Excel and offer the user a graphical user interface in which user can define pressure-temperature-composition limits and list of properties that need to be calculated.

The program requires an Excel file with sheets (named *model* and *boundaries*), forms (*H2O_NaCl_model* and *Unit_Config*) and modules (*Assemb_module, Driesners_eqs, form_interactions, Math_funcs, Model_eqs, OtherViscModels, Revised_Visc, Water_prop and WaterAndSalt*). The autorun of the workbook initialize form *H2O_NaCl_model* after opening of the file

1.1 Form H_2O_NaCl_model

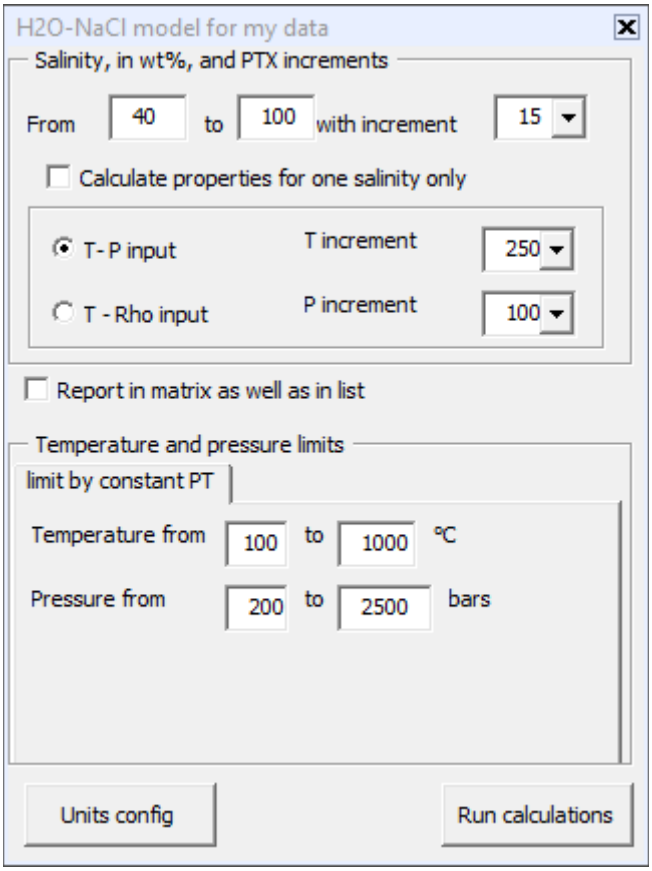

Figure 1 screenshot of the main form, demonstrating graphical user interface. Salinity TextBoxes named in code as *S_start, S_end* and ComboBox *Salt_incr*. CheckBox "**Calculate properties for one salininy only**" defines Boolean parameter *OneSalt*. OptionButton "**T-P input**" is only one functioning selection in this version of the program and define Boolean parameter *TP_Choice*. ComboBoxes next to "**T increment**" and "**P increment**" are defining *T_incr* and *P_incr* correspondingly. TextBoxes for lower and upper limits of the temperature and pressure are defining *T_start*, *T_end*, *P_start* and *P_end* in code. Button "Units config" initialize the form *Unit_config.*

```
Private Sub OneSalt_Click()

If OneSalt.Value = True Then
Label3.Visible = False: Label4.Visible = False
Salt_incr.Visible = False: S_End.Visible = False
Label2.Caption = "NaCl %"
Else
Label3.Visible = True: Label4.Visible = True
Salt_incr.Visible = True: S_End.Visible = True
Label2.Caption = "From"
End If
```

```
End Sub
Private Sub Run_Model_Click()

Dim S_St As Single, S_En As Single, S_Inc As Single, S_Am_st As Single,
SaltRun As Integer
Dim T_st As Single, T_en As Single, T_inc As Single, T_Am_St As Single
Dim P_St As Single, P_En As Single, P_inc As Single, P_Am_St As Single

Dim i As Integer, j As Integer, k%, Rw As Long

Dim PureH2O As Boolean, ClAddr$, ClFrml$
Dim CP_array() As Single, Phase_Boundary() As Single

Dim S As Integer, T As Single, P As Single, mH2O As Single, mNaCl As Single,
XNaCl As Double, RhoH2O As Single, RhoNaCl As Single

Dim Rho_Water#, TmpUnt1#, TmpUnt2#, P_tmp1#, P_tmp2#, P_Der#, T_Tmp#

mH2O = 18.015268
mNaCl = 58.4428
RhoH2O = 1
RhoNaCl = 2.16

SetupExcelForCalc (True)

ActiveWorkbook.Sheets("model").Select

If OneSalt.Value = False Then
    S_St = Val(S_start.Value) / 100: S_En = Val(S_End.Value) / 100: S_Inc =
Val(Salt_incr.Value) / 100
    If S_En <= S_St Or S_St < 0 Then
        MsgBox "Please check initial and final salinities", vbCritical
        S_start.SetFocus
        Exit Sub
    End If
Else
    S_St = Val(S_start.Value) / 100
    S_En = S_St: S_Inc = 0
    If S_St < 0 Then
        MsgBox "Please check salinity", vbCritical
        S_start.SetFocus
        Exit Sub
    End If
End If

T_st = Val(T_Start.Value): T_en = Val(T_End.Value): T_inc = Val(T_incr.Value)
If T_en <= T_st Or T_st < 0 Then
    MsgBox "Please check initial and final Temperatures", vbCritical
    T_Start.SetFocus
    Exit Sub
```

```
End If

P_St = Val(P_start.Value): P_En = Val(P_End.Value): P_inc = Val(P_incr.Value)
If P_En <= P_St Or P_St < 0 Then
    MsgBox "Please check initial and final pressures", vbCritical
    P_start.SetFocus
    Exit Sub
End If

S_Am_st = 1
If S_St <> S_En Then
    While S_Am_st * S_Inc + S_St <= S_En
        S_Am_st = S_Am_st + 1
    Wend
End If

T_Am_St = Int((T_en - T_st) / T_inc)
P_Am_St = Int((P_En - P_St) / P_inc)

' CP_array  store Critical parameters, first number - step in salt starts
from 1
' 0 to 3 used for to store 0 - XNaCl, 1 - TCrit, 2 - PCrit, 3 - RhoCrit, 4
and 5 used to show crit isochore
' hence 4 is equal to 1000°C, and 5 is P(Rho_crit, 1000°C)
ReDim CP_array(1 To S_Am_st, 0 To 5) As Single

' Phase_Boundary created to store phase boundary PT at given x. First number
- T, second - P
ReDim Phase_Boundary(1 To S_Am_st, 0 To T_Am_St, 0 To 1) As Single

S_St = Val(S_start.Value) / 100
T_st = Val(T_Start.Value)
P_St = Val(P_start.Value)

Unload H2O_NaCl_model
Model_Page_setup

Rw = 2

'global cycle for salinity
ProgressInStatusBar True
For SaltRun = 1 To S_Am_st

    If S_Unit = "WtPer" Then
        S_Tmp = S_St + S_Inc * (SaltRun - 1)
    ElseIf S_Unit = "MolPer" Then
        S_Tmp = (S_St + S_Inc * (SaltRun - 1)) * mNaCl / ((S_St + S_Inc *
(SaltRun - 1)) * mNaCl + (1 - (S_St + S_Inc * (SaltRun - 1))) * mH2O)
    ElseIf S_Unit = "VolPer" Then
```

```
         S_Tmp = (S_St + S_Inc * (SaltRun - 1)) * RhoNaCl / ((S_St + S_Inc *
(SaltRun - 1)) * RhoNaCl + (1 - S_St - S_Inc * (SaltRun - 1)) * RhoH2O)
    Else
         S_Tmp = (S_St + S_Inc * (SaltRun - 1)) * mNaCl * 100 / (1000 + (S_St
+ S_Inc * (SaltRun - 1)) * mNaCl * 100)
    End If
    S_Tmp = Round(S_Tmp, 6)
    Crit_Array_Filling S_Tmp, SaltRun, CP_array
    XNaCl = CP_array(SaltRun, 0)

    'global cycle for temperature
    For i = 0 To T_Am_St
    DoEvents
        T = Round(T_st + i * T_inc - T_Unit, 3)
        If XNaCl = 0 And T > CP_array(SaltRun, 1) Then
            Phase_Boundary(SaltRun, i, 0) = CP_array(SaltRun, 1)
            Phase_Boundary(SaltRun, i, 1) = CP_array(SaltRun, 2)
        Else
            Phase_Boundary(SaltRun, i, 0) = T
            Phase_Boundary(SaltRun, i, 1) = New_LV_P(T, 1, XNaCl, True)
'LV_Pressure(T, XNaCl)
        End If
        'function ot make inverted calculations in T-Rho space
        'currently unfinished
        If T_Rho_Input = False Then
            'global cycle for pressure in PT space
            For j = 0 To P_Am_St
                P = (P_St + j * P_inc) / P_Unit
                If P > Phase_Boundary(SaltRun, i, 1) And XNaCl <> 0 And XNaCl
< X_L_Sat(T, P) Then
                    ' phase boundary appearance in table
                    If T - T_Unit - Phase_Boundary(SaltRun, i, 0) <= T_inc
And P - Phase_Boundary(SaltRun, i, 1) < P_inc / P_Unit And
Phase_Boundary(SaltRun, i, 1) >= P_St / P_Unit Then
                        Cells(Rw, 1) = CStr(Round((S_St + S_Inc * (SaltRun -
1)) * 100, 1))
                        Cells(Rw, 2) = Phase_Boundary(SaltRun, i, 0)
                        Cells(Rw, 3) = Phase_Boundary(SaltRun, i, 1)
                        Cells(Rw, 5) = "Phase Boundary " & (S_St + (SaltRun -
1) * S_Inc) * 100 & " " & S_Unit
                        Rw = Rw + 1
                    End If

                    ' first row at new T
                    Cells(Rw, 1) = CStr(Round((S_St + (SaltRun - 1) * S_Inc)
* 100, 1))
                    Cells(Rw, 2) = Round(T + T_Unit, 4)
                    Cells(Rw, 3) = P
                    Rw = Rw + 1
```

```
                    'copying formula from lower pressure to highest
                    If P < (P_St + P_Am_St * P_inc) / P_Unit Then
                        ClAddr = CStr("A" & Rw & ":" & "A" & Rw + P_Am_St - j
- 1)
                        ClFrml = "=R[-1]C"
                        Range(ClAddr).Formula = ClFrml
                        ClAddr = CStr("B" & Rw & ":" & "B" & Rw + P_Am_St - j
- 1)
                        Range(ClAddr).Formula = ClFrml
                        ClAddr = CStr("C" & Rw & ":" & "C" & Rw + P_Am_St - j
- 1)
                        ClFrml = "=R[-1]C+" & P_inc
                        Range(ClAddr).Formula = ClFrml
                        Rw = Rw + P_Am_St - j
                        Exit For
                    End If

                Else
                    'pure water region should be plotted
                    If XNaCl = 0 Then
                        Cells(Rw, 1) = 0
                        Cells(Rw, 2) = Round(T, 4)
                        Cells(Rw, 3) = (P_St + j * P_inc)
                        Rw = Rw + 1
                        If (P_St + j * P_inc) / P_Unit < (P_St + P_Am_St *
P_inc) / P_Unit Then
                            ClFrml = "=R[-1]C"
                            ClAddr = CStr("A" & Rw & ":" & "A" & Rw + P_Am_St
- j - 1)
                            Range(ClAddr).Formula = ClFrml
                            ClAddr = CStr("B" & Rw & ":" & "B" & Rw + P_Am_St
- j - 1)
                            Range(ClAddr).Formula = ClFrml
                            ClFrml = "=R[-1]C+" & P_inc
                            ClAddr = CStr("C" & Rw & ":" & "C" & Rw + P_Am_St
- j - 1)
                            Range(ClAddr).Formula = ClFrml

                            Rw = Rw + P_Am_St - j
                            Exit For
                        End If

                        Exit For
                    End If
                End If
            Next j
        Else
        End If

        If XNaCl = 0 Then
```

```
            If T - Phase_Boundary(SaltRun, i, 0) <= T_inc And P_St + j *
P_inc - Phase_Boundary(SaltRun, i, 1) < P_inc And Phase_Boundary(SaltRun, i,
1) >= P_St Then
                Cells(Rw, 1) = Round((S_St + (SaltRun - 1) * S_Inc) * 100, 1)
                Cells(Rw, 2) = Phase_Boundary(SaltRun, i, 0)
                Cells(Rw, 3) = Phase_Boundary(SaltRun, i, 1)
                Cells(Rw, 5) = "Phase Boundary " & (S_St + (SaltRun - 1) *
S_Inc) * 100 & " wt% NaCl"
                Rw = Rw + 1
            End If
        End If
    Next i

ProgressInStatusBar False, "Table calculation", SaltRun, S_Am_st
Next SaltRun

Application.StatusBar = "writing of the result on sheet in progress"

For SaltRun = 1 To S_Am_st
    i = 0
    j = 0
    While i < T_Am_St + 1
        If Phase_Boundary(SaltRun, i, 1) <> 0 Then
            Phase_Boundary(SaltRun, j, 1) = Phase_Boundary(SaltRun, i, 1)
            Phase_Boundary(SaltRun, j, 0) = Phase_Boundary(SaltRun, i, 0)
            If i <> j Then
                Phase_Boundary(SaltRun, i, 1) = Phase_Boundary(SaltRun,
T_Am_St, 1)
                Phase_Boundary(SaltRun, i, 0) = Phase_Boundary(SaltRun,
T_Am_St, 0)
            End If
            j = j + 1
        End If
        i = i + 1
    Wend
    Cells(SaltRun + 1, 10) = CP_array(SaltRun, 1)
    Cells(SaltRun + 1, 11) = CP_array(SaltRun, 2)
Next SaltRun

Cells(1, 10) = "Critical point position"

For SaltRun = 1 To S_Am_st
    For i = 0 To T_Am_St
        Cells(1, SaltRun * 2 + 12) = "Salinity " & (S_St + (SaltRun - 1) *
S_Inc) * 100
        Cells(i + 2, SaltRun * 2 + 12) = Phase_Boundary(SaltRun, i, 0)
        Cells(i + 2, SaltRun * 2 + 13) = Phase_Boundary(SaltRun, i, 1)
    Next i
Next SaltRun
```

```
''REPLACING EXCEL FORMULAS BY NUMBERS VALUES
Range("A2").Select
Range(Selection, Selection.End(xlToRight)).Select
Range(Selection, Selection.End(xlDown)).Select
Selection.Copy
Range("A2").Select
Selection.PasteSpecial Paste:=xlPasteValues, Operation:=xlNone,
SkipBlanks:=False, Transpose:=False

SetupExcelForCalc (False)

'CALL FOR MAJOR CALCULATION FUNCTION
'Concurents_Viscosity_calcs
Rho_AND_Visc
If Matrix_Report_page = True Then Matrix_Transpose

ActiveWorkbook.Sheets("model").Activate

Application.ScreenUpdating = True
End Sub
Private Sub P_End_Change()
    If Not IsNumeric(P_End) Or Val(T_End) < 0 Then
    P_End.Value = ""
    MsgBox "Numbers only", vbOKOnly
    P_End.SetFocus
    End If
End Sub
Private Sub P_Start_Change()
    If Not IsNumeric(P_start) Or Val(o_start) < 0 Then
    P_start.Value = ""
    MsgBox "Numbers only", vbOKOnly
    P_start.SetFocus
    End If
End Sub
Private Sub S_End_Change()
    If Not IsNumeric(S_End) Or Val(T_End) < 0 Then
    S_End.Value = ""
    MsgBox "Numbers only", vbOKOnly
    S_End.SetFocus
    End If

End Sub
Private Sub S_Start_Change()
    If Not IsNumeric(S_start) Or Val(S_start) < 0 Then
    S_start.Value = ""
    MsgBox "Positive numbers only", vbOKOnly
    S_start.SetFocus
    End If
End Sub
```

```
Private Sub T_End_Change()
    If Not IsNumeric(T_End) Or Val(T_End) < 0 Then
    T_End.Value = ""
    MsgBox "Numbers only", vbOKOnly
    T_End.SetFocus
    End If
End Sub
Private Sub T_Start_Change()
    If Not IsNumeric(T_Start) Or Val(T_Start) < 0 Then
    T_Start.Value = ""
    MsgBox "Numbers only", vbOKOnly
    T_Start.SetFocus
    End If
End Sub

Private Sub TP_Choice_Click()

T_Rho_switcher True

End Sub
Private Sub TRho_Choice_Click()

T_Rho_switcher False

End Sub
Private Sub T_Rho_switcher(P_True)

If P_True = False Then
    Label7.Caption = "Rho increment"
    Label10.Caption = "Density from"
    Label13.Caption = "kg*m-3"
    'TP_Choice.Value = False
    T_Rho_Input = True
Else
    Label7.Caption = "P increment"
    Label10.Caption = "Pressure from"
    Label13.Caption = "bars"
    'TP_Choice.Value = True
    T_Rho_Input = False
End If

End Sub
Private Sub Units_Click()
Unit_config.Show
End Sub
Private Sub UserForm_Initialize()

S_Unit = "WtPer"
P_Unit = 1
T_Unit = 0
```

```
Dens_Unit = 1000
TP_Choice.Value = True
TRho_Choice.Value = False

With Salt_incr
    .AddItem 0.1
    .AddItem 0.2
    .AddItem 0.5
    .AddItem 1
    .AddItem 2
    .AddItem 3
    .AddItem 5
    .AddItem 10
    .AddItem 20
    .AddItem 25
End With
With T_incr
    .AddItem 0.2
    .AddItem 0.5
    .AddItem 1
    .AddItem 2
    .AddItem 3
    .AddItem 5
    .AddItem 10
End With
With P_incr
    .AddItem 0.2
    .AddItem 0.5
    .AddItem 1
    .AddItem 2
    .AddItem 3
    .AddItem 5
    .AddItem 10
    .AddItem 50
End With

End Sub
```

1.2 Form Unit

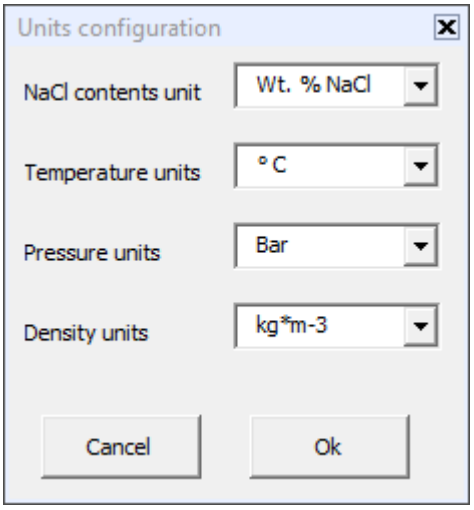

Figure 2 screenshot of the units configuration form. ComboBoxes in this window define parameters named in code as *NaCl, Temp, Pres, Dens.*

```
Private Sub Cancel_Units_Click()
    Unit_config.Hide
End Sub

Public Sub Ok_Click()

If Temp.Value = "° K" Then T_Unit = 273.15 Else T_Unit = 0
If Pres.Value = "MPa" Then P_Unit = 10 Else P_Unit = 1
If Dens.Value = "kg*m-3" Then Dens_Unit = 1 Else Dens_Unit = 0.001

If NaCl.Value = "Wt. % NaCl" Then
    S_Unit = "WtPer"
ElseIf NaCl.Value = "mol. % NaCl" Then
    S_Unit = "MolPer"
ElseIf NaCl.Value = "v. % NaCl" Then
    S_Unit = "VolPer"
Else
    S_Unit = "Molal"
End If

H2O_NaCl_model.Frame2.Caption = "Salinity, in " + NaCl + ", and PTX
increments"
H2O_NaCl_model.Label11.Caption = Temp.Value
H2O_NaCl_model.Label13.Caption = Pres.Value

Unit_config.Hide

End Sub

Private Sub UserForm_Initialize()
```

```
With NaCl
    .AddItem "Wt. % NaCl"
    .AddItem "mol. % NaCl"
    .AddItem "v. % NaCl"
    .AddItem "molality"
End With

With Temp
    .AddItem "° C"
    .AddItem "° K"
End With

With Pres
    .AddItem "Bar"
    .AddItem "MPa"
End With

With Dens
    .AddItem "kg*m-3"
    .AddItem "g*cm-3"
End With

End Sub
```

1.3 Module Assemb_module

```
Private Sub Reset_Excel()

Application.ScreenUpdating = True
Application.Calculation = xlCalculationAutomatic
Application.EnableEvents = True

End Sub
Sub ReArranger()

Dim P(0 To 30) As Single, roW(0 To 30) As Integer, i As Integer
SetupExcelForCalc True

P(0) = 1:     P(1) = 50:    P(2) = 100:   P(3) = 150:   P(4) = 200:   P(5) =
250:   P(6) = 300:   P(7) = 350: P(8) = 400
P(9) = 450:   P(10) = 500:  P(11) = 550:  P(12) = 600:  P(13) = 650:  P(14) =
700:  P(15) = 750:  P(16) = 800
P(17) = 850:  P(18) = 900:  P(19) = 950:  P(20) = 1000: P(21) = 1050: P(22) =
1100: P(23) = 1150: P(24) = 1200
P(25) = 1250: P(26) = 1300: P(27) = 1350: P(28) = 1400: P(29) = 1450: P(30) =
1500

roW(0) = 2: roW(8) = 10:  roW(16) = 18: roW(24) = 26
roW(1) = 3: roW(9) = 11:  roW(17) = 19: roW(25) = 27
roW(2) = 4: roW(10) = 12: roW(18) = 20: roW(26) = 28
roW(3) = 5: roW(11) = 13: roW(19) = 21: roW(27) = 29
roW(4) = 6: roW(12) = 14: roW(20) = 22: roW(28) = 30
roW(5) = 7: roW(13) = 15: roW(21) = 23: roW(29) = 31
roW(6) = 8: roW(14) = 16: roW(22) = 24: roW(30) = 32
roW(7) = 9: roW(15) = 17: roW(23) = 25

ProgressInStatusBar True
RowNumber = 1

For i = 2 To 27932
    DoEvents
    j = 0
    While Cells(i, 3) <> P(j)
        j = j + 1
    Wend
        Cells(1, 8 + j * 4) = Cells(i, 3)
        If Cells(i, 3) = 1 Then RowNumber = RowNumber + 1
        Cells(RowNumber, 8 + j * 4) = Cells(i, 2)
        Cells(RowNumber, 9 + j * 4) = Cells(i, 4)
        Cells(RowNumber, 10 + j * 4) = Cells(i, 5)

        ProgressInStatusBar False, "", i, 27932

Next i
```

```
SetupExcelForCalc False

End Sub

Private Function Divisible(i As Integer) As Integer
Divisible = Round_Down((i Mod 30), 0)
End Function

Public Function FindRhoForVisc(T, P, Rho, Visc)
T1 = 40
T2 = T1 - 0.1
Rho1 = Rho_Water(T1, P)
Rho2 = Rho_Water(T2, P)
Visc_Tmp1 = Water_Viscosity_calc(T1 + 273.15, Rho1)

While Abs(Visc - Visc_Tmp1) > 0.04

    Visc_Tmp1 = Water_Viscosity_calc(T1 + 273.15, Rho1) - Visc
    Visc_Tmp2 = Water_Viscosity_calc(T2 + 273.15, Rho2) - Visc

    visc_der = CDec((Visc_Tmp1 - Visc_Tmp2) / (T1 - T2))
    T1 = T1 - Visc_Tmp1 / visc_der

    Visc_Tmp1 = Visc_Tmp1 + Visc
    T2 = T1 - 1
    Rho1 = Rho_Water(T1, P)
    Rho2 = Rho_Water(T2, P)
    Step = Step + 1
    If Step = 1000 Then
        MsgBox "!!! Too much iterations in pressure calcs " & i, vbOKOnly
        Application.ScreenUpdating = True
        Stop
    End If
Wend

FindRhoForVisc = Rho1 'Visc_Tmp1
T = T1
Rho = Rho1

End Function

' this sub is responsible for assembling all of the functions and user input,
to form an output
Sub Rho_AND_Visc()
Dim k As Long, i As Long, XNaCl As Double, slt As Single, T As Double, P As
Double, Rho#, Visc As Double
Dim mH2O As Single, mNaCl As Single, RhoH2O#, RhoNaCl As Single, StTime As
Single, CurTime As Single
Dim RhoWater#, T_Star As Double, PreviousRho#, Tmp#, Tmp2#, q2h#, tStarH#,
Main_Rho As Boolean ', a#(0 To 9)
```

```
Dim dRho#
Dim CP_array(0, 0 To 5) As Single

SetupExcelForCalc (True)

mH2O = 18.015268
mNaCl = 58.4428

RhoH2O = 1
RhoNaCl = 2.16
i = 2
While Cells(i, 2) <> ""
i = i + 1
Wend
i = i - 1
'If MsgBox("stop here?", vbYesNo) = vbYes Then Exit Sub
ProgressInStatusBar True

For k = 2 To i
    DoEvents
    CurTime = Timer
    q2h = 1
    slt = ActiveWorkbook.Sheets("model").Cells(k, 1) / 100
    XNaCl = slt / mNaCl / (slt / mNaCl + (1 - slt) / mH2O)
    T = ActiveWorkbook.Sheets("model").Cells(k, 2) - T_Unit
    P = ActiveWorkbook.Sheets("model").Cells(k, 3) '* P_Unit

    If ActiveWorkbook.Sheets("model").Cells(k, 4) = "" Then
        'True stand to mark calculations of Rho in main cycle, not in the
derivative functions
        Rho = Rho_Brine(XNaCl, T, P)
        ActiveWorkbook.Sheets("model").Cells(k, 4) = Rho
    Else
        Rho = ActiveWorkbook.Sheets("model").Cells(k, 4)
    End If

    'Cells(k, 5) = Viscosity_1Brines_CHOOSEN(slt * 100, T, p, Rho)
    beeta = beta(XNaCl, T, P, Rho)
    Cells(k, 5) = XsiCapital(beeta, slt, T, P, Rho)
    'Cells(k, 6) = beeta
    Cells(k, 7) = Fluxibility(slt, T, P, Rho)
    Cells(k, 6) = P
    'Cells(k, 6) = Palliser_1998_visc(slt, T + 273.15, P, Rho_Water(T, P))


    ProgressInStatusBar False, "Calculation of the density and other
parameters", k - 1, i - 1
Next k

SetupExcelForCalc (False)
```

```
End Sub
Public Function T_finder_PXvsLH(slt, P) As Double
Dim S#
S = slt
XNaCl = WtToMol(S) / 100
a = 420
b = 1000

n = 1
Toler = 0.001
While n <= 1000
    c = (a + b) / 2
    If (b - a) / 2 < Toler Then
        T_finder_PXvsLH = b
        n = 1001
    End If

    n = n + 1
    aa = X_L_Sat(c, P) - XNaCl
    bb = X_L_Sat(b, P) - XNaCl
    If Sgn(aa) = Sgn(bb) Then b = c Else a = c
Wend


End Function
```

1.4 Module Driesner_eqs

```
Public Function T_Star_V(XNaCl, T, P) As Double
'Driesner 2007 Tv*  for density,
Dim n10 As Double, n11 As Double, n12 As Double
Dim n20 As Double, n23 As Double, n21 As Double, n22 As Double, n300 As
Double, n301 As Double
Dim n302 As Double, n310 As Double, n311 As Double, n312 As Double, n30 As
Double, n31 As Double
Dim n1 As Double, n2 As Double, d As Double, n_oneNaCl As Double, n_twoNaCl
As Double

xH2O = 1 - XNaCl

n11 = -54.2958 - 45.7623 * Exp(-9.44785 * 10 ^ -4 * P)
n21 = -2.6142 - 0.000239092 * P
n22 = 0.0356828 + 4.37235 * 10 ^ -6 * P + 2.0566 * 10 ^ -9 * P ^ 2

n300 = 7.60664 * 10 ^ 6 / ((P + 472.051) ^ 2)
n301 = -50 - 86.1446 * Exp(-6.21128 * 10 ^ -4 * P)
n302 = 294.318 * Exp(-5.66735 * 10 ^ -3 * P)
n310 = -0.0732761 * Exp(-2.3772 * 10 ^ -3 * P) - 5.2948 * 10 ^ -5 * P
n311 = -47.2747 + 24.3653 * Exp(-1.25533 * 10 ^ -3 * P)
```

```
n312 = -0.278529 - 0.00081381 * P
n30 = n300 * (Exp(n301 * XNaCl) - 1) + n302 * XNaCl
n31 = n310 * Exp(n311 * XNaCl) + n312 * XNaCl

n_oneNaCl = 330.47 + 0.942876 * P ^ 0.5 + 0.0817193 * P - 2.47556 * 10 ^ -8 *
P ^ 2 + 3.45052 * 10 ^ -10 * P ^ 3
n10 = n_oneNaCl
n12 = -n11 - n10
n20 = 1 - n21 * n22 ^ 0.5
n_twoNaCl = -0.0370751 + 0.00237723 * P ^ 0.5 + 5.42049 * 10 ^ -5 * P +
5.84709 * 10 ^ -9 * P ^ 2 - 5.99373 * 10 ^ -13 * P ^ 3
n23 = n_twoNaCl - n20 - n21 * (1 + n22) ^ 0.5
n1 = n10 + n11 * xH2O + n12 * xH2O ^ 2
n2 = n20 + n21 * (XNaCl + n22) ^ 0.5 + n23 * XNaCl
d = n30 * Exp(n31 * T)

T_Star_V = n1 + n2 * T + d

End Function

Public Function T_star_H(XNaCl, q2h, T, P) As Double
'Driesner's Th* for enthalpy
Dim q10#, q11#, q12#
Dim q20#, q21#, q22#, q23#
Dim q1#, q2#, q_oneNaCl#, q_twoNaCl#, xH2O#

xH2O = 1 - XNaCl

q11 = -32.1724 + 0.0621255 * P
q21 = -1.69513 - 4.52781 * 10 ^ -4 * P - 6.04279 * 10 ^ -8 * P ^ 2
q22 = 0.0612567 + 1.88082 * 10 ^ -5 * P
q_oneNaCl = 47.9048 - 9.36994 * 10 ^ -3 * P + 6.51059 * 10 ^ -6 * P ^ 2
q_twoNaCl = 0.241022 + 3.45087 * 10 ^ -5 * P - 4.28356 * 10 ^ -9 * P ^ 2

q10 = q_oneNaCl
q12 = -q11 - q10

q20 = 1 - q21 * q22 ^ 0.5
q23 = q_twoNaCl - q20 - q21 * (1 + q22) ^ 0.5

q1 = q10 + q11 * xH2O + q12 * xH2O ^ 2
q2 = q20 + q21 * (XNaCl + q22) ^ 0.5 + q23 * XNaCl

T_star_H = q1 + q2 * T + 273.15
q2h = q2
End Function

'halite melting curve
'Eq 1 from Driesner and Heinrich 2007
Public Function T_hm(P) As Double
```

```
Dim a As Double, T_tr_NaCl As Single, P_tr_NaCl As Single
a = 2.4726 * 10 ^ -2
T_tr_NaCl = 800.7
P_tr_NaCl = 5 * 10 ^ -4

T_hm = T_tr_NaCl + a * (P - P_tr_NaCl)

End Function

'Halite sublimation curve,
'eq 2 Driesner and Heinrich 2007
Private Function P_Subl(T)
Dim B_subl As Single, P_Triple_NaCl As Single, T_Triple_NaCl As Single
B_subl = 1.18061 * 10 ^ 4
T_Triple_NaCl = 800.7
P_Triple_NaCl = 5 * 10 ^ -4

P_Subl = 10 ^ (Log10(P_Triple_NaCl) + B_subl * (1 / (T_Triple_NaCl + 273.15)
- 1 / (T + 273.15)))

End Function
'Halite boiling curve,
'eq 3 Driesner and Heinrich 2007
Public Function P_Boil(T)
Dim B_boil As Single, P_Triple_NaCl As Single, T_Triple_NaCl As Single
B_boil = 0.941812 * 10 ^ 4
T_Triple_NaCl = 800.7
P_Triple_NaCl = 5 * 10 ^ -4

P_Boil = 10 ^ (Log10(P_Triple_NaCl) + B_boil * (1 / (T_Triple_NaCl + 273.15)
- 1 / (T + 273.15)))

End Function

'eq 5 and eq 7
Public Function X_and_P_crit(T_in, Xcrit_Out, Pcrit_Out)
Dim i As Integer, j As Integer, GotIt As Boolean
Dim Sum1 As Double, PH2O_Crit As Double, TH2O_Crit As Double

Dim c(1 To 14) As Double, cA(1 To 11) As Single, d(1 To 11) As Double
Dim T As Double, P_Crit As Double, X_Crit As Double, X_Crit_2 As Double
''IAPS-84
'PH2O_Crit = 2.2054915 * 10 ^ 2: TH2O_Crit = 373.976
'IAPWS-95
PH2O_Crit = 2.2064 * 10 ^ 2: TH2O_Crit = 373.946

c(1) = -2.36:               c(2) = 1.28534 * 10 ^ -1:  c(3) = -2.3707 * 10 ^
-2:   c(4) = 3.20089 * 10 ^ -3
c(5) = -1.38917 * 10 ^ -4:  c(6) = 1.02789 * 10 ^ -7:  c(7) = -4.8376 * 10 ^
-11:  c(8) = 2.36
```

```
c(9) = -1.31417 * 10 ^ -2:  c(10) = 2.98491 * 10 ^ -3: c(11) = -1.30114 * 10
^ -4: c(14) = -4.88336 * 10 ^ -4

cA(1) = 1: cA(2) = 1.5:  cA(3) = 2: cA(4) = 2.5
cA(5) = 3: cA(6) = 4:    cA(7) = 5: cA(8) = 1
cA(9) = 2: cA(10) = 2.5: cA(11) = 3

For i = 8 To 11
    Sum1 = Sum1 + c(i) * (500 - TH2O_Crit) ^ cA(i)
    c(13) = c(13) + c(i) * cA(i) * (500 - TH2O_Crit) ^ (cA(i) - 1)
Next i
c(12) = PH2O_Crit + Sum1

d(1) = 8 * 10 ^ -5:         d(2) = 1 * 10 ^ -5:          d(3) = -1.37125 * 10
^ -7:  d(4) = 9.46822 * 10 ^ -10
d(5) = -3.50549 * 10 ^ -12: d(6) = 6.57369 * 10 ^ -15:   d(7) = -4.89423 * 10
^ -18: d(8) = 7.77761 * 10 ^ -2
d(9) = 2.7042 * 10 ^ -4:    d(10) = -4.244821 * 10 ^ -7: d(11) = 2.580872 *
10 ^ -10

Sum1 = 0
T = T_in
If T < TH2O_Crit Then
    'eq. 5a, for unknown reasons tends to overestimate pressure in comparison
    'with paper pictures/SoWat program
    'For j = 1 To 7
    'Sum1 = Sum1 + c(j) * (TH2O_Crit - T) ^ cA(j)
    'Next j
    'P_Crit = PH2O_Crit + Sum1

    'eq 5a replaced by an equation which used to estimate pressure
    'for phase boundary at given temperature
    T = T + 273.15
    T_inv = 1 - T / 647.096
    RhoUpUp = Exp(-2.0315024 * T_inv ^ (1 / 3) - 2.6830294 * T_inv ^ (2 / 3)
- 5.38626492 * T_inv ^ (4 / 3) - 17.2991605 * T_inv ^ 3 - 44.7586581 * T_inv
^ (37 / 6) - 63.9201063 * T_inv ^ (71 / 6)) * 322
    P = Water_Pressure_calc(T, RhoUpUp)
    T = T - 273.15
    P_Crit = P * 10
    X_Crit = 0

Else
    If T >= TH2O_Crit And T <= 500 Then
        'eq 5b
        For j = 8 To 11
        Sum1 = Sum1 + c(j) * (T - TH2O_Crit) ^ cA(j)
        Next j
        P_Crit = PH2O_Crit + Sum1
    Else
```

```
        'eq. 5c
        For j = 12 To 14
        Sum1 = Sum1 + c(j) * (T - 500) ^ (j - 12)
        Next j
        P_Crit = Sum1
    End If
End If
Sum1 = 0

If T >= TH2O_Crit And T <= 600 Then
    'eq. 7a
    For j = 1 To 7
    Sum1 = Sum1 + d(j) * (T - TH2O_Crit) ^ j
    Next j
    X_Crit = Sum1
ElseIf T > 600 Then ' And T <= 1000
    'eq. 7b
    For j = 8 To 11
    Sum1 = Sum1 + d(j) * (T - 600) ^ (j - 8)
    Next j
    X_Crit = Sum1
End If

Xcrit_Out = X_Crit
Pcrit_Out = P_Crit
X_and_P_crit = Pcrit_Out
End Function

'Halite Liquidus
'Eq 8 from Driesner and Heinrich 2007
Public Function X_L_Sat(T, P) As Double
Dim E(0 To 5) As Double, i As Integer, TmpUnt As Double
E(0) = 0.0989944 + 3.30796 * 10 ^ -6 * P - 4.71759 * 10 ^ -10 * P ^ 2
E(1) = 0.00947257 - 8.6646 * 10 ^ -6 * P + 1.69417 * 10 ^ -9 * P ^ 2
E(2) = 0.610863 - 1.51716 * 10 ^ -5 * P + 1.1929 * 10 ^ -8 * P ^ 2
E(3) = -1.64994 + 2.03441 * 10 ^ -4 * P - 6.46015 * 10 ^ -8 * P ^ 2
E(4) = 3.36474 - 1.54023 * 10 ^ -4 * P + 8.17048 * 10 ^ -8 * P ^ 2
E(5) = 1

For i = 0 To 4
    E(5) = E(5) - E(i)
Next i

TmpUnt = T / T_hm(P)
For i = 0 To 5
    X_L_Sat = X_L_Sat + E(i) * TmpUnt ^ i
Next i

If X_L_Sat < 0 Then Stop
```

```
End Function

'eq 9
Public Function X_V_Sat(T, P)
Dim j(0 To 3) As Double, k(0 To 15) As Double, Log_K_supScr As Double,
Log_K_Line As Double, P_Line As Double, P_NaCl As Double
Dim ii%, X_L_St#, P_Crit#

k(0) = -0.235694:       k(1) = -0.188838:           k(2) = 0.004:
k(3) = 0.0552466:       k(4) = 0.66918
k(5) = 396.848:         k(6) = 45:                  k(7) = -3.2719 * 10 ^ -7:
k(8) = 141.699:         k(9) = -0.292631
k(10) = -0.00139991:    k(11) = 1.95965 * 10 ^ -6:  k(12) = -7.3653 * 10 ^ -
10: k(13) = 0.904411:       k(14) = 0.000769766
k(15) = -1.18658 * 10 ^ -6

j(0) = k(0) + k(1) * Exp(-k(2) * T)
j(1) = k(4) + (k(3) - k(4)) / (1 + Exp((T - k(5)) / k(6))) + k(7) * (T -
k(8)) ^ 2
j(2) = 0
For ii = 0 To 3
    j(2) = j(2) + k(ii + 9) * T ^ ii
Next ii
j(3) = 0
For ii = 0 To 2
    j(3) = j(3) + k(ii + 13) * T ^ ii
Next ii

If T > 800.7 Then
    P_NaCl = P_Boil(T)
Else
    P_NaCl = P_Subl(T)
End If

X_L_St = X_L_Sat(T, P)
X_and_P_crit T, 0, P_Crit

P_Line = (P - P_NaCl) / (P_Crit - P_NaCl)
Log_K_Line = 1 + j(0) * (1 - P_Line) ^ j(1) + j(2) * (1 - P_Line) + j(3) * (1
- P_Line) ^ 2 - (1 + j(0) + j(2) + j(3)) * (1 - P_Line) ^ 3
Log_K_supScr = Log_K_Line * (Log10(P_NaCl / P_Crit) - Log10(X_L_Sat(T,
P_Crit))) + Log10(X_L_Sat(T, P_Crit))

'If P > Pvlh Then
    X_V_Sat = X_L_St * P_NaCl / 10 ^ Log_K_supScr / P
'Else
'    MsgBox "OOOPS"
'    Stop
'End If
End Function
```

```
'Vapor-Liquid-Halite coexistense
'eq 10 from Driesner and Heinrigch 2007
Public Function P_VLH(T)
Dim i As Integer, f(0 To 10) As Double, P_tr_NaCl As Single, T_tr_NaCl As
Single
T_tr_NaCl = 800.7
P_tr_NaCl = 5 * 10 ^ -4

f(0) = 4.64 * 10 ^ -3:   f(1) = 5 * 10 ^ -7:       f(2) = 1.69078 * 10:
f(3) = -2.69148 * 10 ^ 2: f(4) = 7.63204 * 10 ^ 3: f(5) = -4.95636 * 10 ^ 4
f(6) = 2.33119 * 10 ^ 5: f(7) = -5.13556 * 10 ^ 5: f(8) = 5.49708 * 10 ^ 5:
f(9) = -2.84628 * 10 ^ 5: f(10) = P_tr_NaCl

For i = 0 To 9
    f(10) = f(10) - f(i)
Next i

For i = 0 To 10
    P_VLH = P_VLH + f(i) * (T / T_tr_NaCl) ^ i
Next i

End Function

'Eq 11
Public Function X_VL_Liq(T, P) As Double

Dim d#(1 To 11), XN_Crit#, TmpUnit#, ii%, TH2O_Crit#
Dim h#(1 To 11), G0#, G1#, G2#, P_Crit#

h(1) = 0.00168486:        h(2) = 0.000219379:   h(3) = 438.58:         h(4) =
18.4508
h(5) = -0.00000000056765: h(6) = 0.00000673704: h(7) = 0.000000144951: h(8) =
384.904
h(9) = 7.07477:           h(10) = 0.0000606896: h(11) = 0.00762859

G1 = h(2) + (h(1) - h(2)) / (1 + Exp((T - h(3)) / h(4))) + h(5) * T ^ 2
G2 = h(7) + (h(6) - h(7)) / (1 + Exp((T - h(8)) / h(9))) + h(10) * Exp(-h(11)
* T)
X_and_P_crit T, XN_Crit, P_Crit

If T < 800.7 Then
    TmpUnit = P_VLH(T)
    G0 = (X_L_Sat(T, TmpUnit) - G1 * (P_Crit - TmpUnit) - G2 * (P_Crit -
TmpUnit) ^ 2 - XN_Crit) / (P_Crit - TmpUnit) ^ 0.5
Else
    TmpUnit = P_Boil(T)
    G0 = (1 - G1 * (P_Crit - TmpUnit) - G2 * (P_Crit - TmpUnit) ^ 2 -
XN_Crit) / (P_Crit - TmpUnit) ^ 0.5
End If
```

```
X_VL_Liq = XN_Crit + G0 * (P_Crit - P) ^ 0.5 + G1 * (P_Crit - P) + G2 *
(P_Crit - P) ^ 2

End Function

'Eq 13 Eq 14 Eq 15 Eq 16 Eq 17
Public Function X_VL_Vap(T, P) As Double
Dim j#(0 To 3), k#(0 To 15), Log_K_supScr#, Log_K_Line#, P_Line#, P_NaCl#
Dim ii%, X_VL_Lq#, P_Crit#, Tmp#

k(0) = -0.235694:       k(1) = -0.188838:           k(2) = 0.004:
k(3) = 0.0552466:       k(4) = 0.66918
k(5) = 396.848:         k(6) = 45:                  k(7) = -3.2719 * 10 ^ -7:
k(8) = 141.699:         k(9) = -0.292631
k(10) = -0.00139991:    k(11) = 1.95965 * 10 ^ -6:  k(12) = -7.3653 * 10 ^ -
10: k(13) = 0.904411:       k(14) = 0.000769766
k(15) = -1.18658 * 10 ^ -6

j(0) = k(0) + k(1) * Exp(-k(2) * T)
j(1) = k(4) + (k(3) - k(4)) / (1 + Exp((T - k(5)) / k(6))) + k(7) * (T +
k(8)) ^ 2
j(2) = 0
For ii = 0 To 3
    j(2) = j(2) + k(ii + 9) * T ^ ii
Next ii
j(3) = 0
For ii = 0 To 2
    j(3) = j(3) + k(ii + 13) * T ^ ii
Next ii

If T >= 800.7 Then
    P_NaCl = P_Boil(T)
Else
    P_NaCl = P_Subl(T)
End If

X_VL_Lq = X_VL_Liq(T, P)

X_and_P_crit T, X, P_Crit

P_Line = (P - P_NaCl) / (P_Crit - P_NaCl)
Log_K_Line = 1 + j(0) * (1 - P_Line) ^ j(1) + j(2) * (1 - P_Line) + j(3) * (1
- P_Line) ^ 2 - (1 + j(0) + j(2) + j(3)) * (1 - P_Line) ^ 3

Tmp = X_L_Sat(T, P_NaCl)
Log_K_supScr = Log_K_Line * (Log10(P_NaCl / P_Crit) - Log10(Tmp)) +
Log10(Tmp)
```

```
If P > P_VLH(T) Then
    X_VL_Vap = X_VL_Lq / 10 ^ Log_K_supScr * P_NaCl / P
Else
    X_VL_Vap = X_VL_Lq / 10 ^ Log_K_supScr * P_NaCl / P
    X_VL_Vap = X_L_Sat(T, P) / X_VL_Lq * X_VL_Vap
    'MsgBox "OOOPS"
    'Stop
End If

End Function

Public Function Rho_Liq_NaCl(T_in_C, P_in_Bar)
Dim m#(0 To 5), Rho_Zero#, KNaCl#, T#, P#
T = T_in_C
P = P_in_Bar
m(0) = 58443
m(1) = 23.772
m(2) = 0.018639
m(3) = -0.0000019687
m(4) = -0.000015259
m(5) = 0.000000055058

KNaCl = m(4) + m(5) * T
Rho_Zero = m(0) / (m(1) + m(2) * T + m(3) * T ^ 2)
Rho_Liq_NaCl = Rho_Zero / (1 - 0.1 * LogExp(1 + 10 * P * KNaCl))

End Function
```

1.5 Module Form_interactions

```
Global S_Unit As String, T_Unit As Single, P_Unit As Single, Dens_Unit As
Single, T_Rho_Input As Boolean

'verification that viscosity of pure water meet the requirements
'T in °C, P in bars
Public Function Visc_Inc_data_Fit(T, P) As Boolean

If T > -22.15 And P > 0 And P > -94.765 * T + 0.947 And P < 161.22 * T +
5671.1 And T <= 900 And P <= 10000 Then

    If T < 100 Then
        Visc_Inc_data_Fit = True
        Exit Function
    ElseIf T >= 100 And T < 160 And P < 5000 Then
        Visc_Inc_data_Fit = True
        Exit Function
    ElseIf T >= 160 And T < 600 And P < 3500 Then
        Visc_Inc_data_Fit = True
        Exit Function
    ElseIf T >= 600 And P < 3000 Then
        Visc_Inc_data_Fit = True
        Exit Function
    Else
        Visc_Inc_data_Fit = False
        Exit Function
    End If
Else
    Visc_Inc_data_Fit = False
End If

End Function

Public Static Function ProgressInStatusBar(Func_Initialisation As Boolean,
Optional Label$, Optional Curr_Counter, Optional Max_Counter)
Dim Starting_Time!, Current_Time!, Label_Text$, Progress_Text$, Time_Text$,
Time_Left!, Fract_Progress!

If Func_Initialisation = True Then
    Starting_Time = Round(Timer, 0)
    Application.StatusBar = True
Else
    Current_Time = Round(Timer, 0)
    Fract_Progress = Curr_Counter / Max_Counter

    Label_Text = Label & ", "
    Progress_Text = "progress: " & Curr_Counter & " of " & Max_Counter & ": "
& Round(Fract_Progress * 100, 1) & " %"
```

```
    Time_Text = " Time to finish(min) " & Round((Current_Time -
Starting_Time) / Fract_Progress * (1 - Fract_Progress) / 60, 0)

    Application.StatusBar = Label_Text & Progress_Text & Time_Text
End If

End Function
Private Function SheetExist(n As String) As Boolean
Dim ws As Worksheet
  SheetExist = False
  For Each ws In Worksheets
    If n = ws.Name Then
      SheetExist = True
      Exit Function
    End If
  Next ws
End Function

'this function should be ready to plot the data in TP or TRho space
Public Function Matrix_Transpose() '(TP_Space As Boolean)

Dim i%, j%, k%, n%, m%, MaxRow%, TotalTables%, TotalColumns%

SetupExcelForCalc (True)
GrabDataForMatrix TotalSlts, TotalRows, TotalProps, S_Border, T_Array,
Prop_Array

If SheetExist("Matrix result") = True Then ActiveWorkbook.Sheets("Matrix
result").Delete
Sheets.Add.Name = "Matrix result"

TotalTables = UBound(S_Border, 1) - 1
i = 2
j = 3

While Prop_Array(i, 1) <> Prop_Array(j, 1)
    j = j + 1
Wend
TotalColumns = j - 1
j = i

While ActiveWorkbook.Sheets("model").Cells(S_Border(1), 1) =
ActiveWorkbook.Sheets("model").Cells(j, 1)
    j = j + 1
    If Prop_Array(TotalColumns, 1) = Prop_Array(TotalColumns + j, 1) Then
MaxRow = MaxRow + 1
Wend

With ActiveWorkbook.Sheets("Matrix result")
    For i = 1 To TotalProps - 1
```

```
        For j = 1 To TotalTables
            'headers
            .Cells(1 + (i - 1) * (MaxRow + 3), 1 + (j - 1) * TotalProps) =
"Salinity " & ActiveWorkbook.Sheets("model").Cells(S_Border(j), 1)
            .Cells(1 + (i - 1) * (MaxRow + 3), 2 + (j - 1) * TotalProps) =
ActiveWorkbook.Sheets("model").Cells(1, i + 3)
            'Temperature
            For k = 2 To MaxRow + 1
                .Cells(1 + k + (i - 1) * (MaxRow + 3), 1 + (j - 1) *
TotalProps) = T_Array(2 + (k - 2) * (TotalColumns - 1))
            Next k
            'Pressure and properties
            For k = 2 To TotalColumns
                m = 0
                .Cells(2 + (i - 1) * (MaxRow + 3), (j - 1) * TotalProps + k)
= Prop_Array(k, 1)
                    For n = S_Border(j) To S_Border(j + 1) - 1
                        If Prop_Array(n, 1) = .Cells(2 + (i - 1) * (MaxRow +
3), (j - 1) * TotalProps + k) Then 'And .Cells(2 + (i - 1) * (MaxRow + 3), (j
- 1) * TotalProps + k - 1) <> "" Then
                            m = m + 1
                            .Cells(2 + m + (i - 1) * (MaxRow + 3), k + (j -
1) * TotalProps) = Prop_Array(n, i + 1)
                        End If
                    Next n
            Next k


        Next j
    Next i
End With

SetupExcelForCalc (False)

End Function
Private Function CollapseMatrixes(MaxRows%, TotalColumns%, TTablesH%,
TTablesW%)
Dim i%, j%

For i = 1 To TTablesH
    For j = 1 To TTablesW
        Selection.Rows.Group
        Selection.Columns.Group
    Next j
Next i

End Function

Private Function GrabDataForMatrix(TotalSlts, TotalRows, TotalProps, S_Border
As Variant, T_Array As Variant, Prop_Array As Variant)
```

```
Dim i%, j%, k%

TotalRows = 2
TotalProps = 3

With ActiveWorkbook.Sheets("model")
    While .Cells(TotalRows, 1) <> ""
        TotalRows = TotalRows + 1
        If .Cells(TotalRows, 1) <> .Cells(TotalRows - 1, 1) Then TotalSlts =
TotalSlts + 1
    Wend
    While .Cells(2, TotalProps) <> ""
        TotalProps = TotalProps + 1
    Wend

    TotalProps = TotalProps - 1
    TotalRows = TotalRows - 1

    ReDim S_Border(1 To TotalSlts + 1)
    ReDim T_Array(2 To TotalRows)
    ReDim Prop_Array(2 To TotalRows, 1 To TotalProps)

    For i = 2 To TotalRows
        T_Array(i) = .Cells(i, 2)
        For j = 1 To TotalProps
            Prop_Array(i, j) = .Cells(i, j + 2)
        Next j
    Next i

    k = 1
    j = 2
    S_Border(k) = 2
    S_Border(TotalSlts + 1) = TotalRows + 1
    For i = 2 To TotalRows
        If .Cells(S_Border(k), 1) = .Cells(i, 1) Then
            j = j + 1
        Else
            k = k + 1
            S_Border(k) = i
        End If
    Next i
End With



End Function


Public Function SetupExcelForCalc(Start As Boolean)
```

```
If Start = True Then
    Application.ScreenUpdating = False
    Application.Calculation = xlCalculationManual
    Application.EnableEvents = False
    Application.DisplayAlerts = False
    Application.StatusBar = False
Else
    Application.ScreenUpdating = True
    Application.Calculation = xlCalculationAutomatic
    Application.EnableEvents = True
    Application.DisplayAlerts = True
    Application.StatusBar = True
End If

End Function

Sub StartIt()
    SetupExcelForCalc True
End Sub

Public Function Crit_Array_Filling(S_Tmp, SaltRun, CP_array)
Dim n As Integer, mH2O As Single, mNaCl As Single, XNaCl As Double, T_min As
Single, T_Max As Single

Dim i As Integer, j As Integer
Dim Sum1 As Double, PH2O_Crit As Double, TH2O_Crit As Double

Dim c(1 To 14) As Double, cA(1 To 11) As Single, d(1 To 11) As Double
Dim T As Double, P As Single, P_Crit As Single
Dim X_Crit As Double, X_Crit_der As Double, T2 As Double, X_Crit2 As Double

mH2O = 18.015268
mNaCl = 58.4428
XNaCl = S_Tmp / mNaCl / (S_Tmp / mNaCl + (1 - S_Tmp) / mH2O)
TH2O_Crit = 373.973 - 0.027

T = 0
'estimation of T
For j = 1 To 80
    If XNaCl = 0 Then
        T = TH2O_Crit
        Exit For
    End If
    T = j * 25
    X_Crit = 0: P_Crit = 0
    X_and_P_crit T, X_Crit, P_Crit

    If X_Crit >= XNaCl Then Exit For
Next j
```

```
j = 0
'Newtons algorythm to obtain X_Crit
While Abs(X_Crit - XNaCl) > 0.000001
    X_Crit = 0: X_Crit2 = 0: X_Crit_der = 0
    X_and_P_crit T, X_Crit, P_Crit
    X_Crit = X_Crit - XNaCl

    T2 = T - 0.001
    X_and_P_crit T2, X_Crit2, P_Crit
    X_Crit2 = X_Crit2 - XNaCl

    X_Crit_der = (X_Crit - X_Crit2) / (T - T2)
    T = T - X_Crit / X_Crit_der
    X_Crit = X_Crit + XNaCl

    If XNaCl = 0 Then X_Crit = 0
    j = j + 1
    If j > 1000 Then Stop
Wend

If T = 0 Then T = 0.01
X_and_P_crit T, X_Crit, P_Crit
    'TEMPERATURE AND PRESSURE CORRECTED FOR CRITICAL POINT OF PURE WATER,
    'ACCORDING TO ITS POSITION IN IAPWS 95


'Savings data in array
CP_array(SaltRun, 0) = XNaCl
CP_array(SaltRun, 1) = T
CP_array(SaltRun, 2) = P_Crit
If T < 1000 Then
    CP_array(SaltRun, 3) = Rho_Brine(XNaCl, T, P_Crit)
    ' 1000 °C and pressure at this temperature for drawing isochores
    CP_array(SaltRun, 4) = 1000
    Sum1 = CP_array(SaltRun, 3) * mH2O / (mH2O * (1 - XNaCl) + mNaCl * XNaCl)
    CP_array(SaltRun, 5) = Water_Pressure_calc(1273.15, Sum1) * 10
End If

End Function
Public Function WtToMol(wtPecent As Double)
mH2O = 18.015268
mNaCl = 58.4428
WtToMol = wtPecent / mNaCl / (wtPecent / 100 / mNaCl + (1 - wtPecent / 100) /
mH2O)
End Function
Public Function MolToWt(MolPercent As Double)
mH2O = 18.015268
mNaCl = 58.4428
```

```
MolToWt = mNaCl * MolPercent / (mNaCl * MolPercent / 100 + (1 - MolPercent /
100) * mH2O)
End Function

Sub Model_Page_setup()

Dim Ttxt As String, Ptxt As String, Dtxt As String

With Sheets("model").Cells
.Clear
.RowHeight = 15
.ColumnWidth = 8.43
End With

'If Temp.Value = "° K" Then T_Unit = 273.15 Else T_Unit = 0
'If Pres.Value = "MPa" Then P_Unit = 10 Else P_Unit = 1
'If Dens.Value = "kg*m-3" Then Dens_Unit = 1 Else Dens_Unit = 0.001

If T_Unit = 273.15 Then Ttxt = "°K" Else Ttxt = "°C"
If P_Unit = 10 Then Ptxt = "MPa" Else Ptxt = "bar"
If Dens_Unit = 1 Then Dtxt = "kg*m-3" Else Dtxt = "g*cm-3"

Cells(1, 1) = "Salt, " & S_Unit
Cells(1, 2) = "T, " & Ttxt
Cells(1, 3) = "P, " & Ptxt
Cells(1, 4) = "Density, " & Dtxt
Columns("E:E").ColumnWidth = 35
Cells(1, 5) = "Notes"

Rows("2:2").Select
With ActiveWindow
    .SplitColumn = 0
    .SplitRow = 1
End With
ActiveWindow.FreezePanes = True
Columns("A:F").Select
Range("F1").Activate
Selection.AutoFilter
Columns("D:D").Select
Selection.NumberFormat = "0.0"
Columns("C:C").Select
Selection.NumberFormat = "0.0"

End Sub
```

1.6 Module Math_funcs

```
Public Function LogExp(X) As Double
Dim Tmp As Double
Tmp = Exp(1)
LogExp = Log(X) / Log(Tmp#)
End Function
Public Static Function Log10(X) As Double
Log10 = Log(X) / Log(10#)
End Function
Public Function Arccos(X) As Double
If Round(X, 8) = 1# Then Arccos = 0#: Exit Function
If Round(X, 8) = -1# Then Arccos = Pi: Exit Function
Arccos = Atn(-X / Sqr(-X * X + 1)) + 2 * Atn(1)
End Function
Public Function Round_Down(Nmbr As Double, DecPl As Integer) As Double
    Round_Down = Sgn(Nmbr) * Fix(Abs(Nmbr) * 10 ^ (DecPl)) / 10 ^ DecPl
End Function
Public Function Round_Up(Nmbr As Double, DecPl As Integer) As Double
    Round_Up = -Sgn(Nmbr) * Int(-Abs(Nmbr) * 10 ^ (DecPl)) / 10 ^ DecPl
End Function
Public Function Arccs(X) As Double
If Round(X, 12) = 1# Then Arccs = 0#: Exit Function
If Round(X, 12) = -1# Then Arccs = Pi: Exit Function
Arccs = Atn(-X / Sqr(-X * X + 1)) + 2 * Atn(1)
End Function
```

1.7 Module Model_eqs

```
' reduced susceptibility parameter
Public Function XsiCapital(bbeta, SltWtFrac, Ti, Pi, rhoi) As Double
Dim CP_array(0, 0 To 5) As Double, PCrit#, RhoCrit#, XNaCl#, mH2O#, mNaCl#

mH2O = 18.015268
mNaCl = 58.4428

XNaCl = Salinity / mNaCl / (SltWtFrac / mNaCl + (1 - SltWtFrac) / mH2O)
Crit_Array_Filling Salinity, 0, CP_array
PCrit = CP_array(0, 2)
RhoCrit = CP_array(0, 3)

XsiCapital = rhoi ^ 2 * bbeta * PCrit / RhoCrit ^ 2


End Function

' Akinfief and Diamond 2009
Public Function Qtz_solubility(xnacli, Ti, rhoi) As Double
Dim a#(0 To 3), At#, b#(0 To 3), Bt#, mH2O#, mNaCl#, VH2O#, T!, LogSolub#,
XNaCl!

Dim i%

mH2O = 18.015268
mNaCl = 58.4428
XNaCl = xnacli

T = Ti + 273.15
a(0) = 4.262:  a(1) = -5764.2: a(2) = 1.7513 * 10 ^ 6: a(3) = -2.2869 * 10 ^
8
b(0) = 2.8454: b(1) = -1006.9: b(2) = 3.5689 * 10 ^ 5: b(3) = 0

For i = 0 To 3
    At = At + a(i) * T ^ -i
    Bt = Bt + b(i) * T ^ -i
Next i
VH2O = 1 / rhoi * 1000 * (mNaCl * XNaCl + mH2O * (1 - XNaCl))
VH2O = (VH2O - 30.8 * XNaCl) / (1 - XNaCl)
LogSolub = At + Bt * Log10(18.0152 / VH2O) + 2 * Log10(1 - XNaCl)
Qtz_solubility = 10 ^ LogSolub

End Function
Public Function dQtzDP_const_T(xnacli, Ti, Pi, rhoi) As Double
Dim Rho2#, dP#, mH2O#, mNaCl#, slnty#, tmpPPPPP#
'step in pressure for (dQ/dP)T
dP = 0.5
```

```
mH2O = 18.015268
mNaCl = 58.4428

Rho2 = Rho_Brine(xnacli, Ti, Pi + dP)
slnty = Round(1 - xnacli * mNaCl / (xnacli * mNaCl + (1 - xnacli) * mH2O), 4)
tmpPPPPP = Qtz_solubility(xnacli, Ti, rhoi)
''NOTE THAT (1-Xnacl) moved from final eq to Slnty above
dQtzDP_const_T = (tmpPPPPP - Qtz_solubility(xnacli, Ti, Rho2)) / (-dP) /
tmpPPPPP '* rhoi * (slnty)

End Function

Public Function dQtzDT_const_P(xnacli, Ti, Pi, rhoi) As Double
Dim Rho2#, dT#, mH2O#, mNaCl#, slnty#, tmpPPPPP#
'step in pressure for (dQ/dT)P
dT = -0.5
mH2O = 18.015268
mNaCl = 58.4428

Rho2 = Rho_Brine(xnacli, Ti + dT, Pi)
slnty = Round(1 - xnacli * mNaCl / (xnacli * mNaCl + (1 - xnacli) * mH2O), 4)
tmpPPPPP = Qtz_solubility(xnacli, Ti, rhoi)
''NOTE THAT (1-Xnacl) moved from final eq to Slnty above
''dQtzDT_const_P = -(Qtz_solubility(xnacli, Ti, rhoi) -
Qtz_solubility(xnacli, Ti + dT, Rho2)) / (dT) * rhoi * slnty
dQtzDT_const_P = -(tmpPPPPP - Qtz_solubility(xnacli, Ti + dT, Rho2)) / (dT) /
tmpPPPPP '* rhoi * slnty

End Function
'isotermal compressibility
Public Function beta(xnacli, Ti, Pi, rhoi) As Double
Dim Delta#, P2#, Rho2#
Delta = 0.1  '0.5 '

P2 = Pi + Delta
Rho2 = Rho_Brine(xnacli, Ti, P2)

beta = 1 / rhoi * (rhoi - Rho2) / (Pi - P2)

End Function
'isobaric expansivity
Public Function Alpha(xnacli, Ti, Pi, rhoi) As Double
Dim Delta#, P2
Delta = -0.5
T2 = Ti + Delta
Rho2 = Rho_Brine(xnacli, T2, Pi)

Alpha = -1 / rhoi * (rhoi - Rho2) / (Ti - T2)
End Function
```

```
'isotermal compressibility
Public Function dRhoDX(xnacli, Ti, Pi, rhoi) As Double
Dim xNaCl2#, Delta#, Rho2#

Delta = 0.00001
xNaCl2 = xnacli + Delta
Delta = LV_Pressure(Ti, xNaCl2)

If Delta <= Pi Then
    Rho2 = Rho_Brine(xNaCl2, Ti, Pi, False)
    dRhoDX = 1 / rhoi * (rhoi - Rho2) / (xnacli - xNaCl2)
    rhoi = Allpha(xnacli, Ti, Pi, rhoi)
End If

End Function
'Total derviative approximate estimation
http://www.solitaryroad.com/c353.html
Public Function Allpha(xnacli, Ti, Pi, rhoi) As Double
Dim DeltaT#, DeltaP#, DeltaX#
DeltaT = -0.5
DeltaP = 0.1
DeltaX = 0.00001

Rho2 = Rho_Brine(xnacli + DeltaX, Ti + DeltaT, Pi + DeltaP, False)

Allpha = 1 / rhoi * (rhoi - Rho2) / -0.5 / 0.1 / 0.00001
End Function

Public Function Fluxibility(S_in, T_in, P_in, Rho_in) As Double

Dim tStarH#, RhoWater#, Enthalpy#, Viscosity#, T#, P#, q2h#

T = T_in
P = P_in
Rho = Rho_in
XNaCl = WtToMol(S_in * 100) / 100

tStarH = T_star_H(XNaCl, q2h, T, P)
RhoWater = Rho_Water(tStarH - 273.15, P)
Enthalpy = Round(Water_Enthalpy_calc(tStarH, RhoWater) * 1000, 1)
Viscosity = Viscosity_1Brines_CHOOSEN(S_in * 100, T, P, Rho)
'Pin used to return volumetric temperature from the flux calcs
P_in = Rho * (Enthalpy - 44311.8)
Fluxibility = P_in * (1037.2 - Rho) / Viscosity

End Function
```

1.8 Module OtherViscModels

```
Public Function Mao_Duan_Visc(S_Wt_Frac, T_in_C, P_bars) As Double

Dim Molarity#, T_K#, ViscH2O#, ViscRatio#, RhoH2O#
Dim a#(0 To 2), b#(0 To 2), c#(0 To 2), d#(1 To 10)
Dim A_cap#, B_cap#, C_cap#

T_K = T_in_C + 273.15
RhoH2O = Rho_Water(T_in_C, P_bars)

If S_Wt_Frac >= 1 Then Molarity = 7 Else Molarity = 1000 * S_Wt_Frac /
58.4428 / (1 - S_Wt_Frac)

If Molarity <= 6 Then

    ViscH2O = Water_Viscosity_calc(T_K, RhoH2O)

    a(0) = -0.21319213: a(1) = 0.0013651583:     a(2) = -0.0000012191756
    b(0) = 0.069161945: b(1) = -0.00027292263:    b(2) = 0.00000020852448
    c(0) = -0.0025988855: c(1) = 0.0000077989227: c(2) = 0#

    For i = 0 To 2
        A_cap = A_cap + a(i) * T_K ^ i
        B_cap = B_cap + b(i) * T_K ^ i
        C_cap = C_cap + c(i) * T_K ^ i
    Next i
    ViscRatio = A_cap * Molarity + B_cap * Molarity ^ 2 + C_cap * Molarity ^
3
    ViscRatio = Exp(ViscRatio)
    Mao_Duan_Visc = ViscRatio * ViscH2O
Else
    Mao_Duan_Visc = 0.123456789
End If

End Function



'salinity in wt fracts, temperature in K, pressure in bars, density of the
water at given PT
Public Function Palliser_1998_visc(slt, Ti, P, Di)

Dim h#(1 To 4), HH(1 To 6, 1 To 7) As Double, DR As Double, TR As Single, VR
As Double, d As Double, T As Double
Dim Total#, i As Integer, j As Integer, V0 As Double, PWViscosity As Double
Dim MuWater As Double, MuSalt As Double, MuSalt_800 As Double, MuBrine As
Double, XNaCl#
Dim CP_array#(1 To 1, 0 To 5)
```

```
h(1) = 1: h(2) = 0.978197: h(3) = 0.579829: h(4) = -0.202354

HH(1, 1) = 0.5132047:  HH(1, 2) = 0.2151778: HH(1, 3) = -0.2818107: HH(1, 4)
= 0.1778064:  HH(1, 5) = -0.0417661: HH(1, 6) = 0:          HH(1, 7) = 0
HH(2, 1) = 0.3205656:  HH(2, 2) = 0.7317883: HH(2, 3) = -1.070786:  HH(2, 4)
= 0.460504:   HH(2, 5) = 0:          HH(2, 6) = -0.01578386: HH(2, 7) = 0
HH(3, 1) = 0:          HH(3, 2) = 1.241044:  HH(3, 3) = -1.263184:  HH(3, 4)
= 0.2340379:  HH(3, 5) = 0:          HH(3, 6) = 0:          HH(3, 7) = 0
HH(4, 1) = 0:          HH(4, 2) = 1.476783:  HH(4, 3) = 0:          HH(4, 4)
= -0.4924179: HH(4, 5) = 0.1600435:  HH(4, 6) = 0:          HH(4, 7) = -
0.003629481
HH(5, 1) = -0.7782567: HH(5, 2) = 0:         HH(5, 3) = 0:          HH(5, 4)
= 0:          HH(5, 5) = 0:          HH(5, 6) = 0:          HH(5, 7) = 0
HH(6, 1) = 0.1885447:  HH(6, 2) = 0:         HH(6, 3) = 0:          HH(6, 4)
= 0:          HH(6, 5) = 0:          HH(6, 6) = 0:          HH(6, 7) = 0

DR = 0.317763:         TR = 647.27:          VR = 0.00055071
' water viscosity calculations based on what Palliser used (Kissling 1995 ?)

d = Di * 0.001 / DR
T = Ti / TR
Total = 0

For i = 1 To 4
    Total = Total + h(i) / T ^ (i - 1)
Next i

V0 = T ^ 0.5 / Total
Total = 0

For i = 1 To 6
    For j = 1 To 7
        Total = Total + d * HH(i, j) * (1# / T - 1#) ^ (i - 1) * (d - 1#) ^
(j - 1)
    Next j
Next i

PWViscosity = V0 * Exp(Total) * VR * 0.1
' viscosity calculations
If Ti >= 1273.15 Then
    MuSalt = 4.71624 * 10 ^ -3 + (-4.0203 * 10 ^ -6) * (1000)
Else
    MuSalt = 4.71624 * 10 ^ -3 + (-4.0203 * 10 ^ -6) * (Ti - 273.15)
End If

MuSalt_800 = 4.71624 * 10 ^ -3 + (-4.0203 * 10 ^ -6) * 800 ' (Ti - 273.15) '
If Ti < 1073.15 Then
    MuBrine = (PWViscosity * (1 + 3 * slt) * ((800 - (Ti - 273.15)) / 800) ^
9 + ((Ti - 273.15) / 800) ^ 9 * (PWViscosity * (1 - slt) + MuSalt_800 * slt))
/ (((800 - (Ti - 273.15)) / 800) ^ 9 + ((Ti - 273.15) / 800) ^ 9)
```

```
Else
    MuBrine = PWViscosity * (1 - slt) + MuSalt * slt
End If

Palliser_1998_visc = MuBrine * 1000000#

End Function

Public Function Palliser_1998_visc2ndHalf(slt, Ti, P, Di)

Dim h#(1 To 4), HH(1 To 6, 1 To 7) As Double, DR As Double, TR As Single, VR
As Double, d As Double, T As Double
Dim Total#, i As Integer, j As Integer, V0 As Double, PWViscosity As Double
Dim MuWater As Double, MuSalt As Double, MuSalt_800 As Double, MuBrine As
Double, XNaCl#
Dim CP_array#(1 To 1, 0 To 5)

h(1) = 1: h(2) = 0.978197: h(3) = 0.579829: h(4) = -0.202354

HH(1, 1) = 0.5132047:  HH(1, 2) = 0.2151778: HH(1, 3) = -0.2818107: HH(1, 4)
= 0.1778064:  HH(1, 5) = -0.0417661: HH(1, 6) = 0:           HH(1, 7) = 0
HH(2, 1) = 0.3205656:  HH(2, 2) = 0.7317883: HH(2, 3) = -1.070786:  HH(2, 4)
= 0.460504:   HH(2, 5) = 0:          HH(2, 6) = -0.01578386: HH(2, 7) = 0
HH(3, 1) = 0:          HH(3, 2) = 1.241044:  HH(3, 3) = -1.263184:  HH(3, 4)
= 0.2340379:  HH(3, 5) = 0:          HH(3, 6) = 0:           HH(3, 7) = 0
HH(4, 1) = 0:          HH(4, 2) = 1.476783:  HH(4, 3) = 0:           HH(4, 4)
= -0.4924179: HH(4, 5) = 0.1600435:  HH(4, 6) = 0:           HH(4, 7) = -
0.003629481
HH(5, 1) = -0.7782567: HH(5, 2) = 0:         HH(5, 3) = 0:          HH(5, 4)
= 0:          HH(5, 5) = 0:          HH(5, 6) = 0:           HH(5, 7) = 0
HH(6, 1) = 0.1885447:  HH(6, 2) = 0:         HH(6, 3) = 0:          HH(6, 4)
= 0:          HH(6, 5) = 0:          HH(6, 6) = 0:           HH(6, 7) = 0

DR = 0.317763:         TR = 647.27:          VR = 0.00055071
' water viscosity calculations based on what Palliser used (Kissling 1995 ?)

d = Di * 0.001 / DR
T = Ti / TR
Total = 0

For i = 1 To 4
    Total = Total + h(i) / T ^ (i - 1)
Next i

V0 = T ^ 0.5 / Total
Total = 0

For i = 1 To 6
    For j = 1 To 7
```

```
        Total = Total + d * HH(i, j) * (1# / T - 1#) ^ (i - 1) * (d - 1#) ^
(j - 1)
    Next j
Next i

PWViscosity = V0 * Exp(Total) * VR * 0.1
' viscosity calculations
If Ti >= 1273.15 Then
    MuSalt = 4.71624 * 10 ^ -3 + (-4.0203 * 10 ^ -6) * (1000)
Else
    MuSalt = 4.71624 * 10 ^ -3 + (-4.0203 * 10 ^ -6) * (Ti - 273.15)
End If

MuSalt_800 = 4.71624 * 10 ^ -3 + (-4.0203 * 10 ^ -6) * 800
If Ti < 1073.15 Then
    MuBrine = (PWViscosity * (1 + 3 * slt) * ((800 - (Ti - 273.15)) / 800) ^
9) / (((800 - (Ti - 273.15)) / 800) ^ 9 + ((Ti - 273.15) / 800) ^ 9)
Else
    MuBrine = PWViscosity * (1 - slt) + MuSalt * slt
End If

Palliser_1998_visc2ndHalf = MuBrine * 1000000#

End Function
Public Function Palliser_1998_visc1StHalf(slt, Ti, P, Di)

Dim h#(1 To 4), HH(1 To 6, 1 To 7) As Double, DR As Double, TR As Single, VR
As Double, d As Double, T As Double
Dim Total#, i As Integer, j As Integer, V0 As Double, PWViscosity As Double
Dim MuWater As Double, MuSalt As Double, MuSalt_800 As Double, MuBrine As
Double, XNaCl#
Dim CP_array#(1 To 1, 0 To 5)

h(1) = 1: h(2) = 0.978197: h(3) = 0.579829: h(4) = -0.202354

HH(1, 1) = 0.5132047:  HH(1, 2) = 0.2151778: HH(1, 3) = -0.2818107: HH(1, 4)
= 0.1778064:  HH(1, 5) = -0.0417661: HH(1, 6) = 0:           HH(1, 7) = 0
HH(2, 1) = 0.3205656:  HH(2, 2) = 0.7317883: HH(2, 3) = -1.070786:  HH(2, 4)
= 0.460504:   HH(2, 5) = 0:          HH(2, 6) = -0.01578386: HH(2, 7) = 0
HH(3, 1) = 0:          HH(3, 2) = 1.241044:  HH(3, 3) = -1.263184:  HH(3, 4)
= 0.2340379:  HH(3, 5) = 0:          HH(3, 6) = 0:           HH(3, 7) = 0
HH(4, 1) = 0:          HH(4, 2) = 1.476783:  HH(4, 3) = 0:           HH(4, 4)
= -0.4924179: HH(4, 5) = 0.1600435:  HH(4, 6) = 0:           HH(4, 7) = -
0.003629481
HH(5, 1) = -0.7782567: HH(5, 2) = 0:         HH(5, 3) = 0:           HH(5, 4)
= 0:          HH(5, 5) = 0:          HH(5, 6) = 0:           HH(5, 7) = 0
HH(6, 1) = 0.1885447:  HH(6, 2) = 0:         HH(6, 3) = 0:           HH(6, 4)
= 0:          HH(6, 5) = 0:          HH(6, 6) = 0:           HH(6, 7) = 0

DR = 0.317763:         TR = 647.27:          VR = 0.00055071
```

```
' water viscosity calculations based on what Palliser used (Kissling 1995 ?)

d = Di * 0.001 / DR
T = Ti / TR
Total = 0

For i = 1 To 4
    Total = Total + h(i) / T ^ (i - 1)
Next i

V0 = T ^ 0.5 / Total
Total = 0

For i = 1 To 6
    For j = 1 To 7
        Total = Total + d * HH(i, j) * (1# / T - 1#) ^ (i - 1) * (d - 1#) ^
(j - 1)
    Next j
Next i

PWViscosity = V0 * Exp(Total) * VR * 0.1
' viscosity calculations
If Ti >= 1273.15 Then
    MuSalt = 4.71624 * 10 ^ -3 + (-4.0203 * 10 ^ -6) * (1000)
Else
    MuSalt = 4.71624 * 10 ^ -3 + (-4.0203 * 10 ^ -6) * (Ti - 273.15)
End If

MuSalt_800 = 4.71624 * 10 ^ -3 + (-4.0203 * 10 ^ -6) * 800
If Ti < 1073.15 Then
    MuBrine = (((Ti - 273.15) / 800) ^ 9 * (PWViscosity * (1 - slt) +
MuSalt_800 * slt)) / (((800 - (Ti - 273.15)) / 800) ^ 9 + ((Ti - 273.15) /
800) ^ 9)
Else
    MuBrine = PWViscosity * (1 - slt) + MuSalt * slt
End If

Palliser_1998_visc1StHalf = MuBrine * 1000000#

End Function

'25-200 °C, 0.1-30 mpa, 0-6 mol/kg
'Public Function Kestin_1984_Visc(slt, T, P, RhoWater)
'limits between 10-350 °C, 0.1-50 mpa, 0-5 m
Public Function Phillips_1981(slt, Ti, RhoWater)
Dim MuW#, m#, i%, j%, a!, b!, c!, d!, k!, ak#(0 To 3), bij#(0 To 5, 0 To 4),
tstar#, RhoStar#
Dim MuZero#, RhoRatio#, TRatio#

'A. Nagashima 1977 water viscosity code
```

```
ak(0) = 0.0181583:  ak(1) = 0.0177624: ak(2) = 0.0105207: ak(3) = -0.0036744

bij(0, 0) = 0.501938:  bij(0, 1) = 0.235622:  bij(0, 2) = -0.274637: bij(0,
3) = 0.145831:  bij(0, 4) = -0.0270448
bij(1, 0) = 0.162888:  bij(1, 1) = 0.789393:  bij(1, 2) = -0.743539: bij(1,
3) = 0.263129:  bij(1, 4) = -0.0253093
bij(2, 0) = -0.130356: bij(2, 1) = 0.673665:  bij(2, 2) = 0.959456:  bij(2,
3) = 0.347247:  bij(2, 4) = -0.0267758
bij(3, 0) = 0.907919:  bij(3, 1) = 1.207552:  bij(3, 2) = -0.687343: bij(3,
3) = 0.213486:  bij(3, 4) = -0.0822904
bij(4, 0) = -0.551119: bij(4, 1) = 0.0670665: bij(4, 2) = -0.497089: bij(4,
3) = 0.100754:  bij(4, 4) = 0.0602253
bij(5, 0) = 0.146543:  bij(5, 1) = -0.084337: bij(5, 2) = 0.195286:  bij(5,
3) = -0.032932: bij(5, 4) = -0.0202595
tstar = 647.27
RhoStar = 317.763

TRatio = (tstar / (Ti + 273.15)) ^ -1
RhoRatio = RhoWater / RhoStar

For i = 0 To 3
    MuZero = MuZero + ak(i) * TRatio ^ i
Next i
MuZero = TRatio ^ -0.5 * MuZero ^ -1

For i = 0 To 5
    For j = 0 To 4
        MuW = MuW + bij(i, j) * (TRatio - 1) ^ i * (RhoRatio - 1) ^ j
    Next j
Next i

MuW = Water_Viscosity_calc(Ti + 273.15, RhoWater) 'MuZero * Exp(RhoRatio *
MuW)

a = 0.0816: b = 0.0122: c = 0.000128: d = 0.000629: k = -0.7


m = 1000 * slt / ((1 - slt) * 58.4428)

Philllips_1981 = MuW * (1 + a * m + b * m ^ 2 + c * m ^ 3 + d * Ti * (1 -
Exp(k * m)))

End Function

'Leyendekkers 1979
Public Function TTG_model(slt, T, P, RhoWater)
T_Star = 647.27
D_star = 317.763
m = 1000 * slt / (58.4428 * (1 - slt))
Fmi = 100# * 9.1625 * m + 100# * 3.253 * m ^ 2
```

```
ViscW = Water_Viscosity_calc(T, RhoWater)
TTG_model = ViscW * Exp(Fmi)

End Function

Public Function Kestin_1984_Visc(slt, T_in_K, P_in_mPa, RhoWater)

Dim i As Integer, j As Integer
Dim mH2O As Double, mNaCl As Single, m As Double, XNaCl As Single, Rho As
Double, Visc As Double
Dim a(1 To 3) As Double, b(1 To 3) As Double, A_Up As Double, B_Up As Double,
d(1 To 3, 0 To 2) As Double, D_i As Double, Eta_R As Double
Dim beta_ij(1 To 3, 0 To 3) As Double, beta_E As Double, beta_0 As Double,
beta As Double

mH2O = 18.015268
mNaCl = 58.4428
XNaCl = slt / mNaCl / (slt / mNaCl + (1 - slt) / mH2O)
T = T_in_K
P = P_in_mPa
a(1) = 8.4142 * 10 ^ -2:  a(2) = 2.98 * 10 ^ -3:  a(3) = 3.11 * 10 ^ -4
b(1) = -3.7797 * 10 ^ -2: b(2) = 6.205 * 10 ^ -3: b(3) = -9.68 * 10 ^ -5

d(1, 0) = 6.596 * 10 ^ -2: d(1, 1) = 1.063 * 10 ^ -3:   d(1, 2) = -3.164 * 10
^ -6
d(2, 0) = 6.271 * 10 ^ -3: d(2, 1) = -1.313 * 10 ^ -4:  d(2, 2) = 6.067 * 10
^ -7
d(3, 0) = 1.489 * 10 ^ -3: d(3, 1) = -1.359 * 10 ^ -6:  d(3, 2) = -3.094 * 10
^ -8

beta_ij(1, 0) = 6.26 * 10 ^ -1:    beta_ij(2, 0) = -1.64 * 10 ^ -1:
beta_ij(3, 0) = 1.88 * 10 ^ -2
beta_ij(1, 1) = -1.64 * 10 ^ -2:   beta_ij(2, 1) = 5.24 * 10 ^ -3:
beta_ij(3, 1) = -6.36 * 10 ^ -4
beta_ij(1, 2) = 1.35 * 10 ^ -4:    beta_ij(2, 2) = -4.9 * 10 ^ -5:
beta_ij(3, 2) = 6.11 * 10 ^ -6
beta_ij(1, 3) = -3.65 * 10 ^ -7:   beta_ij(2, 3) = 1.36 * 10 ^ -7:
beta_ij(3, 3) = -1.69 * 10 ^ -8

m = 1000 * slt / (mNaCl * (1 - slt))
A_Up = 0
B_Up = 0

For i = 1 To 3
    A_Up = A_Up + a(i) * m ^ i
    B_Up = B_Up + b(i) * m ^ i
Next i
' this value is from J. Kestin, M. Sokolov, and W. A. Wakeham, J. Phys. Chem.
Ref Data 7:941 (1978).
```

```
mu20 = 1002

Rho = RhoWater

'ViscW = Water_Viscosity_calc(T, RhoWater)

Eta_R = 1

For i = 1 To 3
    For j = 0 To 2
        D_i = D_i + d(i, j) * (T - 273.15) ^ j
    Next j
    Eta_R = Eta_R + D_i * m ^ i
    D_i = 0
Next i

For i = 1 To 3
    For j = 0 To 3
        beta_E = beta_E + beta_ij(i, j) * m ^ i * (T - 273.15) ^ j
    Next j
Next i

beta_0 = -0.7879 + 2.927 * 10 ^ -2 * (T - 273.15) - 1.584 * 10 ^ -4 * (T -
273.15) ^ 2 + 3.775 * 10 ^ -7 * (T - 273.15) ^ 3

beta = beta_E + beta_0

ViscW = 10 ^ ((20 - T + 273.15) * (1.2378 - 1.303 * 10 ^ -3 * (20 - T +
273.15) + 3.06 * 10 ^ -6 * (20 - T + 273.15) ^ 2 + 2.55 * 10 ^ -8 * (20 - T +
273.15) ^ 3) / (96 + T - 273.15)) * 1002


Kestin_1984_Visc = Exp(A_Up + B_Up * LogExp(ViscW / mu20)) * ViscW * (1 +
beta * P / 1000)

End Function
```

1.9 Module Revised_Visc

```
Public Function T_star_visc_Salt_Corrected(wt_Percent, T_in_C) As Double
Dim z0#, b#, c#, d#, E#, f#, Wt_frac#

Wt_frac = wt_Percent / 100


z0 = 0
b = -35.9858
c = 0.80017
d = 1 * 10 ^ -6
E = -0.05239
f = 1.32936

T_star_visc_Salt_Corrected = b * Wt_frac ^ c + T_in_C * (1 - d * T_in_C ^ E -
f * Wt_frac ^ c * T_in_C ^ E)
T_star_visc_Salt_Corrected = Round(T_star_visc_Salt_Corrected + 273.15, 3)

End Function


Public Function Viscosity_1Brines_CHOOSEN(S_in_Wt_Per, T_in_C, P_in_Bar,
Rho_in_KGM) As Double
Dim T_Star#, Rho_W#, Pres#, Tmp#
'MODEL LIMITATION: T_STAR HAVE TO BE <=900 AND APPROX. >40 °C

Pres = P_in_Bar

T_Star = T_star_visc_Salt_Corrected(S_in_Wt_Per, T_in_C)
If T_Star > 1173.15 Then
    Viscosity_1Brines_CHOOSEN = 0
Else
    If S_in_Wt_Per < 100 And S_in_Wt_Per <> 0 Then

        If Pres <= 15 And T_Star <= 487.85 And MolToWt(X_L_Sat(T, P) * 100) -
S_in_Wt_Per < 0.1 Then
            'Never worked, because it requires either pressure below 1 bar
(below limits of our model)
            'or PTx conditions in 2 phase field, which also the limit of the
model

            Exit Function
            Tmp = P_H2O_Boiling_Curve(T_Star - 273.15)
            If Pres < Tmp Then
                Pres = Water_Pressure_calc(T_Star, Rho_in_KGM) * 10
                If Pres < Tmp Then Pres = Tmp
            End If
        End If
```

```
    ElseIf S_in_Wt_Per = 100 Then

        Tmp = P_H2O_Boiling_Curve(T_Star - 273.15)
        If Pres < Tmp Then Pres = Tmp

    End If

    Rho_W = Rho_Water(T_Star - 273.15, Pres)
    Viscosity_1Brines_CHOOSEN = Water_Viscosity_calc(T_Star, Rho_W)

End If
End Function
```

1.10 Module Water_prop

```
'water constants and equation of state from W. WAGNER AND A. PRUß
'J. Phys. Chem. Ref. Data, Vol. 31, No. 2, 2002
'
'
'DERIVATIVES OF THE RESIDUAL PART IN EQ 16, PhiR
'
'
'dDeltaddelta = (Delta_Rho - 1) * (A_CAPS(i) * Theta * 2 / Beta(i) *
((Delta_Rho - 1) ^ 2) ^ (1 / (2 * Beta(i)) - 1) + 2 * B_CAPS(i) * A(i) *
((Delta_Rho - 1) ^ 2) ^ (A(i) - 1))
'd2Deltaddeltadelta = 1 / (Delta_Rho - 1) * dDeltaddelta + (Delta_Rho - 1) ^
2 * (4 * B_CAPS(i) * A(i) * (A(i) - 1) * ((Delta_Rho - 1) ^ 2) ^ (A(i) - 2) +
2 * A_CAPS(i) ^ 2 * Beta(i) ^ -2 * (((Delta_Rho - 1) ^ 2) ^ (1 / 2 / Beta(i)
- 1)) ^ 2 + A_CAPS(i) * Theta * 4 / Beta(i) * (1 / 2 / Beta(i) - 1) *
((Delta_Rho - 1) ^ 2) ^ (1 / 2 / Beta(i) - 2))
'
'dDeltaBIdDelta = B(i) * Delta ^ (B(i) - 1) * dDeltaddelta
'd2DeltaBIddeltadelta = B(i) * (Delta ^ (B(i) - 1) * d2Deltaddeltadelta +
(B(i) - 1) * Delta ^ (B(i) - 2) * dDeltaddelta ^ 2)
'dDeltaBIdTau = -2 * Theta * B(i) * Delta ^ (B(i) - 1)
'd2DeltaBIDTauTau = 2 * B(i) * Delta ^ (B(i) - 1) + 4 * Theta ^ 2 * B(i) *
(B(i) - 1) * Delta ^ (B(i) - 2)
'd2DeltaBIdRhoTau = -A_CAPS(i) * B(i) * 2 / Beta(i) * Delta ^ (B(i) - 1) *
(Delta_Rho - 1) * ((Delta_Rho - 1) ^ 2) ^ (1 / (2 * Beta(i)) - 1) - 2 * Theta
* B(i) * (B(i) - 1) * Delta ^ (B(i) - 2) * dDeltaddelta
'
'
'dPsidDelta = -2 * C_CAPS(i) * (Delta_Rho - 1) * Psi
'd2Psiddeltadelta = (2 * C_CAPS(i) * (Delta_Rho - 1) ^ 2 - 1) * 2 * C_CAPS(i)
* Psi
'dPsidTau = -2 * D_CAPS(i) * (Tau - 1) * Psi
'd2PsidTauTau = (2 * D_CAPS(i) * (Delta_Rho - 1) ^ 2 - 1) * 2 * D_CAPS(i) *
Psi
'd2PsidTauDelta = 4 * C_CAPS(i) * Psi * D_CAPS(i) * (Delta_Rho - 1) * (Tau -
1)



'WAGNER 2002
Public Function Water_Pressure_calc(T, Rho)

Dim R_constant As Double, Delta_Rho As Variant, Tau As Variant
R_constant = 0.46151805
Delta_Rho = CDec(Rho / 322): Tau = CDec(647.096 / T)

Water_Pressure_calc = ((1 + Delta_Rho * PhiR_Delta(Delta_Rho, Tau)) * Rho *
R_constant * T) / 1000
End Function
```

```
'WAGNER 2002
'Units - Joule per kg
Public Function Water_Enthalpy_calc(T_in_K, Rho_in_kgm3)
Dim R_constant As Double, Delta_Rho As Variant, T#, Tau As Variant
R_constant = 0.46151805
Delta_Rho = CDec(Rho_in_kgm3 / 322): Tau = CDec(647.096 / T_in_K)

Water_Enthalpy_calc = (1 + Tau * (Phi0_Tau(Delta_Rho, Tau) +
PhiR_Tau(Delta_Rho, Tau)) + Delta_Rho * PhiR_Delta(Delta_Rho, Tau)) *
R_constant * T_in_K
End Function

'WAGNER 2002
Public Function Water_Isobaric_Heat_capacity_calc(T, Rho)
Dim R_constant As Double, Delta_Rho As Variant, Tau As Variant, PhirDelta#
R_constant = 0.46151805
Delta_Rho = CDec(Rho / 322): Tau = CDec(647.096 / T)
PhirDelta = PhiR_Delta(Delta_Rho, Tau)

Water_Isobaric_Heat_capacity_calc = Water_Isochoric_Heat_capacity_calc(T,
Rho) + R_constant * (1 + Delta_Rho * PhirDelta - Delta_Rho * Tau *
PhiR_DeltaTau(Delta_Rho, Tau)) ^ 2 / (1 + 2 * Delta_Rho * PhirDelta +
Delta_Rho ^ 2 * PhiR_DeltaDelta(Delta_Rho, Tau))
End Function

'WAGNER 2002
Public Function Water_Isochoric_Heat_capacity_calc(T, Rho)
Dim R_constant As Double, Delta_Rho As Variant, Tau As Variant
R_constant = 0.46151805
Delta_Rho = CDec(Rho / 322): Tau = CDec(647.096 / T)

Water_Isochoric_Heat_capacity_calc = (-Tau ^ 2 * (Phi0_TauTau(Delta_Rho, Tau)
+ PhiR_TauTau(Delta_Rho, Tau))) * R_constant
End Function

'WAGNER 2002
Private Function Phi0_TauTau(Delta_Rho, Tau) As Double
Dim i As Integer
'constants from table 6.1
Dim n0(3 To 8) As Double, gamma0(4 To 8) As Double, Sum1 As Double

'constants from table 6.1
n0(3) = 3.00632:        n0(4) = 0.012436
n0(5) = 0.97315:        n0(6) = 1.2795:       n0(7) = 0.96956: n0(8) =
0.24873

gamma0(4) = 1.28728967: gamma0(5) = 3.53734222: gamma0(6) = 7.74073708
```

```
gamma0(7) = 9.24437796: gamma0(8) = 27.5075105

For i = 4 To 8
    Sum1 = Sum1 + n0(i) * gamma0(i) ^ 2 * Exp(-gamma0(i) * Tau) * (1 - Exp(-
gamma0(i) * Tau)) ^ -2
Next i
Phi0_TauTau = -n0(3) / Tau ^ 2 - Sum1

End Function

'WAGNER 2002 eq from table 6.5
Private Function PhiR_TauTau(Delta_Rho, Tau) As Variant
Dim i As Integer
Dim c(1 To 54) As Integer, d(1 To 54) As Integer
Dim T(1 To 54) As Single, n(1 To 56) As Double
Dim Alpha(52 To 54) As Integer, epsilon(52 To 54) As Integer
Dim beta(52 To 56) As Single, gamma(52 To 54) As Single
Dim a(55 To 56) As Single, b(55 To 56) As Single, B_CAPS(55 To 56) As Single,
A_CAPS(55 To 56) As Single
Dim C_CAPS(55 To 56) As Integer, D_CAPS(55 To 56) As Integer
'declaring of  components for F0+Fr and experimental PT spaces
Dim Delta#, Theta#, Psi#
'temporary double units
Dim Sum1 As Double, Sum2 As Double, Sum3 As Double, Sum4 As Double,
d2DeltaBIDTauTau#, dDeltaBIdTau#, dPsidTau#, d2PsidTauTau#
'table 6.2
For i = 1 To 54
    c(i) = 0
Next i

For i = 8 To 22
c(i) = 1
Next i

For i = 23 To 42
c(i) = 2
Next i

For i = 43 To 46
c(i) = 3
Next i

c(47) = 4

For i = 48 To 51
c(i) = 6
Next i

d(1) = 1:   d(2) = 1:  d(3) = 1:  d(4) = 2:  d(5) = 2:   d(6) = 3:   d(7) = 4
```

```
d(8) = 1:   d(9) = 1:  d(10) = 1: d(11) = 2: d(12) = 2:  d(13) = 3:  d(14) =
4
d(15) = 4:  d(16) = 5: d(17) = 7: d(18) = 9: d(19) = 10: d(20) = 11: d(21) =
13
d(22) = 15: d(23) = 1: d(24) = 2: d(25) = 2: d(26) = 2:  d(27) = 3:  d(28) =
4
d(29) = 4:  d(30) = 4: d(31) = 5: d(32) = 6: d(33) = 6:  d(34) = 7:  d(35) =
9
d(36) = 9:  d(37) = 9: d(38) = 9: d(39) = 9: d(40) = 10: d(41) = 10: d(42) =
12
d(43) = 3:  d(44) = 4: d(45) = 4: d(46) = 5: d(47) = 14: d(48) = 3:  d(49) =
6
d(50) = 6:  d(51) = 6: d(52) = 3: d(53) = 3: d(54) = 3

T(1) = -0.5: T(2) = 0.875: T(3) = 1:   T(4) = 0.5: T(5) = 0.75: T(6) = 0.375
T(7) = 1:    T(8) = 4:     T(9) = 6:   T(10) = 12: T(11) = 1:   T(12) = 5
T(13) = 4:   T(14) = 2:    T(15) = 13: T(16) = 9:  T(17) = 3:   T(18) = 4
T(19) = 11:  T(20) = 4:    T(21) = 13: T(22) = 1:  T(23) = 7:   T(24) = 1
T(25) = 9:   T(26) = 10:   T(27) = 10: T(28) = 3:  T(29) = 7:   T(30) = 10
T(31) = 10:  T(32) = 6:    T(33) = 10: T(34) = 10: T(35) = 1:   T(36) = 2
T(37) = 3:   T(38) = 4:    T(39) = 8:  T(40) = 6:  T(41) = 9:   T(42) = 8
T(43) = 16:  T(44) = 22:   T(45) = 23: T(46) = 23: T(47) = 10:  T(48) = 50
T(49) = 44:  T(50) = 46:   T(51) = 50: T(52) = 0:  T(53) = 1:   T(54) = 4

n(1) = 0.12533547935523 * 10 ^ -1:    n(2) = 0.78957634722828 * 10 ^ 1
n(3) = -0.87803203303561 * 10 ^ 1:    n(4) = 0.31802509345418 * 10 ^ 0
n(5) = -0.26145533859358 * 10 ^ 0:    n(6) = -0.78199751687981 * 10 ^ -2
n(7) = 0.88089493102134 * 10 ^ -2:    n(8) = -0.66856572307965 * 10 ^ 0
n(9) = 0.20433810950965 * 10 ^ 0:     n(10) = -0.66212605039687 * 10 ^ -4
n(11) = -0.19232721156002 * 10 ^ 0:   n(12) = -0.25709043003438 * 10 ^ 0
n(13) = 0.16074868486251 * 10 ^ 0:    n(14) = -0.40092828925807 * 10 ^ -1
n(15) = 0.39343422603254 * 10 ^ -6:   n(16) = -0.75941377088144 * 10 ^ -5
n(17) = 0.56250979351888 * 10 ^ -3:   n(18) = -0.15608652257135 * 10 ^ -4
n(19) = 0.11537996422951 * 10 ^ -8:   n(20) = 0.36582165144204 * 10 ^ -6
n(21) = -0.13251180074668 * 10 ^ -11: n(22) = -0.62639586912454 * 10 ^ -9
n(23) = -0.10793600908932 * 10 ^ 0:   n(24) = 0.17611491008752 * 10 ^ -1
n(25) = 0.22132295167546 * 10 ^ 0:    n(26) = -0.40247669763528 * 10 ^ 0
n(27) = 0.58083399985759 * 10 ^ 0:    n(28) = 0.49969146990806 * 10 ^ -2
n(29) = -0.31358700712549 * 10 ^ -1:  n(30) = -0.74315929710341 * 10 ^ 0
n(31) = 0.4780732991548 * 10 ^ 0:     n(32) = 0.20527940895948 * 10 ^ -1
n(33) = -0.13636435110343 * 10 ^ 0:   n(34) = 0.14180634400617 * 10 ^ -1
n(35) = 0.83326504880713 * 10 ^ -2:   n(36) = -0.29052336009585 * 10 ^ -1
n(37) = 0.38615085574206 * 10 ^ -1:   n(38) = -0.20393486513704 * 10 ^ -1
n(39) = -0.16554050063734 * 10 ^ -2:  n(40) = 0.19955571979541 * 10 ^ -2
n(41) = 0.15870308324157 * 10 ^ -3:   n(42) = -0.1638856834253 * 10 ^ -4
n(43) = 0.43613615723811 * 10 ^ -1:   n(44) = 0.34994005463765 * 10 ^ -1
n(45) = -0.76788197844621 * 10 ^ -1:  n(46) = 0.22446277332006 * 10 ^ -1
n(47) = -0.62689710414685 * 10 ^ -4:  n(48) = -0.55711118565645 * 10 ^ -9
n(49) = -0.19905718354408 * 10 ^ 0:   n(50) = 0.31777497330738 * 10 ^ 0
n(51) = -0.11841182425981 * 10 ^ 0:   n(52) = -0.31306260323435 * 10 ^ 2
```

```
n(53) = 0.31546140237781 * 10 ^ 2:    n(54) = -0.25213154341695 * 10 ^ 4
n(55) = -0.14874640856724 * 10 ^ 0:   n(56) = 0.31806110878444 * 10 ^ 0

Alpha(52) = 20: Alpha(53) = 20: Alpha(54) = 20

beta(52) = 150: beta(53) = 150: beta(54) = 250: beta(55) = 0.3: beta(56) =
0.3

gamma(52) = 1.21: gamma(53) = 1.21: gamma(54) = 1.25

epsilon(52) = 1: epsilon(53) = 1: epsilon(54) = 1

a(55) = 3.5:      a(56) = 3.5:      b(55) = 0.85:      b(56) = 0.95
B_CAPS(55) = 0.2: B_CAPS(56) = 0.2: C_CAPS(55) = 28:   C_CAPS(56) = 32
D_CAPS(55) = 700: D_CAPS(56) = 800: A_CAPS(55) = 0.32: A_CAPS(56) = 0.32
'END OF CONSTANT DECLARING

For i = 1 To 7
    Sum1 = Sum1 + n(i) * T(i) * (T(i) - 1) * Delta_Rho ^ d(i) * Tau ^ (T(i) -
2)
Next i
For i = 8 To 51
    Sum2 = Sum2 + n(i) * T(i) * (T(i) - 1) * Delta_Rho ^ d(i) * Tau ^ (T(i) -
2) * Exp(-Delta_Rho ^ c(i))
Next i
For i = 52 To 54
    Sum3 = Sum3 + n(i) * Delta_Rho ^ d(i) * Tau ^ T(i) * Exp(-Alpha(i) *
(Delta_Rho - epsilon(i)) ^ 2 - beta(i) * (Tau - gamma(i)) ^ 2) * ((T(i) / Tau
- 2 * beta(i) * (Tau - gamma(i))) ^ 2 - T(i) / Tau ^ 2 - 2 * beta(i))
Next i
For i = 55 To 56

    Theta = (1 - Tau) + A_CAPS(i) * ((Delta_Rho - 1) ^ 2) ^ (1 / (2 *
beta(i)))

    Delta = Theta ^ 2 + B_CAPS(i) * ((Delta_Rho - 1) ^ 2) ^ a(i)

    Psi = Exp(-C_CAPS(i) * (Delta_Rho - 1) ^ 2 - D_CAPS(i) * (Tau - 1) ^ 2)

    d2DeltaBIDTauTau = 2 * b(i) * Delta ^ (b(i) - 1) + 4 * Theta ^ 2 * b(i) *
(b(i) - 1) * Delta ^ (b(i) - 2)
    dDeltaBIdTau = -2 * Theta * b(i) * Delta ^ (b(i) - 1)
    dPsidTau = -2 * D_CAPS(i) * (Tau - 1) * Psi
    d2PsidTauTau = (2 * D_CAPS(i) * (Delta_Rho - 1) ^ 2 - 1) * 2 * D_CAPS(i)
* Psi

    Sum4 = Sum4 + n(i) * Delta_Rho * (d2DeltaBIDTauTau * Psi + 2 *
dDeltaBIdTau * dPsidTau + Delta ^ b(i) * d2PsidTauTau)

Next i
```

```
PhiR_TauTau = CDec(Sum1 + Sum2 + Sum3 + Sum4)

End Function

'WAGNER 2002 eq from table 6.5
Public Function PhiR_DeltaDelta(Delta_Rho, Tau) As Variant
Dim i As Integer
Dim c(1 To 54) As Integer, d(1 To 54) As Integer
Dim T(1 To 54) As Single, n(1 To 56) As Double
Dim Alpha(52 To 54) As Integer, epsilon(52 To 54) As Integer
Dim beta(52 To 56) As Single, gamma(52 To 54) As Single
Dim a(55 To 56) As Single, b(55 To 56) As Single, B_CAPS(55 To 56) As Single,
A_CAPS(55 To 56) As Single
Dim C_CAPS(55 To 56) As Integer, D_CAPS(55 To 56) As Integer
'declaring of  components for F0+Fr and experimental PT spaces
Dim Delta#, Theta#, Delta2#, Theta2#, Psi#
'temporary double units
Dim Sum1 As Double, Sum2 As Double, Sum3 As Double, Sum4 As Double, TmpUnit#,
dPsidTau#, dDeltaddelta#, d2PsidTauDelta#
Dim dDeltaBIdDelta#, dDeltaBIdTau#, dPsidDelta#, d2DeltaBIdRhoTau#,
d2Psiddeltadelta#, d2DeltaBIddeltadelta#, d2Deltaddeltadelta#
'table 6.2
For i = 1 To 54
    c(i) = 0
Next i

For i = 8 To 22
c(i) = 1
Next i

For i = 23 To 42
c(i) = 2
Next i

For i = 43 To 46
c(i) = 3
Next i

c(47) = 4

For i = 48 To 51
c(i) = 6
Next i

d(1) = 1:   d(2) = 1:  d(3) = 1:  d(4) = 2:  d(5) = 2:   d(6) = 3:   d(7) = 4
d(8) = 1:   d(9) = 1:  d(10) = 1: d(11) = 2: d(12) = 2:  d(13) = 3:  d(14) =
4
d(15) = 4:  d(16) = 5: d(17) = 7: d(18) = 9: d(19) = 10: d(20) = 11: d(21) =
13
```

```
d(22) = 15: d(23) = 1: d(24) = 2: d(25) = 2: d(26) = 2:  d(27) = 3:  d(28) =
4
d(29) = 4:  d(30) = 4: d(31) = 5: d(32) = 6: d(33) = 6:  d(34) = 7:  d(35) =
9
d(36) = 9:  d(37) = 9: d(38) = 9: d(39) = 9: d(40) = 10: d(41) = 10: d(42) =
12
d(43) = 3:  d(44) = 4: d(45) = 4: d(46) = 5: d(47) = 14: d(48) = 3:  d(49) =
6
d(50) = 6:  d(51) = 6: d(52) = 3: d(53) = 3: d(54) = 3

T(1) = -0.5: T(2) = 0.875: T(3) = 1:   T(4) = 0.5: T(5) = 0.75: T(6) = 0.375
T(7) = 1:    T(8) = 4:     T(9) = 6:   T(10) = 12: T(11) = 1:   T(12) = 5
T(13) = 4:   T(14) = 2:    T(15) = 13: T(16) = 9:  T(17) = 3:   T(18) = 4
T(19) = 11:  T(20) = 4:    T(21) = 13: T(22) = 1:  T(23) = 7:   T(24) = 1
T(25) = 9:   T(26) = 10:   T(27) = 10: T(28) = 3:  T(29) = 7:   T(30) = 10
T(31) = 10:  T(32) = 6:    T(33) = 10: T(34) = 10: T(35) = 1:   T(36) = 2
T(37) = 3:   T(38) = 4:    T(39) = 8:  T(40) = 6:  T(41) = 9:   T(42) = 8
T(43) = 16:  T(44) = 22:   T(45) = 23: T(46) = 23: T(47) = 10:  T(48) = 50
T(49) = 44:  T(50) = 46:   T(51) = 50: T(52) = 0:  T(53) = 1:   T(54) = 4

n(1) = 0.12533547935523 * 10 ^ -1:    n(2) = 0.78957634722828 * 10 ^ 1
n(3) = -0.87803203303561 * 10 ^ 1:    n(4) = 0.31802509345418 * 10 ^ 0
n(5) = -0.26145533859358 * 10 ^ 0:    n(6) = -0.78199751687981 * 10 ^ -2
n(7) = 0.88089493102134 * 10 ^ -2:    n(8) = -0.66856572307965 * 10 ^ 0
n(9) = 0.20433810950965 * 10 ^ 0:     n(10) = -0.66212605039687 * 10 ^ -4
n(11) = -0.19232721156002 * 10 ^ 0:   n(12) = -0.25709043003438 * 10 ^ 0
n(13) = 0.16074868486251 * 10 ^ 0:    n(14) = -0.40092828925807 * 10 ^ -1
n(15) = 0.39343422603254 * 10 ^ -6:   n(16) = -0.75941377088144 * 10 ^ -5
n(17) = 0.56250979351888 * 10 ^ -3:   n(18) = -0.15608652257135 * 10 ^ -4
n(19) = 0.11537996422951 * 10 ^ -8:   n(20) = 0.36582165144204 * 10 ^ -6
n(21) = -0.13251180074668 * 10 ^ -11: n(22) = -0.62639586912454 * 10 ^ -9
n(23) = -0.10793600908932 * 10 ^ 0:   n(24) = 0.17611491008752 * 10 ^ -1
n(25) = 0.22132295167546 * 10 ^ 0:    n(26) = -0.40247669763528 * 10 ^ 0
n(27) = 0.58083399985759 * 10 ^ 0:    n(28) = 0.49969146990806 * 10 ^ -2
n(29) = -0.31358700712549 * 10 ^ -1:  n(30) = -0.74315929710341 * 10 ^ 0
n(31) = 0.4780732991548 * 10 ^ 0:     n(32) = 0.20527940895948 * 10 ^ -1
n(33) = -0.13636435110343 * 10 ^ 0:   n(34) = 0.14180634400617 * 10 ^ -1
n(35) = 0.83326504880713 * 10 ^ -2:   n(36) = -0.29052336009585 * 10 ^ -1
n(37) = 0.38615085574206 * 10 ^ -1:   n(38) = -0.20393486513704 * 10 ^ -1
n(39) = -0.16554050063734 * 10 ^ -2:  n(40) = 0.19955571979541 * 10 ^ -2
n(41) = 0.15870308324157 * 10 ^ -3:   n(42) = -0.1638856834253 * 10 ^ -4
n(43) = 0.43613615723811 * 10 ^ -1:   n(44) = 0.34994005463765 * 10 ^ -1
n(45) = -0.76788197844621 * 10 ^ -1:  n(46) = 0.22446277332006 * 10 ^ -1
n(47) = -0.62689710414685 * 10 ^ -4:  n(48) = -0.55711118565645 * 10 ^ -9
n(49) = -0.19905718354408 * 10 ^ 0:   n(50) = 0.31777497330738 * 10 ^ 0
n(51) = -0.11841182425981 * 10 ^ 0:   n(52) = -0.31306260323435 * 10 ^ 2
n(53) = 0.31546140237781 * 10 ^ 2:    n(54) = -0.25213154341695 * 10 ^ 4
n(55) = -0.14874640856724 * 10 ^ 0:   n(56) = 0.31806110878444 * 10 ^ 0

Alpha(52) = 20: Alpha(53) = 20: Alpha(54) = 20
```

```
beta(52) = 150: beta(53) = 150: beta(54) = 250: beta(55) = 0.3: beta(56) =
0.3

gamma(52) = 1.21: gamma(53) = 1.21: gamma(54) = 1.25

epsilon(52) = 1: epsilon(53) = 1: epsilon(54) = 1

a(55) = 3.5:      a(56) = 3.5:      b(55) = 0.85:      b(56) = 0.95
B_CAPS(55) = 0.2: B_CAPS(56) = 0.2: C_CAPS(55) = 28:   C_CAPS(56) = 32
D_CAPS(55) = 700: D_CAPS(56) = 800: A_CAPS(55) = 0.32: A_CAPS(56) = 0.32
'END OF CONSTANT DECLARING

For i = 1 To 7
    Sum1 = Sum1 + n(i) * d(i) * (d(i) - 1) * Delta_Rho ^ (d(i) - 2) * Tau ^
T(i)
Next i
For i = 8 To 51
    Sum2 = Sum2 + n(i) * Exp(-Delta_Rho ^ c(i)) * (Delta_Rho ^ (d(i) - 2) *
Tau ^ T(i) * ((d(i) - c(i) * Delta_Rho ^ c(i)) * (d(i) - 1 - c(i) * Delta_Rho
^ c(i)) - c(i) ^ 2 * Delta_Rho ^ c(i)))
Next i
For i = 52 To 54
    Sum3 = Sum3 + n(i) * Tau ^ T(i) * Exp(-Alpha(i) * (Delta_Rho -
epsilon(i)) ^ 2 - beta(i) * (Tau - gamma(i)) ^ 2) * (-2 * Alpha(i) *
Delta_Rho ^ d(i) + 4 * Alpha(i) ^ 2 * Delta_Rho ^ d(i) * (Delta_Rho -
epsilon(i)) ^ 2 - 4 * d(i) * Alpha(i) * Delta_Rho ^ (d(i) - 1) * (Delta_Rho -
epsilon(i)) + d(i) * (d(i) - 1) * Delta_Rho ^ (d(i) - 2))
Next i
For i = 55 To 56

    Theta = (1 - Tau) + A_CAPS(i) * ((Delta_Rho - 1) ^ 2) ^ (1 / (2 *
beta(i)))

    Delta = Theta ^ 2 + B_CAPS(i) * ((Delta_Rho - 1) ^ 2) ^ a(i)

    Psi = Exp(-C_CAPS(i) * (Delta_Rho - 1) ^ 2 - D_CAPS(i) * (Tau - 1) ^ 2)

    dPsidTau = -2 * D_CAPS(i) * (Tau - 1) * Psi
    d2PsidTauDelta = 4 * C_CAPS(i) * Psi * D_CAPS(i) * (Delta_Rho - 1) * (Tau
- 1)
    dDeltaddelta = (Delta_Rho - 1) * (A_CAPS(i) * Theta * 2 / beta(i) *
((Delta_Rho - 1) ^ 2) ^ (1 / (2 * beta(i)) - 1) + 2 * B_CAPS(i) * a(i) *
((Delta_Rho - 1) ^ 2) ^ (a(i) - 1))
    dDeltaBIdDelta = b(i) * Delta ^ (b(i) - 1) * dDeltaddelta
    dDeltaBIdTau = -2 * Theta * b(i) * Delta ^ (b(i) - 1)
    dPsidDelta = -2 * C_CAPS(i) * (Delta_Rho - 1) * Psi
    d2DeltaBIdRhoTau = -A_CAPS(i) * b(i) * 2 / beta(i) * Delta ^ (b(i) - 1) *
(Delta_Rho - 1) * ((Delta_Rho - 1) ^ 2) ^ (1 / (2 * beta(i)) - 1) - 2 * Theta
* b(i) * (b(i) - 1) * Delta ^ (b(i) - 2) * dDeltaddelta
```

```
    d2Psiddeltadelta = (2 * C_CAPS(i) * (Delta_Rho - 1) ^ 2 - 1) * 2 *
C_CAPS(i) * Psi
    d2Deltaddeltadelta = 1 / (Delta_Rho - 1) * dDeltaddelta + (Delta_Rho - 1)
^ 2 * (4 * B_CAPS(i) * a(i) * (a(i) - 1) * ((Delta_Rho - 1) ^ 2) ^ (a(i) - 2)
+ 2 * A_CAPS(i) ^ 2 * beta(i) ^ -2 * (((Delta_Rho - 1) ^ 2) ^ (1 / 2 /
beta(i) - 1)) ^ 2 + A_CAPS(i) * Theta * 4 / beta(i) * (1 / 2 / beta(i) - 1) *
((Delta_Rho - 1) ^ 2) ^ (1 / 2 / beta(i) - 2))
    d2DeltaBIddeltadelta = b(i) * (Delta ^ (b(i) - 1) * d2Deltaddeltadelta +
(b(i) - 1) * Delta ^ (b(i) - 2) * dDeltaddelta ^ 2)

    Sum4 = Sum4 + n(i) * (Delta ^ b(i) * (2 * dPsidDelta + Delta_Rho *
d2Psiddeltadelta) + 2 * dDeltaBIdDelta * (Psi + Delta_Rho * dPsidDelta) +
d2DeltaBIddeltadelta * Psi * Delta_Rho)


Next i
PhiR_DeltaDelta = CDec(Sum1 + Sum2 + Sum3 + Sum4)

End Function

'WAGNER 2002 eq from table 6.5
Private Function PhiR_DeltaTau(Delta_Rho, Tau) As Variant
Dim i As Integer
Dim c(1 To 54) As Integer, d(1 To 54) As Integer
Dim T(1 To 54) As Single, n(1 To 56) As Double
Dim Alpha(52 To 54) As Integer, epsilon(52 To 54) As Integer
Dim beta(52 To 56) As Single, gamma(52 To 54) As Single
Dim a(55 To 56) As Single, b(55 To 56) As Single, B_CAPS(55 To 56) As Single,
A_CAPS(55 To 56) As Single
Dim C_CAPS(55 To 56) As Integer, D_CAPS(55 To 56) As Integer
'declaring of  components for F0+Fr and experimental PT spaces
Dim Delta#, Theta#, Delta2#, Theta2#, Psi#
'temporary double units
Dim Sum1 As Double, Sum2 As Double, Sum3 As Double, Sum4 As Double, TmpUnit#,
dPsidTau#, dDeltaddelta#
Dim d2PsidTauDelta#, dDeltaBIdDelta#, dDeltaBIdTau#, dPsidDelta#,
d2DeltaBIdRhoTau#
'table 6.2
For i = 1 To 54
    c(i) = 0
Next i

For i = 8 To 22
c(i) = 1
Next i

For i = 23 To 42
c(i) = 2
Next i
```

```
For i = 43 To 46
c(i) = 3
Next i

c(47) = 4

For i = 48 To 51
c(i) = 6
Next i

d(1) = 1:   d(2) = 1:  d(3) = 1:  d(4) = 2:  d(5) = 2:   d(6) = 3:   d(7) = 4
d(8) = 1:   d(9) = 1:  d(10) = 1: d(11) = 2: d(12) = 2:  d(13) = 3:  d(14) =
4
d(15) = 4:  d(16) = 5: d(17) = 7: d(18) = 9: d(19) = 10: d(20) = 11: d(21) =
13
d(22) = 15: d(23) = 1: d(24) = 2: d(25) = 2: d(26) = 2:  d(27) = 3:  d(28) =
4
d(29) = 4:  d(30) = 4: d(31) = 5: d(32) = 6: d(33) = 6:  d(34) = 7:  d(35) =
9
d(36) = 9:  d(37) = 9: d(38) = 9: d(39) = 9: d(40) = 10: d(41) = 10: d(42) =
12
d(43) = 3:  d(44) = 4: d(45) = 4: d(46) = 5: d(47) = 14: d(48) = 3:  d(49) =
6
d(50) = 6:  d(51) = 6: d(52) = 3: d(53) = 3: d(54) = 3

T(1) = -0.5: T(2) = 0.875: T(3) = 1:   T(4) = 0.5: T(5) = 0.75: T(6) = 0.375
T(7) = 1:    T(8) = 4:     T(9) = 6:   T(10) = 12: T(11) = 1:   T(12) = 5
T(13) = 4:   T(14) = 2:    T(15) = 13: T(16) = 9:  T(17) = 3:   T(18) = 4
T(19) = 11:  T(20) = 4:    T(21) = 13: T(22) = 1:  T(23) = 7:   T(24) = 1
T(25) = 9:   T(26) = 10:   T(27) = 10: T(28) = 3:  T(29) = 7:   T(30) = 10
T(31) = 10:  T(32) = 6:    T(33) = 10: T(34) = 10: T(35) = 1:   T(36) = 2
T(37) = 3:   T(38) = 4:    T(39) = 8:  T(40) = 6:  T(41) = 9:   T(42) = 8
T(43) = 16:  T(44) = 22:   T(45) = 23: T(46) = 23: T(47) = 10:  T(48) = 50
T(49) = 44:  T(50) = 46:   T(51) = 50: T(52) = 0:  T(53) = 1:   T(54) = 4

n(1) = 0.12533547935523 * 10 ^ -1:    n(2) = 0.78957634722828 * 10 ^ 1
n(3) = -0.87803203303561 * 10 ^ 1:    n(4) = 0.31802509345418 * 10 ^ 0
n(5) = -0.26145533859358 * 10 ^ 0:    n(6) = -0.78199751687981 * 10 ^ -2
n(7) = 0.88089493102134 * 10 ^ -2:    n(8) = -0.66856572307965 * 10 ^ 0
n(9) = 0.20433810950965 * 10 ^ 0:     n(10) = -0.66212605039687 * 10 ^ -4
n(11) = -0.19232721156002 * 10 ^ 0:   n(12) = -0.25709043003438 * 10 ^ 0
n(13) = 0.16074868486251 * 10 ^ 0:    n(14) = -0.40092828925807 * 10 ^ -1
n(15) = 0.39343422603254 * 10 ^ -6:   n(16) = -0.75941377088144 * 10 ^ -5
n(17) = 0.56250979351888 * 10 ^ -3:   n(18) = -0.15608652257135 * 10 ^ -4
n(19) = 0.11537996422951 * 10 ^ -8:   n(20) = 0.36582165144204 * 10 ^ -6
n(21) = -0.13251180074668 * 10 ^ -11: n(22) = -0.62639586912454 * 10 ^ -9
n(23) = -0.10793600908932 * 10 ^ 0:   n(24) = 0.17611491008752 * 10 ^ -1
n(25) = 0.22132295167546 * 10 ^ 0:    n(26) = -0.40247669763528 * 10 ^ 0
n(27) = 0.58083399985759 * 10 ^ 0:    n(28) = 0.49969146990806 * 10 ^ -2
n(29) = -0.31358700712549 * 10 ^ -1:  n(30) = -0.74315929710341 * 10 ^ 0
```

```
n(31) = 0.4780732991548 * 10 ^ 0:     n(32) = 0.20527940895948 * 10 ^ -1
n(33) = -0.13636435110343 * 10 ^ 0:   n(34) = 0.14180634400617 * 10 ^ -1
n(35) = 0.83326504880713 * 10 ^ -2:   n(36) = -0.29052336009585 * 10 ^ -1
n(37) = 0.38615085574206 * 10 ^ -1:   n(38) = -0.20393486513704 * 10 ^ -1
n(39) = -0.16554050063734 * 10 ^ -2:  n(40) = 0.19955571979541 * 10 ^ -2
n(41) = 0.15870308324157 * 10 ^ -3:   n(42) = -0.1638856834253 * 10 ^ -4
n(43) = 0.43613615723811 * 10 ^ -1:   n(44) = 0.34994005463765 * 10 ^ -1
n(45) = -0.76788197844621 * 10 ^ -1:  n(46) = 0.22446277332006 * 10 ^ -1
n(47) = -0.62689710414685 * 10 ^ -4:  n(48) = -0.55711118565645 * 10 ^ -9
n(49) = -0.19905718354408 * 10 ^ 0:   n(50) = 0.31777497330738 * 10 ^ 0
n(51) = -0.11841182425981 * 10 ^ 0:   n(52) = -0.31306260323435 * 10 ^ 2
n(53) = 0.31546140237781 * 10 ^ 2:    n(54) = -0.25213154341695 * 10 ^ 4
n(55) = -0.14874640856724 * 10 ^ 0:   n(56) = 0.31806110878444 * 10 ^ 0

Alpha(52) = 20: Alpha(53) = 20: Alpha(54) = 20

beta(52) = 150: beta(53) = 150: beta(54) = 250: beta(55) = 0.3: beta(56) =
0.3

gamma(52) = 1.21: gamma(53) = 1.21: gamma(54) = 1.25

epsilon(52) = 1: epsilon(53) = 1: epsilon(54) = 1

a(55) = 3.5:      a(56) = 3.5:      b(55) = 0.85:      b(56) = 0.95
B_CAPS(55) = 0.2: B_CAPS(56) = 0.2: C_CAPS(55) = 28:   C_CAPS(56) = 32
D_CAPS(55) = 700: D_CAPS(56) = 800: A_CAPS(55) = 0.32: A_CAPS(56) = 0.32
'END OF CONSTANT DECLARING

For i = 1 To 7
    Sum1 = Sum1 + n(i) * d(i) * T(i) * Delta_Rho ^ (d(i) - 1) * Tau ^ (T(i) -
1)
Next i
For i = 8 To 51
    Sum2 = Sum2 + n(i) * T(i) * Delta_Rho ^ (d(i) - 1) * Tau ^ (T(i) - 1) *
(d(i) - c(i) * Delta_Rho ^ c(i)) * Exp(-Delta_Rho ^ c(i))
Next i
For i = 52 To 54
    Sum3 = Sum3 + n(i) * Delta_Rho ^ d(i) * Tau ^ T(i) * Exp(-Alpha(i) *
(Delta_Rho - epsilon(i)) ^ 2 - beta(i) * (Tau - gamma(i)) ^ 2) * (d(i) /
Delta_Rho - 2 * Alpha(i) * (Delta_Rho - epsilon(i))) * (T(i) / Tau - 2 *
beta(i) * (Tau - gamma(i)))
Next i
For i = 55 To 56

    Theta = 0: Delta = 0: Psi = 0: dPsidTau = 0: d2PsidTauDelta = 0:
dDeltaddelta = 0: dDeltaBIdDelta = 0: dDeltaBIdTau = 0: dPsidDelta = 0:
d2DeltaBIdRhoTau = 0

    Theta = (1 - Tau) + A_CAPS(i) * ((Delta_Rho - 1) ^ 2) ^ (1 / (2 *
beta(i)))
```

```
    Delta = Theta ^ 2 + B_CAPS(i) * ((Delta_Rho - 1) ^ 2) ^ a(i)

    Psi = Exp(-C_CAPS(i) * (Delta_Rho - 1) ^ 2 - D_CAPS(i) * (Tau - 1) ^ 2)

    dPsidTau = -2 * D_CAPS(i) * (Tau - 1) * Psi
    d2PsidTauDelta = 4 * C_CAPS(i) * Psi * D_CAPS(i) * (Delta_Rho - 1) * (Tau
- 1)
    dDeltaddelta = (Delta_Rho - 1) * (A_CAPS(i) * Theta * 2 / beta(i) *
((Delta_Rho - 1) ^ 2) ^ (1 / (2 * beta(i)) - 1) + 2 * B_CAPS(i) * a(i) *
((Delta_Rho - 1) ^ 2) ^ (a(i) - 1))
    dDeltaBIdDelta = b(i) * Delta ^ (b(i) - 1) * dDeltaddelta
    dDeltaBIdTau = -2 * Theta * b(i) * Delta ^ (b(i) - 1)
    dPsidDelta = -2 * C_CAPS(i) * (Delta_Rho - 1) * Psi
    d2DeltaBIdRhoTau = -A_CAPS(i) * b(i) * 2 / beta(i) * Delta ^ (b(i) - 1) *
(Delta_Rho - 1) * ((Delta_Rho - 1) ^ 2) ^ (1 / (2 * beta(i)) - 1) - 2 * Theta
* b(i) * (b(i) - 1) * Delta ^ (b(i) - 2) * dDeltaddelta

    Sum4 = Sum4 + n(i) * (Delta ^ b(i) * (dPsidTau + Delta_Rho *
d2PsidTauDelta) + Delta_Rho * dDeltaBIdDelta * dPsidTau + dDeltaBIdTau * (Psi
+ Delta_Rho * dPsidDelta) + d2DeltaBIdRhoTau * Delta_Rho * Psi)


Next i
PhiR_DeltaTau = CDec(Sum1 + Sum2 + Sum3 + Sum4)

End Function

'WAGNER 2002 eq from table 6.5
Public Function PhiR_Delta(Delta_Rho, Tau) As Variant
Dim i As Integer
Dim c(1 To 54) As Integer, d(1 To 54) As Integer
Dim T(1 To 54) As Single, n(1 To 56) As Double
Dim Alpha(52 To 54) As Integer, epsilon(52 To 54) As Integer
Dim beta(52 To 56) As Single, gamma(52 To 54) As Single
Dim a(55 To 56) As Single, b(55 To 56) As Single, B_CAPS(55 To 56) As Single,
A_CAPS(55 To 56) As Single
Dim C_CAPS(55 To 56) As Integer, D_CAPS(55 To 56) As Integer
'declaring of  components for F0+Fr and experimental PT spaces
Dim Theta#, Delta#, Psi#, dPsidDelta#, dDeltaddelta#, dDeltaBIdDelta#
'temporary double units
Dim Sum1 As Double, Sum2 As Double, Sum3 As Double, Sum4 As Double


'table 6.2
For i = 1 To 54
    c(i) = 0
Next i

For i = 8 To 22
```

```
c(i) = 1
Next i

For i = 23 To 42
c(i) = 2
Next i

For i = 43 To 46
c(i) = 3
Next i

c(47) = 4

For i = 48 To 51
c(i) = 6
Next i

d(1) = 1:   d(2) = 1:  d(3) = 1:  d(4) = 2:  d(5) = 2:   d(6) = 3:   d(7) = 4
d(8) = 1:   d(9) = 1:  d(10) = 1: d(11) = 2: d(12) = 2:  d(13) = 3:  d(14) =
4
d(15) = 4:  d(16) = 5: d(17) = 7: d(18) = 9: d(19) = 10: d(20) = 11: d(21) =
13
d(22) = 15: d(23) = 1: d(24) = 2: d(25) = 2: d(26) = 2:  d(27) = 3:  d(28) =
4
d(29) = 4:  d(30) = 4: d(31) = 5: d(32) = 6: d(33) = 6:  d(34) = 7:  d(35) =
9
d(36) = 9:  d(37) = 9: d(38) = 9: d(39) = 9: d(40) = 10: d(41) = 10: d(42) =
12
d(43) = 3:  d(44) = 4: d(45) = 4: d(46) = 5: d(47) = 14: d(48) = 3:  d(49) =
6
d(50) = 6:  d(51) = 6: d(52) = 3: d(53) = 3: d(54) = 3

T(1) = -0.5: T(2) = 0.875: T(3) = 1:   T(4) = 0.5: T(5) = 0.75: T(6) = 0.375
T(7) = 1:    T(8) = 4:     T(9) = 6:   T(10) = 12: T(11) = 1:   T(12) = 5
T(13) = 4:   T(14) = 2:    T(15) = 13: T(16) = 9:  T(17) = 3:   T(18) = 4
T(19) = 11:  T(20) = 4:    T(21) = 13: T(22) = 1:  T(23) = 7:   T(24) = 1
T(25) = 9:   T(26) = 10:   T(27) = 10: T(28) = 3:  T(29) = 7:   T(30) = 10
T(31) = 10:  T(32) = 6:    T(33) = 10: T(34) = 10: T(35) = 1:   T(36) = 2
T(37) = 3:   T(38) = 4:    T(39) = 8:  T(40) = 6:  T(41) = 9:   T(42) = 8
T(43) = 16:  T(44) = 22:   T(45) = 23: T(46) = 23: T(47) = 10:  T(48) = 50
T(49) = 44:  T(50) = 46:   T(51) = 50: T(52) = 0:  T(53) = 1:   T(54) = 4

n(1) = 0.12533547935523 * 10 ^ -1:    n(2) = 0.78957634722828 * 10 ^ 1
n(3) = -0.87803203303561 * 10 ^ 1:    n(4) = 0.31802509345418 * 10 ^ 0
n(5) = -0.26145533859358 * 10 ^ 0:    n(6) = -0.78199751687981 * 10 ^ -2
n(7) = 0.88089493102134 * 10 ^ -2:    n(8) = -0.66856572307965 * 10 ^ 0
n(9) = 0.20433810950965 * 10 ^ 0:     n(10) = -0.66212605039687 * 10 ^ -4
n(11) = -0.19232721156002 * 10 ^ 0:   n(12) = -0.25709043003438 * 10 ^ 0
n(13) = 0.16074868486251 * 10 ^ 0:    n(14) = -0.40092828925807 * 10 ^ -1
n(15) = 0.39343422603254 * 10 ^ -6:   n(16) = -0.75941377088144 * 10 ^ -5
```

```
n(17) = 0.56250979351888 * 10 ^ -3:   n(18) = -0.15608652257135 * 10 ^ -4
n(19) = 0.11537996422951 * 10 ^ -8:   n(20) = 0.36582165144204 * 10 ^ -6
n(21) = -0.13251180074668 * 10 ^ -11: n(22) = -0.62639586912454 * 10 ^ -9
n(23) = -0.10793600908932 * 10 ^ 0:   n(24) = 0.17611491008752 * 10 ^ -1
n(25) = 0.22132295167546 * 10 ^ 0:    n(26) = -0.40247669763528 * 10 ^ 0
n(27) = 0.58083399985759 * 10 ^ 0:    n(28) = 0.49969146990806 * 10 ^ -2
n(29) = -0.31358700712549 * 10 ^ -1:  n(30) = -0.74315929710341 * 10 ^ 0
n(31) = 0.4780732991548 * 10 ^ 0:     n(32) = 0.20527940895948 * 10 ^ -1
n(33) = -0.13636435110343 * 10 ^ 0:   n(34) = 0.14180634400617 * 10 ^ -1
n(35) = 0.83326504880713 * 10 ^ -2:   n(36) = -0.29052336009585 * 10 ^ -1
n(37) = 0.38615085574206 * 10 ^ -1:   n(38) = -0.20393486513704 * 10 ^ -1
n(39) = -0.16554050063734 * 10 ^ -2:  n(40) = 0.19955571979541 * 10 ^ -2
n(41) = 0.15870308324157 * 10 ^ -3:   n(42) = -0.1638856834253 * 10 ^ -4
n(43) = 0.43613615723811 * 10 ^ -1:   n(44) = 0.34994005463765 * 10 ^ -1
n(45) = -0.76788197844621 * 10 ^ -1:  n(46) = 0.22446277332006 * 10 ^ -1
n(47) = -0.62689710414685 * 10 ^ -4:  n(48) = -0.55711118565645 * 10 ^ -9
n(49) = -0.19905718354408 * 10 ^ 0:   n(50) = 0.31777497330738 * 10 ^ 0
n(51) = -0.11841182425981 * 10 ^ 0:   n(52) = -0.31306260323435 * 10 ^ 2
n(53) = 0.31546140237781 * 10 ^ 2:    n(54) = -0.25213154341695 * 10 ^ 4
n(55) = -0.14874640856724 * 10 ^ 0:   n(56) = 0.31806110878444 * 10 ^ 0

Alpha(52) = 20: Alpha(53) = 20: Alpha(54) = 20

beta(52) = 150: beta(53) = 150: beta(54) = 250: beta(55) = 0.3: beta(56) =
0.3

gamma(52) = 1.21: gamma(53) = 1.21: gamma(54) = 1.25

epsilon(52) = 1: epsilon(53) = 1: epsilon(54) = 1

a(55) = 3.5:      a(56) = 3.5:      b(55) = 0.85:      b(56) = 0.95
B_CAPS(55) = 0.2: B_CAPS(56) = 0.2: C_CAPS(55) = 28:   C_CAPS(56) = 32
D_CAPS(55) = 700: D_CAPS(56) = 800: A_CAPS(55) = 0.32: A_CAPS(56) = 0.32
'END OF CONSTANT DECLARING

For i = 1 To 7
    Sum1 = Sum1 + n(i) * d(i) * Delta_Rho ^ (d(i) - 1) * (Tau) ^ T(i)
Next i
For i = 8 To 51
    Sum2 = Sum2 + n(i) * Exp(-Delta_Rho ^ c(i)) * (Delta_Rho ^ (d(i) - 1) *
Tau ^ T(i) * (d(i) - c(i) * Delta_Rho ^ c(i)))
Next i
For i = 52 To 54
    Sum3 = Sum3 + n(i) * Delta_Rho ^ d(i) * Tau ^ T(i) * Exp(-Alpha(i) *
(Delta_Rho - epsilon(i)) ^ 2 - beta(i) * (Tau - gamma(i)) ^ 2) * (d(i) /
Delta_Rho - 2 * Alpha(i) * (Delta_Rho - epsilon(i)))
Next i
For i = 55 To 56
    Theta = (1 - Tau) + A_CAPS(i) * ((Delta_Rho - 1) ^ 2) ^ (1 / (2 *
beta(i)))
```

```
    Delta = Theta ^ 2 + B_CAPS(i) * ((Delta_Rho - 1) ^ 2) ^ a(i)
    Psi = Exp(-C_CAPS(i) * (Delta_Rho - 1) ^ 2 - D_CAPS(i) * (Tau - 1) ^ 2)

    dPsidDelta = -2 * C_CAPS(i) * (Delta_Rho - 1) * Psi
    dDeltaddelta = (Delta_Rho - 1) * (A_CAPS(i) * Theta * 2 / beta(i) *
((Delta_Rho - 1) ^ 2) ^ (1 / (2 * beta(i)) - 1) + 2 * B_CAPS(i) * a(i) *
((Delta_Rho - 1) ^ 2) ^ (a(i) - 1))
    If Delta = 0 Then
        dDeltaBIdDelta = 0
    Else
        dDeltaBIdDelta = dDeltaddelta * b(i) * Delta ^ (b(i) - 1)
    End If

    Sum4 = Sum4 + n(i) * (Delta ^ b(i) * (Psi + Delta_Rho * dPsidDelta) +
dDeltaBIdDelta * Delta_Rho * Psi)
Next i
PhiR_Delta = CDec(Sum1 + Sum2 + Sum3 + Sum4)

End Function

Private Function PhiR_Tau(Delta_Rho, Tau)
Dim i As Integer
Dim c(1 To 54) As Integer, d(1 To 54) As Integer
Dim T(1 To 54) As Single, n(1 To 56) As Double
Dim Alpha(52 To 54) As Integer, epsilon(52 To 54) As Integer
Dim beta(52 To 56) As Single, gamma(52 To 54) As Single
Dim a(55 To 56) As Single, b(55 To 56) As Single, B_CAPS(55 To 56) As Single,
A_CAPS(55 To 56) As Single
Dim C_CAPS(55 To 56) As Integer, D_CAPS(55 To 56) As Integer
'declaring of  components for F0+Fr and experimental PT spaces
Dim Delta#, Theta#, Psi#, dDeltaBIdTau#, dPsidTau#
'temporary double units
Dim Sum1 As Double, Sum2 As Double, Sum3 As Double, Sum4 As Double, Pwr#
'table 6.2
For i = 1 To 54
    c(i) = 0
Next i

For i = 8 To 22
c(i) = 1
Next i

For i = 23 To 42
c(i) = 2
Next i

For i = 43 To 46
c(i) = 3
Next i
```

```
c(47) = 4

For i = 48 To 51
c(i) = 6
Next i

d(1) = 1:   d(2) = 1:  d(3) = 1:  d(4) = 2:  d(5) = 2:   d(6) = 3:   d(7) = 4
d(8) = 1:   d(9) = 1:  d(10) = 1: d(11) = 2: d(12) = 2:  d(13) = 3:  d(14) =
4
d(15) = 4:  d(16) = 5: d(17) = 7: d(18) = 9: d(19) = 10: d(20) = 11: d(21) =
13
d(22) = 15: d(23) = 1: d(24) = 2: d(25) = 2: d(26) = 2:  d(27) = 3:  d(28) =
4
d(29) = 4:  d(30) = 4: d(31) = 5: d(32) = 6: d(33) = 6:  d(34) = 7:  d(35) =
9
d(36) = 9:  d(37) = 9: d(38) = 9: d(39) = 9: d(40) = 10: d(41) = 10: d(42) =
12
d(43) = 3:  d(44) = 4: d(45) = 4: d(46) = 5: d(47) = 14: d(48) = 3:  d(49) =
6
d(50) = 6:  d(51) = 6: d(52) = 3: d(53) = 3: d(54) = 3

T(1) = -0.5: T(2) = 0.875: T(3) = 1:   T(4) = 0.5: T(5) = 0.75: T(6) = 0.375
T(7) = 1:    T(8) = 4:     T(9) = 6:   T(10) = 12: T(11) = 1:   T(12) = 5
T(13) = 4:   T(14) = 2:    T(15) = 13: T(16) = 9:  T(17) = 3:   T(18) = 4
T(19) = 11:  T(20) = 4:    T(21) = 13: T(22) = 1:  T(23) = 7:   T(24) = 1
T(25) = 9:   T(26) = 10:   T(27) = 10: T(28) = 3:  T(29) = 7:   T(30) = 10
T(31) = 10:  T(32) = 6:    T(33) = 10: T(34) = 10: T(35) = 1:   T(36) = 2
T(37) = 3:   T(38) = 4:    T(39) = 8:  T(40) = 6:  T(41) = 9:   T(42) = 8
T(43) = 16:  T(44) = 22:   T(45) = 23: T(46) = 23: T(47) = 10:  T(48) = 50
T(49) = 44:  T(50) = 46:   T(51) = 50: T(52) = 0:  T(53) = 1:   T(54) = 4

n(1) = 0.12533547935523 * 10 ^ -1:    n(2) = 0.78957634722828 * 10 ^ 1
n(3) = -0.87803203303561 * 10 ^ 1:    n(4) = 0.31802509345418 * 10 ^ 0
n(5) = -0.26145533859358 * 10 ^ 0:    n(6) = -0.78199751687981 * 10 ^ -2
n(7) = 0.88089493102134 * 10 ^ -2:    n(8) = -0.66856572307965 * 10 ^ 0
n(9) = 0.20433810950965 * 10 ^ 0:     n(10) = -0.66212605039687 * 10 ^ -4
n(11) = -0.19232721156002 * 10 ^ 0:   n(12) = -0.25709043003438 * 10 ^ 0
n(13) = 0.16074868486251 * 10 ^ 0:    n(14) = -0.40092828925807 * 10 ^ -1
n(15) = 0.39343422603254 * 10 ^ -6:   n(16) = -0.75941377088144 * 10 ^ -5
n(17) = 0.56250979351888 * 10 ^ -3:   n(18) = -0.15608652257135 * 10 ^ -4
n(19) = 0.11537996422951 * 10 ^ -8:   n(20) = 0.36582165144204 * 10 ^ -6
n(21) = -0.13251180074668 * 10 ^ -11: n(22) = -0.62639586912454 * 10 ^ -9
n(23) = -0.10793600908932 * 10 ^ 0:   n(24) = 0.17611491008752 * 10 ^ -1
n(25) = 0.22132295167546 * 10 ^ 0:    n(26) = -0.40247669763528 * 10 ^ 0
n(27) = 0.58083399985759 * 10 ^ 0:    n(28) = 0.49969146990806 * 10 ^ -2
n(29) = -0.31358700712549 * 10 ^ -1:  n(30) = -0.74315929710341 * 10 ^ 0
n(31) = 0.4780732991548 * 10 ^ 0:     n(32) = 0.20527940895948 * 10 ^ -1
n(33) = -0.13636435110343 * 10 ^ 0:   n(34) = 0.14180634400617 * 10 ^ -1
n(35) = 0.83326504880713 * 10 ^ -2:   n(36) = -0.29052336009585 * 10 ^ -1
n(37) = 0.38615085574206 * 10 ^ -1:   n(38) = -0.20393486513704 * 10 ^ -1
```

```
n(39) = -0.16554050063734 * 10 ^ -2:  n(40) = 0.19955571979541 * 10 ^ -2
n(41) = 0.15870308324157 * 10 ^ -3:   n(42) = -0.1638856834253 * 10 ^ -4
n(43) = 0.43613615723811 * 10 ^ -1:   n(44) = 0.34994005463765 * 10 ^ -1
n(45) = -0.76788197844621 * 10 ^ -1:  n(46) = 0.22446277332006 * 10 ^ -1
n(47) = -0.62689710414685 * 10 ^ -4:  n(48) = -0.55711118565645 * 10 ^ -9
n(49) = -0.19905718354408 * 10 ^ 0:   n(50) = 0.31777497330738 * 10 ^ 0
n(51) = -0.11841182425981 * 10 ^ 0:   n(52) = -0.31306260323435 * 10 ^ 2
n(53) = 0.31546140237781 * 10 ^ 2:    n(54) = -0.25213154341695 * 10 ^ 4
n(55) = -0.14874640856724 * 10 ^ 0:   n(56) = 0.31806110878444 * 10 ^ 0

Alpha(52) = 20: Alpha(53) = 20: Alpha(54) = 20

beta(52) = 150: beta(53) = 150: beta(54) = 250: beta(55) = 0.3: beta(56) =
0.3

gamma(52) = 1.21: gamma(53) = 1.21: gamma(54) = 1.25

epsilon(52) = 1: epsilon(53) = 1: epsilon(54) = 1

a(55) = 3.5:      a(56) = 3.5:      b(55) = 0.85:      b(56) = 0.95
B_CAPS(55) = 0.2: B_CAPS(56) = 0.2: C_CAPS(55) = 28:   C_CAPS(56) = 32
D_CAPS(55) = 700: D_CAPS(56) = 800: A_CAPS(55) = 0.32: A_CAPS(56) = 0.32
'END OF CONSTANT DECLARING

For i = 1 To 7
    Sum1 = Sum1 + n(i) * T(i) * Delta_Rho ^ d(i) * Tau ^ (T(i) - 1)
Next i
For i = 8 To 51
    Sum2 = Sum2 + n(i) * T(i) * Delta_Rho ^ d(i) * Tau ^ (T(i) - 1) * Exp(-
Delta_Rho ^ c(i))
Next i
For i = 52 To 54
    Sum3 = Sum3 + n(i) * Delta_Rho ^ d(i) * Tau ^ T(i) * Exp(-Alpha(i) *
(Delta_Rho - epsilon(i)) ^ 2 - beta(i) * (Tau - gamma(i)) ^ 2) * (T(i) / Tau
- 2 * beta(i) * (Tau - gamma(i)))
Next i
For i = 55 To 56
    Theta = (1 - Tau) + A_CAPS(i) * ((Delta_Rho - 1) ^ 2) ^ (1 / (2 *
beta(i)))
    Delta = Theta ^ 2 + B_CAPS(i) * ((Delta_Rho - 1) ^ 2) ^ a(i)
    Psi = Exp(-C_CAPS(i) * (Delta_Rho - 1) ^ 2 - D_CAPS(i) * (Tau - 1) ^ 2)

    dDeltaBIdTau = -2 * Theta * b(i) * Delta ^ (b(i) - 1)
    dPsidTau = -2 * D_CAPS(i) * (Tau - 1) * Psi

    Sum4 = Sum4 + n(i) * Delta_Rho * (dDeltaBIdTau * Psi + Delta ^ b(i) *
dPsidTau)
Next i
PhiR_Tau = CDec(Sum1 + Sum2 + Sum3 + Sum4)
End Function
```

```
'WAGNER 2002
Private Function Phi0_Tau(Delta_Rho, Tau) As Double
Dim i%, n0#(2 To 8), gamma0#(4 To 8), sum#

n0(2) = 6.6832105268: n0(3) = 3.00632: n0(4) = 0.012436: n0(5) = 0.97315:
n0(6) = 1.2795: n0(7) = 0.96956: n0(8) = 0.24873

gamma0(4) = 1.28728967: gamma0(5) = 3.53734222: gamma0(6) = 7.74073708:
gamma0(7) = 9.24437796: gamma0(8) = 27.5075105

For i = 4 To 8
    sum = sum + n0(i) * gamma0(i) * ((1 - Exp(-gamma0(i) * Tau)) ^ -1 - 1)
Next i

Phi0_Tau = n0(2) + n0(3) / Tau + sum
End Function

'WAGNER 2002
Private Function Phi0(Delta_Rho, Tau) As Double

Dim i As Integer
'constants from table 6.1
Dim n0(1 To 8) As Double, gamma0(4 To 8) As Double, Sum1 As Double

'constants from table 6.1
n0(1) = -8.32044648201: n0(2) = 6.6832105268: n0(3) = 3.00632: n0(4) =
0.012436
n0(5) = 0.97315:        n0(6) = 1.2795:       n0(7) = 0.96956: n0(8) =
0.24873

gamma0(4) = 1.28728967: gamma0(5) = 3.53734222: gamma0(6) = 7.74073708
gamma0(7) = 9.24437796: gamma0(8) = 27.5075105

For i = 4 To 8
    Sum1 = Sum1 + n0(i) * LogExp(1 - Exp(1) ^ (-gamma0(i) * Tau))
Next i
Phi0 = LogExp(Delta_Rho) + n0(1) + n0(2) * Tau + n0(3) * LogExp(Tau) + Sum1

End Function


'WAGNER 2002
Private Function PhiR(Delta_Rho, Tau) As Variant

Dim i As Integer
Dim c(1 To 54) As Integer, d(1 To 54) As Integer
Dim T(1 To 54) As Single, n(1 To 56) As Double
Dim Alpha(52 To 54) As Integer, epsilon(52 To 54) As Integer
Dim beta(52 To 56) As Single, gamma(52 To 54) As Single
```

```
Dim a(55 To 56) As Single, b(55 To 56) As Single, B_CAPS(55 To 56) As Single,
A_CAPS(55 To 56) As Single
Dim C_CAPS(55 To 56) As Integer, D_CAPS(55 To 56) As Integer
'declaring of  components for F0+Fr and experimental PT spaces
Dim Delta As Double, Theta As Double, Psi As Double
'temporary double units
Dim Sum1 As Double, Sum2 As Double, Sum3 As Double, Sum4 As Double
'table 6.2
For i = 1 To 54
    c(i) = 0
Next i

For i = 8 To 22
c(i) = 1
Next i

For i = 23 To 42
c(i) = 2
Next i

For i = 43 To 46
c(i) = 3
Next i

c(47) = 4

For i = 48 To 51
c(i) = 6
Next i

d(1) = 1:   d(2) = 1:  d(3) = 1:  d(4) = 2:  d(5) = 2:   d(6) = 3:   d(7) = 4
d(8) = 1:   d(9) = 1:  d(10) = 1: d(11) = 2: d(12) = 2:  d(13) = 3:  d(14) =
4
d(15) = 4:  d(16) = 5: d(17) = 7: d(18) = 9: d(19) = 10: d(20) = 11: d(21) =
13
d(22) = 15: d(23) = 1: d(24) = 2: d(25) = 2: d(26) = 2:  d(27) = 3:  d(28) =
4
d(29) = 4:  d(30) = 4: d(31) = 5: d(32) = 6: d(33) = 6:  d(34) = 7:  d(35) =
9
d(36) = 9:  d(37) = 9: d(38) = 9: d(39) = 9: d(40) = 10: d(41) = 10: d(42) =
12
d(43) = 3:  d(44) = 4: d(45) = 4: d(46) = 5: d(47) = 14: d(48) = 3:  d(49) =
6
d(50) = 6:  d(51) = 6: d(52) = 3: d(53) = 3: d(54) = 3

T(1) = -0.5: T(2) = 0.875: T(3) = 1:   T(4) = 0.5: T(5) = 0.75: T(6) = 0.375
T(7) = 1:    T(8) = 4:     T(9) = 6:   T(10) = 12: T(11) = 1:   T(12) = 5
T(13) = 4:   T(14) = 2:    T(15) = 13: T(16) = 9:  T(17) = 3:   T(18) = 4
T(19) = 11:  T(20) = 4:    T(21) = 13: T(22) = 1:  T(23) = 7:   T(24) = 1
T(25) = 9:   T(26) = 10:   T(27) = 10: T(28) = 3:  T(29) = 7:   T(30) = 10
```

```
T(31) = 10:  T(32) = 6:    T(33) = 10: T(34) = 10: T(35) = 1:   T(36) = 2
T(37) = 3:   T(38) = 4:    T(39) = 8:  T(40) = 6:  T(41) = 9:   T(42) = 8
T(43) = 16:  T(44) = 22:   T(45) = 23: T(46) = 23: T(47) = 10:  T(48) = 50
T(49) = 44:  T(50) = 46:   T(51) = 50: T(52) = 0:  T(53) = 1:   T(54) = 4

n(1) = 0.12533547935523 * 10 ^ -1:    n(2) = 0.78957634722828 * 10 ^ 1
n(3) = -0.87803203303561 * 10 ^ 1:    n(4) = 0.31802509345418 * 10 ^ 0
n(5) = -0.26145533859358 * 10 ^ 0:    n(6) = -0.78199751687981 * 10 ^ -2
n(7) = 0.88089493102134 * 10 ^ -2:    n(8) = -0.66856572307965 * 10 ^ 0
n(9) = 0.20433810950965 * 10 ^ 0:     n(10) = -0.66212605039687 * 10 ^ -4
n(11) = -0.19232721156002 * 10 ^ 0:   n(12) = -0.25709043003438 * 10 ^ 0
n(13) = 0.16074868486251 * 10 ^ 0:    n(14) = -0.40092828925807 * 10 ^ -1
n(15) = 0.39343422603254 * 10 ^ -6:   n(16) = -0.75941377088144 * 10 ^ -5
n(17) = 0.56250979351888 * 10 ^ -3:   n(18) = -0.15608652257135 * 10 ^ -4
n(19) = 0.11537996422951 * 10 ^ -8:   n(20) = 0.36582165144204 * 10 ^ -6
n(21) = -0.13251180074668 * 10 ^ -11: n(22) = -0.62639586912454 * 10 ^ -9
n(23) = -0.10793600908932 * 10 ^ 0:   n(24) = 0.17611491008752 * 10 ^ -1
n(25) = 0.22132295167546 * 10 ^ 0:    n(26) = -0.40247669763528 * 10 ^ 0
n(27) = 0.58083399985759 * 10 ^ 0:    n(28) = 0.49969146990806 * 10 ^ -2
n(29) = -0.31358700712549 * 10 ^ -1:  n(30) = -0.74315929710341 * 10 ^ 0
n(31) = 0.4780732991548 * 10 ^ 0:     n(32) = 0.20527940895948 * 10 ^ -1
n(33) = -0.13636435110343 * 10 ^ 0:   n(34) = 0.14180634400617 * 10 ^ -1
n(35) = 0.83326504880713 * 10 ^ -2:   n(36) = -0.29052336009585 * 10 ^ -1
n(37) = 0.38615085574206 * 10 ^ -1:   n(38) = -0.20393486513704 * 10 ^ -1
n(39) = -0.16554050063734 * 10 ^ -2:  n(40) = 0.19955571979541 * 10 ^ -2
n(41) = 0.15870308324157 * 10 ^ -3:   n(42) = -0.1638856834253 * 10 ^ -4
n(43) = 0.43613615723811 * 10 ^ -1:   n(44) = 0.34994005463765 * 10 ^ -1
n(45) = -0.76788197844621 * 10 ^ -1:  n(46) = 0.22446277332006 * 10 ^ -1
n(47) = -0.62689710414685 * 10 ^ -4:  n(48) = -0.55711118565645 * 10 ^ -9
n(49) = -0.19905718354408 * 10 ^ 0:   n(50) = 0.31777497330738 * 10 ^ 0
n(51) = -0.11841182425981 * 10 ^ 0:   n(52) = -0.31306260323435 * 10 ^ 2
n(53) = 0.31546140237781 * 10 ^ 2:    n(54) = -0.25213154341695 * 10 ^ 4
n(55) = -0.14874640856724 * 10 ^ 0:   n(56) = 0.31806110878444 * 10 ^ 0

Alpha(52) = 20: Alpha(53) = 20: Alpha(54) = 20

beta(52) = 150: beta(53) = 150: beta(54) = 250: beta(55) = 0.3: beta(56) =
0.3

gamma(52) = 1.21: gamma(53) = 1.21: gamma(54) = 1.25

epsilon(52) = 1: epsilon(53) = 1: epsilon(54) = 1

a(55) = 3.5:      a(56) = 3.5:      b(55) = 0.85:      b(56) = 0.95
B_CAPS(55) = 0.2: B_CAPS(56) = 0.2: C_CAPS(55) = 28:   C_CAPS(56) = 32
D_CAPS(55) = 700: D_CAPS(56) = 800: A_CAPS(55) = 0.32: A_CAPS(56) = 0.32
'END OF CONSTANT DECLARING

For i = 1 To 7
    Sum1 = Sum1 + n(i) * Delta_Rho ^ d(i) * (Tau) ^ T(i)
```

```
Next i
For i = 8 To 51
    Sum2 = Sum2 + n(i) * Delta_Rho ^ d(i) * (Tau) ^ T(i) * Exp(1) ^ (-
Delta_Rho ^ c(i))
Next i
For i = 52 To 54
    Sum3 = Sum3 + n(i) * Delta_Rho ^ d(i) * (Tau) ^ T(i) * Exp(1) ^ (-
Alpha(i) * (Delta_Rho - epsilon(i)) ^ 2 - beta(i) * (Tau - gamma(i)) ^ 2)
Next i
For i = 55 To 56
    Theta = (1 - Tau) + A_CAPS(i) * ((Delta_Rho - 1) ^ 2) ^ (1 / (2 *
beta(i)))
    Delta = Theta ^ 2 + B_CAPS(i) * ((Delta_Rho - 1) ^ 2) ^ a(i)
    Psi = Exp(1) ^ (-C_CAPS(i) * (Delta_Rho - 1) ^ 2 - D_CAPS(i) * (Tau - 1)
^ 2)
    Sum4 = Sum4 + n(i) * Delta ^ b(i) * Delta_Rho * Psi
Next i
PhiR = CDec(Sum1 + Sum2 + Sum3 + Sum4)
End Function



'Huber et al 2009, New International Formulation for the Viscosity of H2O
'Valid up to 1173 °K and 1000 MPa or 10 kBar
' T in K, Rho in kg/m-3, output viscosity in micropascal/second (NOT
MILIPASCAL/SEC!!!) or 1000 Cp
Public Function Water_Viscosity_calc(T_inc, Rho_inc)
Dim i As Integer, j As Integer
Dim T As Single, T_Star As Single, T_ As Double
Dim Rho As Double, Rho_star As Single, Rho_ As Double, Rho2 As Single, Rho_2
As Double
Dim P As Single, P_Star As Single, P_ As Double
Dim Mu As Double, Mu_star As Single, Mu_ As Double
Dim Mu_0 As Double, Mu_1 As Double, Mu_2 As Double
Dim Tmp_Sum1 As Double, Tmp_Sum2 As Double, Tmp_Sum3 As Double
Dim Hi(0 To 3) As Single, Hij(0 To 5, 0 To 6) As Double
Dim Psi_D As Double, L As Double, w As Double
Dim Chi_ As Single, Chi1 As Double, Chi2 As Double
Dim Chi_Mu As Single, qc As Double, qd As Double, Upsilon As Single, gamma As
Single
Dim Xi As Double, Xi0 As Single, gamma0 As Single, T_r As Single
Dim Y As Double

T_Star = 647.096
Rho_star = 322
P_Star = 22.064

Mu_star = 1 * 10 ^ -6
Hi(0) = 1.67752:  Hi(1) = 2.20462: Hi(2) = 0.6366564: Hi(3) = -0.241605
```

```
Hij(0, 0) = 0.520094:  Hij(1, 0) = 0.0850895:   Hij(2, 0) = -1.08374:  Hij(3,
0) = -0.289555
Hij(0, 1) = 0.222531:  Hij(1, 1) = 0.999115:    Hij(2, 1) = 1.88797:   Hij(3,
1) = 1.26613
Hij(5, 1) = 0.120573:  Hij(0, 2) = -0.281378:   Hij(1, 2) = -0.906851: Hij(2,
2) = -0.772479
Hij(3, 2) = -0.489837: Hij(4, 2) = -0.25704:    Hij(0, 3) = 0.161913:  Hij(1,
3) = 0.257399
Hij(0, 4) = -0.0325372: Hij(3, 4) = 0.0698452:  Hij(4, 5) = 0.00872102:
Hij(3, 6) = -0.00435673
Hij(5, 6) = -0.000593264

Chi_Mu = 0.068: qc = 1.9 ^ -1:    qd = 1.1 ^ -1: Upsilon = 0.63: gamma =
1.239
Xi0 = 0.13:     gamma0 = 0.06: T_r = 1.5
T = T_inc
T_ = T / T_Star

Rho = Rho_inc
Rho2 = Rho * 0.9995
Rho_ = Rho / Rho_star
Tmp_Sum2 = T_Star * 1.5

Chi1 = ((Rho - Rho2) / (Water_Pressure_calc(T, Rho) - Water_Pressure_calc(T,
Rho2))) * P_Star / Rho_star
Chi2 = ((Rho - Rho2) / (Water_Pressure_calc(Tmp_Sum2, Rho) -
Water_Pressure_calc(Tmp_Sum2, Rho2))) * P_Star / Rho_star

Chi_ = (Chi1 - Chi2 * Tmp_Sum2 / T) * Rho_

If Chi_ < 0 Then Chi_ = 0

Tmp_Sum2 = 0
For i = 0 To 3
    Tmp_Sum1 = Tmp_Sum1 + Hi(i) / T_ ^ i
Next i

Mu_0 = 100 * T_ ^ 0.5 / Tmp_Sum1
Tmp_Sum1 = 0

For i = 0 To 5
    For j = 0 To 6
        Tmp_Sum1 = Tmp_Sum1 + Hij(i, j) * (Rho_ - 1) ^ j
    Next j
    Tmp_Sum2 = Tmp_Sum2 + ((1 / T_ - 1) ^ i) * Tmp_Sum1
    Tmp_Sum1 = 0
Next i
Mu_1 = Exp(Rho_ * Tmp_Sum2)
Tmp_Sum2 = 0
Tmp_Sum1 = 0
```

```
Xi = Xi0 * (Chi_ / gamma0) ^ (Upsilon / gamma)

If Xi < 0 Then Xi = 0
If Xi >= 0 And Xi <= 0.3817016416 Then
    Y = 0.2 * qc * Xi * (qd * Xi) ^ 5 * (1 - qc * Xi + (qc * Xi) ^ 2 - 765 /
504 * (qd * Xi) ^ 2)
Else
    'Psi_D = WorksheetFunction.Acos((1 + (qd * Xi) ^ 2) ^ -0.5)
    'arccs function have two strings removed from calculation
    Psi_D = Arccs((1 + (qd * Xi) ^ 2) ^ -0.5)
    w = Abs((qc * Xi - 1) / (qc * Xi + 1)) ^ 0.5 * Tan(Psi_D / 2)
    If qc * Xi > 1 Then L = LogExp((1 + w) / (1 - w)) Else L = 2 *
Atn(Abs(w))
    Y = 1 / 12 * Sin(3 * Psi_D) - 0.25 / (qc * Xi) * Sin(2 * Psi_D) + 1 / (qc
* Xi) ^ 2 * (1 - 1.25 * (qc * Xi) ^ 2) * Sin(Psi_D) - 1 / (qc * Xi) ^ 3 * ((1
- 1.5 * (qc * Xi) ^ 2) * Psi_D - Abs((qc * Xi) ^ 2 - 1) ^ 1.5 * L)
End If
Mu_2 = Exp(Chi_Mu * Y)

Mu = Mu_0 * Mu_1 * Mu_2
Water_Viscosity_calc = Mu

End Function

Public Function Rho_Water_Vap_sat(Ti) As Double
Dim T#, T_inv#, RhoVapSat#, c#(1 To 6)
'used eq 2.7 to obtain liquid density from Wagner and Pruss, output in bars
T = Ti
'If T > 373.946 Then T = 373.945
If T = 0 Then T = 0.01
T = T + 273.15
T_inv = 1 - T / 647.096

c(1) = -2.0315024: c(2) = -2.6830294: c(3) = -5.38626492
c(4) = -17.2991605: c(5) = -44.7586581: c(6) = -63.9201063

Rho_Water_Vap_sat = Exp(c(1) * T_inv ^ (1 / 3) + c(2) * T_inv ^ (2 / 3) +
c(3) * T_inv ^ (4 / 3) + c(4) * T_inv ^ 3 + c(5) * T_inv ^ (37 / 6) + c(6) *
T_inv ^ (71 / 6)) * 322

End Function
Public Function Rho_Water_Liq_sat(Ti) As Double
Dim T#, T_inv#, RhoLiqSat#, b#(1 To 6)
'used eq 2.6 to obtain liquid density from Wagner and Pruss, output in bars
T = Ti
'If T > 373.946 Then T = 373.945
If T = 0 Then T = 0.01
T = T + 273.15
T_inv = 1 - T / 647.096
```

```
b(1) = 1.99274064:  b(2) = 1.09965342:  b(3) = -0.510839303
b(4) = -1.75493479: b(5) = -45.5170352: b(6) = -674694.45

Rho_Water_Liq_sat = (1 + b(1) * T_inv ^ (1 / 3) + b(2) * T_inv ^ (2 / 3) +
b(3) * T_inv ^ (5 / 3) + b(4) * T_inv ^ (16 / 3) + b(5) * T_inv ^ (43 / 3) +
b(6) * T_inv ^ (110 / 3)) * 322

End Function
Public Function P_H2O_Boiling_Curve(Ti_C) As Double
'Output is in bars
Dim T#, T_inv#, RhoVapSat#, a#(1 To 6)

T = Ti_C
If T = 0 Then T = 0.01
T = T + 273.15
T_inv = 1 - T / 647.096

a(1) = -7.85951783: a(2) = 1.84408259:  a(3) = -11.7866497
a(4) = 22.6807411:  a(5) = -15.9618719: a(6) = 1.80122502

P_H2O_Boiling_Curve = Exp(647.096 / T * (a(1) * T_inv + a(2) * T_inv ^ 1.5 +
a(3) * T_inv ^ 3 + a(4) * T_inv ^ 3.5 + a(5) * T_inv ^ 4 + a(6) * T_inv ^
7.5)) * 220.64

End Function


Public Function Water_boiling_Curve(Ti) As Double
Dim T#, T_inv#, RhoVapSat#, c#(1 To 6)
'used eq 2.7 to obtain liquid density from Wagner and Pruss, output in bars
    T = Ti
    If T > 373.946 Then T = 373.945
    If T = 0 Then T = 0.01
    T = T + 273.15
    T_inv = 1 - T / 647.096


    c(1) = -2.0315024: c(2) = -2.6830294: c(3) = -5.38626492
    c(4) = -17.2991605: c(5) = -44.7586581: c(6) = -63.9201063

    RhoVapSat = Exp(c(1) * T_inv ^ (1 / 3) + c(2) * T_inv ^ (2 / 3) + c(3) *
T_inv ^ (4 / 3) + c(4) * T_inv ^ 3 + c(5) * T_inv ^ (37 / 6) + c(6) * T_inv ^
(71 / 6)) * 322

    'SO IF REQUEST RHO BASED ON PRESSURE, VALUES CAN FELT INTO VAPOR STATE
    Water_boiling_Curve = Water_Pressure_calc(T, RhoVapSat) * 10
    'Water_boiling_Curve = Water_Pressure_calc(T, RhoLiqSat) * 10

End Function
```

```
Public Function Rho_Water(T_in_C, P_in_Bar) As Double

Dim T_K#, P_mPa#, n#, aa#, bb#, Toler#, TH2O_Crit#, RhoH2O_Crit#
Dim Rho1#, Rho2#, RhoAprx#, P_tmp1#, P_tmp2#, P_Der#, EndLoop As Boolean

T_K = T_in_C + 273.15
P_mPa = P_in_Bar / 10
TH2O_Crit = 647.096
RhoH2O_Crit = 322

If T_K <= TH2O_Crit Then
    If P_mPa * 10 < Round_Down(P_H2O_Boiling_Curve(T_in_C), 2) Then
        '0.001021135 stands for density of vapor at T=1000 C and P=0.006 bars
        Rho1 = 0.001021135
        Rho2 = Rho_Water_Vap_sat(T_in_C) + 1
    Else
        Rho1 = Rho_Water_Liq_sat(T_in_C) - 1
        Rho2 = 1701
    End If
Else
    Rho1 = 0.001021135
    Rho2 = 1701
End If

'Bisscectional aproximation first
Toler = 1
While n <= 1000
    DoEvents
    RhoAprx = (Rho1 + Rho2) / 2
    If Abs(Rho2 - Rho1) / 2 < Toler Then
        RhoAprx = Rho2
        n = 1000
    End If
    n = n + 1
    aa = Water_Pressure_calc(T_K, RhoAprx) - P_mPa
    bb = Water_Pressure_calc(T_K, Rho1) - P_mPa
    If Sgn(aa) = Sgn(bb) Then Rho1 = RhoAprx Else Rho2 = RhoAprx
Wend

'newthon method compare desired P_in with pressure,
'to get accuracy less than 0.01 mPa (0.1 Bar)
Rho1 = RhoAprx
Rho2 = Rho1 - 0.0001
Toler = 0.0001
n = 0
While EndLoop = False
    DoEvents
    RhoAprx = Rho2
    P_tmp1 = Water_Pressure_calc(T_K, Rho1) - P_mPa
```

```
    P_tmp2 = Water_Pressure_calc(T_K, Rho2) - P_mPa
    P_Der = CDec((P_tmp1 - P_tmp2) / (Rho1 - Rho2))
    Rho1 = Rho1 - P_tmp1 / P_Der

    P_tmp1 = P_tmp1 + P_mPa
    Rho2 = Rho1 - 0.0001
    n = n + 1
    If n >= 10000 Then
        'MsgBox "!!! Too much iterations in pressure calcs " & i, vbOKOnly
        'Application.ScreenUpdating = True
        Rho1 = 123456789
        EndLoop = True
    End If
    If Abs(CDec(1 - P_mPa / P_tmp1)) <= 10 ^ -8 Or Abs(RhoAprx - Rho1) <
Toler Then EndLoop = True
Wend
Rho_Water = Rho1
End Function
```

1.11 Module WaterAndSalt

```
Public Function New_LV_P(Ti, Pi, XNaCl_Moli, FindWhereItIs) As Double
Dim n%, a#, b#, c#, Toler#, chckr1 As Boolean, chckr2 As Boolean

If XNaCl_Moli = 0 Then
    If Ti < 373.947 Then New_LV_P = P_H2O_Boiling_Curve(Ti) Else New_LV_P = 0
Else
    'defining upper P limit along L+H curve
    If XNaCl_Moli >= 0.098994534 And X_L_Sat(Ti, P_VLH(Ti)) >= XNaCl_Moli And
X_L_Sat(Ti, 5000) <= XNaCl_Moli Then
        a = P_VLH(Ti)
        b = 5000
        n = 1
        Toler = 0.001
        While n <= 1000
            c = (a + b) / 2
            If (b - a) / 2 < Toler Then
                n = 1001
            End If

            n = n + 1
            aa = X_L_Sat(Ti, c) - XNaCl_Moli
            bb = X_L_Sat(Ti, b) - XNaCl_Moli
            If Sgn(aa) = Sgn(bb) Then b = c Else a = c
        Wend

    Else
        b = 5000
    End If
    'defining lower P limit
    If FindWhereItIs = False Then a = Pi Else a = 0.001

    n = 1
    Toler = 0.001
    While n <= 1000
        c = (a + b) / 2
        If (b - a) / 2 < Toler Then
            New_LV_P = b
            n = 1001
        End If
        n = n + 1
        aa = AbovePhases(Ti, c, XNaCl_Moli, chckr1)
        bb = AbovePhases(Ti, a, XNaCl_Moli, chckr2)
        'If aa <> bb And bb <> True Then a = c Else b = c
        If chckr1 = chckr2 And chckr1 = True Then
            If aa = True Then b = c Else a = c
        ElseIf chckr1 <> chckr2 And chckr1 = False Then
            b = c
```

```
        End If

    Wend
    New_LV_P = Round_Down(New_LV_P, 3)
End If

End Function

Public Function AbovePhases(Ti, Pi, XNaCl_Moli, NoErrors As Boolean) As
Boolean
Dim n%, j%, T#, P#, XNaCl#, XNaCl_Crit#, PCrit#, a#, b#, c#, Toler#, Tmp#,
Tmp2#
Dim TLSat#, TVSat#, TVLliq#, TVLvap#
T = Ti
P = Pi
XNaCl = XNaCl_Moli
X_and_P_crit T, XNaCl_Crit, PCrit
Toler = 0.001
'On Error GoTo msge
If XNaCl = 0 Then
    If P > P_H2O_Boiling_Curve(T) Then AbovePhases = True: NoErrors = True
ElseIf XNaCl = 1 Then
    If T > 800.7 Then
        Tmp = P_Boil(T)
        If Tmp < P Then
            NoErrors = True
            AbovePhases = True
        Else
            NoErrors = True
            AbovePhases = False
        End If
    End If
Else
    Tmp = X_L_Sat(Ti, Pi)
    If Tmp >= XNaCl Then
        NoErrors = True
        AbovePhases = True
    Else
        NoErrors = True
        AbovePhases = False
        GoTo GetOut
    End If

    If P > PCrit Then
        NoErrors = True
        AbovePhases = True
    Else
        If P < P_VLH(T) Then
            NoErrors = True
```

```
            AbovePhases = False
        Else
            Tmp = X_VL_Liq(T, P)
            Tmp2 = X_VL_Vap(T, P)

            If Tmp < XNaCl Or Tmp2 > XNaCl Then
                 NoErrors = True
                AbovePhases = True
            Else
                NoErrors = True
                AbovePhases = False
            End If
        End If
    End If

End If
GetOut:
End Function

Public Function V_Extrapol(x_in, T_in, P_in) As Double

Dim o0#, o1#, o2#, T_inv#, mH2O#, mNaCl#, T#, P#, P2#, Rho#, Rho2#, V#, V2#,
XNaCl#
Dim o3#, o4#, o5#, Vsat#, Vwat#

Dim V1000#, dVdP390#

mH2O = 18.015268
mNaCl = 58.4428

T = T_in
XNaCl = x_in
P = P_in

V = X_L_Sat(T, P)

If P <= 15 And T <= 214.7 Then
    T = T_Star_V(XNaCl, T, P)
    Vsat = mH2O / Rho_Water_Liq_sat(T) * 1000
    Vwat = mH2O / Rho_Water(T, P) * 1000

    If Vsat < Vwat Then

        o2 = 2.0125 * 10 ^ -7 + 3.29977 * 10 ^ -9 * Exp(-4.31279 * Log10(P))
- 1.17748 * 10 ^ -7 * Log10(P) + 7.58009 * 10 ^ -8 * (Log10(P)) ^ 2

        V = mH2O / Rho_Water_Liq_sat(T) * 1000
        V2 = mH2O / Rho_Water_Liq_sat(T - 0.005) * 1000
        o1 = (V - V2) / 0.005 - 3 * o2 * T ^ 2
        o0 = V - o1 * T - o2 * T ^ 3
```

```
        V_Extrapol = o0 + (o2 * T ^ 3) + (o1 * T)
    End If

ElseIf P <= 350 And T >= 600 Then
    V = X_VL_Liq(T, P)
    If Round_Down(XNaCl, 5) >= Round_Down(X_VL_Liq(T, P), 5) Then
'        If P >= New_LV_P(T, P, XNaCl, True) Then

            V1000 = (mH2O * (1 - XNaCl) + mNaCl * XNaCl) /
Rh_Br_for_V_extr(XNaCl, T, 1000) * 1000
            V = (mH2O * (1 - XNaCl) + mNaCl * XNaCl) /
Rh_Br_for_V_extr(XNaCl, T, 390.147) * 1000
            V2 = (mH2O * (1 - XNaCl) + mNaCl * XNaCl) /
Rh_Br_for_V_extr(XNaCl, T, 390.137) * 1000

            dVdP390 = (V - V2) / (0.01)

            o4 = (V - V1000 + dVdP390 * 1609.853) / (LogExp(1390.147 / 2000)
- 2390.147 / 1390.147)
            o3 = V - o4 * LogExp(1390.147) - 390.147 * dVdP390 + 390.147 /
1390.147 * o4
            o5 = dVdP390 - o4 / (1390.147)

        V_Extrapol = o3 + o4 * LogExp(P + 1000) + o5 * P
'        End If
    End If
Else
    V_Extrapol = 0
End If

End Function

Public Function Rho_Brine(XNaCl_Frac, T_in_C, P_in_Bar) As Double
Dim T#, P#, T_Star#, V_water#
SetupExcelForCalc True
Dim mH2O#, mNaCl#
mH2O = 18.015268
mNaCl = 58.4428

T = T_in_C
P = P_in_Bar
T_Star = T_Star_V(XNaCl_Frac, T, P)

V_water = V_Extrapol(XNaCl_Frac, T, P)
If V_water = 0 Then V_water = mH2O / Rho_Water(T_Star, P) * 1000#

Rho_Brine = (mH2O * (1 - XNaCl_Frac) + mNaCl * XNaCl_Frac) / V_water * 1000#
' FOR CRITICAL POINT OF PURE WATER 373.946 °C, 220.64 B RHO RETURNED AS
316.29
```

```
End Function

Private Function Rh_Br_for_V_extr(XNaCl_Frac, T_in_C, P_in_Bar) As Double
Dim T#, P#, T_Star#, V_water#

Dim mH2O#, mNaCl#

mH2O = 18.015268
mNaCl = 58.4428

T = T_in_C
P = P_in_Bar
T_Star = T_Star_V(XNaCl_Frac, T, P)

V_water = mH2O / Rho_Water(T_Star, P) * 1000#

Rh_Br_for_V_extr = (mH2O * (1 - XNaCl_Frac) + mNaCl * XNaCl_Frac) / V_water *
1000#
End Function

Public Function Isob_Heat_cap(XNaCl, T_in_C, rhoi) As Double
Dim ThSt#, q2#
ThSt = T_star_H(XNaCl, q2, T_in_C, P)
Isob_Heat_cap = Water_Isobaric_Heat_capacity_calc(T_in_C, rhoi) * q2


End Function
```

2. Appendix B

Table 1 Dynamic viscosity of H_2O-NaCl, experimentally measured (Exp. Data) obtained from referred literature, and calculated by different models Palliser and McKibbin 1998, revised model discussed in Chapter 2 and Mao and Duan 2009. All references provided in Chapter 2 references section

Salt, wt%	T, °C	P, bar	Density, $kg*m^{-3}$	Reference	Exp data	Palliser and McKibbin 1998	Revised model	Mao Duan 2009
0.01	0	1	999.9	Ozbek 1977	1787.7	1793.2	1792.6	1792.0
0.02	0	1	1000.0	Ozbek 1977	1787.7	1793.8	1793.6	1792.2
0.05	0	1	1000.1	Ozbek 1977	1788.3	1795.4	1796.3	1792.8
0.11	0	1	1000.5	Ozbek 1977	1789.3	1798.6	1800.8	1794.1
0.29	0	1	1001.5	Ozbek 1977	1798.8	1808.3	1812.3	1797.9
0.58	0	1	1003.1	Ozbek 1977	1793.8	1823.9	1828.2	1804.3
1.15	0	1	1006.1	Ozbek 1977	1799.4	1854.5	1856.0	1817.2
2.85	0	1	1015.7	Ozbek 1977	1821.1	1946.0	1929.5	1859.3
5.6	0	1	1036.1	Ozbek 1977	1874.6	2093.9	2039.5	1940.5
10.78	0	1	1080.1	Ozbek 1977	2050.6	2372.4	2244.3	2148.2

0.57	10	1	1003.8	Ozbek 1977	1314.6	1328.9	1335.2	1315.7
2.82	10	1	1019.9	Ozbek 1977	1347.9	1417.1	1416.2	1358.7
5.45	10	1	1039.2	Ozbek 1977	1398.1	1520.2	1501.8	1418.3
10.43	10	1	1077.2	Ozbek 1977	1529.9	1715.4	1663.9	1566.1
14.61	10	1	1109.9	Ozbek 1977	1697.3	1879.3	1807.5	1737.0
16.92	10	1	1128.2	Ozbek 1977	1816.2	1969.8	1891.3	1855.8
18.89	10	1	1143.9	Ozbek 1977	1930.0	2047.1	1965.9	1974.0
24.3	10	1	1187.6	Ozbek 1977	2383.3	2259.1	2187.6	2403.6
25.32	10	1	1196.0	Ozbek 1977	2489.2	2299.1	2232.5	2506.2
0	12.5	1	999.4	Ozbek 1977	1218.8	1217.7	1217.1	1217.1
0.01	12.5	1	999.5	Ozbek 1977	1219.0	1218.1	1218.1	1217.2
0.02	12.5	1	999.6	Ozbek 1977	1219.4	1218.4	1218.9	1217.4
0.05	12.5	1	999.8	Ozbek 1977	1220.0	1219.5	1220.9	1217.9
0.11	12.5	1	1000.3	Ozbek 1977	1221.0	1221.7	1224.4	1218.8
1.15	12.5	1	1007.8	Ozbek 1977	1237.1	1259.7	1266.3	1236.3
2.3	12.5	1	1016.0	Ozbek 1977	1254.7	1301.7	1304.8	1257.2
2.86	12.5	1	1020.1	Ozbek 1977	1263.7	1322.2	1322.7	1268.0
0	15	1	999.1	Ozbek 1977	1139.3	1138.1	1137.6	1137.6
0.01	15	1	999.2	Ozbek 1977	1139.4	1138.5	1138.6	1137.7
0.02	15	1	999.2	Ozbek 1977	1139.8	1138.8	1139.3	1137.9
0.05	15	1	999.5	Ozbek 1977	1140.4	1139.8	1141.3	1138.3
0.11	15	1	999.9	Ozbek 1977	1141.4	1141.9	1144.5	1139.3
1.16	15	1	1007.5	Ozbek 1977	1157.4	1177.7	1184.4	1156.1
2.3	15	1	1015.8	Ozbek 1977	1174.8	1216.7	1220.6	1175.8
2.86	15	1	1019.8	Ozbek 1977	1183.7	1235.8	1237.5	1186.0
19.45	17.99	1	1144.9	Ozbek 1977	1631.9	1668.2	1633.1	1630.2
2.7	18	36.2	1019.6	Ozbek 1977	1087.0	1136.5	1139.9	1094.3
2.7	18	70.7	1021.2	Ozbek 1977	1086.0	1134.7	1138.1	1093.0
2.7	18	139.9	1024.2	Ozbek 1977	1084.0	1131.4	1134.7	1090.5
2.7	18	157.9	1024.9	Ozbek 1977	1084.0	1130.6	1133.9	1089.9
2.7	18	206.1	1027.0	Ozbek 1977	1081.0	1128.5	1131.8	1088.4
2.7	18	239.9	1028.4	Ozbek 1977	1084.0	1127.2	1130.4	1087.5
2.7	18	264.4	1029.4	Ozbek 1977	1085.1	1126.3	1129.4	1086.8
2.7	18	302.7	1031.0	Ozbek 1977	1082.0	1125.0	1128.0	1085.8
2.7	18	1	1018.1	Ozbek 1977	1090.0	1138.5	1141.9	1095.7
19.45	18	1	1144.8	Ozbek 1977	1628.3	1667.7	1632.7	1629.8
19.45	18.01	1	1144.8	Ozbek 1977	1625.3	1667.3	1632.4	1629.4
19.45	18.01	1	1144.8	Ozbek 1977	1628.5	1667.3	1632.4	1629.4
19.45	18.02	1	1144.8	Ozbek 1977	1626.2	1666.9	1632.0	1629.0
19.45	18.05	34.5	1145.8	Ozbek 1977	1625.7	1662.9	1625.0	1625.8
19.45	18.05	205	1151.5	Ozbek 1977	1641.7	1651.2	1598.6	1617.2
19.45	18.05	205	1151.5	Ozbek 1977	1644.4	1651.2	1598.6	1617.2
19.45	18.05	243	1152.8	Ozbek 1977	1645.7	1649.0	1593.3	1615.5

19.45	18.06	34.5	1145.8	Ozbek 1977	1625.4	1662.5	1624.7	1625.4
19.45	18.06	137.9	1149.2	Ozbek 1977	1634.5	1655.0	1608.1	1619.9
19.45	18.06	137.9	1149.2	Ozbek 1977	1636.8	1655.0	1608.1	1619.9
19.45	18.06	172.8	1150.4	Ozbek 1977	1638.9	1652.7	1602.8	1618.2
19.45	18.06	172.8	1150.4	Ozbek 1977	1640.2	1652.7	1602.8	1618.2
19.45	18.06	243	1152.8	Ozbek 1977	1646.0	1648.6	1592.9	1615.2
19.45	18.06	274.7	1153.8	Ozbek 1977	1648.0	1647.0	1588.7	1613.9
19.45	18.06	274.7	1153.8	Ozbek 1977	1648.1	1647.0	1588.7	1613.9
19.45	18.06	307.8	1154.9	Ozbek 1977	1651.6	1645.3	1584.5	1612.7
19.45	18.06	307.8	1154.9	Ozbek 1977	1652.9	1645.3	1584.5	1612.7
19.45	18.07	69.3	1146.9	Ozbek 1977	1628.4	1659.4	1618.5	1623.1
19.45	18.07	69.3	1146.9	Ozbek 1977	1628.8	1659.4	1618.5	1623.1
19.45	18.08	104.2	1148.1	Ozbek 1977	1632.0	1656.5	1612.6	1620.8
19.45	18.08	14.2	1145.1	Ozbek 1977	1632.5	1663.3	1627.4	1625.8
13.19	18.14	1	1095.9	Ozbek 1977	1338.4	1464.8	1430.1	1353.1
13.19	18.26	173.4	1102.1	Ozbek 1977	1341.1	1449.5	1407.2	1341.7
13.19	18.46	274	1105.6	Ozbek 1977	1338.7	1437.7	1391.5	1332.0
13.19	18.46	274	1105.6	Ozbek 1977	1339.8	1437.7	1391.5	1332.0
13.19	18.48	309.9	1106.9	Ozbek 1977	1339.8	1435.5	1387.8	1330.3
13.19	18.49	309.9	1106.9	Ozbek 1977	1342.5	1435.2	1387.5	1330.0
13.19	18.5	172.7	1101.9	Ozbek 1977	1332.6	1441.1	1399.5	1334.1
13.19	18.51	206.5	1103.2	Ozbek 1977	1334.3	1439.0	1395.9	1332.6
13.19	18.51	242.3	1104.5	Ozbek 1977	1334.9	1437.3	1392.7	1331.4
13.19	18.52	172.7	1101.9	Ozbek 1977	1331.8	1440.4	1398.9	1333.4
13.19	18.52	242.3	1104.5	Ozbek 1977	1336.6	1437.0	1392.4	1331.1
13.19	18.53	138.9	1100.7	Ozbek 1977	1329.3	1441.8	1401.9	1334.4
13.19	18.53	138.9	1100.7	Ozbek 1977	1331.0	1441.8	1401.9	1334.4
13.19	18.54	103.4	1099.4	Ozbek 1977	1330.4	1443.5	1405.2	1335.5
13.19	18.54	206.5	1103.2	Ozbek 1977	1332.3	1438.0	1395.0	1331.6
13.19	18.55	103.4	1099.4	Ozbek 1977	1326.1	1443.2	1404.9	1335.2
13.19	18.56	68.9	1098.1	Ozbek 1977	1324.6	1444.9	1408.2	1336.3
13.19	18.56	68.9	1098.1	Ozbek 1977	1327.0	1444.9	1408.2	1336.3
13.19	18.67	34.8	1096.9	Ozbek 1977	1323.2	1443.1	1408.4	1334.3
13.19	18.69	34.8	1096.9	Ozbek 1977	1322.1	1442.4	1407.7	1333.6
13.19	18.72	1	1095.7	Ozbek 1977	1320.6	1443.6	1410.5	1334.2
13.19	18.73	1	1095.7	Ozbek 1977	1320.6	1443.3	1410.2	1333.9
7.91	19	35.5	1057.2	Ozbek 1977	1164.0	1268.9	1251.2	1173.1
7.91	19	66.5	1058.4	Ozbek 1977	1167.0	1267.2	1248.8	1171.9
7.91	19	104.4	1060.0	Ozbek 1977	1168.0	1265.2	1246.1	1170.6
7.91	19	138.9	1061.3	Ozbek 1977	1166.0	1263.6	1243.8	1169.4
7.91	19	174.8	1062.8	Ozbek 1977	1166.0	1262.0	1241.4	1168.3
7.91	19	207.9	1064.1	Ozbek 1977	1165.0	1260.6	1239.3	1167.4
7.91	19	241.4	1065.4	Ozbek 1977	1133.0	1259.2	1237.3	1166.4

7.91	19	272.3	1066.6	Ozbek 1977	1165.0	1258.1	1235.5	1165.7
7.91	19	309.6	1068.0	Ozbek 1977	1166.0	1256.9	1233.5	1164.8
7.91	19	156.8	1062.0	Ozbek 1977	1166.0	1262.8	1242.6	1168.9
7.91	19	1	1055.8	Ozbek 1977	1166.0	1270.9	1253.8	1174.4
7.91	19	1	1055.8	Ozbek 1977	1161.0	1270.9	1253.8	1174.4
7.91	19	35.5	1057.2	Ozbek 1977	1160.0	1268.9	1251.2	1173.1
12.97	19	1	1093.9	Ozbek 1977	1289.0	1426.8	1394.8	1317.8
12.97	19	36.5	1095.1	Ozbek 1977	1293.0	1424.5	1390.9	1316.3
12.97	19	74.1	1096.5	Ozbek 1977	1293.0	1422.2	1387.0	1314.7
12.97	19	107.2	1097.7	Ozbek 1977	1293.0	1420.3	1383.6	1313.4
12.97	19	143.4	1099.0	Ozbek 1977	1293.0	1418.4	1380.1	1312.1
12.97	19	175.4	1100.2	Ozbek 1977	1295.0	1416.8	1377.1	1311.0
12.97	19	206.5	1101.3	Ozbek 1977	1302.0	1415.3	1374.3	1309.9
12.97	19	233.4	1102.3	Ozbek 1977	1298.0	1414.1	1371.9	1309.1
12.97	19	270.6	1103.6	Ozbek 1977	1299.0	1412.5	1368.8	1308.0
12.97	19	302.8	1104.8	Ozbek 1977	1304.0	1411.3	1366.2	1307.2
16.03	19.5	1	1117.3	Ozbek 1977	1401.0	1502.4	1468.9	1414.4
16.03	19.5	35.5	1118.4	Ozbek 1977	1401.0	1500.1	1464.5	1412.8
16.03	19.5	70.7	1119.6	Ozbek 1977	1405.0	1497.9	1460.2	1411.4
16.03	19.5	139.1	1121.9	Ozbek 1977	1407.0	1494.1	1452.2	1408.7
16.03	19.5	173.4	1123.1	Ozbek 1977	1411.0	1492.3	1448.4	1407.5
16.03	19.5	203.6	1124.2	Ozbek 1977	1412.0	1490.9	1445.2	1406.5
16.03	19.5	243	1125.6	Ozbek 1977	1415.0	1489.1	1441.1	1405.3
16.03	19.5	278	1126.8	Ozbek 1977	1417.0	1487.7	1437.7	1404.3
16.03	19.5	312.5	1128.0	Ozbek 1977	1419.0	1486.4	1434.5	1403.4
16.03	19.5	154.8	1122.5	Ozbek 1977	1409.0	1493.3	1450.4	1408.1
16.03	19.5	1	1117.3	Ozbek 1977	1403.0	1502.4	1468.9	1414.4
0.57	20	1	1002.3	Ozbek 1977	1010.1	1019.2	1025.1	1009.8
2.82	20	1	1018.5	Ozbek 1977	1042.6	1086.9	1090.4	1045.1
5.45	20	1	1037.5	Ozbek 1977	1092.0	1165.9	1159.7	1093.4
10.43	20	1	1074.3	Ozbek 1977	1198.7	1315.7	1291.7	1210.5
14.61	20	1	1106.1	Ozbek 1977	1328.1	1441.3	1409.8	1343.3
16.92	20	1	1124.0	Ozbek 1977	1417.4	1510.8	1479.2	1434.5
18.89	20	1	1139.5	Ozbek 1977	1505.7	1570.0	1541.1	1524.8
24.3	20	1	1182.9	Ozbek 1977	1834.5	1732.6	1726.8	1849.5
25.64	20	1	1193.8	Ozbek 1977	1912.8	1772.9	1776.8	1951.9
26.4	20	1	1200.1	Ozbek 1977	2040.0	1795.8	1806.0	**
13.19	22.8	1	1094.1	Ozbek 1977	1204.7	1307.8	1283.7	1212.6
13.19	23	173.4	1100.1	Ozbek 1977	1208.9	1295.5	1264.8	1203.4
19.45	23.02	1	1142.5	Ozbek 1977	1447.5	1476.1	1457.6	1447.3
19.45	23.09	1	1142.5	Ozbek 1977	1444.1	1473.7	1455.4	1445.0
19.45	23.11	1	1142.4	Ozbek 1977	1443.9	1473.0	1454.7	1444.4
19.45	23.18	35.4	1143.3	Ozbek 1977	1443.7	1469.0	1448.2	1441.1

19.45	23.2	35.4	1143.3	Ozbek 1977	1444.0	1468.3	1447.6	1440.4
13.19	23.24	245.8	1102.6	Ozbek 1977	1206.6	1286.6	1253.5	1196.0
13.19	23.24	280.2	1103.8	Ozbek 1977	1207.5	1285.8	1251.5	1195.5
13.19	23.24	314.7	1105.0	Ozbek 1977	1207.7	1285.2	1249.5	1195.2
13.19	23.26	209.9	1101.3	Ozbek 1977	1204.4	1286.8	1255.3	1195.9
13.19	23.26	314.7	1105.0	Ozbek 1977	1211.5	1284.6	1249.0	1194.7
19.45	23.26	70.9	1144.5	Ozbek 1977	1443.6	1464.8	1441.5	1437.5
13.19	23.27	174.1	1100.0	Ozbek 1977	1201.8	1287.5	1257.4	1196.2
19.45	23.27	70.9	1144.5	Ozbek 1977	1443.6	1464.4	1441.2	1437.2
13.19	23.28	103.7	1097.4	Ozbek 1977	1196.9	1289.3	1262.0	1197.2
13.19	23.28	245.8	1102.5	Ozbek 1977	1208.4	1285.4	1252.5	1194.9
13.19	23.28	280.2	1103.8	Ozbek 1977	1211.6	1284.7	1250.4	1194.5
13.19	23.29	174.1	1100.0	Ozbek 1977	1202.6	1286.9	1256.8	1195.7
13.19	23.29	209.9	1101.2	Ozbek 1977	1206.1	1285.9	1254.4	1195.1
13.19	23.3	69.3	1096.2	Ozbek 1977	1195.8	1289.9	1264.0	1197.4
13.19	23.31	34.8	1095.0	Ozbek 1977	1193.3	1290.9	1266.4	1197.9
13.19	23.31	103.7	1097.4	Ozbek 1977	1198.5	1288.4	1261.2	1196.4
13.19	23.32	69.3	1096.2	Ozbek 1977	1195.4	1289.3	1263.5	1196.9
13.19	23.34	34.8	1094.9	Ozbek 1977	1191.4	1290.0	1265.6	1197.1
13.19	23.35	1	1093.8	Ozbek 1977	1191.5	1291.0	1268.0	1197.6
19.45	23.35	104.1	1145.5	Ozbek 1977	1442.3	1460.4	1434.9	1433.8
19.45	23.35	104.1	1145.5	Ozbek 1977	1444.2	1460.4	1434.9	1433.8
13.19	23.36	1	1093.8	Ozbek 1977	1190.7	1290.7	1267.8	1197.3
19.45	23.41	138.9	1146.7	Ozbek 1977	1442.7	1457.2	1429.3	1431.1
19.45	23.42	138.9	1146.7	Ozbek 1977	1443.8	1456.9	1429.0	1430.8
19.45	23.48	173.4	1147.8	Ozbek 1977	1443.3	1453.8	1423.6	1428.2
19.45	23.48	173.4	1147.8	Ozbek 1977	1444.2	1453.8	1423.6	1428.2
2.7	23.5	1	1016.7	Ozbek 1977	958.0	996.4	1000.9	960.4
2.7	23.5	34.6	1018.1	Ozbek 1977	957.0	995.4	999.9	959.8
2.7	23.5	70.3	1019.7	Ozbek 1977	959.0	994.4	998.9	959.2
2.7	23.5	103.4	1021.1	Ozbek 1977	959.0	993.6	998.0	958.6
2.7	23.5	139.8	1022.6	Ozbek 1977	957.0	992.7	997.1	958.1
2.7	23.5	240.3	1026.8	Ozbek 1977	956.0	990.7	994.9	956.9
2.7	23.5	307.5	1029.6	Ozbek 1977	956.0	989.7	993.7	956.3
2.7	23.5	1	1016.7	Ozbek 1977	960.0	996.4	1000.9	960.4
19.45	23.53	207.1	1148.9	Ozbek 1977	1445.1	1451.1	1418.7	1426.0
19.45	23.53	207.1	1148.9	Ozbek 1977	1445.5	1451.1	1418.7	1426.0
19.45	23.59	138.8	1146.6	Ozbek 1977	1438.5	1451.2	1423.9	1425.4
19.45	23.59	242.3	1150.0	Ozbek 1977	1445.9	1448.3	1413.5	1423.6
19.45	23.59	242.3	1150.0	Ozbek 1977	1446.5	1448.3	1413.5	1423.6
19.45	23.62	1	1142.2	Ozbek 1977	1426.6	1455.6	1438.7	1427.8
19.45	23.63	275.4	1151.1	Ozbek 1977	1447.1	1446.2	1409.3	1421.9
19.45	23.63	275.4	1151.1	Ozbek 1977	1445.6	1446.2	1409.3	1421.9

19.45	23.67	309.8	1152.2	Ozbek 1977	1449.5	1444.2	1405.1	1420.3
19.45	23.68	389.8	1154.9	Ozbek 1977	1447.8	1442.7	1398.3	1419.3
1.72	23.8	1	1009.6	Ozbek 1977	943.0	962.6	968.9	938.9
1.72	23.8	1	1009.6	Ozbek 1977	942.0	962.6	968.9	938.9
12.74	24	1	1090.1	Ozbek 1977	1196.0	1259.4	1238.0	1166.9
0	25	1	997.0	Ozbek 1977	890.6	890.5	890.0	890.0
0.01	25	1	997.1	Ozbek 1977	890.8	890.8	890.8	890.2
0.01	25	1	997.1	Ozbek 1977	890.8	890.8	890.8	890.2
0.02	25	1	997.2	Ozbek 1977	891.1	891.0	891.4	890.3
0.02	25	1	997.2	Ozbek 1977	891.1	891.0	891.4	890.3
0.45	25	1	1000.2	Ozbek 1977	891.3	902.5	907.5	896.0
0.05	25	1	997.4	Ozbek 1977	891.7	891.8	893.0	890.7
0.05	25	1	997.4	Ozbek 1977	891.7	891.8	893.0	890.7
0.07	25	1	997.5	Ozbek 1977	891.9	892.4	893.9	890.9
0.09	25	1	997.7	Ozbek 1977	892.1	892.9	894.8	891.2
0.11	25	1	997.8	Ozbek 1977	892.7	893.4	895.6	891.5
0.11	25	1	997.8	Ozbek 1977	892.6	893.4	895.6	891.5
0.11	25	1	997.8	Ozbek 1977	892.5	893.4	895.6	891.5
0.29	25	1	999.1	Ozbek 1977	895.2	898.2	902.3	893.8
0.35	25	1	999.5	Ozbek 1977	896.3	899.8	904.3	894.6
0.51	25	1	1000.7	Ozbek 1977	898.4	904.1	909.4	896.8
0.54	25	1	1000.9	Ozbek 1977	898.7	904.9	910.3	897.2
0.58	25	1	1001.2	Ozbek 1977	899.0	906.0	911.5	897.7
0.58	25	1	1001.2	Ozbek 1977	899.3	906.0	911.5	897.7
0.58	25	1	1001.2	Ozbek 1977	899.3	906.0	911.5	897.7
0.64	25	1	1001.6	Ozbek 1977	900.0	907.6	913.3	898.5
1.02	25	1	1004.3	Ozbek 1977	905.3	917.7	924.2	903.7
1.15	25	1	1005.2	Ozbek 1977	907.1	921.2	927.7	905.5
1.16	25	1	1005.3	Ozbek 1977	907.3	921.5	928.0	905.7
1.36	25	1	1006.7	Ozbek 1977	909.8	926.8	933.4	908.5
2	25	1	1011.2	Ozbek 1977	918.9	943.9	949.9	917.7
2.3	25	1	1013.4	Ozbek 1977	923.3	951.9	957.4	922.1
2.82	25	1	1017.1	Ozbek 1977	928.8	965.8	970.2	930.0
2.83	25	1	1017.1	Ozbek 1977	931.4	966.1	970.4	930.2
2.83	25	1	1017.1	Ozbek 1977	931.4	966.1	970.4	930.2
2.87	25	1	1017.4	Ozbek 1977	931.4	967.2	971.4	930.8
2.95	25	1	1018.0	Ozbek 1977	932.9	969.3	973.3	932.0
3.21	25	1	1019.8	Ozbek 1977	936.3	976.3	979.6	936.1
3.84	25	1	1024.3	Ozbek 1977	946.3	993.1	994.7	946.2
3.96	25	1	1025.2	Ozbek 1977	947.7	996.3	997.6	948.2
4.75	25	1	1030.8	Ozbek 1977	960.7	1017.4	1016.3	961.6
4.83	25	1	1031.4	Ozbek 1977	962.4	1019.5	1018.2	963.0
5.45	25	1	1035.9	Ozbek 1977	970.9	1036.1	1032.9	974.0

5.52	25	1	1036.4	Ozbek 1977	975.9	1038.0	1034.6	975.3
5.52	25	1	1036.4	Ozbek 1977	975.7	1038.0	1034.6	975.3
5.64	25	1	1037.2	Ozbek 1977	977.7	1041.2	1037.4	977.5
6	25	1	1039.8	Ozbek 1977	981.0	1050.8	1045.9	984.1
6.56	25	1	1043.9	Ozbek 1977	992.5	1065.7	1059.2	994.8
7.63	25	1	1051.7	Ozbek 1977	1013.1	1094.3	1084.6	1016.3
7.91	25	35	1055.1	Ozbek 1977	1019.0	1100.9	1089.8	1021.6
7.91	25	104.4	1057.8	Ozbek 1977	1021.0	1099.1	1086.9	1020.7
7.91	25	138.9	1059.2	Ozbek 1977	1019.0	1098.4	1085.5	1020.3
7.91	25	173.4	1060.5	Ozbek 1977	1022.0	1097.7	1084.2	1019.9
7.91	25	207.9	1061.9	Ozbek 1977	1021.0	1097.1	1083.0	1019.6
7.91	25	241.6	1063.2	Ozbek 1977	1023.0	1096.6	1081.9	1019.4
7.91	25	276.8	1064.5	Ozbek 1977	1023.0	1096.1	1080.8	1019.2
7.91	25	311.6	1065.8	Ozbek 1977	1026.0	1095.8	1079.8	1019.0
7.91	25	156.8	1059.9	Ozbek 1977	1021.0	1098.0	1084.8	1020.1
7.91	25	1	1053.7	Ozbek 1977	1020.0	1101.8	1091.3	1022.1
7.93	25	1	1053.9	Ozbek 1977	1018.5	1102.3	1091.8	1022.5
10.43	25	1	1072.4	Ozbek 1977	1073.3	1169.1	1152.7	1079.7
10.66	25	1	1074.1	Ozbek 1977	1088.0	1175.3	1158.4	1085.5
10.88	25	1	1075.7	Ozbek 1977	1085.3	1181.2	1163.9	1091.0
10.93	25	1	1076.1	Ozbek 1977	1085.0	1182.5	1165.1	1092.3
12.81	25	1	1090.2	Ozbek 1977	1134.2	1232.7	1212.8	1143.3
12.97	25	1	1091.4	Ozbek 1977	1132.0	1237.0	1217.0	1148.0
12.97	25	36.5	1092.6	Ozbek 1977	1136.0	1235.9	1214.5	1147.4
12.97	25	71.3	1093.9	Ozbek 1977	1138.0	1234.9	1212.2	1146.8
12.97	25	107.2	1095.2	Ozbek 1977	1137.0	1233.9	1209.9	1146.3
12.97	25	141.7	1096.4	Ozbek 1977	1142.0	1233.1	1207.8	1145.9
12.97	25	208.5	1098.8	Ozbek 1977	1147.0	1231.7	1203.9	1145.2
12.97	25	242.3	1100.0	Ozbek 1977	1149.0	1231.1	1202.1	1144.9
12.97	25	276.8	1101.3	Ozbek 1977	1151.0	1230.6	1200.4	1144.7
12.97	25	310.6	1102.5	Ozbek 1977	1147.0	1230.2	1198.7	1144.5
13.62	25	1	1096.4	Ozbek 1977	1160.0	1254.4	1233.9	1167.3
14.61	25	1	1103.9	Ozbek 1977	1188.6	1280.8	1260.1	1198.4
15.31	25	1	1109.3	Ozbek 1977	1210.0	1299.5	1278.9	1221.7
15.75	25	1	1112.7	Ozbek 1977	1228.0	1311.3	1290.9	1236.9
15.75	25	1	1112.7	Ozbek 1977	1230.0	1311.3	1290.9	1236.9
16.03	25	36.2	1115.9	Ozbek 1977	1241.0	1317.6	1295.5	1246.2
16.03	25	70.1	1117.0	Ozbek 1977	1243.0	1316.5	1292.7	1245.6
16.03	25	105.1	1118.2	Ozbek 1977	1242.0	1315.5	1289.9	1245.0
16.03	25	206.6	1121.7	Ozbek 1977	1247.0	1313.1	1282.3	1243.8
16.03	25	244.4	1123.1	Ozbek 1977	1248.0	1312.5	1279.7	1243.4
16.03	25	277.2	1124.2	Ozbek 1977	1252.0	1311.9	1277.6	1243.2
16.03	25	312	1125.4	Ozbek 1977	1256.0	1311.5	1275.4	1243.0

16.03	25	1	1114.8	Ozbek 1977	1241.0	1318.7	1298.6	1246.8
16.92	25	1	1121.7	Ozbek 1977	1268.3	1342.5	1323.3	1279.6
17.12	25	1	1123.3	Ozbek 1977	1275.1	1347.9	1329.0	1287.2
18.89	25	1	1137.1	Ozbek 1977	1345.5	1395.1	1379.9	1359.6
20.08	25	1	1146.5	Ozbek 1977	1400.0	1426.9	1415.4	1413.5
20.32	25	1	1148.4	Ozbek 1977	1413.0	1433.3	1422.7	1424.9
20.45	25	1	1149.4	Ozbek 1977	1407.0	1436.8	1426.6	1431.2
23.45	25	1	1173.5	Ozbek 1977	1573.7	1517.0	1521.7	1593.3
23.92	25	1	1177.3	Ozbek 1977	1610.0	1529.5	1537.2	1622.1
24.3	25	1	1180.4	Ozbek 1977	1632.6	1539.7	1550.0	1646.0
24.65	25	1	1183.3	Ozbek 1977	1654.0	1549.0	1561.8	1668.7
24.67	25	1	1183.4	Ozbek 1977	1657.0	1549.6	1562.5	1670.0
25.32	25	1	1188.8	Ozbek 1977	1700.0	1566.9	1584.8	1713.8
25.38	25	1	1189.3	Ozbek 1977	1699.4	1568.5	1586.8	1718.0
26.43	25	1	1197.9	Ozbek 1977	1770.0	1596.6	1623.7	**
20.56	25.5	1	1150.1	Ozbek 1977	1412.0	1423.5	1414.9	1420.7
20.56	25.5	35.5	1151.0	Ozbek 1977	1413.0	1422.3	1411.0	1420.1
20.56	25.5	70.3	1152.1	Ozbek 1977	1415.0	1421.2	1407.1	1419.4
20.56	25.5	141.2	1154.4	Ozbek 1977	1422.0	1419.3	1399.7	1418.4
20.56	25.5	175.5	1155.6	Ozbek 1977	1423.0	1418.5	1396.3	1418.0
20.56	25.5	208.2	1156.7	Ozbek 1977	1428.0	1417.9	1393.3	1417.6
20.56	25.5	277.5	1158.9	Ozbek 1977	1439.0	1416.7	1387.1	1417.1
20.56	25.5	311.5	1160.1	Ozbek 1977	1437.0	1416.3	1384.3	1416.9
20.56	25.5	156.2	1154.9	Ozbek 1977	1422.0	1419.0	1398.2	1418.2
20.56	25.5	1	1150.1	Ozbek 1977	1413.0	1423.5	1414.9	1420.7
20.56	25.5	1	1150.1	Ozbek 1977	1410.0	1423.5	1414.9	1420.7
24	27.5	9.3	1176.8	Ozbek 1977	1525.0	1448.1	1461.2	1539.7
24	27.5	34.8	1177.6	Ozbek 1977	1526.0	1447.4	1458.0	1539.3
24	27.5	69.5	1178.7	Ozbek 1977	1529.0	1446.6	1453.7	1539.0
24	27.5	106.5	1179.9	Ozbek 1977	1534.0	1445.8	1449.4	1538.6
24	27.5	141.1	1181.0	Ozbek 1977	1535.0	1445.2	1445.5	1538.4
24	27.5	176	1182.2	Ozbek 1977	1540.0	1444.6	1441.7	1538.2
24	27.5	246.1	1184.4	Ozbek 1977	1546.0	1443.8	1434.5	1538.0
24	27.5	278.2	1185.4	Ozbek 1977	1551.0	1443.6	1431.4	1538.0
24	27.5	310.9	1186.5	Ozbek 1977	1552.0	1443.4	1428.4	1538.0
24	27.5	158.2	1181.6	Ozbek 1977	1536.0	1444.9	1443.6	1538.3
24	27.5	1	1176.7	Ozbek 1977	1525.0	1448.3	1462.2	1539.8
24.7	27.86	1	1182.3	Ozbek 1977	1546.2	1454.4	1474.0	1569.8
24.7	27.86	33.4	1183.1	Ozbek 1977	1549.2	1453.6	1469.8	1569.4
24.7	27.86	33.4	1183.1	Ozbek 1977	1549.7	1453.6	1469.8	1569.4
24.7	27.87	1	1182.3	Ozbek 1977	1545.2	1454.1	1473.7	1569.4
24.7	27.91	70.3	1184.2	Ozbek 1977	1551.3	1451.2	1463.7	1567.4
24.7	27.92	70.3	1184.2	Ozbek 1977	1552.0	1450.9	1463.5	1567.0

19.45	27.93	33.6	1141.0	Ozbek 1977	1300.6	1320.1	1310.2	1298.9
19.45	27.93	33.6	1141.0	Ozbek 1977	1301.0	1320.1	1310.2	1298.9
19.45	27.94	1	1140.1	Ozbek 1977	1299.4	1320.5	1312.9	1298.9
19.45	27.97	1	1140.1	Ozbek 1977	1298.1	1319.7	1312.1	1298.1
2.72	28	35.8	1016.9	Ozbek 1977	871.0	900.3	905.1	868.8
2.72	28	71	1018.4	Ozbek 1977	870.0	899.8	904.6	868.7
2.72	28	105.5	1019.8	Ozbek 1977	868.0	899.4	904.1	868.5
2.72	28	140.6	1021.3	Ozbek 1977	868.0	899.0	903.7	868.4
2.72	28	175.1	1022.8	Ozbek 1977	868.0	898.8	903.4	868.3
2.72	28	209.9	1024.2	Ozbek 1977	869.0	898.5	903.0	868.3
2.72	28	244.1	1025.6	Ozbek 1977	868.0	898.3	902.8	868.3
2.72	28	275.4	1026.9	Ozbek 1977	870.0	898.2	902.5	868.3
2.72	28	311.6	1028.4	Ozbek 1977	868.0	898.1	902.3	868.4
2.72	28	157.2	1022.0	Ozbek 1977	869.0	898.9	903.5	868.4
2.72	28	1	1015.4	Ozbek 1977	868.0	900.8	905.6	869.0
19.45	28.05	104	1143.2	Ozbek 1977	1302.0	1315.4	1301.0	1295.1
19.45	28.05	104	1143.2	Ozbek 1977	1302.3	1315.4	1301.0	1295.1
24.7	28.05	104.9	1185.3	Ozbek 1977	1549.7	1446.2	1455.6	1562.4
24.7	28.07	104.9	1185.3	Ozbek 1977	1549.7	1445.6	1455.0	1561.7
24.7	28.16	173.4	1187.5	Ozbek 1977	1555.1	1441.8	1444.7	1558.5
24.7	28.21	173.4	1187.4	Ozbek 1977	1552.1	1440.2	1443.3	1556.8
24.7	28.22	173.4	1187.4	Ozbek 1977	1551.4	1439.9	1443.0	1556.5
24.7	28.26	204.4	1188.4	Ozbek 1977	1553.5	1438.4	1438.6	1555.2
24.7	28.27	204.4	1188.4	Ozbek 1977	1554.0	1438.1	1438.4	1554.8
24.7	28.3	238.5	1189.5	Ozbek 1977	1555.6	1436.9	1434.1	1553.9
24.7	28.31	238.5	1189.5	Ozbek 1977	1557.5	1436.6	1433.8	1553.5
24.7	28.33	273.4	1190.6	Ozbek 1977	1559.2	1435.8	1429.8	1553.0
24.7	28.34	273.4	1190.6	Ozbek 1977	1559.0	1435.5	1429.6	1552.7
24.7	28.35	308.5	1191.6	Ozbek 1977	1563.2	1435.1	1426.0	1552.5
24.7	28.36	308.5	1191.6	Ozbek 1977	1561.2	1434.8	1425.8	1552.2
13.19	28.44	1	1091.6	Ozbek 1977	1071.5	1151.3	1136.0	1072.2
19.45	28.45	175.7	1145.4	Ozbek 1977	1295.5	1303.2	1285.1	1284.1
19.45	28.48	175.7	1145.4	Ozbek 1977	1294.3	1302.4	1284.3	1283.3
13.19	28.52	1	1091.5	Ozbek 1977	1067.4	1149.3	1134.1	1070.5
13.19	28.53	1	1091.5	Ozbek 1977	1068.7	1149.1	1133.8	1070.2
13.19	28.54	172.7	1097.6	Ozbek 1977	1074.3	1146.5	1125.3	1069.4
13.19	28.55	35.5	1092.6	Ozbek 1977	1067.5	1148.0	1131.6	1069.6
13.19	28.55	35.5	1092.6	Ozbek 1977	1067.6	1148.0	1131.6	1069.6
24.7	28.56	1	1181.9	Ozbek 1977	1521.0	1432.4	1453.4	1546.3
13.19	28.57	69.9	1093.9	Ozbek 1977	1068.9	1146.9	1129.3	1069.0
13.19	28.57	69.9	1093.9	Ozbek 1977	1069.0	1146.9	1129.3	1069.0
13.19	28.59	104.4	1095.1	Ozbek 1977	1070.2	1146.0	1127.2	1068.4
19.45	28.59	240.9	1147.5	Ozbek 1977	1294.8	1298.9	1277.0	1280.5

13.19	28.6	104.4	1095.1	Ozbek 1977	1070.0	1145.7	1127.0	1068.2
13.19	28.61	139.2	1096.3	Ozbek 1977	1071.1	1145.1	1125.1	1067.9
13.19	28.62	139.2	1096.3	Ozbek 1977	1068.4	1144.9	1124.9	1067.7
13.19	28.64	174.1	1097.6	Ozbek 1977	1072.6	1144.1	1122.9	1067.2
13.19	28.65	174.1	1097.6	Ozbek 1977	1072.5	1143.8	1122.7	1067.0
13.19	28.66	207.8	1098.8	Ozbek 1977	1074.2	1143.3	1121.1	1066.8
13.19	28.66	241.6	1100.0	Ozbek 1977	1076.1	1143.2	1119.7	1066.8
13.19	28.67	207.8	1098.8	Ozbek 1977	1076.0	1143.1	1120.8	1066.5
13.19	28.67	276.1	1101.2	Ozbek 1977	1078.4	1142.8	1118.2	1066.7
13.19	28.67	310.6	1102.4	Ozbek 1977	1078.5	1142.8	1117.0	1066.8
13.19	28.68	241.6	1100.0	Ozbek 1977	1077.6	1142.7	1119.3	1066.4
19.45	28.68	240.9	1147.4	Ozbek 1977	1295.2	1296.4	1274.7	1278.1
13.19	28.69	276.1	1101.2	Ozbek 1977	1077.7	1142.3	1117.8	1066.2
13.19	28.7	310.6	1102.4	Ozbek 1977	1082.8	1142.0	1116.3	1066.2
19.45	28.72	1	1139.7	Ozbek 1977	1276.9	1298.3	1292.0	1277.6
19.45	28.75	107.2	1142.9	Ozbek 1977	1282.1	1295.7	1282.5	1276.3
19.45	28.75	273	1148.5	Ozbek 1977	1294.9	1294.4	1270.9	1276.4
19.45	28.77	205.4	1146.2	Ozbek 1977	1290.6	1294.2	1274.8	1275.7
19.45	28.77	273	1148.5	Ozbek 1977	1294.6	1293.9	1270.4	1275.9
19.45	28.82	307.1	1149.6	Ozbek 1977	1296.9	1292.5	1267.1	1274.7
19.45	28.83	367.1	1151.5	Ozbek 1977	1295.6	1292.3	1263.4	1274.9
0.04	30	1	995.9	Ozbek 1977	798.5	798.7	799.5	797.7
0.07	30	1	996.1	Ozbek 1977	798.9	799.4	800.7	798.1
0.09	30	1	996.3	Ozbek 1977	799.2	799.9	801.6	798.3
0.11	30	1	996.4	Ozbek 1977	799.6	800.3	802.3	798.6
0.35	30	1	998.1	Ozbek 1977	802.5	806.1	810.2	801.5
0.57	30	1	999.6	Ozbek 1977	805.0	811.3	816.4	804.2
0.64	30	1	1000.1	Ozbek 1977	806.6	813.0	818.3	805.1
1.36	30	1	1005.1	Ozbek 1977	816.1	830.2	836.5	814.3
2.82	30	1	1015.4	Ozbek 1977	834.8	865.2	869.9	834.2
3.18	30	1	1017.9	Ozbek 1977	841.1	873.8	877.8	839.4
4.75	30	1	1029.0	Ozbek 1977	864.0	911.4	911.9	863.2
5.45	30	1	1034.0	Ozbek 1977	874.3	928.1	926.9	874.6
5.52	30	1	1034.5	Ozbek 1977	882.3	929.8	928.4	875.7
7.91	30	1	1051.7	Ozbek 1977	918.0	987.0	980.1	918.5
7.91	30	34.8	1053.0	Ozbek 1977	919.0	986.6	979.2	918.4
7.91	30	70.1	1054.4	Ozbek 1977	919.0	986.3	978.3	918.4
7.91	30	104.4	1055.8	Ozbek 1977	920.8	986.0	977.5	918.4
7.91	30	138.9	1057.2	Ozbek 1977	919.0	985.8	976.8	918.4
7.91	30	173.4	1058.5	Ozbek 1977	923.0	985.6	976.1	918.5
7.91	30	238.9	1061.0	Ozbek 1977	926.0	985.5	974.9	918.7
7.91	30	273	1062.3	Ozbek 1977	924.0	985.5	974.3	918.9
7.91	30	307.1	1063.6	Ozbek 1977	925.0	985.6	973.8	919.0

7.91	30	156.8	1057.9	Ozbek 1977	921.0	985.7	976.4	918.4
7.91	30	1	1051.7	Ozbek 1977	920.0	987.0	980.1	918.5
7.93	30	1	1051.9	Ozbek 1977	917.6	987.5	980.5	918.8
8.05	30	1	1052.8	Ozbek 1977	918.7	990.3	983.2	921.2
10.43	30	1	1070.2	Ozbek 1977	968.8	1047.3	1036.0	970.7
10.46	30	1	1070.4	Ozbek 1977	966.6	1048.0	1036.7	971.4
12.74	30	1	1087.5	Ozbek 1977	1024.0	1102.6	1089.2	1026.3
12.81	30	1	1088.0	Ozbek 1977	1022.7	1104.3	1090.9	1028.1
14.61	30	1	1101.6	Ozbek 1977	1072.5	1147.3	1134.0	1077.7
14.91	30	1	1103.9	Ozbek 1977	1081.0	1154.5	1141.4	1086.5
15.31	30	1	1107.0	Ozbek 1977	1091.7	1164.1	1151.3	1098.6
16.92	30	1	1119.3	Ozbek 1977	1142.9	1202.6	1191.9	1150.4
16.98	30	1	1119.8	Ozbek 1977	1144.0	1204.0	1193.4	1152.4
18.89	30	1	1134.7	Ozbek 1977	1212.1	1249.8	1243.7	1221.9
18.94	30	1	1135.1	Ozbek 1977	1214.0	1250.9	1245.0	1223.8
20.82	30	1	1149.9	Ozbek 1977	1287.0	1295.9	1296.9	1301.9
22.61	30	1	1164.2	Ozbek 1977	1363.0	1338.8	1348.6	1386.4
23.45	30	1	1171.0	Ozbek 1977	1412.6	1358.9	1373.7	1429.9
24.3	30	1	1177.9	Ozbek 1977	1463.3	1379.2	1399.7	1476.7
25.32	30	1	1186.3	Ozbek 1977	1522.7	1403.6	1431.7	1536.9
25.38	30	1	1186.8	Ozbek 1977	1521.7	1405.1	1433.7	1540.5
26.52	30	1	1196.3	Ozbek 1977	1610.0	1432.3	1470.6	**
12.97	30.5	1	1089.0	Ozbek 1977	1016.0	1096.4	1083.5	1021.8
12.97	30.5	36.9	1090.1	Ozbek 1977	1017.0	1096.0	1081.9	1021.8
12.97	30.5	72	1091.4	Ozbek 1977	1019.0	1095.7	1080.5	1021.8
12.97	30.5	106.5	1092.6	Ozbek 1977	1022.0	1095.4	1079.1	1021.8
12.97	30.5	141	1093.9	Ozbek 1977	1023.0	1095.3	1077.8	1021.9
12.97	30.5	208.5	1096.3	Ozbek 1977	1026.0	1095.1	1075.4	1022.2
12.97	30.5	276.1	1098.7	Ozbek 1977	1029.0	1095.1	1073.3	1022.6
12.97	30.5	311.3	1100.0	Ozbek 1977	1030.0	1095.2	1072.3	1022.8
12.97	30.5	158.2	1094.5	Ozbek 1977	1024.0	1095.2	1077.2	1022.0
12.97	30.5	1	1089.0	Ozbek 1977	1019.0	1096.4	1083.5	1021.8
16.03	31	1	1112.0	Ozbek 1977	1096.0	1156.6	1145.8	1098.4
16.03	31	35.7	1113.0	Ozbek 1977	1096.0	1156.3	1143.9	1098.4
16.03	31	70.1	1114.2	Ozbek 1977	1097.0	1156.0	1142.1	1098.5
16.03	31	174.8	1117.8	Ozbek 1977	1101.0	1155.5	1137.0	1098.9
16.03	31	208.2	1118.9	Ozbek 1977	1107.0	1155.5	1135.5	1099.1
16.03	31	275.9	1121.3	Ozbek 1977	1111.0	1155.6	1132.8	1099.6
16.03	31	311.3	1122.5	Ozbek 1977	1113.0	1155.8	1131.4	1099.9
16.03	31	156.2	1117.1	Ozbek 1977	1102.0	1155.6	1137.8	1098.8
16.03	31	1	1112.0	Ozbek 1977	1095.0	1156.6	1145.8	1098.4
24.7	34.15	1	1179.1	Ozbek 1977	1359.1	1274.4	1303.2	1377.7
24.7	34.38	173.4	1184.2	Ozbek 1977	1366.5	1269.1	1283.7	1373.7

24.7	34.42	36.5	1179.8	Ozbek 1977	1353.2	1267.5	1293.5	1370.7
24.7	34.43	36.5	1179.8	Ozbek 1977	1356.0	1267.2	1293.3	1370.5
24.7	34.45	70.7	1180.8	Ozbek 1977	1356.4	1266.8	1289.9	1370.4
24.7	34.45	70.7	1180.8	Ozbek 1977	1357.5	1266.8	1289.9	1370.4
24.7	34.45	138.2	1183.0	Ozbek 1977	1362.2	1267.1	1284.6	1371.3
24.7	34.45	138.2	1183.0	Ozbek 1977	1362.4	1267.1	1284.6	1371.3
24.7	34.46	1	1178.9	Ozbek 1977	1349.6	1266.5	1295.6	1369.3
24.7	34.46	105.1	1181.9	Ozbek 1977	1359.5	1266.7	1286.9	1370.6
24.7	34.47	1	1178.9	Ozbek 1977	1350.4	1266.2	1295.3	1369.0
24.7	34.47	174.1	1184.2	Ozbek 1977	1363.4	1266.9	1281.5	1371.3
24.7	34.48	105.1	1181.9	Ozbek 1977	1359.1	1266.2	1286.5	1370.0
24.7	34.48	174.1	1184.1	Ozbek 1977	1365.4	1266.6	1281.3	1371.1
24.7	34.49	207.2	1185.2	Ozbek 1977	1369.5	1266.7	1278.7	1371.4
24.7	34.5	207.2	1185.2	Ozbek 1977	1367.8	1266.4	1278.5	1371.1
24.7	34.5	241.6	1186.3	Ozbek 1977	1371.9	1266.8	1276.1	1371.8
24.7	34.5	275.4	1187.3	Ozbek 1977	1374.2	1267.3	1274.0	1372.4
24.7	34.51	241.6	1186.3	Ozbek 1977	1368.9	1266.6	1275.9	1371.5
24.7	34.51	275.4	1187.3	Ozbek 1977	1373.2	1267.0	1273.7	1372.1
24.7	34.51	311.3	1188.5	Ozbek 1977	1378.4	1267.5	1271.5	1372.9
24.7	34.53	311.3	1188.5	Ozbek 1977	1379.0	1267.0	1271.1	1372.4
0	35	1	994.0	Ozbek 1977	719.6	719.6	719.1	719.1
0.01	35	1	994.1	Ozbek 1977	719.7	719.8	719.8	719.2
0.02	35	1	994.2	Ozbek 1977	720.1	720.0	720.3	719.4
0.05	35	1	994.4	Ozbek 1977	720.6	720.7	721.6	719.7
0.05	35	1	994.4	Ozbek 1977	720.5	720.7	721.6	719.7
0.11	35	1	994.8	Ozbek 1977	721.6	722.0	723.7	720.4
0.11	35	1	994.8	Ozbek 1977	721.4	722.0	723.7	720.4
0.17	35	1	995.2	Ozbek 1977	722.4	723.3	725.7	721.1
0.23	35	1	995.6	Ozbek 1977	723.2	724.6	727.5	721.7
0.29	35	1	996.0	Ozbek 1977	724.1	725.9	729.2	722.4
3.38	35	1	1017.4	Ozbek 1977	724.9	792.6	796.6	761.0
0.4	35	1	996.8	Ozbek 1977	725.7	728.3	732.2	723.7
1.16	35	1	1002.0	Ozbek 1977	734.7	744.7	750.5	732.6
2.31	35	1	1010.0	Ozbek 1977	749.1	769.5	775.0	746.9
2.88	35	1	1013.9	Ozbek 1977	756.4	781.8	786.6	754.3
5.52	35	1	1032.5	Ozbek 1977	785.6	838.8	838.7	791.9
8.05	35	1	1050.6	Ozbek 1977	823.7	893.4	888.7	833.5
10.46	35	1	1068.2	Ozbek 1977	868.3	945.4	937.7	879.4
12.74	35	1	1085.1	Ozbek 1977	918.7	994.7	985.8	929.3
14.91	35	1	1101.5	Ozbek 1977	974.1	1041.5	1033.6	983.8
16.98	35	1	1117.3	Ozbek 1977	1022.0	1086.2	1081.3	1043.3
18.94	35	1	1132.6	Ozbek 1977	1083.0	1128.5	1128.7	1107.6
20.56	35	35.3	1146.2	Ozbek 1977	1171.0	1163.5	1167.6	1167.8

20.56	35	71	1147.3	Ozbek 1977	1170.0	1163.6	1165.5	1168.2
20.56	35	105.1	1148.4	Ozbek 1977	1176.0	1163.8	1163.7	1168.6
20.56	35	140.3	1149.6	Ozbek 1977	1179.0	1164.0	1161.8	1169.1
20.56	35	174.8	1150.7	Ozbek 1977	1180.0	1164.3	1160.1	1169.6
20.56	35	207.9	1151.8	Ozbek 1977	1183.0	1164.7	1158.5	1170.2
20.56	35	243	1152.9	Ozbek 1977	1185.0	1165.1	1156.9	1170.8
20.56	35	278.2	1154.1	Ozbek 1977	1191.0	1165.5	1155.4	1171.4
20.56	35	310.9	1155.2	Ozbek 1977	1193.0	1166.0	1154.0	1172.0
20.56	35	156.2	1150.1	Ozbek 1977	1179.0	1164.2	1161.0	1169.4
20.56	35	1	1145.3	Ozbek 1977	1166.0	1163.5	1169.7	1167.4
20.82	35	1	1147.4	Ozbek 1977	1153.0	1169.1	1176.4	1177.6
22.61	35	1	1161.7	Ozbek 1977	1234.0	1207.7	1223.9	1253.3
20.56	35.5	35.3	1145.9	Ozbek 1977	1153.0	1152.1	1156.6	1156.6
20.56	35.5	70	1147.0	Ozbek 1977	1156.0	1152.2	1154.7	1157.0
20.56	35.5	202.9	1151.4	Ozbek 1977	1164.0	1153.3	1148.1	1159.1
20.56	35.5	244.1	1152.7	Ozbek 1977	1168.0	1153.9	1146.3	1159.8
20.56	35.5	277.3	1153.8	Ozbek 1977	1169.0	1154.3	1144.9	1160.4
20.56	35.5	307.1	1154.8	Ozbek 1977	1173.0	1154.8	1143.7	1161.0
20.56	35.5	1	1145.0	Ozbek 1977	1151.0	1152.0	1158.6	1156.2
20.56	35.5	1	1145.0	Ozbek 1977	1152.0	1152.0	1158.6	1156.2
19.45	35.51	1	1136.3	Ozbek 1977	1115.0	1128.0	1130.4	1114.7
19.45	35.51	1	1136.3	Ozbek 1977	1115.6	1128.0	1130.4	1114.7
19.45	35.53	1	1136.3	Ozbek 1977	1115.6	1127.6	1130.0	1114.2
19.45	35.56	1	1136.3	Ozbek 1977	1112.6	1126.9	1129.3	1113.6
19.45	35.56	34.7	1137.1	Ozbek 1977	1115.8	1127.0	1127.6	1114.0
19.45	35.56	34.7	1137.1	Ozbek 1977	1117.7	1127.0	1127.6	1114.0
19.45	35.58	1	1136.3	Ozbek 1977	1112.7	1126.4	1128.9	1113.2
19.45	35.59	107.9	1139.5	Ozbek 1977	1121.7	1126.7	1123.4	1114.3
19.45	35.6	70	1138.2	Ozbek 1977	1117.1	1126.3	1125.0	1113.6
19.45	35.6	70	1138.2	Ozbek 1977	1117.8	1126.3	1125.0	1113.6
19.45	35.6	70	1138.2	Ozbek 1977	1118.3	1126.3	1125.0	1113.6
19.45	35.64	138.3	1140.5	Ozbek 1977	1128.1	1125.9	1121.0	1113.7
19.45	35.65	138.3	1140.5	Ozbek 1977	1120.5	1125.7	1120.8	1113.5
19.45	35.65	206.6	1142.7	Ozbek 1977	1125.6	1126.4	1117.9	1114.6
19.45	35.66	172.3	1141.6	Ozbek 1977	1122.5	1125.8	1119.1	1113.8
19.45	35.66	172.3	1141.6	Ozbek 1977	1122.7	1125.8	1119.1	1113.8
19.45	35.68	240.3	1143.8	Ozbek 1977	1126.6	1126.1	1115.9	1114.6
19.45	35.69	205	1142.7	Ozbek 1977	1126.0	1125.5	1117.1	1113.7
19.45	35.69	205	1142.7	Ozbek 1977	1126.1	1125.5	1117.1	1113.7
19.45	35.69	240.3	1143.8	Ozbek 1977	1126.4	1125.9	1115.7	1114.4
19.45	35.7	274.2	1145.0	Ozbek 1977	1127.5	1126.2	1114.3	1114.8
19.45	35.7	274.2	1145.0	Ozbek 1977	1128.0	1126.2	1114.3	1114.8
19.45	35.7	306.5	1146.0	Ozbek 1977	1131.1	1126.7	1113.2	1115.4

13.19	35.89	1	1088.0	Ozbek 1977	926.2	986.8	978.6	924.2
13.19	35.96	1	1088.0	Ozbek 1977	926.0	985.4	977.3	922.9
13.19	36.06	35.3	1089.1	Ozbek 1977	922.5	983.6	974.5	921.6
13.19	36.08	35.3	1089.1	Ozbek 1977	922.8	983.2	974.2	921.2
13.19	36.11	1	1087.9	Ozbek 1977	921.1	982.5	974.5	920.3
13.19	36.16	70.4	1090.3	Ozbek 1977	923.8	981.9	971.8	920.2
13.19	36.19	70.4	1090.3	Ozbek 1977	921.7	981.3	971.3	919.7
13.19	36.24	104.4	1091.5	Ozbek 1977	922.8	980.6	969.6	919.3
13.19	36.24	174.1	1094.0	Ozbek 1977	925.6	981.2	968.2	920.2
13.19	36.25	104.4	1091.5	Ozbek 1977	922.6	980.4	969.4	919.1
13.19	36.26	139.2	1092.7	Ozbek 1977	923.0	980.5	968.5	919.4
13.19	36.27	139.2	1092.7	Ozbek 1977	925.3	980.3	968.3	919.2
13.19	36.3	174.1	1094.0	Ozbek 1977	923.4	980.1	967.1	919.2
13.19	36.3	174.1	1094.0	Ozbek 1977	924.7	980.1	967.1	919.2
13.19	36.32	206.5	1095.1	Ozbek 1977	924.7	980.0	966.2	919.3
13.19	36.32	206.5	1095.1	Ozbek 1977	925.0	980.0	966.2	919.3
13.19	36.35	239.7	1096.3	Ozbek 1977	926.9	979.9	965.1	919.3
13.19	36.35	239.7	1096.3	Ozbek 1977	927.1	979.9	965.1	919.3
13.19	36.35	305.1	1098.6	Ozbek 1977	928.4	980.8	964.2	920.4
13.19	36.36	305.1	1098.6	Ozbek 1977	928.1	980.6	964.0	920.3
13.19	36.36	274.7	1097.5	Ozbek 1977	928.6	980.2	964.4	919.7
13.19	36.38	274.7	1097.5	Ozbek 1977	928.4	979.8	964.0	919.4
0.1	40	1	992.9	Ozbek 1977	654.0	655.2	656.6	653.8
0.31	40	1	994.3	Ozbek 1977	656.8	659.3	662.5	656.0
0.57	40	1	996.1	Ozbek 1977	658.5	664.4	668.7	658.8
0.58	40	1	996.1	Ozbek 1977	660.1	664.6	669.0	659.0
0.99	40	1	998.9	Ozbek 1977	665.0	672.6	677.9	663.5
2.82	40	1	1011.4	Ozbek 1977	665.3	708.5	713.3	684.9
3.16	40	1	1013.8	Ozbek 1977	690.9	715.2	719.6	689.1
3.96	40	1	1019.3	Ozbek 1977	701.6	730.8	734.1	699.3
5.45	40	1	1029.8	Ozbek 1977	720.9	760.0	760.9	719.5
5.52	40	1	1030.3	Ozbek 1977	720.8	761.4	762.2	720.4
6	40	1	1033.7	Ozbek 1977	730.0	770.8	770.8	727.3
6.24	40	1	1035.4	Ozbek 1977	732.1	775.5	775.2	730.8
7.63	40	1	1045.3	Ozbek 1977	753.9	802.8	800.4	752.1
8.05	40	1	1048.3	Ozbek 1977	755.4	811.0	808.0	758.9
10.43	40	1	1065.6	Ozbek 1977	801.1	857.6	852.4	800.4
10.46	40	1	1065.8	Ozbek 1977	799.1	858.2	852.9	801.0
12.1	40	1	1077.9	Ozbek 1977	832.0	890.4	884.6	833.2
12.74	40	1	1082.6	Ozbek 1977	842.2	902.9	897.1	846.7
13.62	40	1	1089.2	Ozbek 1977	868.0	920.1	914.7	866.0
14.61	40	1	1096.7	Ozbek 1977	886.7	939.6	934.9	889.0
14.91	40	1	1099.0	Ozbek 1977	896.4	945.4	941.1	896.3

16.03	40	1	1107.5	Ozbek 1977	926.0	967.4	964.6	924.7
16.03	40	34.5	1108.5	Ozbek 1977	928.0	967.8	963.8	925.3
16.03	40	70	1109.7	Ozbek 1977	930.0	968.3	963.0	925.9
16.03	40	103.9	1110.8	Ozbek 1977	931.0	968.8	962.3	926.6
16.03	40	138.6	1112.0	Ozbek 1977	931.0	969.3	961.6	927.3
16.03	40	174.8	1113.3	Ozbek 1977	933.0	969.9	960.9	928.0
16.03	40	242.7	1115.7	Ozbek 1977	937.0	971.2	959.8	929.5
16.03	40	276.8	1116.8	Ozbek 1977	936.0	971.9	959.3	930.2
16.03	40	310.9	1118.0	Ozbek 1977	940.0	972.6	958.9	931.0
16.03	40	1	1107.5	Ozbek 1977	924.0	967.4	964.6	924.7
16.92	40	1	1114.3	Ozbek 1977	944.8	984.8	983.7	948.7
16.98	40	1	1114.8	Ozbek 1977	939.5	986.0	985.0	950.3
17.12	40	1	1115.9	Ozbek 1977	950.8	988.7	988.1	954.2
18.48	40	1	1126.4	Ozbek 1977	987.4	1015.4	1018.2	994.2
18.89	40	1	1129.6	Ozbek 1977	1000.0	1023.4	1027.5	1006.9
18.94	40	1	1130.0	Ozbek 1977	999.6	1024.4	1028.7	1008.5
20.08	40	1	1138.9	Ozbek 1977	1040.0	1046.7	1055.0	1045.9
20.82	40	1	1144.8	Ozbek 1977	1054.0	1061.2	1072.6	1071.8
22.61	40	1	1159.1	Ozbek 1977	1127.0	1096.3	1116.5	1140.1
23.92	40	1	1169.7	Ozbek 1977	1190.0	1122.0	1150.0	1195.7
24.16	40	1	1171.6	Ozbek 1977	1191.5	1126.7	1156.3	1206.4
24.3	40	1	1172.8	Ozbek 1977	1198.5	1129.4	1160.0	1212.8
25.32	40	1	1181.2	Ozbek 1977	1244.0	1149.4	1187.2	1261.1
26.43	40	1	1190.4	Ozbek 1977	1300.0	1171.2	1217.8	**
26.66	40	1	1192.3	Ozbek 1977	1350.0	1175.7	1224.3	**
2.72	40.5	35.7	1012.0	Ozbek 1977	679.0	700.3	705.1	677.8
2.72	40.5	70.8	1013.5	Ozbek 1977	679.0	700.7	705.5	678.3
2.72	40.5	105.1	1015.0	Ozbek 1977	680.0	701.0	705.8	678.8
2.72	40.5	140.6	1016.5	Ozbek 1977	679.0	701.5	706.1	679.4
2.72	40.5	173.4	1017.8	Ozbek 1977	681.0	701.9	706.5	679.9
2.72	40.5	207.2	1019.2	Ozbek 1977	681.0	702.4	706.8	680.4
2.72	40.5	242.3	1020.7	Ozbek 1977	686.0	702.9	707.2	681.0
2.72	40.5	276.1	1022.0	Ozbek 1977	680.0	703.4	707.6	681.6
2.72	40.5	311.3	1023.4	Ozbek 1977	683.0	704.0	708.1	682.2
2.72	40.5	157.9	1017.2	Ozbek 1977	682.0	701.7	706.3	679.6
2.72	40.5	1	1010.5	Ozbek 1977	679.0	700.0	704.9	677.3
7.91	40.5	1	1047.0	Ozbek 1977	751.0	800.7	798.1	749.8
7.91	40.5	34.8	1048.4	Ozbek 1977	753.0	801.1	798.0	750.3
7.91	40.5	70	1049.8	Ozbek 1977	753.0	801.5	798.0	750.9
7.91	40.5	104.4	1051.1	Ozbek 1977	753.0	801.9	798.0	751.4
7.91	40.5	138.6	1052.5	Ozbek 1977	755.0	802.4	798.0	752.0
7.91	40.5	173.4	1053.9	Ozbek 1977	755.0	802.9	798.1	752.6
7.91	40.5	207.2	1055.2	Ozbek 1977	757.0	803.5	798.1	753.2

7.91	40.5	241.6	1056.5	Ozbek 1977	757.0	804.0	798.3	753.8
7.91	40.5	276.5	1057.8	Ozbek 1977	758.0	804.7	798.4	754.5
7.91	40.5	310.6	1059.1	Ozbek 1977	760.0	805.3	798.6	755.2
7.91	40.5	157.2	1053.2	Ozbek 1977	754.0	802.7	798.0	752.3
7.91	40.5	1	1047.0	Ozbek 1977	750.0	800.7	798.1	749.8
7.91	40.5	1	1047.0	Ozbek 1977	748.0	800.7	798.1	749.8
24.7	40.57	176.8	1181.0	Ozbek 1977	1214.9	1128.4	1149.4	1223.1
24.7	40.68	1	1175.7	Ozbek 1977	1198.6	1122.9	1156.5	1216.0
24.7	40.68	104	1178.6	Ozbek 1977	1207.0	1124.7	1150.8	1218.7
24.7	40.68	308.5	1185.1	Ozbek 1977	1222.1	1129.4	1141.7	1224.7
24.7	40.68	308.5	1185.1	Ozbek 1977	1224.0	1129.4	1141.7	1224.7
24.7	40.69	104	1178.6	Ozbek 1977	1205.4	1124.5	1150.6	1218.4
24.7	40.7	36.3	1176.5	Ozbek 1977	1200.4	1123.1	1154.1	1216.4
24.7	40.7	138.2	1179.7	Ozbek 1977	1209.2	1124.9	1148.7	1219.2
24.7	40.7	241.6	1183.0	Ozbek 1977	1218.1	1127.3	1144.0	1222.2
24.7	40.7	241.6	1183.0	Ozbek 1977	1219.3	1127.3	1144.0	1222.2
24.7	40.71	1	1175.7	Ozbek 1977	1196.0	1122.3	1155.9	1215.3
24.7	40.71	70.1	1177.5	Ozbek 1977	1201.5	1123.4	1152.0	1217.1
24.7	40.71	36.3	1176.5	Ozbek 1977	1202.0	1122.8	1153.9	1216.2
24.7	40.71	70.1	1177.5	Ozbek 1977	1202.9	1123.4	1152.0	1217.1
24.7	40.71	138.2	1179.7	Ozbek 1977	1206.9	1124.7	1148.5	1218.9
24.7	40.71	206.5	1181.8	Ozbek 1977	1214.0	1126.2	1145.3	1220.9
24.7	40.71	276.8	1184.1	Ozbek 1977	1222.2	1127.9	1142.3	1223.1
24.7	40.71	276.8	1184.1	Ozbek 1977	1223.0	1127.9	1142.3	1223.1
24.7	40.72	173.4	1180.8	Ozbek 1977	1212.5	1125.3	1146.6	1219.7
24.7	40.72	206.5	1181.8	Ozbek 1977	1215.2	1126.0	1145.1	1220.7
24.7	40.73	173.4	1180.8	Ozbek 1977	1211.4	1125.1	1146.4	1219.5
12.97	41	36.2	1085.0	Ozbek 1977	835.0	891.1	885.0	837.1
12.97	41	71	1086.3	Ozbek 1977	836.0	891.6	884.6	837.7
12.97	41	105.8	1087.6	Ozbek 1977	839.0	892.1	884.2	838.4
12.97	41	142.7	1088.9	Ozbek 1977	840.0	892.7	883.9	839.1
12.97	41	172.7	1090.0	Ozbek 1977	843.0	893.2	883.6	839.7
12.97	41	240.6	1092.4	Ozbek 1977	845.0	894.5	883.2	841.1
12.97	41	267.1	1093.4	Ozbek 1977	844.0	895.1	883.0	841.7
12.97	41	308.3	1094.9	Ozbek 1977	847.0	895.9	882.9	842.6
12.97	41	157.5	1089.4	Ozbek 1977	840.0	893.0	883.7	839.4
12.97	41	1	1083.9	Ozbek 1977	834.0	890.6	885.4	836.5
0	42.5	1	991.2	Ozbek 1977	623.6	623.7	623.2	623.2
0.01	42.5	1	991.3	Ozbek 1977	623.8	623.9	623.8	623.3
0.02	42.5	1	991.4	Ozbek 1977	624.1	624.1	624.2	623.4
0.05	42.5	1	991.6	Ozbek 1977	624.5	624.6	625.3	623.7
0.11	42.5	1	992.0	Ozbek 1977	625.3	625.8	627.2	624.3
1.16	42.5	1	999.1	Ozbek 1977	637.8	645.4	650.6	635.4

0.61	42.5	1	995.3	Ozbek 1977	651.3	635.1	639.4	629.5
2.88	42.5	1	1010.8	Ozbek 1977	658.1	677.6	682.3	655.0
24	44.5	1	1168.0	Ozbek 1977	1092.0	1034.8	1065.2	1106.0
24	44.5	35	1168.7	Ozbek 1977	1094.0	1035.5	1063.8	1107.0
24	44.5	71.2	1169.8	Ozbek 1977	1099.0	1036.4	1062.4	1108.2
24	44.5	110.3	1171.0	Ozbek 1977	1099.0	1037.4	1060.9	1109.4
24	44.5	142.4	1172.1	Ozbek 1977	1105.0	1038.2	1059.8	1110.5
24	44.5	176.5	1173.2	Ozbek 1977	1107.0	1039.1	1058.7	1111.6
24	44.5	208.1	1174.2	Ozbek 1977	1111.0	1040.0	1057.7	1112.7
24	44.5	243.9	1175.3	Ozbek 1977	1112.0	1041.1	1056.7	1113.9
24	44.5	278.6	1176.4	Ozbek 1977	1112.0	1042.1	1055.7	1115.1
24	44.5	313	1177.5	Ozbek 1977	1115.0	1043.2	1054.8	1116.3
24	44.5	173.9	1173.1	Ozbek 1977	1106.0	1039.1	1058.8	1111.5
24	44.5	1	1168.0	Ozbek 1977	1096.0	1034.8	1065.2	1106.0
5.52	45	1	1027.9	Ozbek 1977	659.2	695.0	696.3	659.1
8.05	45	1	1045.9	Ozbek 1977	692.0	740.3	738.5	694.8
10.46	45	1	1063.3	Ozbek 1977	729.5	783.4	779.8	733.6
12.74	45	1	1080.1	Ozbek 1977	770.6	824.2	820.6	775.6
14.91	45	1	1096.4	Ozbek 1977	817.7	863.0	861.1	821.1
16.98	45	1	1112.2	Ozbek 1977	860.0	900.0	901.7	870.4
18.94	45	1	1127.3	Ozbek 1977	907.1	935.1	942.0	923.4
20.56	45	1	1140.1	Ozbek 1977	974.0	964.1	976.8	972.5
20.56	45	34.8	1140.9	Ozbek 1977	973.0	964.8	975.9	973.4
20.56	45	72	1142.1	Ozbek 1977	978.0	965.7	975.0	974.5
20.56	45	105.1	1143.1	Ozbek 1977	980.0	966.5	974.3	975.4
20.56	45	141.1	1144.3	Ozbek 1977	980.0	967.4	973.5	976.5
20.56	45	175.2	1145.4	Ozbek 1977	983.0	968.3	972.8	977.5
20.56	45	208.9	1146.6	Ozbek 1977	985.0	969.2	972.2	978.6
20.56	45	242	1147.7	Ozbek 1977	983.0	970.1	971.6	979.6
20.56	45	312.3	1150.0	Ozbek 1977	988.0	972.2	970.6	981.8
20.56	45	1	1140.1	Ozbek 1977	970.0	964.1	976.8	972.5
20.56	45	1	1140.1	Ozbek 1977	973.0	964.1	976.8	972.5
20.82	45	1	1142.1	Ozbek 1977	964.9	968.7	982.6	980.9
22.61	45	1	1156.4	Ozbek 1977	1032.0	1000.8	1023.2	1042.8
0.1	50	1	988.7	Ozbek 1977	547.8	548.7	549.8	547.5
0.31	50	1	990.1	Ozbek 1977	550.2	552.1	554.7	549.5
0.99	50	1	994.6	Ozbek 1977	557.5	563.3	567.8	556.1
3.16	50	1	1009.2	Ozbek 1977	581.0	598.9	603.0	578.6
5.56	50	1	1025.8	Ozbek 1977	608.6	638.3	639.8	606.5
6.24	50	1	1030.5	Ozbek 1977	617.4	649.5	650.2	615.0
8.05	50	1	1043.4	Ozbek 1977	638.1	679.2	678.1	639.2
10.46	50	1	1060.7	Ozbek 1977	675.3	718.7	716.3	675.2
12.1	50	1	1072.8	Ozbek 1977	703.4	745.6	743.2	702.6

12.74	50	1	1077.5	Ozbek 1977	712.5	756.1	753.9	714.0
14.91	50	1	1093.7	Ozbek 1977	754.6	791.7	791.5	755.9
16.98	50	1	1109.5	Ozbek 1977	792.3	825.7	829.0	801.1
18.48	50	1	1121.1	Ozbek 1977	833.8	850.3	857.4	837.7
18.94	50	1	1124.7	Ozbek 1977	837.2	857.9	866.3	849.6
20.82	50	1	1139.4	Ozbek 1977	886.4	888.7	904.0	902.1
22.61	50	1	1153.7	Ozbek 1977	945.4	918.1	941.6	958.5
24.16	50	1	1166.3	Ozbek 1977	1000.7	943.5	975.8	1013.2
26.84	50	1	1188.6	Ozbek 1977	1120.0	987.5	1038.6	**
2.7	54	1	1004.2	Ozbek 1977	548.0	553.8	558.1	537.6
2.7	54	35.7	1005.7	Ozbek 1977	549.0	554.5	558.7	538.4
2.7	54	70.1	1007.1	Ozbek 1977	544.0	555.3	559.4	539.3
2.7	54	141	1010.1	Ozbek 1977	542.0	556.9	560.8	540.9
2.7	54	174.8	1011.5	Ozbek 1977	544.0	557.7	561.5	541.7
2.7	54	207.9	1012.9	Ozbek 1977	542.0	558.4	562.2	542.5
2.7	54	241.3	1014.3	Ozbek 1977	544.0	559.2	562.9	543.3
2.7	54	275.1	1015.6	Ozbek 1977	547.0	560.1	563.6	544.2
2.7	54	310.4	1017.1	Ozbek 1977	549.0	560.9	564.4	545.0
2.7	54	158.9	1010.9	Ozbek 1977	543.0	557.3	561.2	541.4
7.91	54	1	1040.3	Ozbek 1977	598.0	633.8	633.3	598.1
7.91	54	34.8	1041.6	Ozbek 1977	601.0	634.7	633.8	598.9
7.91	54	70	1043.1	Ozbek 1977	600.0	635.6	634.3	599.9
7.91	54	104.4	1044.4	Ozbek 1977	601.0	636.4	634.8	600.8
7.91	54	139.3	1045.8	Ozbek 1977	600.0	637.3	635.3	601.7
7.91	54	174.1	1047.2	Ozbek 1977	604.0	638.3	635.9	602.6
7.91	54	207.7	1048.6	Ozbek 1977	605.0	639.2	636.4	603.5
7.91	54	243.2	1049.9	Ozbek 1977	605.0	640.1	637.0	604.5
7.91	54	276.1	1051.2	Ozbek 1977	607.0	641.1	637.6	605.3
7.91	54	311.3	1052.6	Ozbek 1977	607.0	642.1	638.2	606.3
7.91	54	158.4	1046.6	Ozbek 1977	603.0	637.8	635.6	602.2
7.91	54	1	1040.3	Ozbek 1977	600.0	633.8	633.3	598.1
5.52	55	1	1023.0	Ozbek 1977	561.0	587.6	589.3	559.7
8.05	55	1	1040.8	Ozbek 1977	589.7	625.9	625.3	590.7
10.46	55	1	1058.1	Ozbek 1977	622.9	662.4	660.7	624.3
12.74	55	1	1074.8	Ozbek 1977	659.2	696.8	695.6	660.2
14.91	55	1	1091.0	Ozbek 1977	696.0	729.7	730.4	698.9
16.03	55	1	1099.5	Ozbek 1977	723.0	746.6	749.0	720.9
16.03	55	1	1099.5	Ozbek 1977	724.0	746.6	749.0	720.9
16.03	55	4.5	1099.6	Ozbek 1977	723.0	746.7	749.0	721.0
16.03	55	14.1	1099.8	Ozbek 1977	725.0	747.0	749.1	721.3
16.03	55	32.9	1100.4	Ozbek 1977	723.0	747.6	749.1	721.9
16.03	55	69.6	1101.7	Ozbek 1977	726.0	748.7	749.3	723.1
16.03	55	104.1	1102.9	Ozbek 1977	728.0	749.8	749.5	724.2

16.03	55	139.3	1104.2	Ozbek 1977	729.0	750.9	749.7	725.4
16.03	55	173.4	1105.4	Ozbek 1977	731.0	752.0	749.9	726.5
16.03	55	207.9	1106.6	Ozbek 1977	733.0	753.1	750.2	727.6
16.03	55	241.4	1107.8	Ozbek 1977	732.0	754.2	750.4	728.8
16.03	55	276.8	1109.0	Ozbek 1977	736.0	755.5	750.7	730.0
16.03	55	310.6	1110.2	Ozbek 1977	739.0	756.6	751.0	731.1
16.03	55	159.6	1104.9	Ozbek 1977	739.0	751.5	749.8	726.0
16.03	55	1	1099.5	Ozbek 1977	725.0	746.6	749.0	720.9
16.98	55	1	1106.8	Ozbek 1977	739.8	761.0	765.2	740.7
18.94	55	1	1121.9	Ozbek 1977	772.6	790.6	799.9	785.2
20.82	55	1	1136.7	Ozbek 1977	819.0	819.0	834.9	833.4
22.61	55	1	1151.0	Ozbek 1977	869.4	846.1	869.9	885.1
20.56	56	1	1134.1	Ozbek 1977	818.0	802.3	817.2	813.8
20.56	56	36.3	1134.9	Ozbek 1977	817.0	803.5	817.0	815.1
20.56	56	70.1	1136.0	Ozbek 1977	821.0	804.7	816.9	816.4
20.56	56	106.5	1137.2	Ozbek 1977	819.0	805.9	816.9	817.8
20.56	56	141	1138.3	Ozbek 1977	823.0	807.2	816.8	819.1
20.56	56	174.8	1139.5	Ozbek 1977	826.0	808.4	816.8	820.4
20.56	56	207.9	1140.6	Ozbek 1977	827.0	809.6	816.8	821.7
20.56	56	241.6	1141.7	Ozbek 1977	828.0	810.8	816.9	823.0
20.56	56	276.8	1142.9	Ozbek 1977	832.0	812.2	817.0	824.4
20.56	56	310.6	1144.0	Ozbek 1977	834.0	813.5	817.1	825.7
20.56	56	158.6	1138.9	Ozbek 1977	825.0	807.8	816.8	819.8
20.56	56	1	1134.1	Ozbek 1977	814.0	802.3	817.2	813.8
0.58	60	1	987.0	Ozbek 1977	472.4	474.7	477.8	471.0
3.96	60	1	1009.6	Ozbek 1977	506.1	522.0	525.0	502.7
6	60	1	1023.7	Ozbek 1977	526.0	550.5	551.7	524.3
7.63	60	1	1035.1	Ozbek 1977	546.5	573.3	573.3	543.1
12.97	60	2.1	1073.8	Ozbek 1977	618.0	648.1	647.6	616.7
12.97	60	37.2	1075.0	Ozbek 1977	619.0	649.2	648.0	617.8
12.97	60	70.7	1076.2	Ozbek 1977	621.1	650.3	648.5	618.9
12.97	60	104.4	1077.5	Ozbek 1977	620.0	651.4	649.0	619.9
12.97	60	141.7	1078.9	Ozbek 1977	622.0	652.6	649.5	621.2
12.97	60	174.4	1080.1	Ozbek 1977	623.0	653.6	650.0	622.2
12.97	60	206.8	1081.3	Ozbek 1977	624.0	654.7	650.5	623.3
12.97	60	276.1	1083.8	Ozbek 1977	631.0	657.1	651.6	625.5
13.62	60	1	1078.6	Ozbek 1977	629.0	657.2	657.1	627.1
17.12	60	1	1105.1	Ozbek 1977	691.3	706.2	711.2	690.3
20.08	60	1	1128.1	Ozbek 1977	750.0	747.6	760.8	755.0
23.92	60	1	1158.9	Ozbek 1977	851.0	801.3	831.4	859.2
24	60	1	1159.5	Ozbek 1977	854.0	802.5	832.9	861.7
24	60	33.3	1160.2	Ozbek 1977	856.0	803.7	832.8	863.1
24	60	72.6	1161.3	Ozbek 1977	859.0	805.2	832.6	864.8

24	60	105.1	1162.3	Ozbek 1977	861.0	806.5	832.4	866.3
24	60	177.5	1164.6	Ozbek 1977	862.0	809.5	832.2	869.6
24	60	210.8	1165.7	Ozbek 1977	867.0	810.8	832.2	871.1
24	60	231.5	1166.4	Ozbek 1977	870.0	811.7	832.2	872.0
24	60	274.7	1167.8	Ozbek 1977	869.0	813.5	832.2	874.0
24	60	313.9	1169.1	Ozbek 1977	875.0	815.2	832.3	875.8
24	60	156	1164.0	Ozbek 1977	864.0	808.6	832.3	868.6
24	60	1	1159.5	Ozbek 1977	855.0	802.5	832.9	861.7
26.43	60	1	1179.7	Ozbek 1977	926.0	836.5	882.0	**
27.04	60	1	1185.0	Ozbek 1977	970.0	845.0	894.9	**
2.7	69	1	996.2	Ozbek 1977	430.0	442.8	446.2	431.3
2.7	69	36.2	997.7	Ozbek 1977	434.0	443.7	447.1	432.3
2.7	69	71	999.2	Ozbek 1977	432.0	444.7	447.9	433.3
2.7	69	106.8	1000.7	Ozbek 1977	433.0	445.7	448.8	434.2
2.7	69	139.8	1002.1	Ozbek 1977	436.0	446.6	449.7	435.1
2.7	69	207.9	1005.0	Ozbek 1977	434.0	448.5	451.4	437.0
2.7	69	241	1006.4	Ozbek 1977	439.0	449.4	452.2	437.9
2.7	69	273.2	1007.7	Ozbek 1977	438.0	450.3	453.0	438.8
2.7	69	309.7	1009.2	Ozbek 1977	441.0	451.3	454.0	439.8
2.7	69	152.7	1002.7	Ozbek 1977	436.0	446.9	450.0	435.5
2.7	69	1	996.2	Ozbek 1977	429.0	442.8	446.2	431.3
7.91	70	36.2	1032.9	Ozbek 1977	477.0	501.0	500.5	476.8
7.91	70	70	1034.3	Ozbek 1977	480.0	502.0	501.3	477.8
7.91	70	131.4	1036.8	Ozbek 1977	480.0	504.0	502.7	479.7
7.91	70	174.8	1038.5	Ozbek 1977	479.0	505.3	503.7	481.1
7.91	70	207.7	1039.9	Ozbek 1977	481.0	506.4	504.5	482.1
7.91	70	242	1041.2	Ozbek 1977	485.0	507.5	505.3	483.1
7.91	70	275.9	1042.6	Ozbek 1977	484.0	508.6	506.1	484.2
7.91	70	310.6	1043.9	Ozbek 1977	484.0	509.7	506.9	485.2
7.91	70	156.5	1037.8	Ozbek 1977	480.0	504.8	503.3	480.5
7.91	70	17.6	1032.1	Ozbek 1977	476.0	500.4	500.1	476.2
16.03	70	7.9	1091.1	Ozbek 1977	584.0	598.6	601.5	583.5
16.03	70	7.9	1091.1	Ozbek 1977	586.0	598.6	601.5	583.5
16.03	70	9	1091.2	Ozbek 1977	587.0	598.6	601.6	583.5
16.03	70	21.7	1091.5	Ozbek 1977	585.0	599.1	601.8	584.0
16.03	70	21.9	1091.5	Ozbek 1977	587.0	599.1	601.8	584.0
16.03	70	35.1	1092.0	Ozbek 1977	586.0	599.6	602.0	584.5
16.03	70	70.4	1093.2	Ozbek 1977	588.0	600.9	602.6	585.8
16.03	70	104.3	1094.4	Ozbek 1977	589.0	602.2	603.2	587.1
16.03	70	139.8	1095.7	Ozbek 1977	590.0	603.5	603.8	588.4
16.03	70	173.4	1096.9	Ozbek 1977	595.0	604.8	604.4	589.7
16.03	70	208.2	1098.2	Ozbek 1977	597.0	606.1	605.1	591.0
16.03	70	242.3	1099.4	Ozbek 1977	596.0	607.4	605.7	592.3

16.03	70	276.8	1100.7	Ozbek 1977	597.0	608.8	606.3	593.6
16.03	70	310.8	1101.9	Ozbek 1977	600.0	610.1	607.0	594.9
16.03	70	158.2	1096.4	Ozbek 1977	591.0	604.2	604.1	589.1
16.03	70	12.4	1091.2	Ozbek 1977	586.0	598.7	601.6	583.6
27.2	70	1	1180.5	Ozbek 1977	840.0	733.7	780.2	**
20.56	71	7.9	1125.6	Ozbek 1977	662.0	644.6	658.3	658.6
20.56	71	34.8	1126.3	Ozbek 1977	662.0	645.7	658.6	659.8
20.56	71	70	1127.4	Ozbek 1977	663.0	647.2	659.0	661.3
20.56	71	207.9	1132.1	Ozbek 1977	671.0	652.9	661.0	667.3
20.56	71	243.4	1133.3	Ozbek 1977	671.0	654.4	661.5	668.8
20.56	71	277.5	1134.5	Ozbek 1977	674.0	655.9	662.0	670.3
20.56	71	311.1	1135.6	Ozbek 1977	676.0	657.3	662.6	671.8
20.56	71	157.5	1130.4	Ozbek 1977	668.0	650.8	660.2	665.1
20.56	71	12.7	1125.7	Ozbek 1977	659.0	644.8	658.3	658.9
20.56	71	7.9	1125.6	Ozbek 1977	663.0	644.6	658.3	658.6
0.58	75	1	978.6	Ozbek 1977	383.6	384.4	386.9	381.7
3.97	75	1	1001.3	Ozbek 1977	412.5	422.8	425.2	409.1
7.65	75	1	1026.7	Ozbek 1977	447.0	464.6	464.4	443.4
17.14	75	1	1096.5	Ozbek 1977	567.1	572.1	576.9	564.4
7.91	78.5	1	1026.4	Ozbek 1977	425.0	446.9	446.5	427.2
7.91	78.5	35.5	1027.8	Ozbek 1977	427.0	448.0	447.4	428.3
7.91	78.5	70	1029.2	Ozbek 1977	427.0	449.1	448.2	429.4
7.91	78.5	173.4	1033.5	Ozbek 1977	431.0	452.5	450.8	432.6
7.91	78.5	207.9	1034.9	Ozbek 1977	433.0	453.7	451.7	433.7
7.91	78.5	242.2	1036.3	Ozbek 1977	433.0	454.8	452.5	434.8
7.91	78.5	275.6	1037.6	Ozbek 1977	433.0	455.9	453.4	435.8
7.91	78.5	311.3	1039.0	Ozbek 1977	436.0	457.1	454.3	437.0
7.91	78.5	156.2	1032.8	Ozbek 1977	431.0	452.0	450.4	432.1
7.91	78.5	1	1026.4	Ozbek 1977	426.0	446.9	446.5	427.2
7.91	78.5	1	1026.4	Ozbek 1977	428.0	446.9	446.5	427.2
12.97	80	36.2	1063.3	Ozbek 1977	476.0	493.6	492.7	475.7
12.97	80	71.3	1064.6	Ozbek 1977	477.0	494.9	493.5	477.0
12.97	80	105.5	1065.9	Ozbek 1977	479.0	496.2	494.3	478.2
12.97	80	141	1067.3	Ozbek 1977	479.0	497.5	495.2	479.5
12.97	80	173.4	1068.5	Ozbek 1977	481.0	498.7	495.9	480.6
12.97	80	206.5	1069.8	Ozbek 1977	482.0	499.9	496.7	481.8
12.97	80	274.7	1072.4	Ozbek 1977	484.0	502.5	498.3	484.2
12.97	80	307.8	1073.6	Ozbek 1977	486.0	503.7	499.1	485.4
24	80	8.6	1147.9	Ozbek 1977	654.0	610.0	634.5	658.9
24	80	34.5	1148.5	Ozbek 1977	656.0	611.2	634.9	660.2
24	80	70.1	1149.6	Ozbek 1977	656.0	612.8	635.4	661.9
24	80	104.4	1150.7	Ozbek 1977	659.0	614.3	635.9	663.6
24	80	138.9	1151.8	Ozbek 1977	664.0	615.9	636.4	665.4

24	80	173.4	1152.9	Ozbek 1977	660.0	617.5	637.0	667.1
24	80	208.6	1154.1	Ozbek 1977	665.0	619.1	637.5	668.8
24	80	243	1155.2	Ozbek 1977	665.0	620.7	638.1	670.5
24	80	276.8	1156.4	Ozbek 1977	667.0	622.3	638.7	672.2
24	80	312.7	1157.6	Ozbek 1977	669.0	623.9	639.3	674.0
24	80	214.1	1154.3	Ozbek 1977	662.0	619.4	637.6	669.1
24	80	10.3	1148.0	Ozbek 1977	653.0	610.1	634.5	658.9
27.5	80	1	1177.3	Ozbek 1977	740.0	646.9	689.9	**
2.7	84	36.9	988.7	Ozbek 1977	358.0	365.8	368.3	357.6
2.7	84	105.5	991.7	Ozbek 1977	359.0	367.8	370.2	359.5
2.7	84	174.1	994.7	Ozbek 1977	360.0	369.8	372.0	361.5
2.7	84	308.9	1000.4	Ozbek 1977	365.0	373.7	375.6	365.3
2.7	84	161.3	994.2	Ozbek 1977	362.0	369.4	371.6	361.1
2.7	84	1	987.2	Ozbek 1977	356.0	364.8	367.4	356.5
16.03	84	8.6	1082.7	Ozbek 1977	494.0	500.0	502.0	491.5
16.03	84	10.3	1082.7	Ozbek 1977	494.0	500.1	502.1	491.6
16.03	84	21.7	1083.1	Ozbek 1977	495.0	500.6	502.3	492.0
16.03	84	35.6	1083.6	Ozbek 1977	496.0	501.1	502.6	492.6
16.03	84	70.1	1084.8	Ozbek 1977	496.0	502.5	503.4	493.9
16.03	84	104.4	1086.1	Ozbek 1977	497.0	503.8	504.2	495.3
16.03	84	173.6	1088.6	Ozbek 1977	499.0	506.6	505.8	498.0
16.03	84	207.5	1089.9	Ozbek 1977	501.0	507.9	506.6	499.3
16.03	84	242.7	1091.2	Ozbek 1977	503.0	509.3	507.4	500.7
16.03	84	276.5	1092.4	Ozbek 1977	504.0	510.7	508.2	502.0
16.03	84	311.1	1093.7	Ozbek 1977	504.0	512.0	509.0	503.3
16.03	84	159.9	1088.1	Ozbek 1977	498.0	506.0	505.5	497.4
16.03	84	10.5	1082.7	Ozbek 1977	493.0	500.1	502.1	491.6
20.56	85	10.8	1117.2	Ozbek 1977	558.0	539.5	550.4	554.8
20.56	85	34.8	1117.9	Ozbek 1977	556.0	540.5	550.9	555.9
20.56	85	71.2	1119.0	Ozbek 1977	560.0	542.1	551.6	557.5
20.56	85	105.5	1120.2	Ozbek 1977	562.0	543.6	552.3	559.0
20.56	85	140.6	1121.4	Ozbek 1977	563.0	545.1	553.0	560.6
20.56	85	174.8	1122.6	Ozbek 1977	563.0	546.6	553.8	562.1
20.56	85	206.8	1123.7	Ozbek 1977	565.0	548.0	554.4	563.5
20.56	85	242.5	1125.0	Ozbek 1977	568.0	549.5	555.2	565.1
20.56	85	276.8	1126.2	Ozbek 1977	569.0	551.0	555.9	566.7
20.56	85	311.3	1127.4	Ozbek 1977	573.0	552.5	556.7	568.2
20.56	85	157	1122.0	Ozbek 1977	563.0	545.8	553.4	561.3
20.56	85	7.6	1117.1	Ozbek 1977	557.0	539.4	550.3	554.6
20.56	85	10.7	1117.2	Ozbek 1977	557.0	539.5	550.4	554.8
24	94	10.2	1139.3	Ozbek 1977	556.0	517.5	537.0	561.3
24	94	34.7	1139.9	Ozbek 1977	557.0	518.7	537.5	562.5
24	94	68.2	1140.9	Ozbek 1977	559.0	520.2	538.2	564.2

24	94	103.9	1142.0	Ozbek 1977	561.0	521.9	539.0	566.0
24	94	137.6	1143.2	Ozbek 1977	561.0	523.4	539.7	567.7
24	94	172.5	1144.3	Ozbek 1977	565.0	525.0	540.4	569.5
24	94	242.9	1146.7	Ozbek 1977	566.0	528.3	542.0	573.0
24	94	279.6	1148.0	Ozbek 1977	568.0	530.0	542.8	574.8
24	94	312.8	1149.2	Ozbek 1977	566.0	531.5	543.5	576.4
24	94	14.3	1139.4	Ozbek 1977	557.0	517.7	537.1	561.5
2.7	96	7.2	979.5	Ozbek 1977	311.0	318.1	320.1	311.7
2.7	96	33.8	980.7	Ozbek 1977	312.0	318.9	320.8	312.5
2.7	96	173.4	986.9	Ozbek 1977	315.0	322.9	324.6	316.5
2.7	96	240.6	989.8	Ozbek 1977	317.0	324.9	326.4	318.4
2.7	96	305.4	992.6	Ozbek 1977	318.0	326.8	328.1	320.2
2.7	96	77.6	982.7	Ozbek 1977	314.0	320.2	322.0	313.8
20.56	97	10	1109.6	Ozbek 1977	489.0	470.8	479.0	486.6
20.56	97	34.8	1110.3	Ozbek 1977	490.0	471.9	479.6	487.8
20.56	97	70.7	1111.5	Ozbek 1977	492.0	473.4	480.4	489.4
20.56	97	105.6	1112.7	Ozbek 1977	493.0	475.0	481.2	491.0
20.56	97	175.5	1115.2	Ozbek 1977	496.0	478.0	482.9	494.1
20.56	97	207.3	1116.3	Ozbek 1977	497.0	479.4	483.7	495.5
20.56	97	270.8	1118.6	Ozbek 1977	499.0	482.1	485.2	498.3
20.56	97	280.9	1119.0	Ozbek 1977	500.0	482.6	485.5	498.8
20.56	97	159.4	1114.6	Ozbek 1977	495.0	477.3	482.5	493.4
20.56	97	10.8	1109.6	Ozbek 1977	488.0	470.8	479.0	486.7
7.91	98.5	4.5	1013.7	Ozbek 1977	340.0	354.4	353.0	342.0
7.91	98.5	34.5	1014.9	Ozbek 1977	341.0	355.4	353.8	343.0
7.91	98.5	67.9	1016.4	Ozbek 1977	341.0	356.5	354.7	344.1
7.91	98.5	140.3	1019.5	Ozbek 1977	344.0	358.9	356.7	346.4
7.91	98.5	175.5	1021.0	Ozbek 1977	344.0	360.0	357.6	347.5
7.91	98.5	206.8	1022.3	Ozbek 1977	346.0	361.1	358.4	348.5
7.91	98.5	242.9	1023.8	Ozbek 1977	346.0	362.3	359.4	349.7
7.91	98.5	276.8	1025.2	Ozbek 1977	348.0	363.4	360.3	350.7
7.91	98.5	310.9	1026.6	Ozbek 1977	348.0	364.5	361.2	351.8
7.91	98.5	12.2	1014.0	Ozbek 1977	340.0	354.6	353.2	342.3
16.03	98.5	7.7	1073.4	Ozbek 1977	421.0	424.3	424.6	420.4
16.03	98.5	9.3	1073.4	Ozbek 1977	422.0	424.3	424.6	420.4
16.03	98.5	22	1073.8	Ozbek 1977	421.0	424.8	424.9	421.0
16.03	98.5	35.1	1074.3	Ozbek 1977	422.0	425.4	425.3	421.5
16.03	98.5	70.1	1075.6	Ozbek 1977	424.0	426.7	426.2	422.9
16.03	98.5	104.1	1076.9	Ozbek 1977	420.8	428.1	427.0	424.2
16.03	98.5	139.9	1078.2	Ozbek 1977	426.0	429.5	427.9	425.6
16.03	98.5	172.5	1079.5	Ozbek 1977	426.0	430.8	428.8	426.9
16.03	98.5	207.9	1080.8	Ozbek 1977	428.0	432.2	429.7	428.3
16.03	98.5	241.6	1082.1	Ozbek 1977	429.0	433.5	430.5	429.6

16.03	98.5	276.3	1083.4	Ozbek 1977	431.0	434.9	431.4	430.9
16.03	98.5	310.9	1084.7	Ozbek 1977	432.0	436.3	432.3	432.3
16.03	98.5	159.9	1079.0	Ozbek 1977	426.0	430.3	428.4	426.4
16.03	98.5	9.5	1073.4	Ozbek 1977	421.0	424.3	424.6	420.5
0.58	100	1	962.2	Ozbek 1977	286.9	12.5	288.5	12.4
3.98	100	1	985.2	Ozbek 1977	309.7	13.7	316.5	13.4
7.66	100	1	1010.8	Ozbek 1977	337.1	15.1	345.3	14.5
16.98	100	1	1079.6	Ozbek 1977	429.9	18.5	426.6	18.5
12.97	101	5.8	1048.7	Ozbek 1977	378.0	387.6	385.5	378.0
12.97	101	35.1	1049.8	Ozbek 1977	378.0	388.6	386.3	379.1
12.97	101	71.3	1051.2	Ozbek 1977	379.0	390.0	387.2	380.4
12.97	101	105.8	1052.6	Ozbek 1977	381.0	391.3	388.2	381.6
12.97	101	139.9	1053.9	Ozbek 1977	362.0	392.5	389.0	382.9
12.97	101	174.4	1055.3	Ozbek 1977	382.0	393.8	390.0	384.1
12.97	101	206.8	1056.6	Ozbek 1977	385.0	395.0	390.8	385.3
12.97	101	238.2	1057.9	Ozbek 1977	385.0	396.2	391.6	386.4
12.97	101	272.7	1059.2	Ozbek 1977	386.0	397.5	392.6	387.7
12.97	101	308.5	1060.6	Ozbek 1977	386.0	398.8	393.5	388.9
12.97	101	161	1054.8	Ozbek 1977	382.0	393.3	389.6	383.6
12.97	101	6.5	1048.7	Ozbek 1977	377.0	387.6	385.5	378.0
24	101	13.8	1134.9	Ozbek 1977	524.0	480.2	497.1	521.9
24	101	35.5	1135.5	Ozbek 1977	523.0	481.2	497.6	523.0
24	101	71.3	1136.5	Ozbek 1977	525.0	482.9	498.4	524.8
24	101	107.2	1137.7	Ozbek 1977	527.0	484.5	499.2	526.6
24	101	139.9	1138.8	Ozbek 1977	528.0	486.0	500.0	528.2
24	101	175.8	1140.0	Ozbek 1977	527.0	487.7	500.8	530.0
24	101	211.3	1141.3	Ozbek 1977	532.0	489.3	501.7	531.8
24	101	244.4	1142.4	Ozbek 1977	534.0	490.8	502.5	533.4
24	101	276.8	1143.5	Ozbek 1977	535.0	492.3	503.2	535.0
24	101	313.7	1144.8	Ozbek 1977	536.0	494.0	504.1	536.8
24	101	155.8	1139.3	Ozbek 1977	529.0	486.8	500.4	529.0
24	101	88.4	1137.1	Ozbek 1977	526.0	483.7	498.8	525.7
24	101	11.9	1134.9	Ozbek 1977	523.0	480.2	497.1	521.8
2.7	108.5	36.5	972.0	Ozbek 1977	275.0	280.5	281.9	275.6
2.7	108.5	102.5	975.0	Ozbek 1977	276.0	282.3	283.6	277.4
2.7	108.5	237.5	981.1	Ozbek 1977	280.0	286.2	287.2	281.2
2.7	108.5	307	984.2	Ozbek 1977	282.0	288.2	289.1	283.1
2.7	108.5	162	977.7	Ozbek 1977	278.0	284.1	285.2	279.1
2.7	108.5	14.1	971.0	Ozbek 1977	274.0	279.8	281.3	274.9
16.03	113	8.8	1063.6	Ozbek 1977	366.0	366.9	365.2	366.2
16.03	113	8.9	1063.6	Ozbek 1977	366.0	366.9	365.2	366.2
16.03	113	21.7	1064.0	Ozbek 1977	366.0	367.4	365.6	366.7
16.03	113	34.8	1064.5	Ozbek 1977	367.0	367.9	365.9	367.2

16.03	113	70	1065.8	Ozbek 1977	368.0	369.3	366.9	368.6
16.03	113	104.1	1067.1	Ozbek 1977	369.0	370.6	367.8	370.0
16.03	113	139.3	1068.5	Ozbek 1977	370.0	372.0	368.7	371.3
16.03	113	174.1	1069.9	Ozbek 1977	371.0	373.3	369.6	372.7
16.03	113	206.7	1071.2	Ozbek 1977	372.0	374.6	370.5	373.9
16.03	113	242.3	1072.6	Ozbek 1977	374.0	376.0	371.5	375.3
16.03	113	275.8	1073.9	Ozbek 1977	375.0	377.3	372.3	376.6
16.03	113	310.8	1075.3	Ozbek 1977	376.0	378.6	373.3	377.9
16.03	113	163.2	1069.5	Ozbek 1977	378.0	372.9	369.4	372.2
16.03	113	8.8	1063.6	Ozbek 1977	365.0	366.9	365.2	366.2
20.56	114	14.7	1098.4	Ozbek 1977	414.0	397.0	401.1	413.2
20.56	114	36.4	1099.1	Ozbek 1977	415.0	398.0	401.7	414.2
20.56	114	70.5	1100.2	Ozbek 1977	415.0	399.4	402.6	415.7
20.56	114	104.4	1101.4	Ozbek 1977	418.0	400.9	403.5	417.2
20.56	114	140.3	1102.8	Ozbek 1977	419.0	402.4	404.4	418.8
20.56	114	210.3	1105.4	Ozbek 1977	421.0	405.4	406.3	421.9
20.56	114	242.3	1106.6	Ozbek 1977	422.0	406.7	407.1	423.3
20.56	114	276.5	1107.8	Ozbek 1977	424.0	408.1	408.0	424.8
20.56	114	307.8	1109.0	Ozbek 1977	426.0	409.5	408.8	426.1
20.56	114	157.9	1103.4	Ozbek 1977	419.0	403.1	404.9	419.6
20.56	114	10	1098.3	Ozbek 1977	413.0	396.8	401.0	413.0
7.91	120	8.3	998.5	Ozbek 1977	278.0	287.4	284.8	280.0
7.91	120	35.8	999.7	Ozbek 1977	278.0	288.3	285.6	280.9
7.91	120	68.8	1001.2	Ozbek 1977	279.0	289.3	286.5	281.9
7.91	120	104.4	1002.8	Ozbek 1977	279.0	290.5	287.4	283.1
7.91	120	138.2	1004.3	Ozbek 1977	281.0	291.6	288.3	284.1
7.91	120	174.4	1005.9	Ozbek 1977	282.0	292.7	289.3	285.3
7.91	120	207.5	1007.4	Ozbek 1977	283.0	293.8	290.2	286.3
7.91	120	241.6	1008.9	Ozbek 1977	284.0	294.9	291.1	287.3
7.91	120	274.1	1010.3	Ozbek 1977	285.0	295.9	292.0	288.3
7.91	120	311.6	1011.9	Ozbek 1977	286.0	297.1	292.9	289.5
7.91	120	153	1005.0	Ozbek 1977	282.0	292.1	288.7	284.6
7.91	120	8.3	998.5	Ozbek 1977	277.0	287.4	284.8	280.0
12.97	121	306.5	1047.1	Ozbek 1977	323.0	330.5	323.9	325.7
12.97	121	10.7	1034.8	Ozbek 1977	313.0	319.9	316.0	315.2
12.97	121	6.5	1034.7	Ozbek 1977	314.0	319.7	315.9	315.1
12.97	121	36.2	1035.8	Ozbek 1977	315.0	320.8	316.7	316.1
12.97	121	68.9	1037.2	Ozbek 1977	315.0	322.0	317.6	317.3
12.97	121	103.8	1038.6	Ozbek 1977	315.0	323.2	318.5	318.6
12.97	121	139.6	1040.2	Ozbek 1977	317.0	324.5	319.5	319.8
12.97	121	172.7	1041.5	Ozbek 1977	319.0	325.7	320.3	321.0
12.97	121	205.4	1042.9	Ozbek 1977	320.0	326.9	321.2	322.2
12.97	121	238.2	1044.3	Ozbek 1977	321.0	328.1	322.1	323.3

12.97	121	272.7	1045.7	Ozbek 1977	322.0	329.3	323.0	324.5
0.58	125	1		Ozbek 1977*	226.0			
4	125	1		Ozbek 1977*	245.2			
7.7	125	1		Ozbek 1977*	267.8			
17.25	125	1		Ozbek 1977*	343.3			
2.7	18	1	1018.1	Ozbek 1977	1089.0	1138.5	1141.9	1095.7
2.7	126	9.3	957.2	Ozbek 1977	234.0	238.3	239.1	234.9
2.7	126	35.1	958.5	Ozbek 1977	234.0	239.0	239.8	235.6
2.7	126	87.2	961.0	Ozbek 1977	237.0	240.4	241.2	237.1
2.7	126	135.5	963.4	Ozbek 1977	237.0	241.8	242.4	238.4
2.7	126	252	968.8	Ozbek 1977	241.0	245.0	245.4	241.6
2.7	126	309.6	971.5	Ozbek 1977	242.0	246.6	246.9	243.1
2.7	126	15.5	957.5	Ozbek 1977	234.0	238.4	239.3	235.1
20.56	129	11.4	1087.8	Ozbek 1977	361.0	347.5	348.4	363.7
20.56	129	33.8	1088.5	Ozbek 1977	365.0	348.5	349.0	364.7
20.56	129	70	1089.7	Ozbek 1977	365.0	350.0	350.0	366.3
20.56	129	105.1	1091.0	Ozbek 1977	366.0	351.4	350.9	367.8
20.56	129	140.8	1092.4	Ozbek 1977	366.0	352.9	351.9	369.3
20.56	129	174.1	1093.7	Ozbek 1977	369.0	354.3	352.8	370.8
20.56	129	207.2	1095.0	Ozbek 1977	369.0	355.7	353.7	372.2
20.56	129	241.6	1096.3	Ozbek 1977	370.0	357.1	354.6	373.7
20.56	129	275.9	1097.6	Ozbek 1977	373.0	358.5	355.5	375.1
20.56	129	303.7	1098.7	Ozbek 1977	373.0	359.6	356.2	376.3
20.56	129	161.4	1093.2	Ozbek 1977	368.0	353.8	352.4	370.2
20.56	129	16.5	1087.9	Ozbek 1977	364.0	347.7	348.6	363.9
24	131	174.4	1119.9	Ozbek 1977	399.0	370.8	375.0	406.4
24	131	243.9	1122.5	Ozbek 1977	403.0	373.8	376.8	409.7
24	131	275.4	1123.7	Ozbek 1977	405.0	375.2	377.6	411.2
24	131	315.4	1125.2	Ozbek 1977	406.0	376.9	378.7	413.1
16.03	131.5	7.2	1050.2	Ozbek 1977	313.0	311.6	307.7	313.7
16.03	131.5	8.5	1050.2	Ozbek 1977	313.0	311.7	307.7	313.8
16.03	131.5	21.7	1050.7	Ozbek 1977	312.0	312.2	308.1	314.3
16.03	131.5	35.1	1051.2	Ozbek 1977	313.0	312.7	308.4	314.8
16.03	131.5	70.1	1052.6	Ozbek 1977	314.0	314.0	309.4	316.2
16.03	131.5	140.3	1055.5	Ozbek 1977	316.0	316.7	311.3	318.8
16.03	131.5	207.7	1058.3	Ozbek 1977	318.0	319.2	313.1	321.4
16.03	131.5	242	1059.7	Ozbek 1977	319.0	320.5	314.0	322.7
16.03	131.5	276.6	1061.1	Ozbek 1977	320.0	321.8	314.9	324.0
16.03	131.5	310.9	1062.5	Ozbek 1977	322.0	323.1	315.8	325.3
16.03	131.5	159.8	1056.3	Ozbek 1977	317.0	317.4	311.8	319.6
7.91	135.5	8.4	986.5	Ozbek 1977	246.0	252.1	248.8	247.2
7.91	135.5	34.1	987.7	Ozbek 1977	245.0	252.9	249.5	248.0
7.91	135.5	70.3	989.4	Ozbek 1977	246.0	254.1	250.5	249.1

7.91	135.5	105.8	991.1	Ozbek 1977	247.0	255.2	251.4	250.2
7.91	135.5	138.9	992.6	Ozbek 1977	248.0	256.2	252.3	251.2
7.91	135.5	174.1	994.3	Ozbek 1977	249.0	257.3	253.2	252.3
7.91	135.5	267.5	998.5	Ozbek 1977	251.0	260.2	255.6	255.2
7.91	135.5	242.3	997.4	Ozbek 1977	251.0	259.5	255.0	254.4
7.91	135.5	277.8	999.0	Ozbek 1977	252.0	260.6	255.9	255.5
7.91	135.5	311.6	1000.5	Ozbek 1977	252.0	261.6	256.8	256.5
7.91	135.5	160.3	993.6	Ozbek 1977	249.0	256.9	252.8	251.9
7.91	135.5	11.7	986.7	Ozbek 1977	245.0	252.2	248.9	247.3
12.97	136	7.2	1023.5	Ozbek 1977	278.0	281.9	276.8	279.7
12.97	136	35.5	1024.6	Ozbek 1977	278.0	282.9	277.5	280.7
12.97	136	101.7	1027.4	Ozbek 1977	281.0	285.2	279.3	283.0
12.97	136	206.1	1032.0	Ozbek 1977	283.0	288.9	282.1	286.7
12.97	136	240.6	1033.5	Ozbek 1977	284.0	290.1	283.0	287.9
12.97	136	272.7	1034.9	Ozbek 1977	285.0	291.2	283.8	289.0
12.97	136	307.5	1036.4	Ozbek 1977	286.0	292.4	284.8	290.2
12.97	136	14.5	1023.7	Ozbek 1977	278.0	282.1	277.0	280.0
2.7	148	10	938.5	Ozbek 1977	198.0	200.3	200.5	198.3
2.7	148	51	940.7	Ozbek 1977	201.0	201.4	201.6	199.4
2.7	148	153.4	946.1	Ozbek 1977	202.0	204.2	204.2	202.1
2.7	148	206.5	948.8	Ozbek 1977	203.0	205.6	205.5	203.6
2.7	148	251.6	951.1	Ozbek 1977	204.0	206.8	206.6	204.7
2.7	148	305.1	953.7	Ozbek 1977	205.0	208.2	208.0	206.1
24	148	312.7	1113.1	Ozbek 1977	355.0	331.6	329.2	365.0
0.59	150	1		Ozbek 1977*	185.8			
4.04	150	1		Ozbek 1977*	202.0			
7.78	150	1		Ozbek 1977*	221.3			
17.3900	150	1		Ozbek 1977*	285.2			
12.97	151	7.9	1011.5	Ozbek 1977	249.0	251.8	245.6	251.4
12.97	151	35.8	1012.7	Ozbek 1977	250.0	252.8	246.3	252.4
12.97	151	59.6	1013.8	Ozbek 1977	251.0	253.6	246.9	253.2
12.97	151	104.1	1015.8	Ozbek 1977	251.0	255.1	248.1	254.7
12.97	151	138.2	1017.4	Ozbek 1977	253.0	256.3	249.0	255.9
12.97	151	174.8	1019.1	Ozbek 1977	254.0	257.6	250.0	257.2
12.97	151	206.1	1020.5	Ozbek 1977	255.0	258.6	250.8	258.2
12.97	151	239.9	1022.0	Ozbek 1977	255.0	259.8	251.7	259.4
12.97	151	271.3	1023.5	Ozbek 1977	256.0	260.9	252.5	260.5
12.97	151	305.8	1025.0	Ozbek 1977	257.0	262.0	253.4	261.6
12.97	151	19.3	1012.0	Ozbek 1977	249.0	252.2	245.9	251.8
7.91	152	3.4		Ozbek 1977*	218.0			
7.91	152	35.8	974.1	Ozbek 1977	219.0	223.6	219.4	220.5
7.91	152	70.7	975.9	Ozbek 1977	219.0	224.6	220.4	221.5
7.91	152	140.6	979.3	Ozbek 1977	221.0	226.8	222.2	223.7

7.91	152	172.3	980.9	Ozbek 1977	222.0	227.8	223.0	224.6
7.91	152	211.3	982.8	Ozbek 1977	223.0	228.9	224.0	225.8
7.91	152	243.2	984.4	Ozbek 1977	223.0	229.9	224.8	226.8
7.91	152	276.1	985.9	Ozbek 1977	225.0	230.9	225.6	227.7
7.91	152	311.6	987.6	Ozbek 1977	225.0	232.0	226.5	228.8
7.91	152	159.4	980.3	Ozbek 1977	222.0	227.4	222.6	224.2
7.91	152	20.2	973.4	Ozbek 1977	219.0	223.1	219.0	220.0
16.03	154	16.3	1033.0	Ozbek 1977	265.0	263.1	256.6	267.2
16.03	154	24.8	1033.3	Ozbek 1977	265.0	263.4	256.9	267.5
16.03	154	35.5	1033.8	Ozbek 1977	266.0	263.8	257.1	268.0
16.03	154	70.1	1035.2	Ozbek 1977	267.0	265.1	258.1	269.3
16.03	154	106.2	1036.8	Ozbek 1977	268.0	266.4	259.0	270.6
16.03	154	173.8	1039.8	Ozbek 1977	270.0	268.9	260.8	273.1
16.03	154	208.2	1041.4	Ozbek 1977	271.0	270.2	261.7	274.4
16.03	154	242.3	1042.9	Ozbek 1977	272.0	271.4	262.6	275.7
16.03	154	276.5	1044.4	Ozbek 1977	272.0	272.6	263.5	276.9
16.03	154	312.1	1046.0	Ozbek 1977	273.0	273.9	264.4	278.2
16.03	154	161.7	1039.3	Ozbek 1977	269.0	268.5	260.5	272.7
0	10.54	1	999.7	Kestin 1977	1289.6	1286.5	1285.8	1285.8
0	10.52	34.5	1001.2	Kestin 1977	1285.0	1283.8	1283.8	1283.8
0	10.54	70.6	1002.9	Kestin 1977	1280.4	1279.6	1280.1	1280.1
0	10.54	104.4	1004.5	Kestin 1977	1277.6	1276.4	1277.5	1277.5
0	10.55	138.9	1006.1	Kestin 1977	1272.9	1272.9	1274.5	1274.5
0	10.57	175.8	1007.8	Kestin 1977	1269.2	1269.1	1271.2	1271.2
0	10.59	207.8	1009.3	Kestin 1977	1265.0	1265.8	1268.3	1268.3
0	10.6	242.3	1010.9	Kestin 1977	1262.2	1262.8	1265.7	1265.7
0	10.61	278.2	1012.5	Kestin 1977	1259.6	1259.8	1263.1	1263.1
0	10.62	311.3	1013.9	Kestin 1977	1253.9	1257.2	1260.8	1260.8
0	10.61	138.9	1006.1	Kestin 1977	1273.2	1270.8	1272.4	1272.4
0	10.52	1	999.7	Kestin 1977	1291.3	1287.3	1286.6	1286.6
0	17.19	1	998.7	Kestin 1977	1077.4	1075.1	1074.6	1074.6
0	17.23	17.6	999.5	Kestin 1977	1074.3	1073.1	1072.8	1072.8
0	17.27	35.5	1000.3	Kestin 1977	1071.8	1071.0	1070.9	1070.9
0	17.33	70	1001.9	Kestin 1977	1068.2	1067.6	1067.9	1067.9
0	17.36	104.4	1003.4	Kestin 1977	1065.0	1065.1	1065.8	1065.8
0	17.39	138.9	1005.0	Kestin 1977	1063.2	1062.7	1063.8	1063.8
0	17.42	173.4	1006.5	Kestin 1977	1059.7	1060.4	1061.8	1061.8
0	17.46	205.1	1007.9	Kestin 1977	1058.2	1058.0	1059.8	1059.8
0	17.49	240.3	1009.5	Kestin 1977	1055.8	1055.9	1057.9	1057.9
0	17.52	274.7	1011.0	Kestin 1977	1054.0	1053.9	1056.2	1056.2
0	17.55	309.9	1012.5	Kestin 1977	1052.3	1051.9	1054.5	1054.5
0	17.52	272.7	1010.9	Kestin 1977	1054.4	1053.9	1056.3	1056.3
0	17.5	205.1	1007.9	Kestin 1977	1057.1	1057.0	1058.7	1058.7

0	17.46	137.9	1004.9	Kestin 1977	1062.3	1060.8	1062.0	1062.0
0	17.45	69.3	1001.8	Kestin 1977	1065.2	1064.4	1064.7	1064.7
0	17.47	1	998.7	Kestin 1977	1069.3	1067.4	1066.9	1066.9
0	22.43	1	997.7	Kestin 1977	945.9	945.2	944.7	944.7
0	22.45	17.6	998.4	Kestin 1977	944.7	944.2	943.9	943.9
0	22.46	35.5	999.2	Kestin 1977	943.4	943.4	943.3	943.3
0	22.51	69.3	1000.7	Kestin 1977	942.0	941.3	941.6	941.6
0	22.55	104.4	1002.3	Kestin 1977	939.9	939.5	940.0	940.0
0	22.57	138.9	1003.8	Kestin 1977	937.7	938.2	939.0	939.0
0	22.61	173.5	1005.3	Kestin 1977	937.0	936.5	937.6	937.6
0	22.64	205.8	1006.7	Kestin 1977	934.5	935.2	936.5	936.5
0	22.71	240.3	1008.2	Kestin 1977	932.6	933.1	934.6	934.6
0	22.76	276.1	1009.7	Kestin 1977	930.6	931.4	933.2	933.2
0	22.78	309.9	1011.2	Kestin 1977	929.4	930.5	932.4	932.4
0	22.7	205.1	1006.7	Kestin 1977	933.8	933.9	935.3	935.3
0	22.7	136.8	1003.7	Kestin 1977	935.8	935.4	936.2	936.2
0	22.69	70	1000.7	Kestin 1977	937.7	937.4	937.6	937.6
0	22.68	1	997.6	Kestin 1977	940.2	939.6	939.2	939.2
0	22.77	1	997.6	Kestin 1977	938.0	937.7	937.2	937.2
0	29.94	1	995.7	Kestin 1977	799.6	798.7	798.2	798.2
0	29.96	17.2	996.4	Kestin 1977	799.5	798.2	797.9	797.9
0	30	35.5	997.2	Kestin 1977	798.0	797.4	797.2	797.2
0	30.09	69.3	998.6	Kestin 1977	796.3	795.6	795.6	795.6
0	30.06	103.4	1000.1	Kestin 1977	796.0	795.9	796.1	796.1
0	30.03	108.2	1000.4	Kestin 1977	795.8	796.4	796.6	796.6
0	30.03	174.1	1003.2	Kestin 1977	796.6	796.1	796.7	796.7
0	30.11	208.5	1004.7	Kestin 1977	794.8	794.7	795.5	795.5
0	30.14	241.6	1006.1	Kestin 1977	794.1	794.2	795.1	795.1
0	30.06	275.4	1007.5	Kestin 1977	795.5	795.5	796.6	796.6
0	30.05	310.6	1009.0	Kestin 1977	795.1	795.7	796.9	796.9
0	29.93	140.4	1001.8	Kestin 1977	798.9	797.9	798.3	798.3
0	29.83	1	995.7	Kestin 1977	801.5	800.6	800.1	800.1
0	38.72	1	992.7	Kestin 1977	669.8	669.3	668.7	668.7
0	38.69	16.5	993.4	Kestin 1977	670.5	669.7	669.3	669.3
0	38.63	35.5	994.2	Kestin 1977	670.8	670.6	670.3	670.3
0	38.67	70	995.7	Kestin 1977	670.8	670.4	670.2	670.2
0	38.65	104.4	997.2	Kestin 1977	671.5	670.9	670.9	670.9
0	38.66	139.2	998.7	Kestin 1977	671.6	671.1	671.2	671.2
0	38.65	173.4	1000.2	Kestin 1977	671.6	671.6	671.8	671.8
0	38.61	207.8	1001.6	Kestin 1977	672.2	672.4	672.7	672.7
0	38.62	242.3	1003.1	Kestin 1977	673.5	672.7	673.1	673.1
0	38.62	277.5	1004.5	Kestin 1977	673.5	673.1	673.6	673.6
0	38.62	311.3	1005.9	Kestin 1977	673.4	673.6	674.1	674.1

0	38.5	141	998.8	Kestin 1977	672.8	673.1	673.2	673.2
0	38.41	1	992.8	Kestin 1977	674.2	673.2	672.7	672.7
13.19	18.56	68.9	1098.1	Kestin 1977	1327.0	1444.9	1408.2	1336.3
13.19	18.56	68.9	1098.1	Kestin 1977	1324.6	1444.9	1408.2	1336.3
13.19	18.53	138.9	1100.7	Kestin 1977	1331.0	1441.8	1401.9	1334.4
13.19	18.53	138.9	1100.7	Kestin 1977	1329.3	1441.8	1401.9	1334.4
13.19	18.51	242.3	1104.5	Kestin 1977	1334.8	1437.3	1392.7	1331.4
13.19	18.46	274	1105.6	Kestin 1977	1339.8	1437.7	1391.5	1332.0
13.19	18.46	274	1105.6	Kestin 1977	1338.7	1437.7	1391.5	1332.0
13.19	23.3	139.6	1098.7	Kestin 1977	1200.6	1287.6	1258.9	1196.0
13.19	23.27	139.6	1098.7	Kestin 1977	1200.2	1288.5	1259.7	1196.8
13.19	28.55	35.5	1092.6	Kestin 1977	1067.6	1148.0	1131.6	1069.6
13.19	28.55	35.5	1092.6	Kestin 1977	1067.5	1148.0	1131.6	1069.6
13.19	28.57	69.9	1093.9	Kestin 1977	1069.0	1146.9	1129.3	1069.0
13.19	28.57	69.9	1093.9	Kestin 1977	1068.9	1146.9	1129.3	1069.0
13.19	28.7	310.6	1102.4	Kestin 1977	1082.8	1142.0	1116.3	1066.2
13.19	36.3	174.1	1094.0	Kestin 1977	923.4	980.1	967.1	919.2
13.19	36.3	174.1	1094.0	Kestin 1977	924.7	980.1	967.1	919.2
13.19	36.32	206.5	1095.1	Kestin 1977	924.7	980.0	966.2	919.3
13.19	36.32	206.5	1095.1	Kestin 1977	925.0	980.0	966.2	919.3
13.19	36.35	239.7	1096.3	Kestin 1977	926.9	979.9	965.1	919.3
13.19	36.35	239.7	1096.3	Kestin 1977	927.1	979.9	965.1	919.3
19.45	17.99	1	1144.9	Kestin 1977	1631.9	1668.2	1633.1	1630.2
19.45	18.01	1	1144.8	Kestin 1977	1628.5	1667.3	1632.4	1629.4
19.45	18.07	69.3	1146.9	Kestin 1977	1628.8	1659.4	1618.5	1623.1
19.45	18.07	69.3	1146.9	Kestin 1977	1628.4	1659.4	1618.5	1623.1
19.45	18.08	104.2	1148.1	Kestin 1977	1632.5	1656.5	1612.6	1620.8
19.45	18.08	104.2	1148.1	Kestin 1977	1632.0	1656.5	1612.6	1620.8
19.45	18.06	137.9	1149.2	Kestin 1977	1634.5	1655.0	1608.1	1619.9
19.45	18.06	137.9	1149.2	Kestin 1977	1636.8	1655.0	1608.1	1619.9
19.45	18.06	172.8	1150.4	Kestin 1977	1638.9	1652.7	1602.8	1618.2
19.45	18.06	172.8	1150.4	Kestin 1977	1640.2	1652.7	1602.8	1618.2
19.45	18.05	205	1151.5	Kestin 1977	1641.7	1651.2	1598.6	1617.2
19.45	18.05	205	1151.5	Kestin 1977	1644.4	1651.2	1598.6	1617.2
19.45	18.06	274.7	1153.8	Kestin 1977	1648.0	1647.0	1588.7	1613.9
19.45	18.06	274.7	1153.8	Kestin 1977	1648.1	1647.0	1588.7	1613.9
19.45	18.06	307.8	1154.9	Kestin 1977	1651.6	1645.3	1584.5	1612.7
19.45	18.06	307.8	1154.9	Kestin 1977	1652.9	1645.3	1584.5	1612.7
19.45	18.01	1	1144.8	Kestin 1977	1625.3	1667.3	1632.4	1629.4
19.45	23.35	104.1	1145.5	Kestin 1977	1444.2	1460.4	1434.9	1433.8
19.45	23.35	104.1	1145.5	Kestin 1977	1442.3	1460.4	1434.9	1433.8
19.45	23.48	173.4	1147.8	Kestin 1977	1443.3	1453.8	1423.6	1428.2
19.45	23.48	173.4	1147.8	Kestin 1977	1444.2	1453.8	1423.6	1428.2

19.45	23.53	207.1	1148.9	Kestin 1977	1445.1	1451.1	1418.7	1426.0
19.45	23.53	207.1	1148.9	Kestin 1977	1445.5	1451.1	1418.7	1426.0
19.45	23.59	242.3	1150.0	Kestin 1977	1446.5	1448.3	1413.5	1423.6
19.45	23.59	242.3	1150.0	Kestin 1977	1445.9	1448.3	1413.5	1423.6
19.45	23.63	275.4	1151.1	Kestin 1977	1447.1	1446.2	1409.3	1421.9
19.45	23.63	275.4	1151.1	Kestin 1977	1445.6	1446.2	1409.3	1421.9
19.45	23.68	309.8	1152.2	Kestin 1977	1447.8	1443.9	1404.8	1420.0
19.45	27.93	33.6	1141.0	Kestin 1977	1300.6	1320.1	1310.2	1298.9
19.45	27.93	33.6	1141.0	Kestin 1977	1301.0	1320.1	1310.2	1298.9
19.45	27.99	69.8	1142.1	Kestin 1977	1300.8	1317.7	1305.4	1296.9
19.45	28	69.8	1142.1	Kestin 1977	1302.1	1317.4	1305.2	1296.7
19.45	28.05	104	1143.2	Kestin 1977	1302.3	1315.4	1301.0	1295.1
19.45	28.05	104	1143.2	Kestin 1977	1302.0	1315.4	1301.0	1295.1
19.45	28.12	139.6	1144.3	Kestin 1977	1303.3	1312.9	1296.3	1293.0
19.45	28.14	139.6	1144.3	Kestin 1977	1302.4	1312.3	1295.8	1292.5
19.45	28.53	205.1	1146.3	Kestin 1977	1297.1	1300.8	1280.9	1282.0
19.45	28.54	205.1	1146.3	Kestin 1977	1293.5	1300.5	1280.7	1281.7
19.45	28.75	273	1148.5	Kestin 1977	1294.6	1294.4	1270.9	1276.4
19.45	28.83	307.1	1149.6	Kestin 1977	1295.6	1292.2	1266.8	1274.5
19.45	35.51	1	1136.3	Kestin 1977	1115.0	1128.0	1130.4	1114.7
19.45	35.51	1	1136.3	Kestin 1977	1115.6	1128.0	1130.4	1114.7
19.45	35.56	34.7	1137.1	Kestin 1977	1115.8	1127.0	1127.6	1114.0
19.45	35.56	34.7	1137.1	Kestin 1977	1117.7	1127.0	1127.6	1114.0
19.45	35.6	70	1138.2	Kestin 1977	1117.8	1126.3	1125.0	1113.6
19.45	35.6	70	1138.2	Kestin 1977	1117.1	1126.3	1125.0	1113.6
19.45	35.6	70	1138.2	Kestin 1977	1118.3	1126.3	1125.0	1113.6
19.45	35.62	103.8	1139.3	Kestin 1977	1119.2	1126.0	1122.9	1113.6
19.45	35.63	103.8	1139.3	Kestin 1977	1118.9	1125.8	1122.7	1113.4
19.45	35.64	138.3	1140.5	Kestin 1977	1120.1	1125.9	1121.0	1113.7
19.45	35.66	172.3	1141.6	Kestin 1977	1122.7	1125.8	1119.1	1113.8
19.45	35.66	172.3	1141.6	Kestin 1977	1122.5	1125.8	1119.1	1113.8
19.45	35.69	205	1142.7	Kestin 1977	1126.0	1125.5	1117.1	1113.7
19.45	35.69	205	1142.7	Kestin 1977	1126.1	1125.5	1117.1	1113.7
19.45	35.7	274.2	1145.0	Kestin 1977	1128.0	1126.2	1114.3	1114.8
19.45	35.7	274.2	1145.0	Kestin 1977	1127.5	1126.2	1114.3	1114.8
19.45	35.7	304.4	1146.0	Kestin 1977	1131.0	1126.6	1113.3	1115.3
19.45	35.59	107.5	1139.5	Kestin 1977	1121.7	1126.7	1123.4	1114.3
24.7	27.86	33.4	1183.1	Kestin 1977	1549.2	1453.6	1469.8	1569.4
24.7	27.86	33.4	1183.1	Kestin 1977	1549.7	1453.6	1469.8	1569.4
24.7	28.13	139.6	1186.4	Kestin 1977	1548.9	1443.1	1449.3	1559.6
24.7	28.15	139.6	1186.4	Kestin 1977	1550.4	1442.5	1448.7	1558.9
24.7	28.31	238.5	1189.5	Kestin 1977	1557.5	1436.6	1433.8	1553.5
24.7	34.45	70.7	1180.8	Kestin 1977	1356.4	1266.8	1289.9	1370.4

24.7	34.45	70.7	1180.8	Kestin 1977	1357.5	1266.8	1289.9	1370.4
24.7	34.45	138.2	1183.0	Kestin 1977	1362.2	1267.1	1284.6	1371.3
24.7	34.45	138.2	1183.0	Kestin 1977	1362.4	1267.1	1284.6	1371.3
24.7	40.71	70.1	1177.5	Kestin 1977	1201.5	1123.4	1152.0	1217.1
24.7	40.71	70.1	1177.5	Kestin 1977	1202.9	1123.4	1152.0	1217.1
24.7	40.7	241.6	1183.0	Kestin 1977	1218.1	1127.3	1144.0	1222.2
24.7	40.7	241.6	1183.0	Kestin 1977	1219.3	1127.3	1144.0	1222.2
24.7	40.71	276.8	1184.1	Kestin 1977	1223.0	1127.9	1142.3	1223.1
24.7	40.71	276.8	1184.1	Kestin 1977	1222.2	1127.9	1142.3	1223.1
24.7	40.68	308.5	1185.1	Kestin 1977	1222.1	1129.4	1141.7	1224.7
24.7	40.68	308.5	1185.1	Kestin 1977	1224.0	1129.4	1141.7	1224.7
24.7	40.47	1	1175.8	Kestin 1977	1203.6	1127.3	1160.8	1220.7
2.7	18	1	1018.1	Kestin 1978	1089.0	1138.5	1141.9	1095.7
2.7	18	104.8	1022.6	Kestin 1978	1087.0	1133.0	1136.4	1091.7
2.7	18	175.1	1025.7	Kestin 1978	1083.0	1129.8	1133.1	1089.4
2.7	18	264.4	1029.4	Kestin 1978	1085.0	1126.3	1129.4	1086.8
2.7	18	1	1018.1	Kestin 1978	1090.0	1138.5	1141.9	1095.7
2.7	23.5	1	1016.7	Kestin 1978	958.0	996.4	1000.9	960.4
2.7	23.5	174.2	1024.1	Kestin 1978	957.0	992.0	996.3	957.7
2.7	23.5	204.6	1025.3	Kestin 1978	956.0	991.4	995.6	957.3
2.7	23.5	274.4	1028.2	Kestin 1978	956.0	990.2	994.2	956.6
2.7	23.5	157.2	1023.4	Kestin 1978	957.0	992.3	996.7	957.9
2.7	23.5	1	1016.7	Kestin 1978	960.0	996.4	1000.9	960.4
2.7	28	35.8	1016.7	Kestin 1978	871.0	899.8	904.6	868.5
2.7	28	71	1018.2	Kestin 1978	870.0	899.3	904.1	868.4
2.7	28	105.5	1019.7	Kestin 1978	868.0	898.9	903.7	868.2
2.7	28	140.6	1021.2	Kestin 1978	868.0	898.5	903.3	868.1
2.7	28	175.1	1022.6	Kestin 1978	868.0	898.3	902.9	868.0
2.7	28	209.9	1024.1	Kestin 1978	869.0	898.0	902.6	868.0
2.7	28	244.1	1025.5	Kestin 1978	868.0	897.8	902.3	868.0
2.7	28	275.4	1026.8	Kestin 1978	870.0	897.7	902.1	868.0
2.7	28	311.6	1028.2	Kestin 1978	868.0	897.6	901.9	868.1
2.7	28	157.2	1021.9	Kestin 1978	869.0	898.4	903.1	868.1
2.7	28	1	1015.2	Kestin 1978	868.0	900.3	905.2	868.8
2.7	40.5	35.7	1011.9	Kestin 1978	679.0	699.9	704.8	677.6
2.7	40.5	70.8	1013.4	Kestin 1978	679.0	700.3	705.1	678.1
2.7	40.5	105.1	1014.8	Kestin 1978	680.0	700.7	705.4	678.6
2.7	40.5	140.6	1016.3	Kestin 1978	679.0	701.1	705.8	679.1
2.7	40.5	173.4	1017.7	Kestin 1978	681.0	701.5	706.1	679.6
2.7	40.5	207.2	1019.1	Kestin 1978	681.0	702.0	706.5	680.2
2.7	40.5	242.3	1020.5	Kestin 1978	686.0	702.5	706.9	680.8
2.7	40.5	276.1	1021.9	Kestin 1978	680.0	703.0	707.3	681.3
2.7	40.5	311.3	1023.3	Kestin 1978	683.0	703.6	707.7	682.0

2.7	40.5	157.9	1017.1	Kestin 1978	682.0	701.3	705.9	679.4
2.7	40.5	1	1010.4	Kestin 1978	679.0	699.6	704.5	677.1
2.7	54	104.6	1008.6	Kestin 1978	543.0	556.0	560.1	540.1
2.7	69	1	996.2	Kestin 1978	430.0	442.8	446.2	431.3
2.7	69	104.8	1000.7	Kestin 1978	433.0	445.6	448.8	434.2
2.7	69	175.1	1003.6	Kestin 1978	439.0	447.5	450.6	436.1
2.7	69	1	996.2	Kestin 1978	429.0	442.8	446.2	431.3
2.7	84	240.1	997.5	Kestin 1978	363.0	371.7	373.7	363.3
2.7	96	103.1	983.8	Kestin 1978	314.0	320.9	322.7	314.5
2.7	108.5	10.7	970.8	Kestin 1978	274.0	279.7	281.2	274.8
2.7	126	185.1	965.7	Kestin 1978	238.0	243.2	243.7	239.8
2.7	126	165.1	964.8	Kestin 1978	238.0	242.6	243.2	239.2
2.7	148	103.8	943.5	Kestin 1978	200.0	202.8	202.9	200.8
7.91	19	35.5	1057.2	Kestin 1978	1164.0	1268.9	1251.2	1173.1
7.91	19	241.4	1065.4	Kestin 1978	1166.0	1259.2	1237.3	1166.4
7.91	19	1	1055.8	Kestin 1978	1166.0	1270.9	1253.8	1174.4
7.91	19	1	1055.8	Kestin 1978	1161.0	1270.9	1253.8	1174.4
7.91	19	35.5	1057.2	Kestin 1978	1160.0	1268.9	1251.2	1173.1
7.91	25	1	1053.7	Kestin 1978	1024.0	1101.8	1091.3	1022.1
7.91	25	69.8	1056.4	Kestin 1978	1019.0	1100.0	1088.3	1021.1
7.91	25	1	1053.7	Kestin 1978	1020.0	1101.8	1091.3	1022.1
7.91	30	1	1051.7	Kestin 1978	918.0	987.0	980.1	918.5
7.91	30	70	1054.4	Kestin 1978	919.0	986.3	978.3	918.4
7.91	30	104.4	1055.8	Kestin 1978	920.0	986.0	977.5	918.4
7.91	30	205.1	1059.7	Kestin 1978	923.0	985.6	975.5	918.6
7.91	30	1	1051.7	Kestin 1978	920.0	987.0	980.1	918.5
7.91	40.5	1	1047.0	Kestin 1978	751.0	800.7	798.1	749.8
7.91	40.5	157.2	1053.2	Kestin 1978	754.0	802.7	798.0	752.3
7.91	40.5	1	1047.0	Kestin 1978	750.0	800.7	798.1	749.8
7.91	40.5	1	1047.0	Kestin 1978	748.0	800.7	798.1	749.8
7.91	54	1	1040.3	Kestin 1978	598.0	633.8	633.3	598.1
7.91	54	1	1040.3	Kestin 1978	600.0	633.8	633.3	598.1
7.91	70	16.2	1032.0	Kestin 1978	478.0	500.4	500.0	476.2
7.91	70	103.8	1035.6	Kestin 1978	479.0	503.1	502.0	478.9
7.91	78.5	1	1026.4	Kestin 1978	425.0	446.9	446.5	427.2
7.91	78.5	104.6	1030.7	Kestin 1978	429.0	450.3	449.1	430.5
7.91	78.5	139.6	1032.1	Kestin 1978	429.0	451.4	450.0	431.6
7.91	78.5	207.9	1034.9	Kestin 1978	433.0	453.7	451.7	433.7
7.91	78.5	1	1026.4	Kestin 1978	426.0	446.9	446.5	427.2
7.91	78.5	1	1026.4	Kestin 1978	428.0	446.9	446.5	427.2
7.91	98.5	103.8	1017.9	Kestin 1978	343.0	357.7	355.7	345.2
7.91	98.5	242.9	1023.8	Kestin 1978	346.0	362.3	359.4	349.7
7.91	98.5	185.1	1021.4	Kestin 1978	345.0	360.4	357.9	347.8

7.91	120	8.3	998.5	Kestin 1978	278.0	287.4	284.8	280.0
7.91	120	8.3	998.5	Kestin 1978	277.0	287.4	284.8	280.0
7.91	135.5	207.5	995.8	Kestin 1978	251.0	258.4	254.1	253.3
7.91	152	8.4	972.8	Kestin 1978	218.0	222.7	218.7	219.6
7.91	152	108.1	977.7	Kestin 1978	220.0	225.8	221.3	222.7
12.97	25	175.1	1097.6	Kestin 1978	1143.0	1232.4	1205.8	1145.5
12.97	25	310.6	1102.5	Kestin 1978	1147.0	1230.2	1198.7	1144.5
12.97	30.5	1	1089.0	Kestin 1978	1016.0	1096.4	1083.5	1021.8
12.97	30.5	175.1	1095.1	Kestin 1978	1023.0	1095.1	1076.6	1022.0
12.97	30.5	239.6	1097.4	Kestin 1978	1026.0	1095.1	1074.4	1022.3
12.97	30.5	1	1089.0	Kestin 1978	1019.0	1096.4	1083.5	1021.8
12.97	41	209.2	1091.3	Kestin 1978	848.0	893.9	883.4	840.5
12.97	41	308.5	1094.9	Kestin 1978	847.0	895.9	882.9	842.6
12.97	60	70.7	1076.2	Kestin 1978	621.0	650.3	648.5	618.9
12.97	60	206	1081.3	Kestin 1978	624.0	654.7	650.5	623.2
12.97	60	239.6	1082.5	Kestin 1978	626.0	655.8	651.0	624.3
12.97	60	309.2	1085.1	Kestin 1978	631.0	658.2	652.1	626.6
12.97	60	1.4	1073.8	Kestin 1978	616.0	648.1	647.6	616.7
12.97	80	239.6	1071.1	Kestin 1978	483.0	501.2	497.5	483.0
12.97	80	1.7	1062.1	Kestin 1978	474.0	492.4	491.9	474.5
12.97	101	139.9	1053.9	Kestin 1978	382.0	392.5	389.0	382.9
12.97	121	6.5	1034.7	Kestin 1978	314.0	319.7	315.9	315.1
12.97	121	36.2	1035.8	Kestin 1978	315.0	320.8	316.7	316.1
12.97	121	68.9	1037.2	Kestin 1978	315.0	322.0	317.6	317.3
12.97	121	103.8	1038.6	Kestin 1978	315.0	323.2	318.5	318.6
12.97	121	139.6	1040.2	Kestin 1978	317.0	324.5	319.5	319.8
12.97	121	172.7	1041.5	Kestin 1978	319.0	325.7	320.3	321.0
12.97	121	205.4	1042.9	Kestin 1978	320.0	326.9	321.2	322.2
12.97	121	238.2	1044.3	Kestin 1978	321.0	328.1	322.1	323.3
12.97	121	272.7	1045.7	Kestin 1978	322.0	329.3	323.0	324.5
12.97	121	306.5	1047.1	Kestin 1978	323.0	330.5	323.9	325.7
12.97	121	10.7	1034.8	Kestin 1978	313.0	319.9	316.0	315.2
12.97	136	68.6	1026.0	Kestin 1978	279.0	284.1	278.4	281.9
12.97	136	139.6	1029.1	Kestin 1978	281.0	286.6	280.3	284.4
12.97	136	175.1	1030.7	Kestin 1978	283.0	287.8	281.3	285.6
16.03	19.5	1	1117.3	Kestin 1978	1401.0	1502.4	1468.9	1414.4
16.03	19.5	104.8	1120.7	Kestin 1978	1405.0	1496.0	1456.1	1410.0
16.03	19.5	1	1117.3	Kestin 1978	1403.0	1502.4	1468.9	1414.4
16.03	25	139.6	1119.4	Kestin 1978	1241.0	1314.6	1287.2	1244.6
16.03	25	173.7	1120.6	Kestin 1978	1242.0	1313.8	1284.7	1244.1
16.03	25	175.1	1120.7	Kestin 1978	1248.0	1313.8	1284.6	1244.1
16.03	31	1	1112.0	Kestin 1978	1096.0	1156.6	1145.8	1098.4
16.03	31	104.8	1115.4	Kestin 1978	1100.0	1155.8	1140.3	1098.6

16.03	31	139.6	1116.6	Kestin 1978	1101.0	1155.6	1138.6	1098.7
16.03	31	242.6	1120.1	Kestin 1978	1106.0	1155.6	1134.1	1099.3
16.03	31	1	1112.0	Kestin 1978	1095.0	1156.6	1145.8	1098.4
16.03	40	1	1107.5	Kestin 1978	926.0	967.4	964.6	924.7
16.03	40	209.2	1114.5	Kestin 1978	934.0	970.5	960.3	928.7
16.03	40	171.7	1113.2	Kestin 1978	931.0	969.9	961.0	928.0
16.03	40	1	1107.5	Kestin 1978	924.0	967.4	964.6	924.7
16.03	55	1	1099.5	Kestin 1978	723.0	746.6	749.0	720.9
16.03	55	1	1099.5	Kestin 1978	724.0	746.6	749.0	720.9
16.03	55	159.6	1104.9	Kestin 1978	730.0	751.5	749.8	726.0
16.03	55	1	1099.5	Kestin 1978	725.0	746.6	749.0	720.9
16.03	70	7.9	1091.1	Kestin 1978	584.0	598.6	601.5	583.5
16.03	70	7.9	1091.1	Kestin 1978	586.0	598.6	601.5	583.5
16.03	70	139.6	1095.7	Kestin 1978	590.0	603.5	603.8	588.4
16.03	84	139.6	1087.4	Kestin 1978	498.0	505.2	505.0	496.6
16.03	98.5	104.1	1076.9	Kestin 1978	425.0	428.1	427.0	424.2
16.03	113	8.8	1063.6	Kestin 1978	366.0	366.9	365.2	366.2
16.03	113	206.7	1071.2	Kestin 1978	372.0	374.6	370.5	373.9
16.03	113	163.2	1069.5	Kestin 1978	370.0	372.9	369.4	372.2
16.03	113	8.8	1063.6	Kestin 1978	365.0	366.9	365.2	366.2
16.03	131.5	104.8	1054.0	Kestin 1978	314.0	315.3	310.3	317.5
16.03	131.5	175.1	1056.9	Kestin 1978	318.0	318.0	312.2	320.2
16.03	131.5	10.7	1050.3	Kestin 1978	312.0	311.8	307.8	313.9
16.03	154	8.1	1032.7	Kestin 1978	265.0	262.8	256.4	266.9
16.03	154	10.3	1032.8	Kestin 1978	265.0	262.9	256.5	267.0
16.03	154	106.2	1036.8	Kestin 1978	268.0	266.4	259.0	270.6
16.03	154	139.6	1038.3	Kestin 1978	270.0	267.7	259.9	271.9
16.03	154	161.7	1039.3	Kestin 1978	269.0	268.5	260.5	272.7
16.03	154	16.9	1033.0	Kestin 1978	266.0	263.1	256.6	267.2
20.56	25.5	1	1150.1	Kestin 1978	1412.0	1423.5	1414.9	1420.7
20.56	25.5	106.3	1153.3	Kestin 1978	1419.0	1420.2	1403.3	1418.9
20.56	25.5	243.7	1157.8	Kestin 1978	1431.0	1417.2	1390.0	1417.3
20.56	25.5	1	1150.1	Kestin 1978	1413.0	1423.5	1414.9	1420.7
20.56	25.5	1	1150.1	Kestin 1978	1410.0	1423.5	1414.9	1420.7
20.56	35	105.1	1148.4	Kestin 1978	1176.0	1163.8	1163.7	1168.6
20.56	35.5	107.3	1148.2	Kestin 1978	1157.0	1152.4	1152.7	1157.5
20.56	35.5	139.6	1149.3	Kestin 1978	1158.0	1152.7	1151.1	1158.0
20.56	35.5	173.7	1150.4	Kestin 1978	1161.0	1153.0	1149.4	1158.6
20.56	35.5	157.2	1149.9	Kestin 1978	1160.0	1152.9	1150.2	1158.3
20.56	35.5	1	1145.0	Kestin 1978	1151.0	1152.0	1158.6	1156.2
20.56	35.5	1	1145.0	Kestin 1978	1152.0	1152.0	1158.6	1156.2
20.56	45	1	1140.1	Kestin 1978	974.0	964.1	976.8	972.5
20.56	45	141	1144.3	Kestin 1978	980.0	967.4	973.5	976.5

20.56	45	274.2	1148.7	Kestin 1978	988.0	971.0	971.1	980.6
20.56	45	159.6	1144.9	Kestin 1978	981.0	967.9	973.1	977.1
20.56	45	1	1140.1	Kestin 1978	970.0	964.1	976.8	972.5
20.56	45	1	1140.1	Kestin 1978	973.0	964.1	976.8	972.5
20.56	56	1	1134.1	Kestin 1978	818.0	802.3	817.2	813.8
20.56	56	174.8	1139.5	Kestin 1978	826.0	808.4	816.8	820.4
20.56	56	1	1134.1	Kestin 1978	814.0	802.3	817.2	813.8
20.56	71	7.9	1125.6	Kestin 1978	662.0	644.6	658.3	658.6
20.56	71	104.6	1128.6	Kestin 1978	664.0	648.6	659.5	662.8
20.56	71	139.6	1129.7	Kestin 1978	666.0	650.1	660.0	664.3
20.56	71	175.1	1131.0	Kestin 1978	670.0	651.5	660.5	665.9
20.56	71	7.9	1125.6	Kestin 1978	663.0	644.6	658.3	658.6
20.56	85	10	1117.2	Kestin 1978	558.0	539.5	550.4	554.7
20.56	85	311.3	1127.4	Kestin 1978	570.0	552.5	556.7	568.2
20.56	97	105	1112.7	Kestin 1978	493.0	474.9	481.2	490.9
20.56	97	142.2	1114.0	Kestin 1978	494.0	476.5	482.1	492.6
20.56	97	239.6	1117.5	Kestin 1978	498.0	480.8	484.5	496.9
20.56	114	174.6	1104.0	Kestin 1978	419.0	403.8	405.3	420.3
24	27.5	209.6	1183.3	Kestin 1978	1545.0	1444.2	1438.2	1538.0
24	27.5	156.2	1181.5	Kestin 1978	1536.0	1444.9	1443.8	1538.3
24	44.5	1	1168.0	Kestin 1978	1092.0	1034.8	1065.2	1106.0
24	44.5	1	1168.0	Kestin 1978	1096.0	1034.8	1065.2	1106.0
24	60	1	1159.5	Kestin 1978	854.0	802.5	832.9	861.7
24	60	137.2	1163.4	Kestin 1978	862.0	807.8	832.3	867.8
24	80	110.6	1150.9	Kestin 1978	654.0	614.6	636.0	664.0
24	94	209.2	1145.6	Kestin 1978	567.0	526.7	541.2	571.3
24	94	161.7	1144.0	Kestin 1978	562.0	524.5	540.2	568.9
5.86	24	1	1039.2	Kestin 1984	1000.5	1071.3	1066.3	1003.8
5.86	24	1	1039.2	Kestin 1984	1001.5	1071.3	1066.3	1003.8
5.86	24	52	1041.3	Kestin 1984	999.9	1069.8	1064.3	1002.9
5.86	24	107	1043.5	Kestin 1984	999.5	1068.3	1062.2	1002.0
5.86	24	156	1045.5	Kestin 1984	1000.0	1067.2	1060.5	1001.4
5.86	24	207	1047.6	Kestin 1984	1001.9	1066.2	1058.9	1000.8
5.86	24	257	1049.5	Kestin 1984	1001.2	1065.3	1057.4	1000.3
5.86	24	307	1051.5	Kestin 1984	1002.7	1064.6	1056.1	999.9
5.86	28.1	1	1037.7	Kestin 1984	916.4	977.1	974.2	917.4
5.86	28.1	1	1037.7	Kestin 1984	917.6	977.1	974.2	917.4
5.86	28.1	54	1039.9	Kestin 1984	916.2	976.3	972.9	917.1
5.86	28.1	104	1041.9	Kestin 1984	916.4	975.6	971.7	916.9
5.86	28.1	155	1044.0	Kestin 1984	917.5	975.1	970.6	916.7
5.86	28.1	206	1046.0	Kestin 1984	918.7	974.7	969.7	916.7
5.86	28.1	254	1047.9	Kestin 1984	920.6	974.4	968.9	916.7
5.86	28.1	303	1049.8	Kestin 1984	921.0	974.3	968.2	916.8

5.86	34	2	1035.3	Kestin 1984	815.0	863.3	862.3	812.9
5.86	34	11	1035.7	Kestin 1984	813.8	863.3	862.2	812.9
5.86	34	53	1037.4	Kestin 1984	814.8	863.3	861.8	813.2
5.86	34	103	1039.5	Kestin 1984	815.8	863.3	861.4	813.6
5.86	34	154	1041.5	Kestin 1984	815.9	863.5	861.1	814.0
5.86	34	205	1043.6	Kestin 1984	817.8	863.7	860.9	814.4
5.86	34	254	1045.5	Kestin 1984	819.4	864.1	860.7	814.9
5.86	34	303	1047.4	Kestin 1984	821.2	864.5	860.6	815.5
5.86	40.5	2	1032.5	Kestin 1984	721.3	760.9	761.2	718.7
5.86	40.5	3	1032.5	Kestin 1984	721.8	760.9	761.2	718.7
5.86	40.5	52	1034.5	Kestin 1984	721.3	761.5	761.4	719.5
5.86	40.5	104	1036.7	Kestin 1984	724.2	762.1	761.6	720.3
5.86	40.5	155	1038.7	Kestin 1984	723.6	762.8	761.8	721.1
5.86	40.5	209	1040.9	Kestin 1984	726.1	763.6	762.1	722.0
5.86	40.5	256	1042.8	Kestin 1984	728.4	764.3	762.4	722.9
5.86	40.5	305	1044.7	Kestin 1984	728.6	765.2	762.8	723.8
5.86	49.3	2	1028.3	Kestin 1984	622.1	650.9	652.0	617.3
5.86	49.3	2	1028.3	Kestin 1984	620.3	650.9	652.0	617.3
5.86	49.3	54	1030.4	Kestin 1984	622.5	651.9	652.6	618.4
5.86	49.3	105	1032.5	Kestin 1984	623.7	653.0	653.3	619.6
5.86	49.3	156	1034.6	Kestin 1984	625.5	654.1	654.1	620.7
5.86	49.3	204	1036.6	Kestin 1984	627.4	655.2	654.8	621.9
5.86	49.3	255	1038.6	Kestin 1984	628.0	656.4	655.6	623.1
5.86	49.3	305	1040.5	Kestin 1984	628.9	657.6	656.4	624.3
5.86	65	3	1020.0	Kestin 1984	491.7	509.6	510.9	486.7
5.86	65	3	1020.0	Kestin 1984	491.6	509.6	510.9	486.7
5.86	65	56	1022.2	Kestin 1984	493.1	511.1	512.1	488.2
5.86	65	105	1024.3	Kestin 1984	493.4	512.5	513.2	489.6
5.86	65	156	1026.4	Kestin 1984	495.9	514.0	514.3	491.0
5.86	65	205	1028.4	Kestin 1984	497.5	515.5	515.4	492.4
5.86	65	256	1030.5	Kestin 1984	499.7	517.0	516.6	493.9
5.86	65	302	1032.3	Kestin 1984	501.8	518.4	517.7	495.2
5.86	97.2	4	1000.2	Kestin 1984	333.6	341.5	341.4	330.4
5.86	97.2	5	1000.2	Kestin 1984	333.5	341.5	341.4	330.4
5.86	97.2	53	1002.3	Kestin 1984	335.1	343.0	342.7	331.9
5.86	97.2	104	1004.5	Kestin 1984	335.3	344.6	344.1	333.5
5.86	97.2	154	1006.7	Kestin 1984	337.5	346.2	345.4	335.0
5.86	97.2	206	1008.9	Kestin 1984	339.4	347.8	346.8	336.6
5.86	97.2	255	1011.0	Kestin 1984	340.8	349.4	348.1	338.1
5.86	97.2	302	1013.0	Kestin 1984	342.2	350.9	349.4	339.5
5.86	127	8	978.6	Kestin 1984	252.7	256.9	255.4	251.3
5.86	127	9	978.6	Kestin 1984	252.9	256.9	255.4	251.3
5.86	127	54	980.7	Kestin 1984	254.1	258.3	256.6	252.7

5.86	127	104	983.1	Kestin 1984	255.6	259.8	258.0	254.2
5.86	127	154	985.4	Kestin 1984	256.9	261.4	259.3	255.7
5.86	127	208	987.9	Kestin 1984	258.0	263.0	260.7	257.2
5.86	127	257	990.1	Kestin 1984	259.0	264.5	262.0	258.7
5.86	127	306	992.3	Kestin 1984	261.1	265.9	263.3	260.1
5.86	148.5	8	960.8	Kestin 1984	213.3	217.0	214.7	213.7
5.86	148.5	9	960.9	Kestin 1984	213.5	217.0	214.7	213.7
5.86	148.5	55	963.2	Kestin 1984	215.1	218.4	215.9	215.1
5.86	148.5	103	965.6	Kestin 1984	216.1	219.8	217.2	216.5
5.86	148.5	163	968.6	Kestin 1984	217.2	221.6	218.7	218.2
5.86	148.5	201	970.5	Kestin 1984	219.4	222.7	219.7	219.3
5.86	148.5	256	973.2	Kestin 1984	220.1	224.3	221.1	220.9
5.86	148.5	306	975.6	Kestin 1984	221.5	225.7	222.3	222.3
5.86	173	15	938.8	Kestin 1984	182.3	184.3	181.4	182.7
5.86	173	17	938.9	Kestin 1984	181.7	184.4	181.4	182.8
5.86	173	67	941.7	Kestin 1984	183.7	185.9	182.7	184.2
5.86	173	71	942.0	Kestin 1984	184.2	186.0	182.8	184.3
5.86	173	121	944.8	Kestin 1984	184.2	187.4	184.1	185.8
5.86	173	169	947.4	Kestin 1984	185.6	188.8	185.2	187.1
5.86	173	220	950.2	Kestin 1984	187.6	190.2	186.5	188.6
5.86	173	296	954.3	Kestin 1984	189.6	192.3	188.4	190.7
5.86	199	22	912.8	Kestin 1984	158.3	159.0	155.7	158.4
5.86	199	29	913.3	Kestin 1984	158.5	159.2	155.8	158.6
5.86	199	78	916.5	Kestin 1984	159.5	160.6	157.1	160.0
5.86	199	122	919.3	Kestin 1984	160.9	161.9	158.1	161.3
5.86	199	128	919.7	Kestin 1984	160.6	162.0	158.3	161.5
5.86	199	182	923.1	Kestin 1984	162.8	163.6	159.6	163.0
5.86	199	239	926.6	Kestin 1984	163.6	165.1	161.0	164.6
5.86	199	303	930.5	Kestin 1984	165.1	166.9	162.5	166.3
10.54	24	8	1073.8	Kestin 1984	1094.4	1199.0	1180.9	1106.6
10.54	24	8	1073.8	Kestin 1984	1097.7	1199.0	1180.9	1106.6
10.54	24	58	1075.7	Kestin 1984	1095.4	1197.4	1177.8	1105.7
10.54	24	107	1077.5	Kestin 1984	1097.7	1195.9	1175.0	1104.8
10.54	24	157	1079.4	Kestin 1984	1098.5	1194.6	1172.3	1104.1
10.54	24	211	1081.4	Kestin 1984	1100.0	1193.4	1169.5	1103.4
10.54	24	261	1083.3	Kestin 1984	1101.5	1192.4	1167.2	1102.9
10.54	24	308	1085.0	Kestin 1984	1103.8	1191.7	1165.2	1102.5
10.54	29	5	1071.6	Kestin 1984	986.0	1072.6	1060.2	993.5
10.54	29	7	1071.7	Kestin 1984	986.2	1072.6	1060.1	993.5
10.54	29	55	1073.4	Kestin 1984	988.5	1071.9	1058.2	993.3
10.54	29	104	1075.3	Kestin 1984	989.3	1071.3	1056.4	993.2
10.54	29	156	1077.2	Kestin 1984	991.1	1070.8	1054.7	993.1
10.54	29	207	1079.1	Kestin 1984	992.0	1070.5	1053.1	993.2

10.54	29	259	1081.1	Kestin 1984	994.0	1070.3	1051.6	993.3
10.54	29	308	1082.9	Kestin 1984	995.4	1070.3	1050.4	993.5
10.54	34.8	6	1069.0	Kestin 1984	881.9	951.0	942.9	884.5
10.54	34.8	11	1069.2	Kestin 1984	882.1	951.0	942.8	884.5
10.54	34.8	54	1070.8	Kestin 1984	883.6	951.0	941.9	884.9
10.54	34.8	106	1072.8	Kestin 1984	884.7	951.2	940.9	885.3
10.54	34.8	156	1074.6	Kestin 1984	886.4	951.4	940.1	885.9
10.54	34.8	207	1076.5	Kestin 1984	888.3	951.8	939.4	886.4
10.54	34.8	256	1078.4	Kestin 1984	889.5	952.3	938.8	887.1
10.54	34.8	306	1080.2	Kestin 1984	891.5	952.8	938.2	887.7
10.54	40.2	6	1066.4	Kestin 1984	800.5	856.6	851.3	799.7
10.54	40.2	11	1066.6	Kestin 1984	801.3	856.7	851.3	799.8
10.54	40.2	54	1068.2	Kestin 1984	802.1	857.2	850.9	800.5
10.54	40.2	105	1070.2	Kestin 1984	802.1	857.8	850.6	801.3
10.54	40.2	156	1072.1	Kestin 1984	804.8	858.6	850.3	802.2
10.54	40.2	207	1074.0	Kestin 1984	806.0	859.4	850.2	803.2
10.54	40.2	256	1075.8	Kestin 1984	808.3	860.3	850.1	804.1
10.54	40.2	306	1077.7	Kestin 1984	810.1	861.2	850.0	805.1
10.54	49.8	7	1061.6	Kestin 1984	682.2	722.6	720.0	678.9
10.54	49.8	10	1061.7	Kestin 1984	682.7	722.6	720.0	678.9
10.54	49.8	54	1063.4	Kestin 1984	683.7	723.7	720.3	680.0
10.54	49.8	107	1065.4	Kestin 1984	686.5	724.9	720.8	681.4
10.54	49.8	157	1067.4	Kestin 1984	687.8	726.2	721.2	682.7
10.54	49.8	208	1069.3	Kestin 1984	689.2	727.5	721.7	684.0
10.54	49.8	260	1071.2	Kestin 1984	690.0	728.9	722.2	685.4
10.54	49.8	305	1072.9	Kestin 1984	692.0	730.2	722.7	686.6
10.54	66.1	5	1052.6	Kestin 1984	539.6	561.7	560.7	533.1
10.54	66.1	10	1052.8	Kestin 1984	539.6	561.8	560.8	533.3
10.54	66.1	55	1054.5	Kestin 1984	540.8	563.3	561.6	534.7
10.54	66.1	106	1056.6	Kestin 1984	542.5	564.9	562.7	536.3
10.54	66.1	158	1058.6	Kestin 1984	544.0	566.6	563.7	538.0
10.54	66.1	205	1060.4	Kestin 1984	545.7	568.2	564.7	539.5
10.54	66.1	254	1062.3	Kestin 1984	547.6	569.8	565.7	541.1
10.54	66.1	306	1064.3	Kestin 1984	549.3	571.6	566.8	542.7
10.54	90.2	7	1038.1	Kestin 1984	403.6	413.2	411.6	397.7
10.54	90.2	12	1038.2	Kestin 1984	403.3	413.4	411.7	397.9
10.54	90.2	55	1040.0	Kestin 1984	404.6	414.9	412.8	399.4
10.54	90.2	105	1042.0	Kestin 1984	406.1	416.6	414.1	401.1
10.54	90.2	156	1044.1	Kestin 1984	408.0	418.5	415.4	402.8
10.54	90.2	206	1046.1	Kestin 1984	410.2	420.2	416.7	404.5
10.54	90.2	256	1048.1	Kestin 1984	411.0	422.0	418.0	406.2
10.54	90.2	307	1050.1	Kestin 1984	412.9	423.8	419.3	407.9
10.54	125.7	18	1013.7	Kestin 1984	288.3	291.1	287.1	285.3

10.54	125.7	21	1013.8	Kestin 1984	289.8	291.2	287.2	285.4
10.54	125.7	77	1016.2	Kestin 1984	289.8	293.2	288.7	287.3
10.54	125.7	135	1018.8	Kestin 1984	291.5	295.1	290.2	289.2
10.54	125.7	195	1021.4	Kestin 1984	294.5	297.2	291.8	291.2
10.54	125.7	264	1024.4	Kestin 1984	296.7	299.5	293.7	293.5
10.54	125.7	312	1026.5	Kestin 1984	298.5	301.1	294.9	295.0
10.54	149.4	25	995.2	Kestin 1984	240.8	241.9	236.4	239.4
10.54	149.4	30	995.5	Kestin 1984	240.7	242.1	236.5	239.6
10.54	149.4	79	997.8	Kestin 1984	242.5	243.7	237.8	241.2
10.54	149.4	134	1000.4	Kestin 1984	243.5	245.5	239.3	243.0
10.54	149.4	196	1003.3	Kestin 1984	245.2	247.5	240.9	245.0
10.54	149.4	257	1006.2	Kestin 1984	247.2	249.5	242.5	246.9
10.54	149.4	314	1008.8	Kestin 1984	248.5	251.3	243.9	248.7
17.04	24.2	52	1124.6	Kestin 1984	1297.5	1368.7	1344.9	1306.0
17.04	24.2	104	1126.3	Kestin 1984	1301.5	1366.9	1340.1	1305.0
17.04	24.2	155	1128.1	Kestin 1984	1301.4	1365.4	1335.6	1304.1
17.04	24.2	206	1129.8	Kestin 1984	1305.8	1364.2	1331.4	1303.4
17.04	24.2	258	1131.6	Kestin 1984	1307.0	1363.0	1327.4	1302.8
17.04	24.2	308	1133.3	Kestin 1984	1312.0	1362.2	1323.8	1302.3
17.04	27.9	51	1122.8	Kestin 1984	1198.1	1260.3	1243.9	1205.8
17.04	27.9	105	1124.6	Kestin 1984	1198.8	1259.4	1240.1	1205.4
17.04	27.9	155	1126.3	Kestin 1984	1202.7	1258.7	1236.7	1205.2
17.04	27.9	206	1128.0	Kestin 1984	1205.2	1258.1	1233.6	1205.1
17.04	27.9	254	1129.7	Kestin 1984	1208.8	1257.7	1230.7	1205.1
17.04	27.9	307	1131.5	Kestin 1984	1210.8	1257.5	1227.9	1205.2
17.04	34.5	54	1119.6	Kestin 1984	1049.0	1098.5	1090.8	1055.8
17.04	34.5	104	1121.3	Kestin 1984	1052.2	1098.6	1088.7	1056.3
17.04	34.5	156	1123.1	Kestin 1984	1054.6	1098.9	1086.7	1056.9
17.04	34.5	207	1124.8	Kestin 1984	1059.0	1099.3	1084.8	1057.6
17.04	34.5	259	1126.6	Kestin 1984	1060.7	1099.8	1083.1	1058.3
17.04	34.5	307	1128.2	Kestin 1984	1063.0	1100.4	1081.7	1059.1
17.04	40.5	55	1116.6	Kestin 1984	941.4	978.7	976.1	944.5
17.04	40.5	105	1118.3	Kestin 1984	943.2	979.5	974.9	945.5
17.04	40.5	154	1120.0	Kestin 1984	945.7	980.3	973.8	946.6
17.04	40.5	206	1121.7	Kestin 1984	948.0	981.3	972.8	947.7
17.04	40.5	253	1123.4	Kestin 1984	950.8	982.3	972.0	948.8
17.04	40.5	304	1125.1	Kestin 1984	952.9	983.4	971.3	950.0
17.04	50	52	1111.5	Kestin 1984	804.2	828.1	829.8	804.0
17.04	50	105	1113.3	Kestin 1984	806.7	829.5	829.6	805.6
17.04	50	156	1115.0	Kestin 1984	808.5	831.0	829.5	807.2
17.04	50	205	1116.7	Kestin 1984	809.8	832.5	829.4	808.7
17.04	50	256	1118.5	Kestin 1984	812.7	834.0	829.5	810.3
17.04	50	307	1120.3	Kestin 1984	815.3	835.7	829.5	812.0

17.04	65.2	9	1101.6	Kestin 1984	643.5	653.4	658.2	640.3
17.04	65.2	10	1101.7	Kestin 1984	643.5	653.4	658.2	640.3
17.04	65.2	54	1103.1	Kestin 1984	645.6	655.0	658.7	642.0
17.04	65.2	105	1104.9	Kestin 1984	648.1	656.9	659.4	643.9
17.04	65.2	154	1106.6	Kestin 1984	650.0	658.7	660.1	645.7
17.04	65.2	207	1108.5	Kestin 1984	652.8	660.7	660.8	647.8
17.04	65.2	256	1110.2	Kestin 1984	654.0	662.6	661.6	649.6
17.04	65.2	305	1111.9	Kestin 1984	656.5	664.5	662.4	651.5
17.04	90	6	1086.5	Kestin 1984	478.8	475.5	478.2	472.6
17.04	90	8	1086.6	Kestin 1984	479.2	475.5	478.2	472.7
17.04	90	52	1088.0	Kestin 1984	480.8	477.3	479.3	474.5
17.04	90	105	1090.0	Kestin 1984	482.1	479.5	480.5	476.6
17.04	90	154	1091.8	Kestin 1984	484.4	481.4	481.7	478.6
17.04	90	204	1093.6	Kestin 1984	485.8	483.5	482.9	480.6
17.04	90	257	1095.6	Kestin 1984	488.3	485.6	484.2	482.8
17.04	90	304	1097.3	Kestin 1984	489.6	487.6	485.3	484.6
17.04	126	19	1062.4	Kestin 1984	341.8	333.5	330.7	337.3
17.04	126	22	1062.5	Kestin 1984	343.7	333.6	330.8	337.5
17.04	126	56	1063.8	Kestin 1984	344.8	334.9	331.7	338.8
17.04	126	105	1065.7	Kestin 1984	346.5	336.8	333.1	340.8
17.04	126	154	1067.7	Kestin 1984	346.5	338.7	334.4	342.7
17.04	126	204	1069.7	Kestin 1984	348.4	340.7	335.7	344.6
17.04	126	255	1071.8	Kestin 1984	350.2	342.7	337.1	346.6
17.04	126	304	1073.7	Kestin 1984	352.0	344.5	338.4	348.5
20.65	24.2	5	1151.5	Kestin 1984	1450.1	1468.7	1457.0	1466.8
20.65	24.2	9	1151.6	Kestin 1984	1449.0	1468.5	1456.5	1466.7
20.65	24.2	55	1153.0	Kestin 1984	1455.3	1466.7	1450.8	1465.6
20.65	24.2	105	1154.6	Kestin 1984	1457.9	1464.9	1444.9	1464.5
20.65	24.2	155	1156.3	Kestin 1984	1460.0	1463.3	1439.4	1463.5
20.65	24.2	208	1158.0	Kestin 1984	1464.3	1461.9	1433.8	1462.7
20.65	24.2	256	1159.6	Kestin 1984	1467.2	1460.8	1429.0	1462.1
20.65	24.2	311	1161.4	Kestin 1984	1474.0	1459.7	1423.9	1461.5
20.65	29.2	3	1149.0	Kestin 1984	1300.4	1314.1	1312.9	1316.2
20.65	29.2	3	1149.0	Kestin 1984	1302.3	1314.1	1312.9	1316.2
20.65	29.2	55	1150.5	Kestin 1984	1304.3	1313.2	1308.3	1315.9
20.65	29.2	103	1152.0	Kestin 1984	1306.7	1312.6	1304.2	1315.8
20.65	29.2	157	1153.8	Kestin 1984	1311.4	1312.0	1299.9	1315.7
20.65	29.2	207	1155.5	Kestin 1984	1315.5	1311.7	1296.2	1315.8
20.65	29.2	259	1157.2	Kestin 1984	1319.9	1311.5	1292.5	1316.0
20.65	29.2	312	1158.9	Kestin 1984	1323.4	1311.5	1289.1	1316.3
20.65	35.8	4	1145.6	Kestin 1984	1143.4	1147.1	1154.2	1153.0
20.65	35.8	6	1145.7	Kestin 1984	1144.4	1147.1	1154.1	1153.0
20.65	35.8	54	1147.0	Kestin 1984	1146.6	1147.3	1151.4	1153.7

20.65	35.8	106	1148.7	Kestin 1984	1149.6	1147.6	1148.6	1154.4
20.65	35.8	159	1150.5	Kestin 1984	1154.0	1148.1	1146.0	1155.2
20.65	35.8	210	1152.1	Kestin 1984	1156.9	1148.7	1143.7	1156.1
20.65	35.8	253	1153.6	Kestin 1984	1160.3	1149.3	1141.9	1156.9
20.65	35.8	304	1155.2	Kestin 1984	1163.4	1150.0	1139.8	1157.9
20.65	40.8	3	1143.0	Kestin 1984	1041.2	1042.2	1053.3	1050.4
20.65	40.8	3	1143.0	Kestin 1984	1040.9	1042.2	1053.3	1050.4
20.65	40.8	54	1144.4	Kestin 1984	1044.0	1043.0	1051.3	1051.6
20.65	40.8	99	1145.9	Kestin 1984	1046.8	1043.8	1049.7	1052.6
20.65	40.8	155	1147.7	Kestin 1984	1049.7	1044.8	1047.9	1054.0
20.65	40.8	207	1149.4	Kestin 1984	1052.9	1045.9	1046.3	1055.3
20.65	40.8	258	1151.1	Kestin 1984	1055.7	1047.1	1044.9	1056.6
20.65	40.8	306	1152.7	Kestin 1984	1059.8	1048.2	1043.8	1057.9
20.65	50.4	6	1137.9	Kestin 1984	886.9	880.2	894.6	891.5
20.65	50.4	11	1138.0	Kestin 1984	888.5	880.3	894.5	891.6
20.65	50.4	52	1139.2	Kestin 1984	889.6	881.5	893.9	893.0
20.65	50.4	107	1141.0	Kestin 1984	892.9	883.2	893.3	894.9
20.65	50.4	154	1142.5	Kestin 1984	894.7	884.6	892.8	896.5
20.65	50.4	209	1144.4	Kestin 1984	897.8	886.4	892.3	898.4
20.65	50.4	257	1146.0	Kestin 1984	901.1	888.0	892.0	900.2
20.65	50.4	308	1147.7	Kestin 1984	904.0	889.8	891.8	902.0
20.65	65.1	7	1129.7	Kestin 1984	716.1	701.1	715.8	715.2
20.65	65.1	10	1129.8	Kestin 1984	716.3	701.2	715.8	715.3
20.65	65.1	55	1131.1	Kestin 1984	718.0	703.0	716.2	717.2
20.65	65.1	106	1132.7	Kestin 1984	721.8	705.0	716.6	719.3
20.65	65.1	157	1134.4	Kestin 1984	723.3	707.0	717.0	721.5
20.65	65.1	208	1136.2	Kestin 1984	726.1	709.1	717.5	723.6
20.65	65.1	259	1137.9	Kestin 1984	728.4	711.2	718.1	725.8
20.65	65.1	308	1139.6	Kestin 1984	730.5	713.3	718.7	727.9
20.65	89.8	8	1114.9	Kestin 1984	532.8	510.8	520.9	526.9
20.65	89.8	54	1116.2	Kestin 1984	534.6	512.8	521.9	529.0
20.65	89.8	106	1118.0	Kestin 1984	537.0	515.0	523.0	531.4
20.65	89.8	156	1119.7	Kestin 1984	539.3	517.2	524.2	533.6
20.65	89.8	210	1121.6	Kestin 1984	541.7	519.6	525.4	536.0
20.65	89.8	259	1123.4	Kestin 1984	545.2	521.7	526.5	538.2
20.65	89.8	310	1125.2	Kestin 1984	547.3	523.9	527.7	540.5
26.08	34.5	24	1190.8	Kestin 1984	1455.4	1295.5	1333.3	**
26.08	34.5	49	1191.5	Kestin 1984	1457.2	1295.6	1331.0	**
26.08	34.5	101	1193.2	Kestin 1984	1464.0	1295.7	1326.3	**
26.08	34.5	151	1194.8	Kestin 1984	1468.8	1296.0	1322.1	**
26.08	34.5	203	1196.4	Kestin 1984	1473.6	1296.5	1317.9	**
26.08	34.5	254	1198.0	Kestin 1984	1479.5	1297.1	1314.1	**
26.08	34.5	304	1199.6	Kestin 1984	1484.7	1297.8	1310.6	**

26.08	40	29	1188.0	Kestin 1984	1306.7	1164.7	1206.1	**
26.08	40	31	1188.1	Kestin 1984	1306.5	1164.8	1206.0	**
26.08	40	53	1188.7	Kestin 1984	1308.9	1165.1	1204.5	**
26.08	40	103	1190.3	Kestin 1984	1314.1	1166.0	1201.4	**
26.08	40	156	1192.0	Kestin 1984	1318.3	1167.0	1198.2	**
26.08	40	202	1193.4	Kestin 1984	1323.0	1168.0	1195.7	**
26.08	40	258	1195.2	Kestin 1984	1328.0	1169.3	1192.8	**
26.08	40	307	1196.7	Kestin 1984	1332.6	1170.5	1190.5	**
26.08	50.5	4	1181.9	Kestin 1984	1090.0	967.0	1012.0	**
26.08	50.5	7	1181.9	Kestin 1984	1092.8	967.1	1011.9	**
26.08	50.5	53	1183.1	Kestin 1984	1095.1	968.6	1010.5	**
26.08	50.5	97	1184.4	Kestin 1984	1098.3	970.1	1009.2	**
26.08	50.5	157	1186.3	Kestin 1984	1103.5	972.1	1007.6	**
26.08	50.5	208	1187.9	Kestin 1984	1108.9	973.9	1006.4	**
26.08	50.5	258	1189.5	Kestin 1984	1110.4	975.8	1005.3	**
26.08	50.5	309	1191.1	Kestin 1984	1115.5	977.7	1004.4	**
26.08	66	3	1173.3	Kestin 1984	868.2	761.6	802.5	**
26.08	66	9	1173.4	Kestin 1984	868.9	761.9	802.5	**
26.08	66	54	1174.5	Kestin 1984	871.9	763.8	802.4	**
26.08	66	104	1176.0	Kestin 1984	873.9	766.0	802.4	**
26.08	66	154	1177.5	Kestin 1984	876.5	768.2	802.4	**
26.08	66	207	1179.2	Kestin 1984	880.6	770.6	802.5	**
26.08	66	257	1180.8	Kestin 1984	882.7	772.9	802.6	**
26.08	66	306	1182.4	Kestin 1984	887.1	775.1	802.8	**
0.58	5	1	1003.9	Out 1980	1525.9	1545.5	1551.5	1529.3
0.58	15	1	1003.3	Out 1980	1147.8	1157.9	1164.1	1146.7
0.58	25	1	1001.2	Out 1980	899.4	906.0	911.5	897.7
0.58	35	1	998.0	Out 1980	727.4	732.1	736.9	725.8
0.58	45	1	994.1	Out 1980	603.1	606.7	610.7	601.6
0.58	55	1	989.5	Out 1980	510.5	512.9	516.3	508.9
0.58	65	1	984.3	Out 1980	439.3	440.9	443.8	437.6
0.58	75	1	978.6	Out 1980	383.4	384.4	386.9	381.7
0.58	85	1	972.4	Out 1980	338.6	339.2	341.4	337.1
0.58	95	1	965.7	Out 1980	301.9	302.5	304.4	300.8
1.15	5	1	1007.7	Out 1980	1533.4	1571.4	1576.5	1540.7
1.15	15	1	1007.5	Out 1980	1155.7	1177.4	1184.1	1155.9
1.15	25	1	1005.2	Out 1980	906.5	921.2	927.7	905.5
1.15	35	1	1001.9	Out 1980	733.4	744.4	750.3	732.5
1.15	45	1	997.9	Out 1980	608.2	616.9	621.9	607.6
1.15	55	1	993.3	Out 1980	515.1	521.5	525.8	514.2
1.15	65	1	988.1	Out 1980	443.6	448.3	452.0	442.4
1.15	75	1	982.4	Out 1980	387.5	390.9	394.0	386.1
1.15	85	1	976.2	Out 1980	342.5	344.9	347.6	341.1

1.15	95	1	969.5	Out 1980	305.6	307.6	309.9	304.5
1.83	5	1	1012.2	Out 1980	1543.8	1602.4	1603.9	1555.0
1.83	15	1	1012.4	Out 1980	1166.2	1200.6	1206.0	1167.5
1.83	25	1	1010.0	Out 1980	916.4	939.4	945.6	915.2
1.83	35	1	1006.6	Out 1980	742.6	759.1	765.0	740.8
1.83	45	1	1002.5	Out 1980	616.3	629.0	634.3	614.8
1.83	55	1	997.8	Out 1980	522.0	531.8	536.4	520.6
1.83	65	1	992.6	Out 1980	449.7	457.2	461.1	448.3
1.83	75	1	986.9	Out 1980	393.0	398.6	401.9	391.4
1.83	85	1	980.7	Out 1980	347.5	351.7	354.5	345.9
1.83	95	1	974.1	Out 1980	310.3	313.7	316.0	309.0
2.83	5	1	1019.1	Out 1980	1559.8	1648.0	1642.0	1577.4
2.83	15	1	1019.6	Out 1980	1182.7	1234.8	1236.6	1185.5
2.83	25	1	1017.1	Out 1980	931.9	966.1	970.4	930.2
2.83	35	1	1013.6	Out 1980	756.7	780.7	785.6	753.6
2.83	45	1	1009.3	Out 1980	629.4	646.9	651.6	626.0
2.83	55	1	1004.6	Out 1980	533.9	547.0	551.1	530.6
2.83	65	1	999.3	Out 1980	460.4	470.2	473.8	457.2
2.83	75	1	993.6	Out 1980	402.6	409.9	412.9	399.5
2.83	85	1	987.4	Out 1980	356.2	361.7	364.2	353.3
2.83	95	1	980.8	Out 1980	318.3	322.6	324.6	315.8
4.46	5	1	1030.9	Out 1980	1589.1	1722.3	1701.6	1617.6
4.46	15	1	1031.4	Out 1980	1210.6	1290.4	1284.6	1217.5
4.46	25	1	1028.8	Out 1980	957.1	1009.6	1009.5	956.6
4.46	35	1	1025.0	Out 1980	778.7	815.9	817.9	776.1
4.46	45	1	1020.6	Out 1980	648.8	676.1	678.8	645.5
4.46	55	1	1015.7	Out 1980	551.1	571.6	574.3	547.7
4.46	65	1	1010.3	Out 1980	475.8	491.4	493.8	472.5
4.46	75	1	1004.6	Out 1980	416.4	428.4	430.4	413.4
4.46	85	1	998.5	Out 1980	368.8	378.0	379.5	366.0
4.46	95	1	991.9	Out 1980	329.8	337.1	338.1	327.5
6.55	5	1	1046.9	Out 1980	1636.6	1817.5	1776.5	1676.7
6.55	15	1	1046.8	Out 1980	1251.9	1361.8	1345.1	1263.9
6.55	25	1	1043.8	Out 1980	992.8	1065.5	1058.9	994.6
6.55	35	1	1039.8	Out 1980	810.0	861.0	859.0	808.1
6.55	45	1	1035.2	Out 1980	676.2	713.5	713.4	673.0
6.55	55	1	1030.2	Out 1980	575.3	603.2	603.9	571.8
6.55	65	1	1024.8	Out 1980	497.5	518.6	519.3	493.9
6.55	75	1	1019.0	Out 1980	435.9	452.1	452.6	432.6
6.55	85	1	1012.9	Out 1980	386.7	398.9	399.0	383.4
6.55	95	1	1006.4	Out 1980	346.2	355.8	355.4	343.4
1	20	20	1006.3	Peninov 1978	1020.4	1031.3	1038.1	1015.6
1	25	20	1005.0	Peninov 1978	910.3	916.8	923.3	903.2

1	30	20	1003.5	Peninov 1978	817.4	821.4	827.6	809.6
1	35	20	1001.7	Peninov 1978	735.2	741.2	746.9	730.8
1	40	20	999.8	Peninov 1978	664.0	673.0	678.3	663.8
1	50	20	995.5	Peninov 1978	560.0	563.8	568.3	556.5
1	75	20	982.2	Peninov 1978	388.9	389.7	392.7	385.5
1	100	20	965.9	Peninov 1978	290.3	290.8	292.9	288.3
1	125	20	946.8	Peninov 1978	228.2	229.3	230.7	227.9
1	150	20	925.1	Peninov 1978	187.9	188.4	189.4	187.6
1	175	20	900.6	Peninov 1978	159.7	159.6	160.4	159.3
1	200	50	875.3	Peninov 1978	138.9	139.2	139.8	139.2
1	225	50	844.6	Peninov 1978	122.7	122.9	123.4	123.0
1	250	50	809.6	Peninov 1978	109.6	109.6	110.1	109.7
1	20	100	1009.8	Peninov 1978	1015.8	1028.1	1035.4	1013.3
1	25	100	1008.5	Peninov 1978	905.9	915.1	922.0	902.2
1	30	100	1006.9	Peninov 1978	811.3	820.8	827.3	809.6
1	35	100	1005.2	Peninov 1978	729.9	741.4	747.3	731.5
1	40	100	1003.3	Peninov 1978	667.0	673.7	679.2	664.9
1	50	100	998.9	Peninov 1978	563.0	565.3	569.8	558.2
1	75	100	985.7	Peninov 1978	391.3	391.8	394.8	387.6
1	100	100	969.6	Peninov 1978	292.8	293.0	295.0	290.5
1	125	100	950.8	Peninov 1978	230.5	231.4	232.8	230.0
1	150	100	929.4	Peninov 1978	190.3	190.4	191.5	189.7
1	175	100	905.6	Peninov 1978	161.5	161.7	162.4	161.4
1	200	100	878.9	Peninov 1978	140.5	140.5	141.1	140.5
1	225	100	849.0	Peninov 1978	124.5	124.2	124.7	124.3
1	250	100	815.0	Peninov 1978	111.2	111.0	111.4	111.1
1	275	100	775.6	Peninov 1978	100.3	99.7	100.2	99.7
1	20	200	1014.2	Peninov 1978	1010.8	1024.7	1032.5	1010.9
1	25	200	1012.8	Peninov 1978	905.0	913.4	920.6	901.3
1	30	200	1011.2	Peninov 1978	810.1	820.4	827.1	809.7
1	35	200	1009.4	Peninov 1978	729.1	741.9	748.0	732.4
1	40	200	1007.5	Peninov 1978	670.7	674.9	680.4	666.4
1	50	200	1003.1	Peninov 1978	567.3	567.3	571.8	560.4
1	75	200	990.0	Peninov 1978	394.6	394.5	397.4	390.3
1	100	200	974.1	Peninov 1978	296.1	295.7	297.7	293.2
1	125	200	955.6	Peninov 1978	233.8	234.1	235.4	232.6
1	150	200	934.7	Peninov 1978	193.7	193.0	194.0	192.3
1	175	200	911.5	Peninov 1978	164.2	164.2	164.9	163.9
1	200	200	885.8	Peninov 1978	143.6	143.0	143.5	143.0
1	225	200	857.2	Peninov 1978	127.0	126.7	127.1	126.9
1	250	200	825.1	Peninov 1978	114.4	113.7	114.0	113.8
1	350	200	621.3	Peninov 1978	72.1	72.5	73.9	71.2
1	20	300	1018.5	Peninov 1978	1019.7	1022.0	1030.1	1008.9

1	25	300	1017.0	Peninov 1978	914.0	912.3	919.7	900.7
1	30	300	1015.4	Peninov 1978	819.4	820.4	827.2	810.1
1	35	300	1013.6	Peninov 1978	741.7	742.7	748.8	733.5
1	40	300	1011.6	Peninov 1978	674.8	676.3	681.8	668.0
1	50	300	1007.3	Peninov 1978	571.8	569.4	573.9	562.6
1	75	300	994.2	Peninov 1978	398.4	397.3	400.1	393.0
1	100	300	978.4	Peninov 1978	299.4	298.5	300.4	295.9
1	125	300	960.3	Peninov 1978	237.0	236.7	238.0	235.2
1	150	300	939.9	Peninov 1978	196.6	195.5	196.4	194.8
1	175	300	917.3	Peninov 1978	166.7	166.6	167.3	166.3
1	200	300	892.3	Peninov 1978	146.7	145.4	145.9	145.4
1	225	300	864.8	Peninov 1978	129.8	129.2	129.5	129.3
1	250	300	834.3	Peninov 1978	116.9	116.2	116.5	116.4
1	350	300	659.3	Peninov 1978	77.9	78.9	79.0	77.6
5	20	20	1035.0	Peninov 1978	1094.9	1151.5	1146.9	1083.9
5	30	20	1031.6	Peninov 1978	870.2	917.1	916.9	867.2
5	40	20	1027.4	Peninov 1978	718.2	751.4	752.9	713.4
5	50	20	1022.7	Peninov 1978	603.4	629.5	631.5	600.1
5	75	20	1009.1	Peninov 1978	422.1	435.1	436.6	418.7
5	100	20	993.0	Peninov 1978	316.8	324.7	324.9	315.3
5	125	20	974.6	Peninov 1978	249.5	256.0	255.1	250.6
5	150	20	953.9	Peninov 1978	205.8	210.3	208.6	207.3
5	175	20	930.7	Peninov 1978	175.8	178.2	176.0	176.8
5	200	50	906.9	Peninov 1978	152.4	155.5	152.8	154.9
5	225	50	878.3	Peninov 1978	134.5	137.2	134.6	137.1
5	250	50	846.2	Peninov 1978	120.1	122.4	120.1	122.4
5	20	100	1038.4	Peninov 1978	1087.0	1147.9	1142.6	1081.5
5	30	100	1034.9	Peninov 1978	874.1	916.5	915.7	867.1
5	40	100	1030.7	Peninov 1978	722.5	752.2	753.2	714.6
5	50	100	1026.0	Peninov 1978	607.6	631.1	632.7	601.9
5	75	100	1012.5	Peninov 1978	425.2	437.5	438.6	421.1
5	100	100	996.6	Peninov 1978	319.4	327.1	327.1	317.7
5	125	100	978.4	Peninov 1978	252.2	258.4	257.3	252.9
5	150	100	958.0	Peninov 1978	208.7	212.6	210.7	209.6
5	175	100	935.3	Peninov 1978	177.0	180.5	178.0	179.0
5	200	100	910.2	Peninov 1978	154.0	156.9	154.1	156.3
5	225	100	882.2	Peninov 1978	136.4	138.7	135.8	138.6
5	250	100	851.0	Peninov 1978	121.7	124.0	121.4	124.0
5	275	100	815.3	Peninov 1978	109.6	111.4	109.4	111.3
5	300	100	773.5	Peninov 1978	98.3	100.0	99.1	99.2
5	20	200	1042.5	Peninov 1978	1090.0	1144.1	1137.9	1078.9
5	30	200	1039.0	Peninov 1978	878.7	916.0	914.4	867.3
5	40	200	1034.8	Peninov 1978	727.3	753.5	753.8	716.2

5	50	200	1030.1	Peninov 1978	612.1	633.4	634.3	604.2
5	75	200	1016.7	Peninov 1978	428.9	440.5	441.1	424.0
5	100	200	1000.9	Peninov 1978	323.1	330.2	329.8	320.6
5	125	200	983.0	Peninov 1978	255.9	261.3	259.9	255.8
5	150	200	963.1	Peninov 1978	212.3	215.5	213.2	212.4
5	175	200	941.0	Peninov 1978	180.0	183.3	180.5	181.8
5	200	200	916.6	Peninov 1978	157.3	159.6	156.5	159.1
5	225	200	889.8	Peninov 1978	139.0	141.5	138.3	141.4
5	250	200	860.0	Peninov 1978	125.2	127.0	123.9	127.1
5	325	200	743.5	Peninov 1978	91.6	94.5	92.9	92.2
5	20	300	1046.5	Peninov 1978	1092.0	1141.1	1133.9	1076.8
5	30	300	1042.9	Peninov 1978	883.3	916.0	913.6	867.7
5	40	300	1038.8	Peninov 1978	732.5	755.1	754.6	717.9
5	50	300	1034.1	Peninov 1978	616.6	635.8	636.0	606.6
5	75	300	1020.8	Peninov 1978	432.8	443.6	443.7	427.0
5	100	300	1005.2	Peninov 1978	327.0	333.3	332.5	323.6
5	125	300	987.6	Peninov 1978	259.4	264.3	262.5	258.7
5	150	300	968.0	Peninov 1978	215.5	218.3	215.7	215.2
5	175	300	946.4	Peninov 1978	182.6	186.0	182.9	184.5
5	200	300	922.8	Peninov 1978	160.5	162.3	158.8	161.8
5	225	300	896.9	Peninov 1978	142.0	144.2	140.6	144.2
5	250	300	868.5	Peninov 1978	128.2	129.8	126.3	130.0
5	350	300	713.3	Peninov 1978	85.4	92.4	87.8	86.2
10	30	20	1067.7	Peninov 1978	962.2	1036.8	1025.7	961.2
10	50	20	1058.1	Peninov 1978	670.7	711.6	709.0	668.5
10	75	20	1044.1	Peninov 1978	471.6	491.8	490.7	469.1
10	100	20	1028.2	Peninov 1978	356.5	367.0	364.7	354.8
10	125	20	1010.4	Peninov 1978	281.8	289.4	285.5	283.2
10	150	20	990.5	Peninov 1978	233.7	237.7	232.5	235.0
10	30	100	1070.8	Peninov 1978	965.3	1036.0	1023.1	961.1
10	50	100	1061.2	Peninov 1978	674.0	713.5	709.7	670.5
10	75	100	1047.3	Peninov 1978	474.9	494.5	492.6	471.7
10	100	100	1031.5	Peninov 1978	359.4	369.8	366.9	357.5
10	125	100	1013.9	Peninov 1978	284.4	292.1	287.7	285.8
10	150	100	994.3	Peninov 1978	236.4	240.3	234.6	237.6
10	200	100	949.1	Peninov 1978	176.5	177.3	170.1	177.9
10	30	200	1074.5	Peninov 1978	969.3	1035.5	1020.4	961.3
10	50	200	1065.0	Peninov 1978	677.1	716.0	710.7	673.0
10	75	200	1051.3	Peninov 1978	478.3	498.0	494.9	475.0
10	100	200	1035.7	Peninov 1978	362.8	373.3	369.5	360.9
10	125	200	1018.3	Peninov 1978	288.0	295.4	290.3	289.1
10	150	200	999.1	Peninov 1978	239.8	243.6	237.2	240.8
10	350	200	751.5	Peninov 1978	91.4	101.6	93.9	89.4

10	30	300	1078.3	Peninov 1978	973.4	1035.5	1018.1	961.8
10	50	300	1068.8	Peninov 1978	681.7	718.7	711.9	675.7
10	75	300	1055.2	Peninov 1978	482.2	501.4	497.3	478.3
10	100	300	1039.8	Peninov 1978	366.6	376.7	372.2	364.2
10	125	300	1022.6	Peninov 1978	291.7	298.7	293.0	292.3
10	150	300	1003.8	Peninov 1978	243.1	246.7	239.8	244.0
20	50	20	1133.4	Peninov 1978	868.3	875.8	887.1	879.0
20	100	20	1103.5	Peninov 1978	459.7	451.7	457.8	464.5
20	150	20	1067.8	Peninov 1978	303.6	292.6	288.8	306.5
20	50	100	1135.9	Peninov 1978	872.7	878.1	886.1	881.7
20	100	100	1106.2	Peninov 1978	463.4	455.1	459.7	468.0
20	150	100	1070.8	Peninov 1978	306.4	295.8	291.0	309.9
20	50	200	1139.2	Peninov 1978	877.6	881.2	885.3	885.0
20	100	200	1109.8	Peninov 1978	467.9	459.4	462.2	472.4
20	150	200	1075.0	Peninov 1978	309.9	299.8	293.7	314.0
20	350	200	862.1	Peninov 1978	116.7	134.0	112.7	115.8
20	50	300	1142.6	Peninov 1978	882.0	884.5	884.7	888.5
20	100	300	1113.4	Peninov 1978	472.1	463.7	464.7	476.7
20	150	300	1079.1	Peninov 1978	313.6	303.7	296.3	318.1
0	106.68	100	958.1	Semenyuk 1977	273.0	265.8	265.7	265.7
0	106.68	200	962.7	Semenyuk 1977	275.8	268.5	268.3	268.3
0	106.68	300	967.2	Semenyuk 1977	278.7	271.1	270.9	270.9
0	106.68	500	975.7	Semenyuk 1977	284.3	276.4	276.1	276.1
0	106.68	700	983.9	Semenyuk 1977	289.1	281.6	281.2	281.2
0	106.68	1000	995.5	Semenyuk 1977	295.7	289.4	288.8	288.8
0	106.68	1200	1002.8	Semenyuk 1977	301.1	294.5	293.9	293.9
0	106.68	1500	1013.3	Semenyuk 1977	309.0	302.2	301.4	301.4
0	154.21	100	918.4	Semenyuk 1977	182.7	179.5	179.7	179.7
0	154.21	200	923.9	Semenyuk 1977	184.7	182.0	182.1	182.1
0	154.21	300	929.2	Semenyuk 1977	186.7	184.4	184.6	184.6
0	154.21	500	939.2	Semenyuk 1977	191.4	189.1	189.3	189.3
0	154.21	700	948.5	Semenyuk 1977	195.8	193.7	193.9	193.9
0	154.21	1000	961.6	Semenyuk 1977	201.7	200.4	200.6	200.6
0	154.21	1200	969.8	Semenyuk 1977	206.4	204.8	205.0	205.0
0	154.21	1500	981.4	Semenyuk 1977	211.8	211.1	211.5	211.5
0	203.44	100	867.0	Semenyuk 1977	134.5	134.0	134.3	134.3
0	203.44	200	874.1	Semenyuk 1977	136.0	136.4	136.7	136.7
0	203.44	300	880.9	Semenyuk 1977	138.5	138.7	139.1	139.1
0	203.44	500	893.5	Semenyuk 1977	142.6	143.2	143.6	143.6
0	203.44	700	905.0	Semenyuk 1977	146.6	147.5	147.9	147.9
0	203.44	1000	920.7	Semenyuk 1977	152.4	153.5	154.1	154.1
0	203.44	1200	930.3	Semenyuk 1977	156.2	157.3	158.0	158.0
0	203.44	1500	943.7	Semenyuk 1977	161.2	162.8	163.8	163.8

0	264.97	100	782.3	Semenyuk 1977	108.0	101.0	101.2	101.2
0	264.97	200	794.4	Semenyuk 1977	109.6	103.8	104.0	104.0
0	264.97	300	805.2	Semenyuk 1977	112.6	106.4	106.6	106.6
0	264.97	500	824.0	Semenyuk 1977	116.0	111.1	111.4	111.4
0	264.97	700	840.3	Semenyuk 1977	120.8	115.4	115.8	115.8
0	264.97	1000	861.4	Semenyuk 1977	125.4	121.2	121.8	121.8
0	264.97	1200	873.8	Semenyuk 1977	129.0	124.8	125.6	125.6
0	264.97	1500	890.6	Semenyuk 1977	134.2	129.8	131.0	131.0
5.05	101.28	100	996.0	Semenyuk 1977	318.6	323.2	323.1	314.0
5.05	101.28	200	1000.4	Semenyuk 1977	320.5	326.3	325.8	317.0
5.05	101.28	300	1004.7	Semenyuk 1977	323.3	329.4	328.5	319.9
5.05	101.28	500	1012.9	Semenyuk 1977	328.5	335.5	333.8	325.8
5.05	101.28	700	1020.7	Semenyuk 1977	333.0	341.6	339.1	331.6
5.05	101.28	1000	1031.9	Semenyuk 1977	341.1	350.7	347.0	340.2
5.05	101.28	1200	1038.9	Semenyuk 1977	347.4	356.8	352.4	345.9
5.05	101.28	1500	1049.1	Semenyuk 1977	355.8	365.8	360.4	354.5
5.05	154.76	100	954.2	Semenyuk 1977	203.8	205.9	203.8	203.3
5.05	154.76	200	959.4	Semenyuk 1977	206.1	208.7	206.3	206.1
5.05	154.76	300	964.4	Semenyuk 1977	211.3	211.5	208.8	208.8
5.05	154.76	500	973.9	Semenyuk 1977	212.5	217.0	213.7	214.2
5.05	154.76	700	982.9	Semenyuk 1977	216.1	222.3	218.5	219.4
5.05	154.76	1000	995.5	Semenyuk 1977	223.2	230.0	225.5	227.0
5.05	154.76	1200	1003.4	Semenyuk 1977	227.1	235.0	230.1	232.0
5.05	154.76	1500	1014.5	Semenyuk 1977	233.7	242.2	236.9	239.4
5.05	206.57	100	903.5	Semenyuk 1977	151.8	151.9	149.0	151.4
5.05	206.57	200	910.2	Semenyuk 1977	154.1	154.6	151.4	154.2
5.05	206.57	300	916.6	Semenyuk 1977	155.2	157.3	153.7	156.9
5.05	206.57	500	928.5	Semenyuk 1977	159.6	162.5	158.3	162.1
5.05	206.57	700	939.4	Semenyuk 1977	164.4	167.3	162.7	167.0
5.05	206.57	1000	954.4	Semenyuk 1977	169.9	174.3	169.0	174.1
5.05	206.57	1200	963.6	Semenyuk 1977	174.4	178.7	173.1	178.6
5.05	206.57	1500	976.4	Semenyuk 1977	180.5	184.9	179.1	185.2
5.05	254.72	100	845.0	Semenyuk 1977	124.3	121.7	119.1	121.7
5.05	254.72	200	854.5	Semenyuk 1977	126.5	124.7	121.6	124.8
5.05	254.72	300	863.2	Semenyuk 1977	128.7	127.6	124.0	127.7
5.05	254.72	500	878.9	Semenyuk 1977	133.8	132.9	128.5	133.1
5.05	254.72	700	892.8	Semenyuk 1977	136.6	137.8	132.8	138.1
5.05	254.72	1000	911.2	Semenyuk 1977	142.3	144.5	138.8	145.0
5.05	254.72	1200	922.2	Semenyuk 1977	145.9	148.6	142.7	149.3
5.05	254.72	1500	937.2	Semenyuk 1977	150.6	154.4	148.2	155.5
19.12	108.4	100	1093.8	Semenyuk 1977	419.2	411.3	412.7	420.5
19.12	108.4	200	1097.5	Semenyuk 1977	423.5	415.5	415.3	424.8
19.12	108.4	300	1101.3	Semenyuk 1977	428.7	419.6	417.9	429.0

19.12	108.4	500	1108.7	Semenyuk 1977	436.6	427.9	423.2	437.3
19.12	108.4	700	1115.9	Semenyuk 1977	446.6	436.1	428.5	445.5
19.12	108.4	1000	1126.2	Semenyuk 1977	457.9	448.3	436.7	457.7
19.12	108.4	1200	1132.7	Semenyuk 1977	462.2	456.3	442.2	465.7
19.12	108.4	1500	1142.0	Semenyuk 1977	478.1	468.2	450.8	477.8
19.12	151.01	100	1063.1	Semenyuk 1977	298.0	288.9	283.2	300.1
19.12	151.01	200	1067.3	Semenyuk 1977	301.9	292.7	285.9	304.2
19.12	151.01	300	1071.5	Semenyuk 1977	304.9	296.6	288.5	308.2
19.12	151.01	500	1079.7	Semenyuk 1977	310.7	304.1	293.7	315.9
19.12	151.01	700	1087.6	Semenyuk 1977	316.1	311.4	298.9	323.5
19.12	151.01	1000	1098.8	Semenyuk 1977	323.9	322.0	306.6	334.6
19.12	151.01	1200	1105.8	Semenyuk 1977	330.2	328.9	311.8	341.8
19.12	151.01	1500	1115.7	Semenyuk 1977	336.9	339.0	319.5	352.5
19.12	203.72	100	1018.6	Semenyuk 1977	216.8	210.6	199.7	221.5
19.12	203.72	200	1023.9	Semenyuk 1977	219.2	214.4	202.2	225.5
19.12	203.72	300	1029.0	Semenyuk 1977	222.8	218.0	204.7	229.4
19.12	203.72	500	1038.9	Semenyuk 1977	226.9	225.0	209.6	236.8
19.12	203.72	700	1048.2	Semenyuk 1977	231.8	231.7	214.3	243.9
19.12	203.72	1000	1061.1	Semenyuk 1977	241.2	241.2	221.3	254.1
19.12	203.72	1200	1069.0	Semenyuk 1977	243.0	247.3	225.9	260.6
19.12	203.72	1500	1080.1	Semenyuk 1977	251.6	255.9	232.6	270.2
19.12	251.76	100	970.8	Semenyuk 1977	171.7	168.5	156.7	177.4
19.12	251.76	200	977.6	Semenyuk 1977	174.4	172.6	159.1	181.8
19.12	251.76	300	984.2	Semenyuk 1977	176.7	176.5	161.5	186.0
19.12	251.76	500	996.6	Semenyuk 1977	181.9	183.7	166.1	193.7
19.12	251.76	700	1007.9	Semenyuk 1977	187.3	190.4	170.6	200.9
19.12	251.76	1000	1023.1	Semenyuk 1977	193.6	199.5	177.0	210.8
19.12	251.76	1200	1032.4	Semenyuk 1977	197.4	205.2	181.2	217.1
19.12	251.76	1500	1045.1	Semenyuk 1977	203.8	213.2	187.3	226.0
19.12	300.31	200	922.4	Semenyuk 1977	148.3	143.7	131.1	148.3
19.12	300.31	300	931.6	Semenyuk 1977	150.7	148.6	133.5	153.5
19.12	300.31	500	947.9	Semenyuk 1977	155.1	157.0	138.0	162.4
19.12	300.31	700	962.3	Semenyuk 1977	159.4	164.2	142.3	170.2
19.12	300.31	1000	981.1	Semenyuk 1977	166.2	173.6	148.4	180.4
19.12	300.31	1200	992.2	Semenyuk 1977	169.9	179.3	152.3	186.7
19.12	300.31	1500	1007.1	Semenyuk 1977	176.4	187.0	158.0	195.4
19.12	356.34	200	842.5	Semenyuk 1977	125.4	132.0	108.8	106.4
19.12	356.34	300	857.7	Semenyuk 1977	127.0	143.1	111.3	118.5
19.12	356.34	500	882.5	Semenyuk 1977	131.6	155.5	116.0	132.1
19.12	356.34	700	902.8	Semenyuk 1977	136.9	164.2	120.3	141.8
19.12	356.34	1000	927.6	Semenyuk 1977	144.0	174.5	126.3	153.3
19.12	356.34	1200	941.7	Semenyuk 1977	147.7	180.3	130.1	159.9
19.12	356.34	1500	960.1	Semenyuk 1977	153.8	187.9	135.5	168.9

0.1	20	1	998.9	Haynes 2014	1004.0	1005.1	1007.3	1003.0
0.2	20	1	999.7	Haynes 2014	1006.0	1008.1	1011.7	1004.4
0.3	20	1	1000.4	Haynes 2014	1008.0	1011.1	1015.5	1005.9
0.4	20	1	1001.1	Haynes 2014	1009.0	1014.1	1019.2	1007.3
0.5	20	1	1001.8	Haynes 2014	1011.0	1017.1	1022.7	1008.8
1	20	1	1005.4	Haynes 2014	1020.0	1032.2	1038.8	1016.1
2	20	1	1012.6	Haynes 2014	1036.0	1062.2	1067.9	1031.7
3	20	1	1019.8	Haynes 2014	1052.0	1092.3	1095.2	1048.2
4	20	1	1027.0	Haynes 2014	1068.0	1122.3	1121.7	1065.8
5	20	1	1034.2	Haynes 2014	1085.0	1152.4	1147.9	1084.5
6	20	1	1041.5	Haynes 2014	1104.0	1182.5	1174.1	1104.6
7	20	1	1048.8	Haynes 2014	1124.0	1212.5	1200.2	1125.9
8	20	1	1056.2	Haynes 2014	1145.0	1242.6	1226.5	1148.6
9	20	1	1063.6	Haynes 2014	1168.0	1272.7	1253.1	1172.9
10	20	1	1071.1	Haynes 2014	1193.0	1302.7	1280.0	1198.8
12	20	1	1086.2	Haynes 2014	1250.0	1362.9	1335.1	1256.1
14	20	1	1101.4	Haynes 2014	1317.0	1423.0	1392.0	1321.5
16	20	1	1116.9	Haynes 2014	1388.0	1483.1	1451.1	1396.4
18	20	1	1132.5	Haynes 2014	1463.0	1543.2	1512.8	1482.5
20	20	1	1148.3	Haynes 2014	1557.0	1603.4	1577.3	1581.4
22	20	1	1164.3	Haynes 2014	1676.0	1663.5	1644.8	1695.7
24	20	1	1180.4	Haynes 2014	1821.0	1723.6	1715.8	1827.9
26	20	1	1196.8	Haynes 2014	1990.0	1783.7	1790.5	**
100	809.85	1	1556.0	Ito 1989	1028.0	1460.4	1112.4	**
100	809.85	1	1556.0	Ito 1989	1023.0	1460.4	1112.4	**
100	809.85	1	1556.0	Ito 1989	1025.0	1460.4	1112.4	**
100	809.85	1	1556.0	Ito 1989	1028.0	1460.4	1112.4	**
100	820.85	1	1550.7	Ito 1989	1016.0	1416.2	1077.1	**
100	820.85	1	1550.7	Ito 1989	1017.0	1416.2	1077.1	**
100	820.85	1	1550.7	Ito 1989	1020.0	1416.2	1077.1	**
100	829.85	1	1546.3	Ito 1989	996.0	1380.0	1049.4	**
100	829.85	1	1546.3	Ito 1989	1003.0	1380.0	1049.4	**
100	829.85	1	1546.3	Ito 1989	1003.0	1380.0	1049.4	**
100	829.85	1	1546.3	Ito 1989	997.0	1380.0	1049.4	**
100	829.85	1	1546.3	Ito 1989	997.0	1380.0	1049.4	**
100	829.85	1	1546.3	Ito 1989	1003.0	1380.0	1049.4	**
100	849.85	1	1536.2	Ito 1989	959.0	1299.6	991.4	**
100	849.85	1	1536.2	Ito 1989	957.0	1299.6	991.4	**
100	849.85	1	1536.2	Ito 1989	957.0	1299.6	991.4	**
100	874.85	1	1523.0	Ito 1989	911.0	1199.1	925.2	**
100	874.85	1	1523.0	Ito 1989	914.0	1199.1	925.2	**
100	874.85	1	1523.0	Ito 1989	914.0	1199.1	925.2	**
100	874.85	1	1523.0	Ito 1989	914.0	1199.1	925.2	**

100	874.85	1	1523.0	Ito 1989	921.0	1199.1	925.2	**
100	874.85	1	1523.0	Ito 1989	914.0	1199.1	925.2	**
100	899.85	1	1509.1	Ito 1989	871.0	1098.6	865.2	**
100	899.85	1	1509.1	Ito 1989	874.0	1098.6	865.2	**
100	899.85	1	1509.1	Ito 1989	872.0	1098.6	865.2	**
100	899.85	1	1509.1	Ito 1989	877.0	1098.6	865.2	**
100	899.85	1	1509.1	Ito 1989	874.0	1098.6	865.2	**
100	899.85	1	1509.1	Ito 1989	874.0	1098.6	865.2	**
100	924.85	1	1494.5	Ito 1989	842.0	998.1	810.7	**
100	924.85	1	1494.5	Ito 1989	840.0	998.1	810.7	**
100	924.85	1	1494.5	Ito 1989	837.0	998.1	810.7	**
100	924.85	1	1494.5	Ito 1989	844.0	998.1	810.7	**
100	924.85	1	1494.5	Ito 1989	839.0	998.1	810.7	**
100	924.85	1	1494.5	Ito 1989	836.0	998.1	810.7	**
100	949.85	1	1479.1	Ito 1989	804.0	897.6	761.1	**
100	949.85	1	1479.1	Ito 1989	804.0	897.6	761.1	**
100	949.85	1	1479.1	Ito 1989	804.0	897.6	761.1	**
100	974.85	1	1462.9	Ito 1989	771.0	797.1	715.8	**
100	974.85	1	1462.9	Ito 1989	773.0	797.1	715.8	**
100	974.85	1	1462.9	Ito 1989	775.0	797.1	715.8	**

Density of the H_2O-NaCl fluid calculated based on salinity, temperature and pressure of experiment using Driesner 2007.

** At this PTx coordinates Driesner and Heinrich 2007 model returns values for L+V two phase field. Viscosity calculations for such experimental data omitted due to inability to evaluate fluid density*

*** reached salinity limit for the model*

3. Appendix C

This appendix consists of microthermometry measurements, interpreted Raman data and measured stable isotope composition of the samples, collected during work with samples obtained from North American Emerald Mine, discussed in Chapter 3.

Table 1 Fluid inclusions data, measured by microthermometry and Raman spectroscopy. TCO_2 trip is referring to triple point of pure CO_2 (-56.6 °C), TCO_2 hom – homogenization temperature of CO_2 phase, Type of homogenization – if omitted then to liquid phase otherwise to vapor (V). ΔCO_2 Fermi Diad shows calculated difference between CO_2 peaks measured by Raman, Density (ρ) given in kg m^{-3}, salinity (NaCl %) measured based on either CO_2-clathrate melting for CO_2 dominant FIs or by temperature of ice (Ti) melting for H_2O-NaCl inclusions. T_hH_2O is referring to temperature of homogenization for H_2O-NaCl FIs.

Sample #	Host min	FIA ID	T CO_2 trip	T CO_2 hom	Type of homog	TCO_2 claths	Δ CO2 Fermi Diad	Notes	ρ	NaCl %	Ti	Th H_2O
58A	Car	FIA1					104.306		701			
58A	Car	FIA2					104.472		771			
58A	Em	FI-1					104.434		755			
58A	Em	FI-10					104.47		770			
58A	Em	FI-13					104.26		680			
58A	Em	FI-14					104.382		733			
58A	Em	FI-15					104.887		926			
58A	Em	FI-2					104.309		702			
58A	Em	FI-4					104.323		708			
58A	Em	FI-6					104.287		692			
58A	Em	FI-7					104.334		713			
58A	Em	FI-8					104.194		651			
58A	Em	FI-9					104.572		811			
58A	Em	FIA1					104.955		948			
58A	Qt	FI-11					102.944		103			
58A	Qt	FI-12					102.933		99			
58A	Qt	FI-5					102.816		57			
HID2015-2a	Qt	FIA1					102.767		40			
HID2015-2a	Qt	FIA1					102.743		32			
HID2015-2a	Qt	FIA2					102.767		40			
HID2015-2a	Qt	FIA3					104.685		855			
HID2015-2a	Qt	FIA3					104.659		845			
HID2015-2a	Qt	FIA4					104.468		769			
HID2015-2a	Qt	FIA4					104.947		946			
HID2015-2a	Qt	FIA5					104.857		916			
HID2015-2a	Qt	FIA5					104.877		923			
HID2015-3	Qt	FIA1					104.492		779			
HID2015-3	Qt	FIA1					104.549		802			
HID2015-3	Qt	FIA1					104.59		818			
HID2015-3	Qt	FIA1					104.477		773			
HID2015-3	Qt	FIA1					104.604		824			
HID2015-6	Qt	49	-56.4	13.1					831			
HID2015-6	Qt	49	-56.4	13.4					828			

HID2015-6	Qt	49	-56.4	13.1		831
HID2015-6	Qt	49	-56.4	13.1		831
HID2015-6	Qt	49	-56.4	13.5		827
HID2015-6	Qt	50	-56.7	23.5		722
HID2015-6	Qt	50	-56.7	23.5		722
HID2015-6	Qt	50	-56.7	23.5		722
HID2015-6	Qt	50	-56.7	23.2		726
HID2015-6	Qt	50	-56.7	23		729
HID2015-6	Qt	51	-56.8	11.5		844
HID2015-6	Qt	51	-56.8	11.5		844
HID2015-6	Qt	51	-56.8	11.5		844
HID2015-6	Qt	51	-56.8	11.5		844
HID2015-6	Qt	51	-56.8	11.5		844
HID2015-6	Qt	52	-56.9	27.9		641
HID2015-6	Qt	52	-56.9	28		638
HID2015-6	Qt	52	-56.9	28.3		629
HID2015-6	Qt	52	-56.9	28.2		632
HID2015-6	Qt	53	-57	6.8		878
HID2015-6	Qt	53	-57	6.2		883
HID2015-6	Qt	53	-57	5.7		886
HID2015-6	Qt	54	-57	21.9		742
HID2015-6	Qt	54	-57	22		741
HID2015-6	Qt	55	-57.2	6.2		883
HID2015-6	Qt	55	-57.2	6.3		882
HID2015-6	Qt	55	-57.2	6.3		882
HID2015-6	Qt	55	-57.2	6.2		883
HID2015-6	Qt	55	-57.2	6.2		883
HID2015-6	Qt	56	-57	25.4		693
HID2015-6	Qt	56	-57	25.4		693
HID2015-6	Qt	56	-57	25.4		693
HID2015-6	Qt	56	-57	25.4		693
HID2015-6	Qt	58	-56.7	28.9		606
HID2015-6	Qt	58	-56.6	20		766
HID2015-6	Qt	58	-56.7	28.8		610
HID2015-6	Qt	58	-56.6	20.2		764
HID2015-6	Qt	58	-56.7	28.8		610
HID2015-6	Qt	58	-56.6	20.2		764
HID2015-6	Qt	59	-56.4	29.4		584
HID2015-6	Qt	59	-56.4	29.3		589
HID2015-6	Qt	59	-56.4	29.5		578
HID2015-6	Qt	59	-56.4	29.3		589

HID2015-6	Qt		60	-56.6		15.7		809
HID2015-6	Qt		60	-56.6		16.6		800
HID2015-6	Qt		61	-56.6	N/A		N/A	
HID2015-6	Qt		61	-56.6	N/A		N/A	
HID2015-6	Qt		62	-56.6		18.5		782
HID2015-6	Qt		62	-56.6		18.5		782
HID2015-6	Qt		62	-56.6		18.6		781
HID2015-6	Qt		62	-56.6		20.1		765
HID2015-6	Qt		63	-56.6		27.1		658
HID2015-6	Qt		63	-56.6		27.1		658
HID2015-6	Qt		63	-56.6		27		660
HID2015-6	Qt		63	-56.6		27.3		653
HID2015-6	Qt		63	-56.6		27.1		658
HID2015-6	Qt		64	-56.7		0.2		923
HID2015-6	Qt		64	-56.7		0.2		923
HID2015-6	Qt		64	-56.7		0.2		923
HID2015-6	Qt		64	-56.7		0.3		922
HID2015-6	Qt		64	-56.7	N/A		N/A	
HID2015-6	Qt		65	-56.8	N/A		N/A	
HID2015-6	Qt		65	-56.8	N/A		N/A	
HID2015-6	Qt		66	-57.2		8.5		868
HID2015-6	Qt		66	-57.2		9.1		863
HID2015-6	Qt		66	-57.2		9.2		863
HID2015-6	Qt	54a		-56.6		24		715
HID2015-6	Qt	54a		-56.6		24		715
HID2015-6	Qt	54a		-56.6		24.1		714
HID2015-6	Qt	54a		-56.6		24		715
HID2015-6	Qt	54a		-56.6		24.1		714
HID2015-6	Qt		67	-57.1		26.7		664
HID2015-6	Qt		67	-57.1		26.7		664
HID2015-6	Qt		67	-57.1		26.7		664
HID2015-6	Qt		68	-57		9.7		858
HID2015-6	Qt		68	-57		9.8		857
HID2015-6	Qt		68	-57		9.7		858
HID2015-6	Qt		68	-57		9.9		857
HID2015-6	Qt		69	-56.6		20.7		757
HID2015-6	Qt		69	-56.6		20.7		757
HID2015-6	Qt		69	-56.6		20.7		757
HID2015-6	Qt		70	-57.1		10		856
HID2015-6	Qt		70	-57.1		9.9		857
HID2015-6	Qt		70	-57.1		10		856

HID2015-6	Qt	70	-57.1	10.5			852			
HID2015-6	Qt	71	-57.1	10.8			850			
HID2015-6	Qt	71	-57.1	10.8			850			
HID2015-6	Qt	71	-57.1	10.8			850			
HID2015-6	Qt	71	-57.1	10.8			850			
HID2015-6	Qt	71	-57.1	10.8			850			
HID2015-6	Qt	72	-56.9	28.3			623			
HID2015-6	Qt	72	-56.9	28			632			
HID2015-6	Qt	72	-56.9	28			632			
HID2015-6	Qt	72	-56.9	27.9			635			
HID2015-6	Qt	72	-56.9	27.8			638			
HID2015-6	Qt	73	-57.4	10.9			849			
HID2015-6	Qt	73	-57.4	11			848			
HID2015-6	Qt	73	-57.4	10.9			849			
HID2015-6	Qt	73	-57.4	10.9			849			
HID2015-6	Qt	73	-57.4	10.9			849			
HID2015-6	Qt	74	-56.8	24.5			706			
HID2015-6	Qt	74	-56.8	24.5			706			
HID2015-6	Qt	74	-56.8	24.5			706			
HID2015-6	Qt	74	-56.8	24.5			706			
HID2015-6	Qt	79	-56.7	22.4			736			
HID2015-6	Qt	79	-56.7	22.6			733			
HID2015-6	Qt	79	-56.7	22.6			733			
HID2015-6	Qt	83	-57.1	25.1			696			
HID2015-6	Qt	83	-57.1	25.8			684			
HID2015-6	Qt	83	-57.1	25.6			688			
HID2015-6	Qt	83	-57.1	25.3			693			
HID2015-6	Qt	84	-56.6	1.6			914			
HID2015-6	Qt	84	-56.6	3.4			903			
HID2015-6	Qt	84	-56.6	4.1			898			
HID2015-6	Qt	85	-56.6	27.8			638			
HID2015-6	Qt	85	-56.6	27.8			638			
HID2015-6	Qt	85	-56.6	N/A		N/A				
HID2015-6	Qt	86	-56.8	24.3			709			
HID2015-6	Qt	86	-56.8	24.3			709			
HID2015-6	Qt	86	-56.8	24.8			701			
HID2015-6	Qt	86	-56.8	24.8			701			
HID2015-6	Qt	86	-56.8	24.8			701			
HID2015-6	Qt	86	-56.8	24.8			701			
HID2015-6	Qt	87			H2O-NaCl FIs		936	4.6	-2.8	166
HID2015-6	Qt	87	N/A		H2O-NaCl FIs		930	4.6		172

HID2015-6	Qt	87				H2O-NaCl FIs	932	4.6	-2.8	170
HID2015-6	Qt	86a	-56.7		22.6		733			
HID2015-6	Qt	86a	-56.7		22.6		733			
HID2015-6	Qt	86a	-56.7		22.8		730			
HID2015-6	Qt	86a	-56.7		23		728			
HID2015-6	Qt	86a	-56.7		23		728			
HID2015-6	Qt	86a	-56.7		23		728			
HID2015-6	Qt	86a	ice melt	Th			N/A			
HID2015-6	Qt	5	-56.5	N/A			N/A			
HID2015-6	Qt	5	-56.5	N/A			N/A			
HID2015-6	Qt	5	-56.5	N/A			N/A			
HID2015-6	Qt	20	-57		20.4		761			
HID2015-6	Qt	20	-57		21.3		751			
HID2015-6	Qt	20	-57	N/A			N/A			
HID2015-6	Qt	22	-56.7		26.8		666			
HID2015-6	Qt	22	-56.7		26.8		666			
HID2015-6	Qt	22	-56.7		26.8		666			
HID2015-6	Qt	75	-57.1		10.4		853			
HID2015-6	Qt	75	-57.1		10.6		851			
HID2015-6	Qt	75	-57.1		10.6		851			
HID2015-6	Qt	75	-57.1		11.1		847			
HID2015-6	Qt	75	-57.1		11		848			
HID2015-6	Qt	76	-57.2		26.5		672			
HID2015-6	Qt	76	-57.2		26.5		672			
HID2015-6	Qt	76	-57.2		26.5		672			
HID2015-6	Qt	76	-57.2		26.5		672			
HID2015-6	Qt	76	-57.2		26.5		672			
HID2015-6	Qt	77	-56.8		10.1		855			
HID2015-6	Qt	77	-56.8		10.1		855			
HID2015-6	Qt	77	-56.8		10.1		855			
HID2015-6	Qt	77	-56.8		10.1		855			
HID2015-6	Qt	77	-56.8		10.1		855			
HID2015-6	Qt	78	-56.6		12		840			
HID2015-6	Qt	78	-56.6		12		840			
HID2015-6	Qt	78	-56.6		12		840			
HID2015-6	Qt	78	-56.6		12.6		835			
HID2015-6	Qt	78	-56.6		12.6		835			
HID2015-6	Qt	80	-57		10.5		852			
HID2015-6	Qt	80	-57		10.5		852			
HID2015-6	Qt	80	-57	N/A			N/A			

HID2015-6	Qt		81	-56.7	10.4	853
HID2015-6	Qt		81	-56.7	11	848
HID2015-6	Qt		81	-56.7	11.5	844
HID2015-6	Qt		82	-56.8	26.7	668
HID2015-6	Qt		82	-56.8	26.7	668
HID2015-6	Qt		82	-56.8	26.7	668
HID2015-6	Qt		82	-56.8	26	682
HID2015-6	Qt	13a		-56.6	26.2	678
HID2015-6	Qt	13a		-56.6	26.2	678
HID2015-6	Qt	13a		-56.6	26.2	678
HID2015-6	Qt	13a		-56.6	26.2	678
HID2015-6	Qt	13a		-56.6	26.2	678
HID2015-6	Qt	13b		-56.6	25.9	684
HID2015-6	Qt	13b		-56.6	26.4	674
HID2015-6	Qt	13b		-56.6	26.4	674
HID2015-6	Qt	13b		-56.6	26.4	674
HID2015-6	Qt	13b		-56.6	26.4	674
HID2015-6	Qt	13c		-56.6	26.5	672
HID2015-6	Qt	13c		-56.6	26.5	672
HID2015-6	Qt	13c		-56.6	26.5	672
HID2015-6	Qt	13c		-56.6	26.5	672
HID2015-6	Qt	13c		-56.6	26.5	672
HID2015-6	Qt	13d		-56.9	24	715
HID2015-6	Qt	13d		-56.9	24	715
HID2015-6	Qt	13d		-56.9	24	715
HID2015-6	Qt	13d		-56.9	24.1	714
HID2015-6	Qt	13d		-56.9	24	715
HID2015-6	Qt		23	-57	-3.2	942
HID2015-6	Qt		23	-57	-2.4	937
HID2015-6	Qt		23	-57	-2.4	937
HID2015-6	Qt		23	-57	-2.8	940
HID2015-6	Qt		24	-57.1	25.9	684
HID2015-6	Qt		24	-57.1	25.9	684
HID2015-6	Qt		24	-57.1	25.9	684
HID2015-6	Qt		24	-57.1	25.9	684
HID2015-6	Qt		28	-57.1	14.5	819
HID2015-6	Qt		28	-57.1	14.5	819
HID2015-6	Qt		28	-57.1	14.5	819
HID2015-6	Qt		29	-57.2	12.5	836
HID2015-6	Qt		29	-57.2	12.5	836
HID2015-6	Qt		29	-57.2	12.5	836

HID2015-6	Qt	30	-56.6		29			606
HID2015-6	Qt	30	-56.6		29			606
HID2015-6	Qt	31	-57.2		9.3			861
HID2015-6	Qt	31	-57.2		9.3			861
HID2015-6	Qt	31	-57.2		9.3			861
HID2015-6	Qt	31	-57.2		9.3			861
HID2015-6	Qt	31	-56.8		12.1			840
HID2015-6	Qt	32	-56.8		12.1			840
HID2015-6	Qt	32	-56.8		12.1			840
HID2015-6	Qt	32	-56.8		12.1			840
HID2015-6	Qt	32	-56.8		12.1			840
HID2015-6	Qt	33	-57.1		25.7			688
HID2015-6	Qt	33	-57.1		25.7			688
HID2015-6	Qt	33	-57.1		25.7			688
HID2015-6	Qt	33	-57.1		25.7			688
HID2015-6	Qt	41	-57		26.1			680
HID2015-6	Qt	41	-57		26.1			680
HID2015-6	Qt	41	-57		26.1			680
HID2015-6	Qt	41	-57		26.1			680
HID2015-6	Qt	42	-57.1		24.2			712
HID2015-6	Qt	42	-57.1		24.2			712
HID2015-6	Qt	42	-57.1		24.3			711
HID2015-6	Qt	42	-57.1		24.2			712
HID2015-6	Qt	43	-57.4		12			840
HID2015-6	Qt	43	-57.4		12			840
HID2015-6	Qt	43	-57.4		12			840
HID2015-6	Qt	43	-57.4		12			840
HID2015-6	Qt	44	-56.8		28			638
HID2015-6	Qt	44	-56.8		28			638
HID2015-6	Qt	44	-56.8	N/A			N/A	
HID2015-6	Qt	45	-56.9		20.6			759
HID2015-6	Qt	45	-56.9		20.6			759
HID2015-6	Qt	45	-56.9		20.6			759
HID2015-6	Qt	45	-56.9		20.6			759
HID2015-6	Qt	45	-56.9		20.6			759
HID2015-6	Qt	45	-56.9		20.6			759
HID2015-6	Qt	46	-56.6		27			662
HID2015-6	Qt	46	-56.6		27			662
HID2015-6	Qt	46	-56.6	N/A			N/A	
HID2015-6	Qt	7	-56.4		28.1	V		307
HID2015-6	Qt	7	-56.4		28.1	V		307

HID2015-6	Qt	7	-56.4	28.1	V	307
HID2015-6	Qt	9	-56.4	26.5		672
HID2015-6	Qt	9	-56.4	26.5		672
HID2015-6	Qt	9	-56.4	26.5		672
HID2015-6	Qt	9	-56.4	26.5		672
HID2015-6	Qt	9	-56.4	26.5		672
HID2015-6	Qt	10	-56.2	27.5	V	293
HID2015-6	Qt	10	-56.2	27.5	V	293
HID2015-6	Qt	10	-56.2	27.5	V	293
HID2015-6	Qt	10	-56.2	27.5	V	293
HID2015-6	Qt	11	-56.2	29	V	333
HID2015-6	Qt	11	N/A	29	V	333
HID2015-6	Qt	14	-56.4	18.2		785
HID2015-6	Qt	14	-56.4	18.2		785
HID2015-6	Qt	14	-56.4	18.2		785
HID2015-6	Qt	15	-56.4	17.1		796
HID2015-6	Qt	15	-56.4	17.1		796
HID2015-6	Qt	15	-56.4	17.1		796
HID2015-6	Qt	15	-56.4	17.1		796
HID2015-6	Qt	19	-56.3	26.3	V	271
HID2015-6	Qt	19	-56.3	26.3	V	271
HID2015-6	Qt	19	-56.3	26.3	V	271
HID2015-6	Qt	19	-56.3	26.3	V	271
HID2015-6	Qt	19	-56.3	26.3	V	271
HID2015-6	Qt	25	-56.4	23.2		726
HID2015-6	Qt	25	-56.4	23.2		726
HID2015-6	Qt	25	-56.4	23.2		726
HID2015-6	Qt	25	-56.4	23.2		726
HID2015-6	Qt	26	-56.3	25.3		694
HID2015-6	Qt	26	-56.3	25.3		694
HID2015-6	Qt	26	-56.3	25.3		694
HID2015-6	Qt	26	-56.3	25.3		694
HID2015-6	Qt	27	-56.4	24.2		712
HID2015-6	Qt	27	-56.4	24.2		712
HID2015-6	Qt	27	-56.4	24.2		712
HID2015-6	Qt	27	-56.4	24.2		712
HID2015-6	Qt	27	-56.4	23.8		718
HID2015-6	Qt	27	-56.4	24.2		712
HID2015-6	Qt	35	-56.8	0.2		922
HID2015-6	Qt	35	-56.8	0.4		921
HID2015-6	Qt	35	-56.8	0.1		923

HID2015-6	Qt	35	-56.8	0.4		921
HID2015-6	Qt	36	-56.5	12		840
HID2015-6	Qt	36	-56.5	12		840
HID2015-6	Qt	36	-56.5	12		840
HID2015-6	Qt	36	-56.5	12		840
HID2015-6	Qt	36	-56.5	12		840
HID2015-6	Qt	40	-56.7	15		815
HID2015-6	Qt	40	N/A	15		815
HID2015-6	Qt	47	-56.4	23.5		722
HID2015-6	Qt	47	-56.4	23.4		724
HID2015-6	Qt	47	-56.4	23.5		722
HID2015-6	Qt	48	-56.6	19.6		770
HID2015-6	Qt	48	-56.6	19.6		770
HID2015-6	Qt	48	-56.6	19.6		770
HID2015-6	Qt	1	-57.3	19.7		768
HID2015-6	Qt	1	-57.3	19.7		768
HID2015-6	Qt	1	-57.3	19.7		768
HID2015-6	Qt	1	-57.3	19.7		768
HID2015-6	Qt	1	-57.3	19.7		768
HID2015-6	Qt	1	-57.3	19.7		768
HID2015-6	Qt	1	-57.3	19.7		768
HID2015-6	Qt	1	-57.3	19.7		768
HID2015-6	Qt	2	-56.9	27.7	V	300
HID2015-6	Qt	2	-56.9	27.7	V	300
HID2015-6	Qt	2	-56.9	27.7	V	300
HID2015-6	Qt	2	-56.9	27.7	V	300
HID2015-6	Qt	3	-56.7	N/A	V	N/A
HID2015-6	Qt	3	N/A	N/A	V	N/A
HID2015-6	Qt	3	N/A	N/A	V	N/A
HID2015-6	Qt	3	N/A	N/A	V	N/A
HID2015-6	Qt	4	-56.3	24.3	V	244
HID2015-6	Qt	4	-56.3	24.5	V	247
HID2015-6	Qt	4	-56.3	21.5	V	214
HID2015-6	Qt	4	-56.3	N/A	V	N/A
HID2015-6	Qt	6	-57.7	25.4		691
HID2015-6	Qt	6	-57.7	25.4		691
HID2015-6	Qt	6	-57.7	25.4		691
HID2015-6	Qt	16	-56.6	29.1	V	341
HID2015-6	Qt	16	-56.6	29.1	V	341
HID2015-6	Qt	16	-56.6	29.1	V	341
HID2015-6	Qt	16	-56.6	29.1	V	341

HID2015-6	Qt	16	-56.6	29.1	V	341
HID2015-6	Qt	17	-56.3	27.1		658
HID2015-6	Qt	17	-56.3	27.1		658
HID2015-6	Qt	17	-56.3	27.1		658
HID2015-6	Qt	17	-56.3	27.1		658
HID2015-6	Qt	34	-56.7	-5.3		954
HID2015-6	Qt	34	-56.7	-5.3		954
HID2015-6	Qt	34	-56.7	-2.3		937
HID2015-6	Qt	34	-56.7	-1.1		930
HID2015-6	Qt	34	-56.7	1.6		913
HID2015-6	Qt	88	-57.7	20.4		760
HID2015-6	Qt	88	-57.7	20.5		759
HID2015-6	Qt	88	-57.7	20.8		756
HID2015-6	Qt	88	-57.7	20.8		756
HID2015-6	Qt	88	-57.7	20.8		756
HID2015-6	Qt	89	-57.7	20.5		759
HID2015-6	Qt	89	-57.7	20.5		759
HID2015-6	Qt	89	-57.7	20.5		759
HID2015-6	Qt	89	-57.7	20.3		761
HID2015-6	Qt	90	-57	28.9		606
HID2015-6	Qt	90	-57	28.9		606
HID2015-6	Qt	90	-57	28.9		606
HID2015-6	Qt	90	-57	28.9		606
HID2015-6	Qt	91	-56.8	16.3		802
HID2015-6	Qt	91	-56.8	22.6		733
HID2015-6	Qt	91	-56.8	22.6		733
HID2015-6	Qt	91	-56.8	22.6		733
HID2015-6	Qt	93	-57.2	28		635
HID2015-6	Qt	93	-57.2	28		635
HID2015-6	Qt	93	-57.2	28		635
HID2015-6	Qt	31a	-57.1	26.8		664
HID2015-6	Qt	31a	-57.1	26.8		664
HID2015-6	Qt	31a	-57.1	26.8		664
HID2015-6	Qt	92	-56.8	17.9		787
HID2015-6	Qt	92	-56.8	17.9		787
HID2015-6	Qt	92	-56.8	17.9		787
HID2015-6	Qt	92	-56.8	17.9		787
HID2015-6	Qt	94	-57.4	27		660
HID2015-6	Qt	94	-57.4	27		660
HID2015-6	Qt	94	-57.4	27		660
HID2015-6	Qt	94	-57.4	27		660

HID2015-6	Qt	94	-57.4	27			660
HID2015-6	Qt	95	-56.7	19.9			766
HID2015-6	Qt	95	-56.7	19.9			766
HID2015-6	Qt	95	-56.7	19.9			766
HID2015-6	Qt	95	-56.7	19.9			766
HID2015-6	Qt	96	-56.3	26.6			668
HID2015-6	Qt	96	-56.3	26.6			668
HID2015-6	Qt	96	-56.3	26.6			668
HID2015-6	Qt	97	-56.7	30.9		N/A	
HID2015-6	Qt	97	-56.7	30.9		N/A	
HID2015-6	Qt	97	-56.7	30.9		N/A	
HID2015-6	Qt	97	-56.7	30.9		N/A	
HID2015-6	Qt	97	-56.7	30.9		N/A	
HID2015-6	Qt	98	-57	21			753
HID2015-6	Qt	98	-57	21			753
HID2015-6	Qt	98	-57	21			753
HID2015-6	Qt	98	-57	21			753
HID2015-6	Qt	98	-57	21			753
HID2015-6	Qt	99	-57.2	20			765
HID2015-6	Qt	99	-57.2	20			765
HID2015-6	Qt	99	-57.2	20			765
HID2015-6	Qt	99	-57.2	20			765
HID2015-6	Qt	99	-57.2	20			765
HID2015-6	Qt	100	-55.8	N/A		N/A	
HID2015-6	Qt	101	-56	26.3			674
HID2015-6	Qt	101	-56	N/A		N/A	
HID2015-6	Qt	102	-56.4	2.5			907
HID2015-6	Qt	102	-56.4	2.5			907
HID2015-6	Qt	102	-56.4	2.5			907
HID2015-6	Qt	102	-56.4	2.5			907
HID2015-6	Qt	102	-56.4	2.5			907
HID2015-6	Qt	103	-56.1	-1.1			929
HID2015-6	Qt	103	-56.1	-0.1			923
HID2015-6	Qt	103	-56.1	0.5			920
HID2015-6	Qt	103	-56.1	0.8			918
HID2015-6	Qt	103	-56.1	0.8			918
HID2015-6	Qt	108	-56.4	20.1			764
HID2015-6	Qt	108	-56.4	20.1			764
HID2015-6	Qt	108	-56.4	20.1			764
HID2015-6	Qt	108	-56.4	20.1			764
HID2015-6	Qt	108	-56.4	20.1			764

HID2015-6	Qt	91a	-56.7	-2			935
HID2015-6	Qt	91a	-56.7	-1.7			933
HID2015-6	Qt	91a	-56.7	-0.7			927
HID2015-6	Qt	91a	-56.7	-0.7			927
HID2015-6	Qt	91a	-56.7	-0.8			N/A
HID2015-6	Qt	99	-57.6	19.8			768
HID2015-6	Qt	99	-57.6	20			766
HID2015-6	Qt	99	-57.6	20			766
HID2015-6	Qt	99	-57.6	20.3			762
HID2015-6	Qt	104	-56.9	25	V		252
HID2015-6	Qt	104	-56.9	N/A			N/A
HID2015-6	Qt	104	-56.9	N/A			N/A
HID2015-6	Qt	104	-56.9	N/A			N/A
HID2015-6	Qt	105	-56.7	30.9			#REF!
HID2015-6	Qt	105	-56.7	30.9			#REF!
HID2015-6	Qt	105	-56.7	30.9			#REF!
HID2015-6	Qt	105	-56.7	30.9			#REF!
HID2015-6	Qt	106	-57.1	-2.6			939
HID2015-6	Qt	106	-57.1	-2.6			939
HID2015-6	Qt	106	-57.1	-2.6			939
HID2015-6	Qt	106	-57.1	-2.6			939
HID2015-6	Qt	106	-57.1	-2.6			939
HID2015-6	Qt	112	-56.1	-0.5			926
HID2015-6	Qt	112	-56.1	-0.1			924
HID2015-6	Qt	112	-56.1	0.2			922
HID2015-6	Qt	112	-56.1	0.2			922
HID2015-6	Qt	121	-56.3	2.2			910
HID2015-6	Qt	121	-56.3	2.2			910
HID2015-6	Qt	121	-56.3	2.2			910
HID2015-6	Qt	121	-56.3	2.2			910
HID2015-6	Qt	121	-56.3	2.2			910
HID2015-6	Qt	122	-56.1	29.5	V		354
HID2015-6	Qt	122	-56.1	29.5	V		354
HID2015-6	Qt	122	-56.1	29.5	V		354
HID2015-6	Qt	122	-56.1	29.5	V		354
HID2015-6	Qt	122	-56.1	29.5	V		354
HID2015-6	Qt	123	-56.5	20.1			765
HID2015-6	Qt	123	-56.5	20.1			765
HID2015-6	Qt	123	-56.5	20.1			765
HID2015-6	Qt	123	-56.5	20.1			765
HID2015-6	Qt	123	-56.5	20.1			765

HID2015-6	Qt	125	-56.3		23.8			718
HID2015-6	Qt	125	-56.3		23.8			718
HID2015-6	Qt	125	-56.3		23.8			718
HID2015-6	Qt	125	-56.3		23.8			718
HID2015-6	Qt	125	-56.3		23.8			718
HID2015-6	Qt	125	-56.3		23.8			718
HID2015-6	Qt	126	-56.2		24.5	V		245
HID2015-6	Qt	126	-56.2		24.2	V		242
HID2015-6	Qt	126	-56.2	N/A			N/A	
HID2015-6	Qt	126	-56.2	N/A			N/A	
HID2015-6	Qt	128	-56.4		9.5			860
HID2015-6	Qt	128	-56.4		9.5			860
HID2015-6	Qt	128	-56.4		9.8			857
HID2015-6	Qt	109	-57		27.5	V		293
HID2015-6	Qt	109	-57		27.5	V		293
HID2015-6	Qt	109	-57		27.5	V		293
HID2015-6	Qt	109	-57		27.5	V		293
HID2015-6	Qt	109	-57		27.5	V		293
HID2015-6	Qt	110	-56.9		27.4			653
HID2015-6	Qt	110	-56.9		27.4			653
HID2015-6	Qt	110	-56.9		27.4			653
HID2015-6	Qt	110	-56.9		27.4			653
HID2015-6	Qt	110	-56.9		27.4			653
HID2015-6	Qt	111	-56.6		-2.3			937
HID2015-6	Qt	111	-56.6		-1.8			934
HID2015-6	Qt	111	-56.6		-1.5			932
HID2015-6	Qt	111	-56.6		-1.5			932
HID2015-6	Qt	124	-56.2		26.2			678
HID2015-6	Qt	124	-56.2		26.2			678
HID2015-6	Qt	124	-56.2		26.2			678
HID2015-6	Qt	76	-56.1		26.8			664
HID2015-6	Qt	76	-56.1		26.8			664
HID2015-6	Qt	76	-56.1		26.8			664
HID2015-6	Qt	113s	-56.2		0.4			921
HID2015-6	Qt	113s	-56.2		0.4			921
HID2015-6	Qt	113s	-56.2		0.5			920
HID2015-6	Qt	113s	-56.2		0.5			920
HID2015-6	Qt	113s	-56.2		3.4			902
HID2015-6	Qt	114s	-56.2		-1.4			932
HID2015-6	Qt	114s	-56.2		-1.4			932
HID2015-6	Qt	114s	-56.2		-1.4			932

HID2015-6	Qt	114s	-56.2	-1.5			932
HID2015-6	Qt	115s	-56.2	1			917
HID2015-6	Qt	115s	-56.2	1			917
HID2015-6	Qt	115s	-56.2	1			917
HID2015-6	Qt	115s	-56.2	1			917
HID2015-6	Qt	115s	-56.2	1			917
HID2015-6	Qt	116	-57.4	26.5			668
HID2015-6	Qt	116	-57.4	26.5			668
HID2015-6	Qt	116	-57.4	26.5			668
HID2015-6	Qt	116	-57.4	26.9			660
HID2015-6	Qt	116	-57.4	26.9			660
HID2015-6	Qt	117	-57.1	17.2			793
HID2015-6	Qt	117	-57.1	17.2			793
HID2015-6	Qt	117	-57.1	17.2			793
HID2015-6	Qt	117	-57.1	17.2			793
HID2015-6	Qt	117	-57.1	17.2			793
HID2015-6	Qt	118	-57.1	27			658
HID2015-6	Qt	118	-57.1	27			658
HID2015-6	Qt	118	-57.1	27			658
HID2015-6	Qt	118	-57.1	27			658
HID2015-6	Qt	118	-57.1	27			658
HID2015-6	Qt	119	-57	-1.2			930
HID2015-6	Qt	119	-57	-0.4			925
HID2015-6	Qt	119	-57	-0.4			925
HID2015-6	Qt	119	-57	0.1			922
HID2015-6	Qt	119	-57	0.1			922
HID2015-6	Qt	120	-57	26.5			668
HID2015-6	Qt	120	-57	26.5			668
HID2015-6	Qt	120	-57	26.5			668
HID2015-6	Qt	120	-57	26.6			666
HID2015-6	Qt	120	-57	26.6			666
HID2015-6	Qt	127	-57	26.8			662
HID2015-6	Qt	127	-57	26.8			662
HID2015-6	Qt	127	-57	26.8			662
HID2015-6	Qt	127	-57	26.8			662
HID2015-6	Qt	127	-57	26.8			662
HID2015-6	Qt	129	-57	26.6			666
HID2015-6	Qt	129	-57	N/A		N/A	
HID2015-6	Qt	129	-57	N/A		N/A	
HID2015-6	Qt	130	-56.8	N/A		N/A	
HID2015-6	Qt	130	-56.8	N/A		N/A	

HID2015-6	Qt	130	-56.8	N/A				N/A	
HID2015-6	Qt	130	-56.8	N/A				N/A	
HID2015-6	Qt	131	-56.8		25	V			254
HID2015-6	Qt	131	N/A	N/A				N/A	
HID2015-6	Qt	132	-56.7		28	V			309
HID2015-6	Qt	132	-56.7		28	V			309
HID2015-6	Qt	132	-56.7		28.1	V			312
HID2015-6	Qt	132	-56.7		28.1	V			312
HID2015-6	Qt	133	N/A	N/A				N/A	
HID2015-6	Qt	134	-56.9		19.3				771
HID2015-6	Qt	134	-56.9		19.3				771
HID2015-6	Qt	134	-56.9		20.1				762
HID2015-6	Qt	134	-56.9		20.1				762
HID2015-6	Qt	135	-56.7		26.7				664
HID2015-6	Qt	135	-56.7		26.7				664
HID2015-6	Qt	135	-56.7		26.7				664
HID2015-6	Qt	135	-56.7		26.7				664
HID2015-6	Qt	136	-57.1		12.6				835
HID2015-6	Qt	136	-57.1		12.6				835
HID2015-6	Qt	136	-57.1		12.6				835
HID2015-6	Qt	136	-57.1		12.6				835
HID2015-6	Qt	136	-57.1		12.6				835
HID2015-6	Qt	137	-56.8		27.6	V			300
HID2015-6	Qt	137	-56.8		27.6	V			300
HID2015-6	Qt	137	-56.8	N/A				N/A	
HID2015-6	Qt	137	-56.8	N/A				N/A	
HID2015-6	Qt	138	-56.9		26.8				662
HID2015-6	Qt	138	-56.9		26.8				662
HID2015-6	Qt	138	-56.9		26.8				662
HID2015-6	Qt	138	-56.9		26.8				662
HID2015-6	Qt	139	-56.2		28	V			309
HID2015-6	Qt	139	-56.2		28	V			309
HID2015-6	Qt	139	-56.2		28	V			309
HID2015-6	Qt	139	-56.2		28	V			309
HID2015-6	Qt	139	-56.2		28	V			309
HID2015-6	Qt	140	-56.2		13.8				825
HID2015-6	Qt	140	-56.2		13.8				825
HID2015-6	Qt	140	-56.2		14.2				821
HID2015-6	Qt	140	-56.2		14.2				821
HID2015-6	Qt	140	-56.2		14.2				821
HID2015-6	Qt	141	-56.4		13.3				829

HID2015-6	Qt	141	-56.4		13.3			829
HID2015-6	Qt	141	-56.4		13.3			829
HID2015-6	Qt	141	-56.4		13.3			829
HID2015-6	Qt	141	-56.4		13.3			829
HID2015-6	Qt	143	-56.4		7.8			871
HID2015-6	Qt	143	-56.4		7.8			871
HID2015-6	Qt	143	-56.4		7.8			871
HID2015-6	Qt	143	-56.4		7.8			871
HID2015-6	Qt	143	-56.4		7.8			871
HID2015-6	Qt	150	-56.5		24.4	V		245
HID2015-6	Qt	150	-56.5	N/A			N/A	
HID2015-6	Qt	151	-56.8		12.3			837
HID2015-6	Qt	151	-56.8		12.3			837
HID2015-6	Qt	151	-56.8		12.7			834
HID2015-6	Qt	151	-56.8		12.7			834
HID2015-6	Qt	151	-56.8		13.9			824
HID2015-6	Qt	152	-56.8	N/A			N/A	
HID2015-6	Qt	153	-56.5		25.4	V		259
HID2015-6	Qt	153	-56.5		25.4	V		259
HID2015-6	Qt	153	-56.5		25.4	V		259
HID2015-6	Qt	153	N/A		25.4	V		259
HID2015-6	Qt	153	N/A		25.4	V		259
HID2015-6	Qt	154	-56.7		9.3			860
HID2015-6	Qt	154	-56.7		9.3			860
HID2015-6	Qt	154	-56.7		9.7			857
HID2015-6	Qt	154	-56.7		9.7			857
HID2015-6	Qt	154	-56.7		9.7			857
HID2015-6	Qt	155	<-180		10	V		139
HID2015-6	Qt	155	<-180		10	V		139
HID2015-6	Qt	155	<-180		10	V		139
HID2015-6	Qt	155	<-180		10	V		139
HID2015-6	Qt	155	<-180	N/A			N/A	
HID2015-6	Qt	156	-56.9		19.9			766
HID2015-6	Qt	156	-56.9		19.9			766
HID2015-6	Qt	156	-56.9		20.5			759
HID2015-6	Qt	156	-56.9		21.2			751
HID2015-6	Qt	156	-56.9		21.2			751
HID2015-6	Qt	157	-56.8		14			823
HID2015-6	Qt	157	-56.8		14			823
HID2015-6	Qt	157	-56.8		14			823
HID2015-6	Qt	157	-56.8		14			823

HID2015-6	Qt	157	-56.8		14				823
HID2015-6	Qt	158	-57.1		3				904
HID2015-6	Qt	158	-57.1		3				904
HID2015-6	Qt	158	-57.1		3.6				900
HID2015-6	Qt	158	-57.1		3.6				900
HID2015-6	Qt	158	-57.1		3.8				899
HID2015-6	Qt	159	-56.8	N/A				N/A	
HID2015-6	Qt	159	-56.8	N/A				N/A	
HID2015-6	Qt	159	-56.8	N/A				N/A	
HID2015-6	Qt	159	-56.8	N/A				N/A	
HID2015-6	Qt	159	-56.8	N/A				N/A	
HID2015-6	Qt	160	-56.7		28	V			307
HID2015-6	Qt	160	-56.7		28	V			307
HID2015-6	Qt	160	-56.7		28	V			307
HID2015-6	Qt	160	-56.7		28	V			307
HID2015-6	Qt	160	-56.7		28	V			307
HID2015-6	Qt	161	-56.9		12				840
HID2015-6	Qt	161	-56.9		12				840
HID2015-6	Qt	161	-56.9		12				840
HID2015-6	Qt	161	-56.9		12.7				834
HID2015-6	Qt	161	-56.9		12.7				834
HID2015-6	Qt	162	-56.6	N/A				N/A	
HID2015-6	Qt	163	N/A	N/A				N/A	
HID2015-6	Qt	164	-56.5		9.3	V			136
HID2015-6	Qt	164	-56.5		10	V			139
HID2015-6	Qt	164	-56.5	N/A				N/A	
HID2015-6	Qt	164	-56.5	N/A				N/A	
HID2015-6	Qt	157a	-56.5		27.9	V			304
HID2015-6	Qt	157a	-56.5		27.9	V			304
HID2015-6	Qt	157a	-56.5		28.7	V			327
HID2015-6	Qt	157a	-56.5		28.7				613
HID2015-6	Qt	157a	-56.5	N/A				N/A	
HID2015-6	Qt	134	-56.3		21				754
HID2015-6	Qt	134	-56.3		21				754
HID2015-6	Qt	134	-56.3		21.9				743
HID2015-6	Qt	142	-56.5		27.9	V			302
HID2015-6	Qt	142	-56.5		28.2	V			309
HID2015-6	Qt	142	-56.5	N/A				N/A	
HID2015-6	Qt	142	-56.5	N/A				N/A	
HID2015-6	Qt	144	-56.6		28.3	V			312
HID2015-6	Qt	144	-56.6	N/A				N/A	

HID2015-6	Qt	144	N/A	N/A			N/A	
HID2015-6	Qt	144	N/A	N/A			N/A	
HID2015-6	Qt	145	-57	12.5				836
HID2015-6	Qt	145	-57	12.5				836
HID2015-6	Qt	145	-57	12.8				834
HID2015-6	Qt	145	-57	12				840
HID2015-6	Qt	147	-56.9	14				824
HID2015-6	Qt	147	-56.9	14				824
HID2015-6	Qt	147	-56.9	14.2				822
HID2015-6	Qt	147	-56.9	14.8				817
HID2015-6	Qt	147	-56.9	N/A			N/A	
HID2015-6	Qt	165	-56.6	27.7	V			298
HID2015-6	Qt	165	-56.6	N/A			N/A	
HID2015-6	Qt	165	-56.6	N/A			N/A	
HID2015-6	Qt	165	-56.6	N/A			N/A	
HID2015-6	Qt	165	-56.6	N/A			N/A	
HID2015-6	Qt	166	-57	2.8				906
HID2015-6	Qt	166	-57	2.8				906
HID2015-6	Qt	166	-57	3.4				902
HID2015-6	Qt	166	-57	3.4				902
HID2015-6	Qt	166	-57	4.5				895
HID2015-6	Qt	68						564
HID2015-6	Qt	68						686
HID2015-6	Qt	100						237
HID2015-6	Qt	100						241
HID2015-6	Qt	101						252
HID2015-6	Qt	101						983
HID2015-6	Qt	104						331
HID2015-6	Qt	104						235
HID2015-6	Qt	133						221
HID2015-6	Qt	133						213
HID2015-6	Qt	144						260
HID2015-6	Qt	144						230
HID2015-6	Qt	149						200
HID2015-6	Qt	149						226
HID2015-6	Qt	155						200
HID2015-6	Qt	155						204
HID2015-6	Qt	159						251
HID2015-6	Qt	159						247
HID2015-6	Qt	162						163
HID2015-6	Qt	162						167

HID2015-6	Qt	163							886			
HID2015-6	Qt	163							872			
HID2015-8	Qt	FIA1					H2O-NaCl FIs	N/A				218
HID2015-8	Qt	FIA1					H2O-NaCl FIs	N/A				218
HID2015-8	Qt	FIA1					H2O-NaCl FIs	N/A				222
HID2015-8	Qt	FIA2					H2O-NaCl FIs	N/A				223
HID2015-8	Qt	FIA2					H2O-NaCl FIs	N/A				227
HID2015-8	Qt	FIA2					H2O-NaCl FIs	N/A				229
HID2015-8	Qt	FIA3					H2O-NaCl FIs	N/A				190
HID2015-8	Qt	FIA3					H2O-NaCl FIs	N/A				195
HID2015-8	Qt	FIA3					H2O-NaCl FIs	N/A				190
HID2015-8	Qt	FIA3					H2O-NaCl FIs	N/A				191
HID2015-8	Qt	FIA3					H2O-NaCl FIs		922	7.0	-4.4	199
HID2015-8	Qt	FIA3					H2O-NaCl FIs		924	7.2	-4.5	198
HID2015-8	Qt	FIA3					H2O-NaCl FIs		925	7.6	-4.8	200
HID2015-8	Qt	FIA3					H2O-NaCl FIs		915	7.0	-4.4	205
HID2015-8	Qt	FIA4					H2O-NaCl FIs		904	6.7	-4.2	213
HID2015-8	Qt	FIA4					H2O-NaCl FIs		905	6.7	-4.2	212
HID2015-8	Qt	FIA4					H2O-NaCl FIs		923	6.7	-4.2	195
HID2015-8	Qt	FIA4					H2O-NaCl FIs		908	6.7	-4.2	209.5
HID2016-19	Dol	FIA1		-56.3	7	10.2			883	0		
HID2016-19	Dol	FIA1		-56.3	7.2	10.2			881	0		
HID2016-19	Dol	FIA1		-56.3	7.2	10.2			881	0		
HID2016-19	Dol	FIA1		-56.3	8.3	10.2			873	0		
HID2016-19	Dol	FIA1		-56.3		10.2		N/A		0		
HID2016-19	Ru		1	-56.4	-13				998			
HID2016-19	Ru		1	-56.3				N/A				
HID2016-19	Ru		2	-56.2	-12.3	9			995	2.5		
HID2016-19	Ru		2	-56.2	-2	8.7			939	4.0		
HID2016-19	Ru		2	-56.2				N/A				
HID2016-19	Ru		3		29.8	9			602	2.5		
HID2016-19	Ru		3			8.7		N/A		4.0		
HID2016-19	Ru		3					N/A		5.7	-3.5	
HID2016-19	Dr	FIA1					104.458		765			
HID2016-19	Dr	FIA1					103.910		523			
HID2016-19-III-Em	Em	02					104.29		694			
HID2016-19-III-Em	Em	04					104.74		874			
HID2016-19-III-Em	Em	11					103.74		443			
HID2016-19-III-	Em	12					104.63		833			

Em											
HID2016-19-III-Em	Em	FIA1			104.40			739			
HID2016-19-Qtz	Qt	FIA1	-57.2	27.2				672			
HID2016-19-Qtz	Qt	FIA1	-57.2	27.5				666			
HID2016-19-Qtz	Qt	FIA1				H2O-NaCl FIs		927	9.9	-6.5	215
HID2016-19-Qtz	Qt	FIA1				H2O-NaCl FIs		927	9.9	-6.5	215
HID2016-19-Qtz	Qt	FIA1				H2O-NaCl FIs	N/A				215
NAEM Apatite	Ap	FIA1			104.868			920			
NAEM Apatite	Ap	FIA1			104.809			900			
NAEM Apatite	Ap	FIA2			104.94			944			
NAEM Apatite	Ap	FIA2			105.079			985			
NAEM030916-4	Qt	FIA1			102.7770			43			
NAEM030916-4	Qt	FIA1			102.8030			52			
NAEM030916-4	Qt	FIA1			102.8490			68			
NAEM030916-4	Qt	FIA2			103.6220			390			
NAEM030916-4	Qt	FIA2			103.5770			370			
NAEM030916-4	Qt	FIA2			103.6060			383			
NAEM030916-4	Qt	FIA3				FIA with decrepitation halo	N/A				
NAEM030916-4	Qt	FIA3				FIA with decrepitation halo	N/A				
NAEM030916-4	Qt	FIA4			103.8220			482			
NAEM030916-4	Qt	FIA4			103.8110			477			
NAEM030916-4	Qt	FIA4			103.8030			473			
NAEM030916-4	Qt	FIA5			104.5880			818			
NAEM030916-4	Qt	FIA5			104.5820			815			
NAEM030916-8	Em	FIA1			104.032	methane and graphite detected		578			
NAEM030916-8	Em	FIA1			104.567	methane detected		809			
NAEM030916-8	Em	02					N/A				
NAEM030916-8	Em	04					N/A				
NAEM030916-8	Em	06					N/A				
NAEM030916-8	Em	09					N/A				
NAEM030916-8	Em	12					N/A				
NAEM030916-8	Em	FIA1		16.2				811			
NAEM030916-8	Em	FIA1		16.4				809			
NAEM030916-8	Em	FIA2		16.3				810			
NAEM030916-8	Em	FIA2		16.1				812			
NAEM030916-8	Em	FIA2		16.2				811			
NAEM030916-8	Em	SEC_FIA3			104.306			701			
NAEM030916-8	Qt	1	-58.8	13.7				832			
NAEM030916-8	Qt	1	-58.9	14.9				822			

NAEM030916-8	Qt		2	-58.6	17.5			799
NAEM030916-8	Qt		2	-58.6	18.6			788
NAEM030916-8	Qt		2		18.6			788
NAEM030916-8	Qt		3	-58	16.1			812
NAEM030916-8	Qt		3	-58	17			803
NAEM030916-8	Qt		3	-58	17			803
NAEM09.9	Dol	FIA1				104.345		717
NAEM09.9	Dol	FIA1				104.336		713
NAEM09.9	Dol	FIA1				104.32		707
NAEM09.9	Dol	FIA1				104.346		718
Spear 8 Em	Dol						N/A	
Spear 8 Em	Em						N/A	
58A	Em	FIA1				104.407		744
58A	Em	FIA1				104.407		744
58A	Em	FIA1				104.438		757
58A	Em	FIA2				104.599		822
58A	Em	FIA2				104.593		820
58A	Em	FIA2				104.574		812
HID2015-9	Dol	FIA1				105.076		984
HID2015-9	Dol	FIA1				105.076		984
HID2015-9	Dol	FIA1				105.058		979
HID2015-9	Dol	FIA2				104.417		748
HID2015-9	Dol	FIA2				104.416		748
HID2015-9	Dol	FIA2				104.431		754
HID2015-11	Dol	FIA1				104.377		731
HID2015-11	Dol	FIA1				103.949		540
HID2015-11	Dol	FIA2				104.646		840
HID2015-11	Dol	FIA2				104.733		873
HID2015-11	Dol	FIA2				104.32		707

Minerals abbreviated as apatite (Ap), carbonate (Car), dolomite (Dol), dravite (Dr), emerald (Em), quartz (Qt), rutile (Ru), zircon (Zr).

Table 2. Measured stable isotopes $\sigma^{18}O$ in samples

Sample #	Mineral	$d^{18}O$	Average	St.Dev	# of analyses
HID2015-12	muscovite	11.947	11.8105	0.1365	3
HID2016-19	muscovite	12.961	13.0135	0.0525	2
HID2015-9	muscovite	11.33	11.537	0.207	1
HID2015-17	quartz	15.394	15.4005	0.0065	2
HID2015-17	quartz	17.806	17.9395	0.1335	3
HID2015-8	quartz	12.928	13.014	0.086	3
NAEM030916-2	quartz	13.71	13.9495	0.2395	2
NAEM030916-4	quartz	12.232	12.236	0.004	2
NAEM030916-7	quartz	13.946	14.3135	0.3675	2
NAEM030916-8	quartz	14.035	14.4525	0.4175	2
HID2015-2	quartz	13.63	13.381	0.249	1
HID2016-19	quartz	14.061	14.136	0.075	1
HID2015-12	rutile	5.696	6.1375	0.4415	2
HID2015-19	rutile	5.519	5.255	0.264	2
HID2015-9	rutile	5.789	5.6755	0.1135	2

Table 3. Measured stable isotopes σD in muscovite from various samples

		H_2 Yield	H_2 Yield	H_2 Yield	Measured	Corrected dD
Sample #	mg	mbar	umol	umol/mg	dD	dD (VSMOW)
HID2015-9	20.71	19.2	42.816	2.067407	-46.78	-67.858
HID2015-9	20.68	20.1	44.823	2.167456	-19.084	-40.162
HID2015-12	20.21	18.5	41.255	2.041316	-9.944	-31.022
HID2015-12	20.59	19.1	42.593	2.068626	-12.328	-33.406
HID2016-19	20.66	27.4	61.102	2.957502	-13.649	-34.727
HID2016-19	20.45	26.1	58.203	2.846112	-6.294	-27.372

Table 4. Measured $\sigma^{13}C$ and $\sigma^{18}O$ in carbonate minerals

Sample #	Mineral	d13C(VPDB)	d18O(VPDB)	d18O(VSMOW)
HID2015-12b	calcite	-3.7	-16.2	14.2
HID2015-12a	calcite	-3.8	-15.5	14.9
HID2015-4	calcite	-6.6	-14.7	15.7
HID2015-3	calcite	-7.8	-19.2	11.1
HID2015-9	dolomite	-5.9	-17.4	13.0
HID2015-11	dolomite	-4.4	-17.5	12.9
HID2015-18	dolomite	-8.5	-17.7	12.7
HID2016-19	dolomite	-11.1	-17.1	13.3